Radiobiological studies for improving the treatment planning of Neutron Capture Therapy

UNIVERSIDAD DE GRANADA

María Pedrosa Rivera

Programa de Doctorado en Física y Ciencias del Espacio

Directors: José Ignacio Porras Sánchez, Maria del Carmen Ruiz Ruiz

ILL Supervisors: Ulli Köster, Trevor Forsyth

NEUTRONS FOR SOCIETY

Editor: Universidad de Granada. Tesis Doctorales
Autor: Pedrosa Rivera, María
ISBN: 978-84-1306-639-4
URI: http://hdl.handle.net/10481/63920

A mi abuela,
que siempre me llamaba valiente
cuando en esta familia todos sabemos
que la más valiente siempre fue ella.

Resumen (Español)

En este trabajo, se ha realizado un análisis tanto teórico como experimental del daño celular producido por la irradiación con neutrones, todo ello con el objetivo de mejorar la estimación de la dosis biológica y, por tanto, la planificación del tratamiento de la terapia conocida como de captura de neutrones por boro (Boron Neutron Capture Therapy o BNCT).

Se presenta un nuevo formalismo para la estimación de la dosis biológica que combina la simplicidad del que se utiliza actualmente con la precisión del llamado iso-efectivo. Este formalismo incluye el uso del modelo lineal cuadrático y unos nuevos factores de ponderación (weighting factors o factores RBE) que dependen solo de la energía del neutrón y del tipo de tejido, de manera que pueden aplicarse independientemente de la dosis o de la supervivencia.

Además, se incluye un desarrollo teórico que sigue el efecto individual de las partículas secundarias creadas cuando los neutrones interaccionan con el tejido. Éste muestra cómo los factores RBE dependen fuertemente de la energía del neutrón y por ello no debe usarse necesariamente el mismo valor para neutrones de baja energía (o térmicos) y neutrones de más altas energías (epitérmicos), hecho que se produce en la actual estimación de la dosis biológica en pacientes de BNCT.

Por último, se han llevado a cabo una serie de experimentos de irradiación celular con el objetivo de obtener datos experimentales para el estudio radiobiológico de los neutrones. Seis líneas celulares de interés en la BNCT se han irradiado en tres centros distintos: Institut Laue-Langevin en Grenoble, Centro Nacional de Aceleradores en Sevilla y Hospital Virgen de las Nieves en Granada. En el primero de ellos se ha utilizado una fuente de neutrones fríos para estudiar el efecto de neutrones de baja energía sin la fuerte influencia de otras partículas, ya que se trata de una fuente muy pura. En este centro se han realizado además otros dos experimentos que incluyen la irradiación de células previamente tratadas con el compuesto de boro BPA, para el estudio del efecto de la reacción principal en BNCT, y la irradiación de células con reemplazo del isotopo de nitrógeno, que permite aislar el efecto de la reacción de captura en este elemento y el efecto de los fotones inducidos por el haz. Este último experimento supone toda una novedad en el campo de estudio radiobiológico de neutrones. Los experimentos realizados en las otras dos instalaciones, consistentes en la irradiación con neutrones epitérmicos en el CNA de Sevilla y con fotones de un acelerador hospitalario de

Granada, ayudarán a la obtención de datos para neutrones de más altas energías y para la radiación de fotones que se utiliza de referencia. En todos los casos, tras las irradiaciones, la supervivencia celular es estudiada mediante ensayos de clonogenicidad y de capacidad proliferativa.

Todos estos experimentos proporcionan datos del efecto celular producido por las principales dosis que componen un tratamiento BNCT: neutrones térmicos, neutrones epitérmicos, captura de neutrones en boro y fotones. Se han calculado los factores RBE correspondientes de todos ellos y además se ha estudiado la influencia del tipo de dosis elegida como dosis de referencia. Los datos de las diferentes irradiaciones proporcionan información sobre el daño en distintos tipos de células tumorales y sanas, conocimiento que podría ser aplicado en los futuros tratamientos con BNCT.

Summary (English)

Theoretical and experimental analyses of the neutron biological damage associated with Boron Neutron Capture Therapy has been performed, both with the objective of improving the treatment planning regimes.

A formalism is presented that combines the simplicity of the currently used one with the accuracy of the iso-effective one. This formalism includes the use of the linear quadratic model as well as the deployment of new weighting factors that are independent of dose and survival.

In addition, a theoretical calculation of the individual effects of each secondary particle resulting from the neutron interaction with the tissue is given. This calculation shows how the weighting factors depend heavily on the neutron energy and should not be considered as currently the same for thermal and epithermal neutrons.

Finally, a series of *in vitro* irradiation experiments have been carried out in order to obtain neutron radiobiological data. Six cell lines with interest in BNCT have been irradiated at three different facilities: the Institut Laue-Langevin (Grenoble), the Centro Nacional de Aceleradores (CNA, Sevilla) and the Virgen de las Nieves Hospital (Granada). Experiments at the cold neutron beam at Institut Laue-Langevin were performed in order to establish the effect of low energy neutrons without the influence of epithermal neutrons and with a minimal influence from the effects of photons. In this beam, two other experiments have been carried out: one in order to study the effect of the boron compound BPA (Boron phenylalanine) in different cell lines, and the other one in order to isolate the effect of neutron capture by nitrogen as well as that of the effect of the gammas produced by the beam. This last experiment used nitrogen isotope labeling and has been received as an innovative approach in this field. The other two irradiation experiments, using epithermal neutrons at the Centro Nacional de Aceleradores and using photons in a hospital accelerator, gives values for other more energetic neutrons and for the reference radiation. In all the experiments cell survival was studied after irradiation with clonogenic and colorimetric assays.

Overall, these experiments provide data of the biological effect after *in vitro* irradiation for the different dose components involved in BNCT irradiation: namely thermal, epithermal, boron and photons. The weighting factors (RBE factors) for each of the dose component and cell line has been obtained. The influence of the type of dose chosen as the reference dose has

also been studied. The data for these different irradiations gives information about the damage in different type of tumor and healthy cells; this is knowledge that may be of value for future BNCT treatments.

Agradecimientos / Acknowledgements

Si encuentras tu nombre en las próximas páginas, es que esta tesis tiene una parte de ti en ella. Si crees que deberías estar y no te has encontrado, debes conocerme lo suficientemente bien para saber de mi característico despiste…/ If you find your name in the next pages, it is because this thesis has a part of you in it. If you think you should be and you haven't found yourself, you should know me well enough to know I am a bit scatterbrain...

Quiero empezar, por supuesto, agradeciendo a los dos directores de tesis, por todo el tiempo dedicado. A Ignacio, porque la pasión con la que él vive este proyecto contagia a todos. Gracias por tus esfuerzos para conseguir que yo siga formando parte de este grupo y trabajando a tu lado, cosa que es un placer gracias a tu optimismo, tu cercanía y, por supuesto, tus grandes conocimientos. A Mari Carmen, por atreverse a dirigir una tesis de una física y por creer en mí para introducirme en este insólito mundo de la biología celular. Has aportado una visión imprescindible a este proyecto, y todo desde el cariño, la empatía y el trabajo duro.

My ILL supervisors, which made me realized how lucky I was to have four person leading my work. Ulli, I still do not understand how a person that is 100% busy with infinite projects can spend three hours answering questions in a meeting with a confused PhD student. Thanks for all the explanations, advices and ideas. Trevor, thanks for trusting me enough to leave me freedom in the labs and for improving the English writing, making this thesis something readable.

A Maria José, por empezar siendo mi maestra en el laboratorio, para convertirse en alguien fundamental en mi trabajo y sobre todo en una importante amiga (aunque tú digas que en una madre). A Javier, por descubrirme cómo funciona la verdadera física experimental y hacerme ver lo mucho que la disfruto. Junto con los dos directores, tengo que agradeceros a los cuatro, por tantas horas de experimentos juntos, entre sonrisas y agobios (y mucho calor).

Cerrando el círculo que compone este grupo de investigación de la UGR, a Manolo, por sus cacharros Mcgyverianos que hicieron posible los experimentos. Y a Pablo, por las dudas resueltas, las pizarras llenas y las charlas de las cuatro de la tarde.

Coming back to ILL, to the Life Sciences group, for the ridiculous talks at lunch and the coffees in the sun. Thanks Juliette for all the help in the labs, always with a smile. Thanks

Lindsay for the empathy. To the NPP group, for their interest in my work and their suggestions. Thanks Torsten for all the help and the organization of the beam times. To the people at ILL that treated me kindly and helped me in the difficult steps to carry out the experiments. To Veronique, for helping me even when the rules made the process almost impossible.

To the BNCT community for teaching me the potential of this treatment. Gracias Marcela por enseñarnos tanto en tan poco tiempo. Thanks to the Pavia group, who made Pavia my home for two weeks. Thanks Ian for your hours of work and your kindness. Back in Grenoble, thanks to Lucie for the generosity, for sharing cells and beam time.

A mis amigos. A los Aldanas, por hacerme desconectar unas pocas horas al día. A Adri, por haber estado ahí y por esta certeza de que siempre lo estarás. A Joaquín, porque mi sueño sigue siendo compartir despacho contigo. A Dani y Sara, de lo más bonito que hay en Málaga.

To the Potorritos, because this crazy thing that is doing a PhD is much more enjoyable with other crazy people around. The Spanish cluster: Palme (y nuestros especiales collares a juego), Javier (y a nuestro banquito), Jangel y Murias; Stella (thanks for your hugs) and Lukas (not thanks for your jokes), with me since the very first day till the last one; Giuseppe, always my perfect dancing partner; Ilaria, because talking for hours is never a problem. Marta, the perfect singer partner (and the reactor breaker); Irina, the lovely discovery; Loreto (the punctual); Ana (the best organizer, n1), Joao (or Juanca); Stas (the craziest); Fra (the cooker); Gaynor (the cinema partner); Quantin (ça va?); Silvia (bella!); Radu (the best organizer, n2); Rafal, Peter, Antonio, Tim. Thank all of you for the adventures, the absurd nights, the coffee breaks, the stupid conversations, the funny pictures…the two unforgettable years.

A mis niñas, esa amistad que perdura siempre, la familia que se escoge. Es precioso sentir cómo estáis tan orgullosas de mí, tanto como yo de vosotras. Fuego, Mariqui, Ranya, Zineb, Anbar, Spi, os quiero.

A mi familia, todos mis tíos y primos. Tengo una suerte enorme de estar rodeada de gente tan cariñosa y de disfrutar siempre de vuestra compañía y de nuestras reuniones. Kiri, gracias por entenderme tanto. Tita Abel, gracias por seguir todos mis pasos desde la distancia. Pero familia, tengo que decir que no todo es agradecimiento, pues es culpa vuestra que se me haga duro estar fuera y que siempre quiera volver a casa, a vuestro lado.

A mis padres, que me dieron estas alas que me han llevado hasta aquí. Mi padre, que me ayudó a ver que las matemáticas podían ser algo divertido, ahí empezó todo. Enseñarme que

no todo es blanco o negro y no darle vueltas a decisiones ya tomadas. A mi madre, por enseñarme lo que es ser una mujer fuerte, a pedir justicia y que nadie es mejor que nadie. Ella es la que mejor sabe aliviarme en esos momentos donde es tan difícil encontrar consuelo. A los dos, por haberme acompañado en todos los pasos de este proceso. No hay paginas suficientes para demostrar lo agradecida que estoy y lo mucho que os quiero.

A mi hermana. Otro agradecimiento a mis padres aquí, por dármela a ella. Por esa semana en la que hiciste kilómetros en avión para cuidarme y cocinarme cosas. Por los desahogos por teléfono. Por esta portada tan especial. Por intentar siempre quitarme algún peso cuando ni tú misma no podías con el tuyo. Haces el papel de hermana mayor tan bien como el de mejor amiga.

A Luis, por aguantar la distancia con una sonrisa, por tus abrazos sanadores, por enseñarme lo que es el amor, por quererme de una manera tan bonita… Por alegrarme el día con tan solo una palabra: “Pronto…”

Acronyms

BED: Biologically Effective Dose

BMRR: Brookhaven Medical Research Reactor

BNCT: Boron Neutron Capture Therapy

BNL: Brookhaven National Laboratory

BPA: Boron phenylalanine

BrdU: Bromodeoxyuridine

BSH: Sodium borocaptate

CBE: Compound Biological Effectiveness

C-BENS: Cyclotron-Based Epi-thermal Neutron Source

CEA: Commissariat à l'Énergie atomique

CIBM: Centro de Investigación Biomédica

CIC: Centro de instrumentacion Cientifica

CNA: Centro Nacional de Aceleradores

CNEA: Comisión Nacional de Energía Atómica

CT: Computed Tomography

ENDF: Evaluated Nuclear Data File

FBS: Fetal Bovine Serum

GBM: Glioblastoma

IAEA: International Atomic Energy Agency

ICP-AES: Inductively coupled plasma atomic emission spectroscopy

ICRP: International Commission on Radiological Protection

ICRU: International Commission on Radiation Units and Measurements

ILL: Institut Laue-Langevin

INFN: Istituto Nazionale di Fisica Nucleare

IPPE: Institute for Physics and Power Engineering

ISNCT: International Society for Neutron Capture Therapy

KURRI: Kyoto University Research Reactor Institute

LBNL: Lawrence Berkeley National Laboratory

LENA: Laboratorio Energia Nucleare Applicata

LET: Linear Energy Transfer

LINAC: Linear Particle Accelerator

LQ model: Linear Quadratic model

MCNP: Monte Carlo N-Particle

MIT: Massachusetts Institute of Technology

NCC: National Cancer Center

NIST: National Institute of Standards and Technology

PET: Positron-emission tomography

SARAF: Soreq Applied Research Accelerator Facility

RBE: Relative Biological Effectiveness

STLD: Single Track Lethal Damage

T/N ratio: tumor/normal tissue ratio

Contents

Introduction

Cancer is a global problem that is of increasing concern as human lifespans increase. Most tumors are treated in hospitals mainly by surgery, radiotherapy, chemotherapy, immunotherapy (and combinations thereof). These treatments palliate cancer effects and in many cases eliminate cancer cells. Unfortunately, there are multiple types of cancer. Each tumor is unique case and requires individual treatment and; in some cases, it is not possible to find a solution among the current treatments. Technology and science are in a constant state of development and with this comes new approaches and therapies for the treatment of those tumors for which there is no current solution. One of these therapies, currently in an experimental phase, is known as Boron Neutron Capture Therapy (BNCT).

Shortly after the discovery of the neutron, the idea of using neutrons in radiation therapy arose [Loch36]. The basis of BNCT is the use of the characteristics of neutron irradiation in a way that hybridizes the properties of classical external beam radiotherapy and the targeted cell selectivity of *e.g.* the novel selective chemotherapy approaches. The strategy of BNCT is only possible using particles (such as neutrons), that do not interact with tissues through direct ionization, but by an indirect ionization that occurs following a nuclear reaction or recoil. Some elements have a higher probability of interacting with neutrons than others and in some of the nuclear reactions the secondary particles release high quantity of energy over a small path. This is what occurs when low-energy neutrons are captured by ^{10}B. Hence, if ^{10}B is accumulated in the tumor and subsequently irradiated by a neutron beam, the neutrons have high probability of interacting with and destroying the highly absorbing boron-containing cells without affecting nearby cells that do not have comparable quantities of boron.

Such an approach offers, in concept, the prospect of an idealized therapy that is highly targeted and controlled – and that could even conceivably be delivered in a single session. However, several difficulties stand in the way of this dream, including the requirement for a well-tailored neutron beam, and the need for boron-based drugs having high tumor specificity.

These problems have meant that even after decades of research, only about 1000 patients have been treated with BNCT [Bart12].

In the recent past, the development of new accelerator technologies in different parts of the world has resulted in new neutron beam facilities that are dedicated to BNCT [Krei16]. It is likely therefore that in the coming years there will be an increased number of clinical trials that will boost progress in BNCT worldwide. Many scientists are currently dedicated to research that is focused on the improvement of this therapy.

The main line of research for this thesis is to obtain better evaluations of the biological damage in tissues associated with BNCT – something that is key for the patients' treatment planning. As mentioned above, it is not the neutrons that damage the cells, but the secondary particles after the nuclear reactions or recoils. Different secondary particles involve different types of tissue damage. This depends on the various beam and tissue characteristics and makes the study of the neutron biological dose a challenge.

The work has been carried out in different research centers such as the Centro de Investigación Biomédica of the University of Granada, the Institut Laue-Langevin in Grenoble, the Hospital Virgen de las Nieves in Granada, the Centro Nacional de Aceleradores in Sevilla, and the Istituto Nazionale di Fisica Nucleare in Pavia. Theoretical developments for dose calculation formalism as well as multiple *in vitro* experiments in different type of beams have helped to gather in this work a collection of data and ideas to expand what is known about neutron - cell interactions.

Outline

In **Chapter 1**, the explanation of BNCT and how it works will be included. Information about clinical trials, the type of beam that BNCT needs, and the characteristics of the boron compound will be provided. In addition, the current method for dosimetry calculation in therapy will be explained. The peculiarity of the study of neutron damage will be analyzed in detail, together with the radioprotection parameters and the results of neutron biological effects in previous experiments.

Chapters 2 and 3 will be dedicated to the theoretical development of dosimetry calculation. In **Chapter 2** a new formalism that is in between the current one, which is characterized by its simplicity, and the iso-effective one, that includes more realistic effects, will be presented and developed at hand of some examples. In **Chapter 3**, the effect of all these secondary particles created by the different neutron interactions with the elements of a tissue will be analyzed individually. By studying properties, such as the energy of these secondary particles, an estimation of the general biological effect of neutrons will be reached.

In Chapters 4 and 5, all the experiments related to obtaining biological effect data for *in vitro* samples will be presented. **Chapter 4** will include the explanation of all the experiments performed. Five different types of experiments will be presented with details of the facilities used, the characteristics of the beams used and the design of the irradiation experiments, customized for each type of result. In addition, the characteristics of cell cultures and the tests performed after irradiation will be described. In **Chapter 5**, all the results of the different experiments will be shown. With them, a series of conclusions will be reached to improve both the irradiation method used and the way to study and share the biological effect data among BNCT researchers.

Chapter 1

Boron Neutron Capture Therapy and dose calculation

In this chapter the treatment called Boron Neutron Capture Therapy (BNCT) will be described - how it works, what kind of tumors have been treated and the features of the neutron beams necessary to carry it out will be included. The currently accepted dose estimation for neutron irradiation of human tissue will be explained as well as the estimation of the biological damage caused. Finally, the data that have been gathered from previous experiments and the radioprotection magnitudes for neutron irradiation will be set out. All of this information is provided within the context of explaining the need for new radiobiological data and formalisms for improved BNCT applications.

1.1 BNCT

Boron Neutron Capture Therapy (BNCT) is an experimental form of radiotherapy that uses external irradiation with neutrons in conjunction with a selective tumor preload of the neutron capturing isotope ^{10}B. The idea is that prior to neutron irradiation, patients are injected with a ^{10}B compound and there is preferential uptake by the tumor cells. As neutrons ionize only indirectly, and since low energy neutrons do not induce ionizing recoils, only a nuclear reaction may induce damage in the tissue. ^{10}B has a high capture cross section for thermal (low-energy) neutrons (3837 barns), and a capture results in the emission of an alpha particle and a lithium ion. Both particles have low range (less than 10 μm) but high-energy deposition and LET (Linear Energy Transfer):

$$\ulcorner \rightarrow \quad {}^{4}\mathrm{He},\ 1.77\mathrm{MeV} + {}^{7}\mathrm{Li},\ 1.01\mathrm{MeV} \qquad (6\%)$$

$${}^{10}\mathrm{B} + n_{th}\ (0.025\mathrm{eV}) \rightarrow [{}^{11}\mathrm{B}]$$

$$\llcorner \rightarrow \quad {}^{4}\mathrm{He},\ 1.47\mathrm{MeV} + {}^{7}\mathrm{Li},\ 0.84\ \mathrm{MeV} \qquad (94\%)$$

$$\downarrow$$

$${}^{7}\mathrm{Li} + \gamma,\ 0.478\ \mathrm{MeV}$$

In consequence, high damage is produced over a very short (cellular) length scale. If sufficient ^{10}B can be accumulated inside the cancer cells, then this nuclear reaction can be used to destroy the cancer cells while leaving the healthy cells unaffected (see Figure 1.1). Clearly, the selectivity in the uptake and accumulation of the ^{10}B by the cancer cells is a crucial aspect of this therapy.

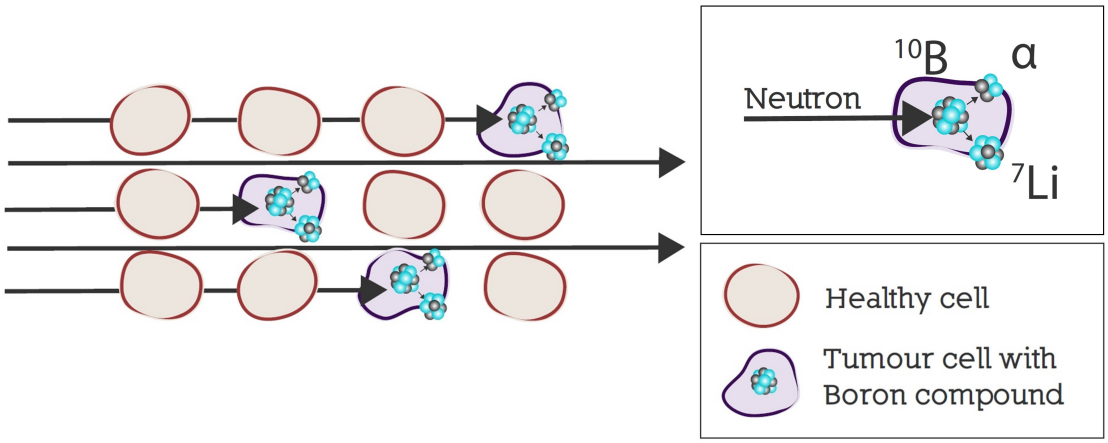

Figure 1.1: Schematic representation of the basics of BNCT. Tumor cells loaded with the boron compound will be destroyed following irradiation with thermal neutrons, while the healthy cells remain safe.

One of the advantages of this therapy is that it is usually performed by a single irradiation and thus completed in just one day. The infusion of the boron compound is realized between 45 minutes and few hours prior to irradiation [Joen03, Wang18]. The accumulation ratio between tumor tissue and healthy tissue (called T/N ratio) is checked by several techniques like Inductively coupled plasma atomic emission spectroscopy (ICP-AES) of a blood sample or Positron-emission tomography (PET) imaging of a patient if the boron compound is labeled by a positron emitter like ^{18}F. In the event that the tumor to normal-tissue boron concentration ratio, T/N, is more than 2.5, the patient is irradiated for the time required to reach the planned

dose (normally around 40 minutes). The patients then remain in the hospital for monitoring, but are usually back home in few days.

Conventional radiotherapy, using photons, is normally executed using fractions of few Grays (Gy=J/Kg), a few times per week, over months. The time in between radiotherapy sessions allows the healthy tissue to repair the sub-lethal damage and to repopulate cells. For BNCT, since cells in the healthy tissue are either unharmed or fully destroyed (due to residual boron uptake in healthy tissue), distributed therapy sessions may be less useful, although more clinical data are required before drawing a firm conclusion on this [Code95]. In addition, it seems that repeated boron infusion is not indicated because the absorption is reduced with each injection [Code93].

1.1.1 Clinical trials

The use of BNCT dates back a few years after the discovery of the neutron, in 1936 from Gordon L. Locher [Loch36]. The first BNCT clinical trials were carried out in the 1950's on brain tumors by W.H. Sweet [Swee51] using a thermal beam from a research reactor at Brookhaven National Laboratory (BNL) with different boron compounds [Farr54]. The insufficient selectivity of the compounds used limited the success of these trials, but they suppose the first implementation of a novelty technique, opening a new research field. Subsequently, H. Hatanaka started a BNCT program in Japan [Hata75], with sodium borocaptate ($Na_2B_{12}H_{11}SH$, called BSH), a new compound synthesized by A.H. Soloway and co-workers [Solo67]. The major limitation of these early clinical trials was the poor penetrability of thermal neutrons through the healthy tissues surrounding the tumor and surgical techniques were used to reach deeply located tumors. Years later, the group of Y. Mishima employed epithermal neutron beams from research reactors [IAEA01] and brought in a more selective compound: the boron phenylalanine (BPA) [Mish89]. The use of this epithermal beam allowed the delivery of neutrons to deeper regions of the body, where they thermalized and deployed their action while delivering less radiation dose to surface tissues.

Since then, clinical trials have been carried out of what can be called "modern BNCT" in Japan, USA, Finland, the Netherlands, Sweden, Argentina, Italy, the Czech Republic and Taiwan, generally for cancers for which there has been poor prognoses. Most of the protocols have been focused on brain tumors, such as glioblastoma multiforme (GBM) [Chad98, Saue02,

Dbal02, Joen03, Yama04, Yama11, Miya05, Miya13, Kawa09 Naka09, Kank11, Naka11, Aiya11], and recurrent head and neck cancers [Kato04, Kato09, Kank11b, Kank12, Wang11]. In addition to this, trials have been performed for malignant melanoma [Mene09], for the treatment of multiple metastases in the liver by extracorporeal irradiation [Zont09] and more recently for lung cancer [Suzu12]. A good review about BNCT in patients with gliomas or head and neck cancer was written by Rolf F. Barth in 2012 [Bart12], showing results such as those seen in Figure 1.2.

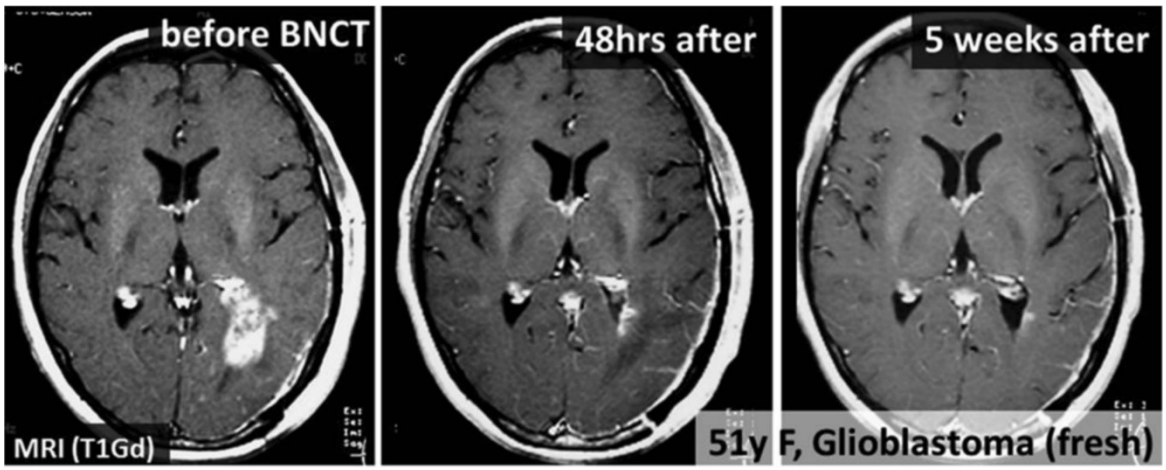

Figure 1.2: MRI images of the follow-up of a patient with glioblastoma treated with BNCT [Bart12].

Since BNCT is an experimental therapy, most of the patients included in the trials were in very bad condition and had received prior conventional therapies. Even if tumors are not totally eliminated, their size is most often reduced after BNCT. Most of the patients have lived longer compared to conventional treatments and often with a better quality of life because of the palliative effects after the reduction of the tumor size.

1.1.2 Boron Compounds

A key point for BNCT is the boron delivery agent, since it is crucial to an effective therapy. It should have enough boron to allow sufficient neutron capture to eliminate the cancer cells ($\geq$20µg ^{10}B/g tumor, approx.), but at the same time be non-toxic to the patient at this concentration [Bart05]. Moreover, it has to be always accumulated much more in tumor cells than in the healthy ones (desired ratio T/N > 2.5), so that the healthy tissues of the patient are not damaged excessively.

The two drugs approved for clinical use are the boron cluster sodium borocaptate (BSH) and the amino acid analogue boronophenylalanine (BPA), as shown in Figure 1.3. BSH was used in brain malignancies and is capable to reach the tumor cells in the brain. Although the mechanism by which this compound can go through the blood-brain barrier is still not clear [Saue12], it has shown good results for BNCT in patients with glioblastoma in the Netherlands and Japan [Saue02, Kage97]. However, the boron accumulations with BSH is frequently insufficient and so BPA is the most used drug in BNCT - mainly because of better uptake selectivity. Nonetheless, there are still some problems: the BPA accumulation is not always as good as it should be to perform the therapy and as a result, some patients cannot be treated; BPA only contains one atom of boron per molecule, and it is therefore necessary to administer high quantities in order to sufficiently load the tumor.

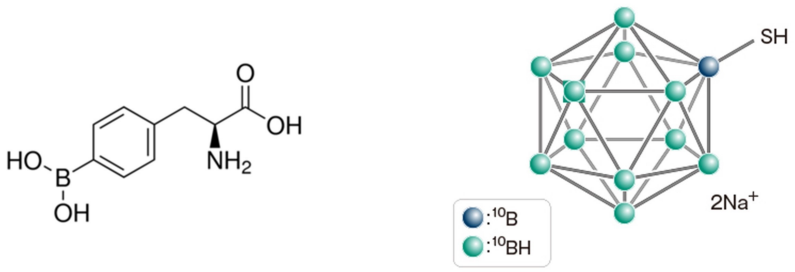

Figure 1.3: BPA (left) and BSH (right), the two boron drugs approved and used in clinical BNCT.

In order to find better compounds that can be approved for future BNCT applications, a lot of research effort is carried out all over the world. Some of the new candidates as future boron carriers developed in the last ten years are: amino acid derivates, nucleic acid derivates, porphyrins, carbohydrates, boron-containing polymers, boron peptides, boron antibodies, emulsions, boron-encapsulated liposomes, and boron-lipid liposomes. For more details on many of those compounds, the chapter about boron in the Neutron Capture Therapy book [Saue12] gives a good overview.

1.1.3 Neutron Beams

The neutron beam to be used in BNCT must fulfil several properties. The International Atomic Energy Agency (IAEA) has published these recommendations for a suitable neutron beam for BNCT. For deep-seated tumors, epithermal neutrons are optimal, *i.e.* neutrons with

energies between 1 eV to 10 keV. They will be thermalized inside the tissue and with thermal energy undergo capture by boron at the tumor. Furthermore, the flux of neutrons must be high in order to maximize the number of captures necessary to eliminate the tumor in a reasonable treatment time (epithermal neutron flux of more than 10^9 neutrons/cm^{2}s) [IAEA01]. Additionally, the dose from gamma rays or fast neutrons coming from the beam should be as low as possible, since they add undesired radiation. The gamma dose rate should be below 1Gy/h and the dose rate from fast neutrons should be below 0.5 Gy/h.

Until a few years ago, only research reactors, with suitable moderators, could reach these requirements. Reactors are big machines and expensive in operation if only a single application is served. In addition, most reactors are not well placed to treat patients; they are normally located far away from hospitals and this may make the transport and stay of patients difficult. This is one of the reasons why BNCT clinical research has not developed as much as might have been expected. BNCT delivery installations should ideally be modified for the neutron moderation in a way that is compatible for the treatment of patients. The places where clinical BNCT trials have been performed are illustrated on the map in Figure 1.4. Most of them are now closed. Only the reactors in Argentina, Taiwan and Japan are still used for patient treatments, and recently another has been built in China [Bava17].

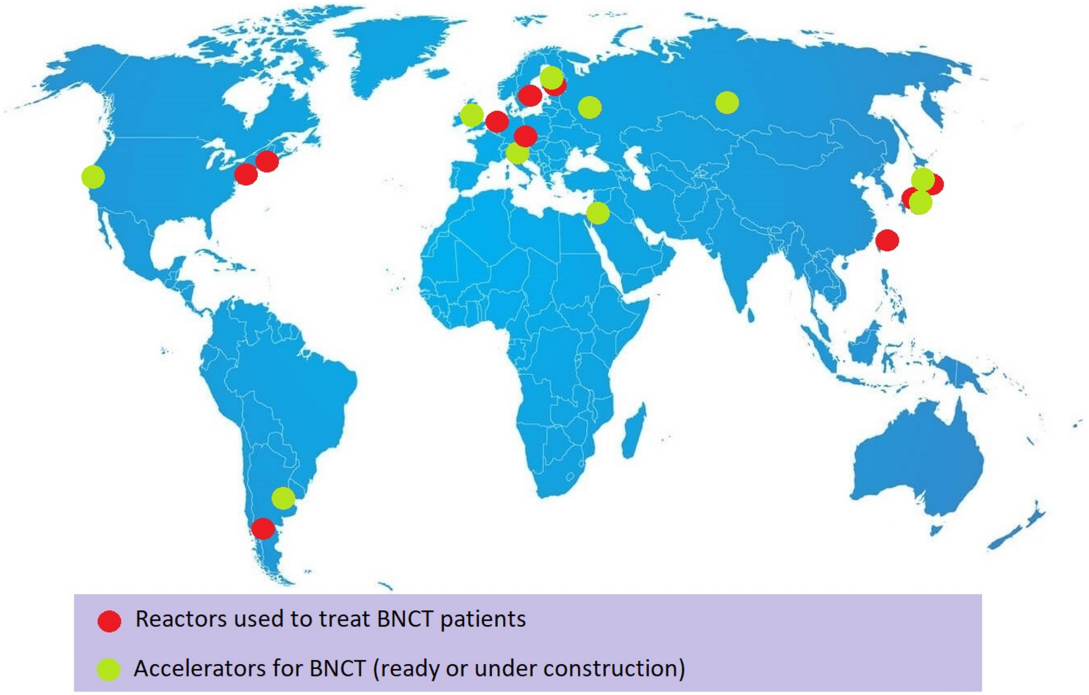

Figure 1.4: BNCT neutron beam sources throughout the world.

However, the advancements in the technology of high intensity compact particle accelerators have opened the way to in-hospital BNCT facilities, and this has allowed an increased number of trials. They are easily turned on and off and are considerably cheaper to construct and operate than a nuclear reactor. A diagram of the general structure of these accelerators is shown in Figure 1.5.

There are a numbers of reactions that will result in the desired neutron spectra [Krei16], for example, the endothermic $^{7}Li(p,n)^{7}Be$ reaction, where the neutrons produced have about 30 keV energy for incident protons of 1880 MeV. To reach sufficient neutron flux with such low-energy protons a high beam current is required [Kono06] and, consequently, high power density is deposited in the target material that has a low melting point (180°C). Therefore, a good cooling system for the target, a proper system to deal with the radioactive ^{7}Be produced and a moderation assembly (not very big if working near the threshold) are required. These are not easy accomplishments, but they may be feasible with the new technologies that are being developed.

Other reactions that can be used for the neutron production are $^{9}Be(p,n)^{9}B$, where the necessary energy to reach significant yield is higher, increasing the neutron energy correspondingly; and $^{9}Be(d,n)^{10}B$, which as exothermic reaction has no threshold, but the energy of the produced neutrons is significantly higher compared to the other reactions.

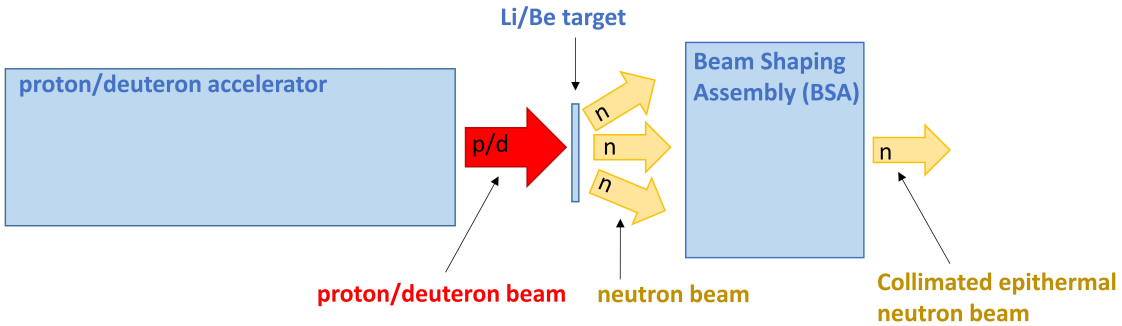

Figure 1.5: Diagram of the general structure of a BNCT neutron accelerator.

The way to reach the proton/deuteron characteristics for the reactions is by electrostatic accelerators like the 3MV Dynamitron in Birmingham [Gree12] or the Tandem-ElectroStatic-Quadrupole (TESQ) facility in Argentina [Krei14]. In addition, radiofrequency (RFQ)

machines like the LINAC in Israel [Half11] or cyclotrons like the 30 MeV proton cyclotron at Kyoto University have been proposed.

Worldwide effort is ongoing in building and trying these new accelerators in countries like Finland, Japan, Taiwan, Israel, Argentina, U.K., Italy or Russia. All of these facilities are aimed at accommodating BNCT patients in the future, increasing the clinical trials and expanding BNCT as an alternative therapy in hospitals.

In Table 1.1 a list is given of the accelerator-based neutron sources that are being developed. Of these, only the first, the C-BENS facility in Kyoto, based on an existing 30-MeV cyclotron, is already in operation and the first clinical trials have started.

1.1.4 Future of BNCT

Despite of the promise of BNCT therapy, there are a relatively small number of cases where the treatment has been used (in the order of just a thousand, including all clinical trials and compassionate use). BNCT therefore requires more experimentation (ideally randomized clinical trials) in order to develop towards a more widely used treatment option.

A strong limitation to the spread of clinical trials comes from the limited availability of suitable neutron sources. Up to now, only research reactors had been used for the clinical trials. However, as explained in the previous section, the new generation of accelerator based BNCT facilities will make trials possible at more places. Another limitation comes from the from the fact that boron carriers are relatively undeveloped; this is still a major hurdle and a topic on which many researchers are working.

A further problem, and the one that will be discussed in this thesis, is the determination of the biological dose – something that is essential for reliable treatment planning. The main problems will be explained in the following sections and the main goal of the present project is the reduction of uncertainties in the biological dose determination.

Despite the difficulties discussed, this special type of hadrontherapy (BNCT is officially a form of hadrontherapy since neutrons are hadrons) is still considered a promising therapy option [Moss14]. This field is a paradigm of interdisciplinary research, where physicists, engineers, biologists, chemists, pharmacologists and of course medical scientists (oncologists,

surgeons and other specialists) work in close connection on a problem which has many different interacting facets.

Institute	Type	Volt, current	Reaction	Max n Energy	Ref
KURRI, Kyoto Univ., Japan (clinical trials)	Cyclotron	30MeV, 1 mA	^{9}Be(p,n)	28 MeV	[Tana11]
South Tohoku Hospital, Fukushima, Japan	Cyclotron	30 MeV, 2 mA	^{9}Be(p,n)	28 MeV	[Tana11]
Helsinki Univ. CH, Finland	Electrostatic (Hyperion)	2.6 MeV, 30 mA	^{7}Li(p,n)	0.89 MeV	I.Auterinen Priv.com.
Budker Institute, Novosibirsk, Russia	Vacuum insulated Tandem	2 MeV, 2 mA	^{7}Li(p,n)	0.23 MeV	[Aley11]
IPPE Obninsk, Russia	Cascade generator KG-2.5	2.3 MeV, 3 mA	^{7}Li(p,n)	0.57 MeV	[Kono04]
Birmingham Univ., UK	Electrostatic (Dynamitron)	2.8 MeV, 1 mA	^{7}Li(p,n)	1.1 MeV	[Gree12]
Tsukuba Univ., Japan	RFQ-DTL	8 MeV, 10 mA	^{9}Be(p,n)	6.1 MeV	[Kuma14]
CNEA Buenos Aires, Argentina	Tandem Electrostatic Quadrupole	1.4 MeV, 30 mA 2.5 MeV, 30 mA	^{9}Be(d,n) ^{7}Li(p,n)	5.7 MeV 0.79 MeV	[Krei14]
INFN Legnaro, Italia	RFQ	5 MeV, 50 mA	^{9}Be(p,n)	3.1 MeV	[Ceba11]
SOREQ, Israel	RFQ-DTL	4 MeV, 2 mA	^{7}Li(p,n)	2.3 MeV	[Half11]
LBNL, USA	DC Electrostatic Quadrupole	2.5 MeV, 50 mA	^{7}Li(p,n)	0.79 MeV	[Kwan95]
NCC, Japan	RFQ	2.5 MeV, 20 mA	^{7}Li(p,n)	0.79 MeV	[CICSweb]
Nagoya Univ., Japan	Electrostatic (Dynamitron)	2.8 MeV, 15 mA	^{7}Li(p,n)	1.1 MeV	[Kiya12]

Table 1.1: Accelerator-based BNCT facilities worldwide.

1.2 BNCT dose estimation

As neutrons irradiate indirectly, the damage caused after neutron irradiation comes from the secondary particles emitted by the recoils or nuclear reactions that occur inside the tissue. This will deliver a dose having a biological effectiveness that depends on the linear energy transfer (LET). It is clear that the capture on boron will release a lot of damage in the tumors, but there are other possible reactions with the other elements in the tissue that may add an undesired dose to healthy tissues. Hence the BNCT dose is the result of a complex mixed field of high and low-LET radiations that depends on the characteristic of the beam as well as the geometry and composition of the tissue being treated.

In BNCT treatment planning, and due to the potential differences in the biological effectiveness, the dose delivered by the neutron field is decomposed into four primary components (illustrated in Figure 1.6):

• $\boldsymbol{D_t}$: thermal neutron component, the dose delivered by neutrons below 0.5 eV, excluding the damage resulting from neutron capture on boron and from the gammas produced in neutron captures. The main reaction which corresponds to this component is the neutron capture reaction by nitrogen, $^{14}N(n,p)^{14}C$. Scattering occurring at these energies with hydrogen will not produce any dose since the resulting proton energy is below the ionization threshold.

• $\boldsymbol{D_f}$: Called “fast neutron dose”, it corresponds to the dose delivered by neutrons of more than 0.5 eV (maximum value depending on the beam characteristics, but it used to be in the order of MeV). Fast neutron dose is mostly due to neutron elastic collision with hydrogen. Other reactions with ^{12}C and ^{16}O (and other elements depending on the tissue [ICRU46]) normally give less than 10% of the dose.

• $\boldsymbol{D_\gamma}$: The gamma dose appears each time that a neutron is captured (mainly by hydrogen) producing prompt gammas of 2.24MeV. The gamma dose will be more important when the size of the sample is bigger, *i.e.* less of the produced photons escape before depositing energy, and when the neutrons are thermalized. Photons coming from the beam are also taking into account in this dose component. For capture on hydrogen, the recoil deuteron (1.3 keV kinetic energy) will leave some dose too, added to the thermal dose component, but much less compared to the recoil proton after capture on nitrogen.

• $\boldsymbol{D_B}$: Each thermal neutron captured by boron will add dose to this component, which will depend on the amount of boron accumulated in the tissue. It is the highest dose component at the tumor. The 478 keV photons released in the 94% of the captures in boron is included in the gamma dose component.

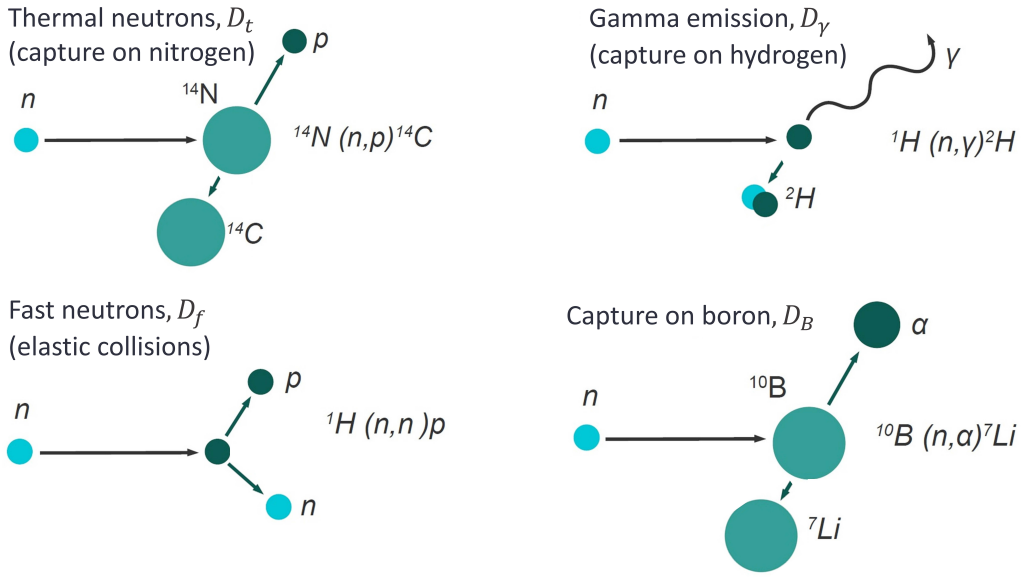

Figure 1.6: The four absorbed dose components that contribute to the radiation dose delivered by BNCT neutron irradiation and the main reactions that cause them.

The total radiation dose will be the sum of all the absorbed dose components. This is known as physical dose or total absorbed dose:

$$D = Df + Dt + D\gamma + D_B \ . \tag{1.1}$$

For the estimation of each term, the absorbed dose is difficult to measure directly. That is why Monte Carlo simulations are used, using the measured neutron flux, to simulate the neutron transport and calculate approximately the absorbed dose. This aspect will be described in more detail in Chapter 3.

1.3 Biological dose in BNCT

1.3.1 Current formalism

In order to introduce the biological effects of BNCT dosage, each dose component previously mentioned is weighted by a weighting factor, w_i, also called Relative Biological Effectiveness (RBE) factors, which include the information about the different biological effects of each dose component. Then, the weighted dose, D_W, is compared to a reference dose, D_0, which is the photon dose required to produce the same final effect as the BNCT treatment.

$$D_W = w_f D_f + w_t D_t + w_\gamma D_\gamma + w_B D_B = D_0. \tag{1.2}$$

The weighting factors (RBE factors), w_i, are defined as the ratio of the reference photon dose, D_0, and the value of the dose component needed to produce the same effect, D_i:

$$w_i = \frac{D_0}{D_i}, \qquad i = t, f, \gamma, B. \tag{1.3}$$

The value of these factors comes from irradiation experiments on *in vivo* and *in vitro* samples. After the irradiation, survival studies are carried out. The results are curves that show survival as a function of increased absorbed dose. The survival will depend on the effect studied, also called the end-point, that can be, for example, the clonogenic ability for *in vitro* samples. w_i factors will then depend on the irradiation type, the reference irradiation chosen, the survival at which the dose ratio is calculated, the tissue irradiated and the end-point studied. The boron weighting factor, w_B, will also depend on the compound used and their biodistribution inside the tissue; this is why it is also called the CBE (compound biological effectiveness) factor [Code99].

1.3.2 *w* factors used in BNCT clinical trials

Since this formalism of dose estimation was initiated by the BNCT community, the RBE factors most used were those proposed by Coderre *et al*. [Code93]. These factors come from BNCT irradiation experiments in rat gliosarcoma, both *in vitro* and *in vivo*. The samples were irradiated in the Brookhaven Medical Research Reactor (BMRR), with estimated dose components for the irradiations of 49% D_f, 34 % D_g, 17% D_t for samples without boron and

17% D_f, 12 % D_g, 6% D_t, 65% D_B for samples with boron compound. Irradiations with 250 kVp X-rays were carried out to obtain the survival curve for the reference photon dose. After comparing the reference data and the data from beam alone irradiations and irradiations with boron compound BPA in samples, they obtained RBE values of between 2.8 and 3.8 for the neutron beam alone, and 3.6 – 9.8 for the samples with BPA (more details in Table 1.3). For reasons that are not clear, the data for the *in vivo* samples at 10% survival, shown in the Table 1.2, were taken as the *w* factors for most of the BNCT treatments applied to patients.

BNCT Dose component	**Weighting factor, w_i (or RBE factor)**
Beam (D_t and D_f)	3.2
Boron capture (with BPA-fructose)	3.8 (tumor), 1.3 (healthy tissue)
Gamma	1

Table 1.2: RBE (relative biological effectiveness) factors for BNCT obtained in the BMRR reactor [Code93].

These factors were applied in most of the cases, independently of the type of cancer or the beam used.

1.3.3 w_t and w_f, previous experiments

There are more experiments apart from the Coderre *et al.* ones, cited in the previous section, and all of them show that RBE factors change a lot depending on the tissue or the beam used for the irradiation.

Of course, the CBE factor will change between experiments since it depends on the boron compound used and its microdistribution in the tissue. Nevertheless, we are going to focus our attention on the previous results of thermal and fast neutron RBE factors, w_t and w_f, showing that even when there is no boron involved, the effect of the neutron irradiation is not easy to quantify.

Currently, in BNCT, the biological effects of thermal and fast neutrons are weighted with the same factor (3.2 from Table 1.2) since it is difficult to separate them. However, there are experiments where experts have tried to study separately the RBE values for the different secondary particles of neutrons of different energies. For that, different neutron sources and

tissues were used. All these experiments follow the definition of RBE as the ratio between a reference photon dose, D_0, and the dose of the neutrons. A summary of these experiments, performed with the objective of improve the BNCT application, is presented in Table 1.3.

There appear to be some inconsistencies in parts of the data that do not correspond to the data given by the survival graphs shown in the respective article. These cases are marked with an asterisk (*) in the table and the values that we extracted from the graphs are given in the caption.

The results in Hall's [Hall75] experiments do not match the studies with mono-energetic proton sources with the same energies as protons from neutron capture on nitrogen [Perr86, Bell89], where RBE in v79 cells appears to be much lower than those obtained from epithermal neutron irradiations. Therefore, no conclusion can be drawn if it can be comparable to the effect of the recoil protons from neutron irradiation.

Mason's experiments obtained much higher values than the others [Maso11], reaching the conclusion that there must be a synergistic interaction between the different dose components.

There are no studies with thermal neutrons only, except for that of Gabel *et al*. [Gabe84] who irradiated cells at Institut Laue-Langevin, but the flux was so low that the data obtained correspond only to high survival fractions.

1.3.4 Problems of the current formalism and *w* factors

Despite the different data shown in Table 1.3, constant factors for all the tissues and irradiations are used in the actual application of the therapy. The reason for this arises from the lack of a proper database that includes all the data for cells, animals and patients that have undergone BNCT irradiations. Furthermore, the simplicity of the formalism has led to a simple use of the RBE factors.

The difficulty of separating the biological effects of the protons from hydrogen recoils and the protons from neutron capture on nitrogen has led to a situation where w_t and w_f are taken to be similar. Hence they were assumed to be the same, called "proton dose" and weighted with the RBE factor of 3.2 shown in the Section 1.3.2 [Code93, Code99]. Nevertheless, protons from capture on nitrogen have different LET than those coming from the scattering of hydrogen (see Table 1.4), and they should therefore have distinguishable biological effects.

Theoretically, the value for the w_t should be the same for each facility (for same tissue and end-point), since the spectra will always include thermal neutrons in the beam. According to the different experiments, for thermal neutron beams, where most of the effect came from the capture on nitrogen, the RBE data shows values from 1.4 to 3.8. However, the w_f parameters may vary between facilities, depending on the maximum energy of their neutron spectra.

The photon weighting factor, w_γ has been taken systematically as one, since it represents the reference radiation type for comparison. However, there has been some discussion on the use of a dose reduction factor [Hope11] because of the different photon dose rate in a BNCT treatment in comparison with that in a conventional radiation study (the former is significantly smaller).

Finally, the boron CBE factor, w_B, in BMRR was calculated for reactor based BNCT evaluating the total beam biological effect for the assumed values of w_f and w_t. Here the weighting factor of the boron dose is obtained as a difference [Code99]. In this way, any deficiency in the formalism or of the other coefficients themselves can be compensated. These factors can be applied reliably to other beams for which the different dose terms are similar to the conditions in which this CBE factor was obtained. However, this may be not the case for very different neutron beams as in the case of the newly-proposed accelerator-based neutron sources [Krei16]. Moreover, ideally the biodistribution profile of the boron compound has to be characterized for each patient.

In addition, low-LET and high-LET secondary particles can interact at the same time giving a higher effect in the tissue. That is why synergies between the different types of irradiation are expected and should be included in the future formalisms [Phoe09].

For all these reasons, a revision of the current framework for the determination of the biological dose is appropriate. The BNCT community, by means of the working groups formed under the auspices of the IAEA and the International Society for Neutron Capture Therapy (ISNCT), is elaborating a new TECDOC for the future practice of BNCT. This includes a revision of the radiobiology of BNCT. The present thesis aims to shed some light on this problem.

Neutron Beam	Tissue	End-point	Survival	RBE factor	Reference
Thermal (BMRR)	Rat skin	Moist desquamation	50%	3.5	[Morr94]
Thermal	Rabbit skin	Moist desquamation	-	2.7	[Yama61]
Thermal	Pig skin	Moist reaction	50%	2.7	[Arch71]
Thermal (BMRR)	Rat spinal cord	myeloparesis	50%	1.4	[Morr94b]
Thermal (ILL) (capture on nitrogen)	V79 cells (hamster)	Clonogenic assay	37%	1.9*[1]	[Gabe84]
Thermal beam (KUR reactor)	B-16 cells Hela Fibroblast	Clonogenic assay	-	2.55 1.33-2.2 2.0	[Fuku89]
Thermal beam (BMRR) (capture on nitrogen + scattering – X-rays)	Rat gliosarcoma *in vitro* *in vivo*	Clonogenic assay Clonogenic assay	10% 1% 0.1% 10% 1% 0.1%	3.7 3.7 3.8 2.8 3.2 3.5	[Code93]
Mix Beam (Studsvik reactor) (High-LET RBE – X-rays)	V79 cells (hamster)	Clonogenic assay	37%	14.5	[Maso11]
Mix Beam (Birmingam accelerator) (High-LET RBE – X-rays)	V79 cells (hamster)	Clonogenic assay	37%	7.1	[Maso11]
Epithermal	Dog brain	MR lesion (Magnetic resonance)	-	3.3-4.4	[Gavi97]
Epithermal	Dog skin	-	-	3.0	[Gavi94]
Epithermal (PLUTO) (24KeV)	V79 cells (hamster)	Clonogenic assay	37%	3.1*[2]	[Morg88]
Epithermal (PLUTO) (24KeV)	Hela cells	Clonogenic assay	37%	5.8*[3]	[Morg88]
Epithermal (RARAF) 0.08 MeV 0.22 MeV 0.34 MeV 0.66 MeV 1 MeV	V79 cells (hamster)	Clonogenic assay	37%	 4.1 6 6.7 5.5 5	[Hall75]

Table 1.3: Summary of the experiments for thermal and epithermal RBE factors, w_t and w_f, for BNCT radiobiological proposes. *[1] A value of 7.5 was deduced from the published graphs. *[2] A value of 4.1 was deduced from the published graphs. *[3] A value of 6.3 was deduced from the published graphs.

Neutron Energy	Particle	Secondary particle maximum energy	Average LET in water
~10 keV	Proton recoil ($^{1}H(n,n)^{1}H$)	10 keV	28 keV/µm
~10 keV	^{12}C recoil ion ($^{12}C(n,n)^{12}C$)	3 keV	770 keV/µm
~10 keV	^{14}N recoil ion ($^{14}N(n,n)^{14}N$)	3 keV	1034 keV/µm
~10 keV	^{16}O recoil ion ($^{16}O(n,n)^{16}O$)	2 keV	1330 keV/µm
< 0.5 eV	Proton ($^{14}N(n,p)^{14}C$)	584 keV	53 keV/µm
< 0.5 eV	^{14}C recoil ion ($^{14}N(n,p)^{14}C$)	42 keV	692 keV/µm

Table 1.4: Average Linear energy transfer (LET) in water of the secondary particles created in the main processes that take place in neutron irradiation.

1.4 Neutrons in radioprotection

1.4.1 Radioprotection concepts

The method used in BNCT of employing a weighting factor to weight a dose depending on the incoming radiation comes from the radiological concept of RBE. RBE is by definition the ratio of the absorbed doses of two types of radiation producing the same specified biological effect in the same conditions [ICRP97]. The values depend on many conditions as the tissue/cell type irradiated, the end-point chosen (the final biological effect investigated), the dose and dose rate, the fractionation scheme, and the reference dose. Therefore, the RBE for each type of irradiation with a certain energy is going to be a range of values. Since the RBE concept would be laborious to apply for general radiological protection, experts decided to use a simpler concept that gives a representative value of the known data called radiation weighting factors, w_R. They are defined as the maximum values of RBE, so they do not depend on the dose and dose rate [ICRP103]. Radiation weighting factors are the ones that are going to be used for dose limitation, assessment and controlling. The ICRP commission emphasizes that for individual risks and more specific applications, the RBE values are the ones that need to be used as well as the specific biological data available. Following the latest advice, the weighting factors used for BNCT dose components are, effectively, the relative biological effectiveness factors, and these do indeed depend on the doses. It is important to point out that even if this RBE factors are called “weighting factors” they must not be confused with the radioprotection concept of a radiation weighting factor.

The objective of this section is to point out that even in radioprotection, where a simpler concept is used independently of the dose, the w_R factors, for evaluating the effect, there are still some problems in describing and taking into account the effect of the neutrons on human tissues.

1.4.2 Radiation weighting factors, w_R, for other particles

Low-LET (less than 10 keV/μm) radiations like photons, electrons and muons are considered, by ICRP Publication 60 [ICRP60], to have a $w_R = 1$. However, the effect of all those particles is not exactly the same (photons of few MeV are less effective than X-rays or Auger electrons that can damage strongly a tissue) and due to all the uncertainties in the estimation, a single value was chosen for practical reasons.

Protons and pions are considered to have a single value of w_R for all the energies. This value is characteristic for protons of high energies since they are the most abundant particles in cosmic radiation. The value selected following the experimentation results was $w_R = 2$.

Alpha particle exposure normally arises from internal emitters. *In vitro* studies evidence strong damage that give RBE values between 10 and 20, depending on the tissue. That is why the final w_R recommended is 20. Heavy ions and fission fragments are considered to have the same w_R as the alpha particles.

In summary, even when the effect of the particles can reach different RBE values, the commission has decided that it is enough safe to choose single values of w_R for general radioprotection purposes. This will not be the case for neutrons.

1.4.3 Radiation weighting factors, w_R, for neutrons

The biological effectiveness of neutrons is estimated according to the secondary particles emitted. In addition, the neutron field will be moderated inside the body, so the dose is induced by the primary neutrons but also by the scattered and moderated ones. The RBE will arise from:

- photons created due to the hydrogen capture where the cross section increases with decreasing neutron energy. It must be taken into account that in humans there are more secondary photons emitted than in smaller animals, since more of the neutrons will be absorbed and less will escape;

• recoil protons from scattering with hydrogen and nitrogen captures;

• heavier charged particles at higher energies; and spallation products at very high energies.

In the ICRP Publication 60 [ICRP60], two different ways of describing the neutron w_R were proposed (See Figure 1.7). The first one is a step function based on the limited available experimental data. A second one, a continuous function based on computational considerations, was chosen for practical reasons, as it is easier to use in real applications. In both of them, a value of about 20 is described for 1 MeV neutrons, as resulting from animal irradiations at reactors [ICRP60].

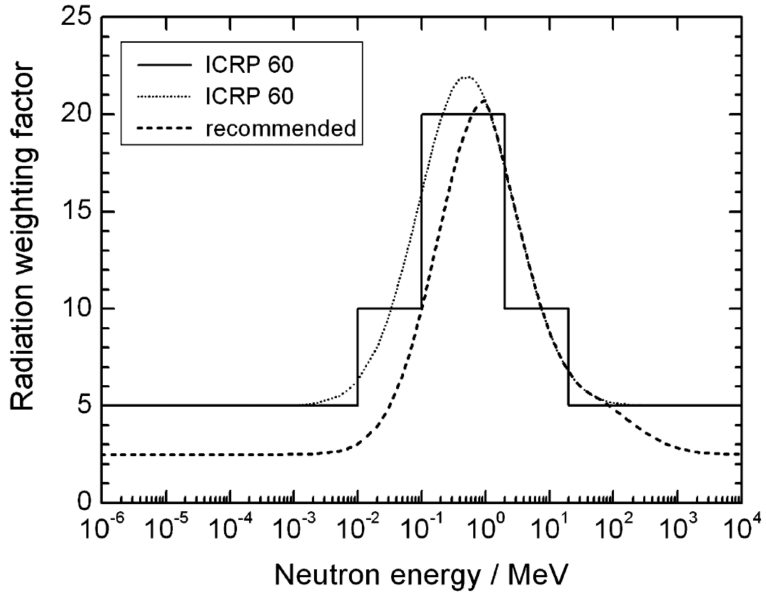

Figure 1.7: ICRP estimation of the radiation weighting factor, w_R, for neutrons. The recommendation corresponds to the last values based on the simulations of 2007.

For energies under 1 MeV, the production of protons is less energetic and the photons from the radiative capture on hydrogen acquire more importance. For this reason, the RBE will decrease. Based on the few experiments with neutrons energies of more than 24 keV [Edwa97], a constant value is fixed for the w_R of neutrons with less than 10 keV.

For neutrons of more than 1 MeV, the few data existing show a decrease of RBE. For very high energies (above 50 MeV) the value is approximately that for protons of similar energy (for which more radiobiological data exist).

After the ICRP Publication 60 [ICRP60], simulations in anthropomorphic phantoms showed data that suggested lower w_R values in neutrons below 1 MeV. This is why the recommended values of w_R are smaller, although they lack supporting experimental data.

1.5 The necessity of new formalism for biological dose estimation and new neutron radiobiological data

A relative lack of data on neutron irradiation of human tissue makes it very difficult to define ideal values for w_R in radioprotection or weighting factors in BNCT. A solution involving the use of approximations is almost inevitable, but as more data is obtained, it is necessary to modify the existing formalism, the description and the weighting factors used.

For radioprotection, more data is necessary for very high energy neutrons (more than 50 MeV) for applications in high altitude or space radiation. Current projects are trying to figure address this problem [Otto15]. Moreover, there also seems to be a lack of data for low-energy neutrons; some assumptions have been made, like the constant w_R value below 10 keV, but without experimental data that really endorse it. In Chapter 3 it will be shown that following a simple theoretical approximation, results do not match this assumption.

In BNCT, constant values of RBE factors are used for all the neutron energy spectra applied in therapy (implying that $w_t = w_f$), however this assumption is not supported by experimental results. In addition, RBE factors, defined as dose and tissue dependent, are adopted as constant for most treatments in all tumors. This practice, in addition to being inconsistent with the definition of RBE factors itself, is not recommended since the biological effect varies depending on the tissue.

A very simple formalism (not very accurate since it equalizes the biological effect, D_W, with a physical dose, D_0) is used in BNCT to estimate the dose to apply in patients. A more realistic view of the step from physical dose to biological dose would help to better predict the damage caused by the BNCT.

More data will help to face all these problems and to improve the precision of treatment planning in BNCT. The big difficulty in obtaining these data is always the mixed field of

neutron dose deposition, but this difficulty has been overcome with the series of experiments that will be described in Chapters 4 and 5, in which different beams has been used to study the effect of the different BNCT dose components separately.

Chapter 2

A radiobiological model for BNCT

The aim of this chapter is to propose a formalism with the use of newly defined weighting factors which are dose-independent. Being a first approximation to other formalism presented in 2012, the iso-effective formalism, this new model will solve some of the problems of the current one, while keeping a simple application structure. It will allow also to compare to conventional fractionated radiotherapy. Before introducing the model, an analysis in depth of the problems of the current weighting factors will be shown as well as some radiobiological concepts needed to introduce the new formalism. Examples of application of the method using data from BNCT clinical trials and the relationship between the current model and the one presented will be displayed.

From now on, different formalisms are going to be mentioned several times. In order to help the reader to follow the notation, the formalisms are going to be referred as:

- Formalism explained in Section 1.3.1 / current formalism / fixed-factor method / weighted dose formalism / formalism that uses w_i. The biological effect will be given by means of the weighted dose or equivalent dose, expressed in $Gy - Eq$ or Gy (RBE), normally denoted by D_w and which will be equal to the reference dose, D_0.

- Formalism explained in Section 2.3 / presented formalism / iso-effective dose method / formalism that uses new weighted factors, w_i^*, and Linear Quadratic model (LQ model) [Pedr20b]. In this case, biological effect will be given by the iso-effective dose in Gy or $Gy(Iso)$, normally denoted by D_0.

• Formalism explained in Section 2.4.1/ Iso-effective formalism / Gonzalez and Santa-Cruz formalism [Gonz12]. It is based in the same concept of iso-effective dose as the presented formalism, but in this case more factors like synergies and repair mechanisms are taken into account. The iso-effective dose in this formalism is expressed in $Gy(Iso)$.

2.1 The dose-dependent problem of the current *w* factors

As it was explained in the previous chapter, in spite of its usefulness demonstrated in the certain clinical trials performed so far by means of research reactors, there are some drawbacks in the current procedure that can be improved. These improvements are very important for the new era of accelerator based BNCT.

One of the handicaps in current BNCT is that the weighting factors (or RBE factors) used for estimating the biological damage (described in Section 1.3.1) depend on:

• Dose and survival: by definition, they are a dose ratio, so they depend on the absorbed dose or on the survival fraction chosen to estimate the dose ratio.

• Tissue and end-point: Different tissues respond differently depending on the radiation type. In addition, different weighting factors must be associated to different biological end-points (effect under study).

• Facility and depth: the neutron spectrum influences the biological effect since the nuclear reactions are different depending on the neutron energy. Also, the beam properties will vary inside the patient depending on the depth.

• Boron compound: there is a dependence on the boron drug used. For the same boron uptake from different compounds, differences in the biological response to the same neutron field have been observed, which has been addressed to differences in the biodistribution within the tissue. Microdistribution in the cell may influence too [Sato18], since alpha particles after boron capture have a range of 5-9 μm, lower than the cell size (>10 μm), so capture in boron accumulated in the nucleus will have stronger effect than if it is accumulated in the membrane.

Notwithstanding, constant w_i are used in BNCT as it was shown in Section 1.3.2, with the only difference between compounds taken into account.

The weighting factors strong dependence on the absorbed dose could lead to some confusions when they are used as constants. Usually different values are reported for different survival fractions of the experiment under which they were measured. The values for doses different to the one of the level of survival chosen would be extrapolated assuming linear dependence of the biological effect on the dose. Although this linear dependence can be approximately assumed for the dose terms D_f, D_t and D_B, because the dose is delivered by heavy charged particles, this is not the case for D_γ and for the reference photon dose D_0.

If, for **example**, in figure 2.1, w_i is obtained as the dose ratio at the survival corresponding to points 1 and 2: $w_i = D_{i1}/D_{02}$, then, to estimate the reference dose corresponding to a particle dose at point 3, D_{i3}, one applies the calculated weighting factor as: $D_0 = w_i D_{i3}$, which gives us the dose in point 4. This, however, does not correspond to the real reference dose, that should be D_{05}. In this example case, the reference photon dose obtained was lower than the real reference photon dose, so the planning dose can be underestimated. The opposite case is also possible, the reference dose can be overestimated and the patient is not receiving enough dose to destroy the tumor. It is a simple way to show the strong effect in which survival is selected to define the "constant" w_i , which should not be a constant. Some other graphical examples of this aspect can be found in the work of González and Santa Cruz [Gonz12].

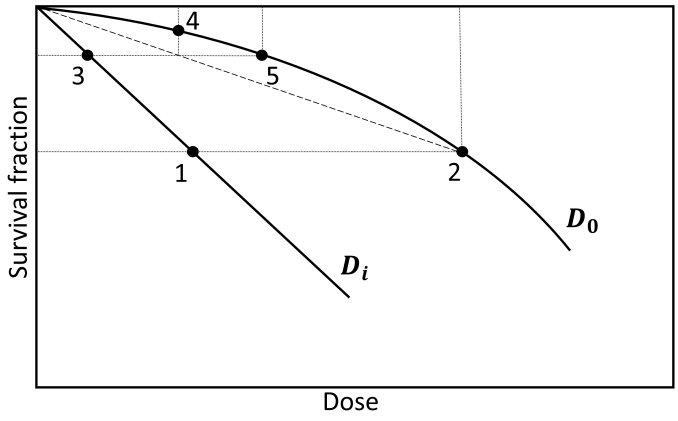

Figure 2.1: Simplification of two survival curves corresponding to two irradiations. The reference one with photon irradiation (curved line, D_0) and the irradiation to study with heavy charged particles (straight line, D_i). If the fixed w_i factor is calculated by the dose ratio in points 1 and 2, for an irradiation with dose in point 3, the estimated equivalent dose will be the one at point 4, while the correct one should be the one in point 5.

Two improvements regarding the dependence problems will be presented in this thesis: in this chapter, a simple model that eliminates some of the dependences and gives a more physically accurate dose estimation; and in Chapter 4 and 5, new measurements providing data for different tissues and beams, so, independently of the formalism used, more RBE for different applications.

2.2 Radiobiology concepts and iso-effect

In current photon radiotherapy, the biological effect is well known and well described by the linear quadratic model (LQ), used in clinical treatments. The biological effect, E comes from the survival fraction, S, of the cells after the irradiation (obtained normally by clonogenic assays), and the common way to describe it, is by the LQ model which is described as [Fowl90]:

$$E \equiv -\ln S = \alpha D + \beta D^2 , \tag{2.1}$$

where D is the absorbed dose, and α and β are constants which depend on the tissue/cell line. Normally, what is known is the ratio α/β, which tipically has a high value for tumors and for the early reaction in healthy tissue, while it has lower values for later response in healthy tissues (See Table 2.1).

Tissue	End-point	α/β (Gy)
Skin	Erythema	8.8
Skin	Subcutaneous fibrosis	1.9
Oral mucosa	Mucositis	9.3
Larynx	Supraglottic larynx	3.8
Lung	Fibrosis	3.1

Tumor	α/β (Gy)
Skin	8.5
Melanoma	0.6
Oral cavity	> 6.5
Larynx	14.5
Lung	~ 50-90

Table 2.1: Values of the parameter α/β for different tissues and end-points and for different tumor types [Ciud03].

On first sight, it may seem a simple model, but it is capable to fit the survival curves that

describe photon irradiation. It allows to include some biological interpretations and it can also be adapted to describe the fractionated treatment. The lineal term is referred to the non-reparable lesions while the quadratic one is related to the cellular death coming from the accumulation of sublethal damage that can be repaired.

As the effect of high LET particles is mostly non-reparable damage, an approximation can be made by describing it with just the linear term, while for photons it is necessary to introduce the possibility of repair. With this idea, the treatment with photons started being applied fractionally, so the final dose applied in the tumor after all the sessions can be higher by irradiating with smaller doses allowing repair of normal tissues between sessions. Therefore, for n sessions, the effect will adopt the form:

$$E = \alpha n d_n + \beta n d_n^2, \tag{2.2}$$

where d_n is the dose in each session, reaching a total dose of $D = \sum_n d_n$.

To describe two different treatments that have the same biological effect in the patients the concept of iso-effect is used. In order to estimate the iso-effect relations of a fractionated treatment with a single photon irradiation, Fowler [Fowl89] introduced the concept of biological effective dose (BED), which is the effect, E, divided by the coefficient α:

$$BED = n d_n \left(1 + \frac{d_n}{\alpha/\beta}\right). \tag{2.3}$$

BED will hence give the dose delivered to the tissue or tumor to obtain the desired iso-effect in infinitely small fractions.

As an **example**, the one single photon irradiation treatment equivalent to a fractionated one of 30 sessions of d_n=2 Gy can be estimated. For a tumor that has a $\alpha/\beta = 10$:

$$BED_1\ (single\ irradiation, dose\ unkown) = BED_2\ (30\ sessions\ of\ 2\ Gy),$$

$$1x\ d\ \left(1 + \frac{d}{10}\right) = 2x30\ \left(1 + \frac{2}{10}\right). \tag{2.4}$$

Resulting in a comparable single fraction of d=22.3 Gy. The dose given by the fractionated treatment is in total 60 Gy, much higher and because of that, more capable to eliminate the tumor and allowing the healthy tissue to be repaired between sessions.

2.3 New formalism proposed

This new formalism for BNCT biological dose description will incorporate two main differences with the current one, explained in Section 1.3.1:

- First, it will include a better description of the biological effect by using the LQ model explained in the previous section. This is especially important in the case of the gamma component for the BNCT irradiation, D_γ, and in the case of the reference photon dose, D_0, since the quadratic term has high impact in the photons effect. This description will avoid the problem of the incorrect comparison of a weighted dose, D_w, which expresses a weighted dose, with a reference dose, D_0, which represents absorbed dose.

- Second, absorbed dose components will be weighted with weighting factors that do not depend on the dose ratio. Thanks to that, problems shown in Section (2.1) are eluded.

Both of these improvements compare with the previous formalism will result in a more accurate formalism for the estimation of the BNCT effect, but keeping an expression quite similar to the one used before and also with the possibility of using old irradiation data. This is important since this formalism will make it easy for treatment planning programs and physicians to adapt, as well as give the possibility of using previous radiobiological data.

To start the formalism description, the LQ model is applied to the different absorbed dose components in BNCT. Therefore, assuming that the biological effect E for each dose component is described by the LQ model, a BNCT treatment provides an effect of:

$$E = \alpha_t D_t + \beta_t D_t^2 + \alpha_f D_f + \beta_f D_f^2 + \alpha_\gamma D_\gamma + \beta_\gamma D_\gamma^2 + \alpha_B D_B + \beta_B D_B^2 \,. \tag{2.5}$$

A reference photon irradiation of dose, D_0, as explained in the previous section, will follow the equation:

$$E = \alpha_0 D_0 + \beta_0 D_0^2 \,. \tag{2.6}$$

In a particular tissue, if both radiations are compared and they have the same effect, they can be equalized:

$$\begin{aligned} &\alpha_t D_t + \beta_t D_t^2 + \alpha_f D_f + \beta_f D_f^2 + \alpha_\gamma D_\gamma + \beta_\gamma D_\gamma^2 + \alpha_B D_B + \beta_B D_B^2 \\ &\quad = \alpha_0 D_0 + \beta_0 D_0^2 \,. \end{aligned} \tag{2.7}$$

Then D_0 denotes the photon iso-effective dose, defined as the photon dose required from a conventional treatment to produce the same biological effect as the BNCT. Here is already visible one of the big differences between both formalisms: while the one given by Eq. (1.2) compares an effect, D_w, with a dose, D_0, in the introduced formalism the biological effects are compared (Eq.(2.7)).

Dividing both components by α_0:

$$\frac{\alpha_t}{\alpha_0}\left(D_t+\frac{D_t^2}{\alpha_t/\beta_t}\right)+\frac{\alpha_f}{\alpha_0}\left(D_f+\frac{D_f^2}{\alpha_f/\beta_f}\right)+\frac{\alpha_\gamma}{\alpha_0}\left(D_\gamma+\frac{D_\gamma^2}{\alpha_\gamma/\beta_\gamma}\right)+\frac{\alpha_B}{\alpha_0}\left(D_B+\frac{D_B^2}{\alpha_B/\beta_B}\right)=D_0+\frac{D_0^2}{\alpha_0/\beta_0}\ . \tag{2.8}$$

At this point, the concept of new weighting factors can be defined as the ratio between the alpha coefficients of each component, α_i, and the one corresponding to photon iso-effective dose, α_0 (notation for the new formalism will be marked by a *):

$$w_i^*=\frac{\alpha_i}{\alpha_0}\ ,\qquad i=t,f,\gamma,B\ . \tag{2.9}$$

These are the key factors of the new formalism, which do not depend either on the dose or on the survival. They are only specific of the tissue and the biological end-point.

Then, Eq.(2.8) reads:

$$w_t^*\left(D_t+\frac{D_t^2}{\alpha_t/\beta_t}\right)+w_f^*\left(D_f+\frac{D_f^2}{\alpha_f/\beta_f}\right)+w_\gamma^*\left(D_\gamma+\frac{D_\gamma^2}{\alpha_\gamma/\beta_\gamma}\right)+w_B^*\left(D_B+\frac{D_B^2}{\alpha_B/\beta_B}\right)=D_0+\frac{D_0^2}{\alpha_0/\beta_0}\ . \tag{2.10}$$

Just for convenience, we will denote the left-hand-side of the equation as:

$$D_W^*=w_t^*\left(D_t+\frac{D_t^2}{\alpha_t/\beta_t}\right)+w_f^*\left(D_f+\frac{D_f^2}{\alpha_f/\beta_f}\right)+w_\gamma^*\left(D_\gamma+\frac{D_\gamma^2}{\alpha_\gamma/\beta_\gamma}\right)+w_B^*\left(D_B+\frac{D_B^2}{\alpha_B/\beta_B}\right). \tag{2.11}$$

The quantity D_W^*, which by definition is equal to $E/\ \alpha_0$, can be considered as an extrapolation to BNCT of the concept of the BED in conventional photon therapy, explained in Section 2.2.

Eq. (2.10) is the key equation for determining the photon iso-effective dose, D_0, just solving a quadratic equation, which leads to:

$$D_0 = \frac{\alpha_0/\beta_0}{2}\left\{-1 + \sqrt{1 + \frac{4}{\alpha_0/\beta_0} D_W^*}\right\}, \tag{2.12}$$

where D_W^* can be obtained from Eq. (2.11). For this, we require the values of the coefficients w_i^*, which are true constants (not depending either on the dose or on the survival), unlike the formerly used w_i factors. Also, the values of α_i/β_i for each component and the one for the reference dose, α_0/β_0, are required. The coefficients w_i^* and α_i/β_i can be obtained from *in vitro*/*in vivo* radiobiology experiments by determining the alpha and beta coefficients in Eq. (2.5) and by a fitting of this equation to the survival data, both for the BNCT irradiation and for the reference photon one (more details in Section 2.3.2). The same for α_0/β_0, but as it corresponds to a well-known radiation, they are tabulated for different tissues and end-points [VanL18, Tham90]

A further simplification can be performed, which is even more closely related to the current formalism, if the β_i factors, for $i = t, f, B$, are neglected. As they are the corresponding high-LET components, the repair is not common and the survival data (in log-scale), as a function of the dose, can be fitted appropriately with a straight line, without quadratic component. In this case Eq. (2.10) reduces to:

$$w_t^*\, D_t + \, w_f^*\, D_f + w_\gamma^* \left(D_\gamma + \frac{D_\gamma^2}{\alpha_\gamma/\beta_\gamma}\right) + w_B^* D_B = D_0 + \frac{D_0^2}{\alpha_0/\beta_0}, \tag{2.13}$$

and then the photon iso-effective dose, D_0, is given by Eq.(2.12), using the value of D_W^* from:

$$D_W^* = \, w_t^*\, D_t + \, w_f^*\, D_f + w_\gamma^* \left(D_\gamma + \frac{D_\gamma^2}{\alpha_\gamma/\beta_\gamma}\right) + w_B^* D_B \,, \tag{2.14}$$

where only the ratios α_0/β_0 and $\alpha_\gamma/\beta_\gamma$ are required (as well as the w_i^*).

2.3.1 Comparison with fractionation treatment

A special interest of the present formalism is that it allows us to compare with conventional fractionated treatments, for which there is an enormous clinical experience. As the right-hand side of both Eqs. (2.10) and (2.13) represents the BED in conventional photon therapy (see Section 2.2) for a comparison to a fractionated treatment, it can be substituted by the right-hand side of Eq.(2.3).:

$$w_t^*\left(D_t+\frac{D_t^2}{\alpha_t/\beta_t}\right)+\ w_f^*\left(D_f+\frac{D_f^2}{\alpha_f/\beta_f}\right)+w_\gamma^*\left(D_\gamma+\frac{D_\gamma^2}{\alpha_\gamma/\beta_\gamma}\right)$$
$$+\,w_B^*\left(D_B+\frac{D_B^2}{\alpha_B/\beta_B}\right)=nd_{n0}\left(1+\frac{d_{n0}}{\alpha_0/\beta_0}\right), \tag{2.15}$$

$$w_t^*\,D_t+\ w_f^*\,D_f+w_\gamma^*\left(D_\gamma+\frac{D_\gamma^2}{\alpha_\gamma/\beta_\gamma}\right)+w_B^*D_B=nd_{n0}\left(1+\frac{d_{n0}}{\alpha_0/\beta_0}\right), \tag{2.16}$$

where n is the corresponding number of sessions of doses d_{n0} that will have the same effect as a single irradiation of D_0. Then, the fractionated photon iso-effective dose, for a given number of sessions, can be obtained as:

$$d_0=\frac{\alpha_0/\beta_0}{2n}\left\{-n+\sqrt{n^2+\frac{4n}{\alpha_0/\beta_0}D_W^*}\right\}. \tag{2.17}$$

Normally, for fractionated treatment, what is fixed is the dose of each session, d_{n0}, which is usually around 2 Gy. That is why the number of sessions has to be calculated to estimate the iso-effective fractionated dose:

$$n=\frac{D_W^*}{d_{n0}+\frac{d_{n0}^2}{\alpha_0/\beta_0}}. \tag{2.18}$$

This comparison must be taken with care, since both BNCT and fractionated photon irradiation may have a different response in tissues. One allows repair (the fractionated) while the other does not. However, as it is done with BED in the comparison of photon single irradiation with fractionated, it gives an idea of the expected effect in the patient.

2.3.2 The new w_i^* factors.

Described in Eq. (2.9), these factors are independent of the dose or survival fractions, but they still depend on the tissue, end-point, facility and boron compound. The concept of these factors is not new, since it corresponds to the maximum RBE values (at low dose and 100% of survival). What is new is their application in the BNCT biological damage estimation.

As w_i^* are dose-independent factors, one important advantage must be emphasized: w_t^* will be the same in all the facilities. In the accelerator-based BNCT one of the principal differences

between facilities is the neutron spectra. The big difference is always in the maximum energy, so in the epithermal part of the neutron spectrum. Nevertheless, all of them will cover in their spectra all the thermalized neutron energies. Therefore, the w_t^* value, as a dose-independent factor, would be transferable between facilities. This makes w_t^* a key factor, which, if it can be obtained isolated, *i.e.* from a pure thermal neutron beam, will be a true constant, for each tissue and end-point, between facilities. That is why, experiments performed at Institut Laue Langevin, described in Chapter 4, will be an important contribution to radiobiology data.

At first sight, one can think that, as the w_i^* factors correspond to a maximum value, the estimated effect is going to be higher than the equivalent dose D_w (Eq. (1.2)) of the older formalism. This is not going to be the case and an example is outlined in Section 2.5.5. Only D_w^* is going to be much higher than D_w, since both use weighting with RBE factors which are maximum for the first. However, with the introduction of the LQ model, the iso-effect is given by D_0 (Eq.(2.12)), and this one will remain moderate.

2.3.3 How to apply the present formalism.

For the application of the formalism to estimate the damage in a BNCT, it is necessary to have the values of the different absorbed dose components: D_t, D_f, D_γ and D_B. Once these values are known:

• We propose the use of Eq. (2.12) with D_W^* given by Eq.(2.11) to obtain the single irradiation treatment photon iso-effective dose. When there is not enough knowledge on the values of the β_i factors, for $i = t, f, B$, then use Eq. (2.14).

The application of Eq.(2.16) (or, alternatively, Eq. (2.17), in the same conditions aforementioned), to obtain the fractionated photon isoeffective dose must be taken with care.

• Quantities D_0 and d_0 can be expressed in Gy, since they are absorbed doses by definition, but always with a specification that they correspond to the photon iso-effective dose (fractionated and non-fractionated).

• For the use of the formulas, knowledge on the w_i^* factors is required. There are different options:

a) The first and best option is to find the radiobiology data of the specific tissue and end-point and apply directly the w_i^* found, for a specific facility. They can be found as RBE_{max}, RBE when survival is 100% or single track lethal damage ($STLD$) [Bare94].

b) When the specific value is not known, there is the option of extracting it from old irradiation experiment data. If the survival curves for the neutron (or neutron + boron compound) irradiation and the one for reference photon dose are shown, the ratio of the α coefficient (Eq. (2.9)) that results from the fitting with LQ in both curves will be the w_i^*.

In this case, it is important to emphasize that the survival curve corresponding to neutron damage also includes the damage by induced gamma radiation from the beam. It is necessary to extract this gamma damage to have just the effect of the neutron dose for having the correct α_i corresponding. This extraction should be done using the LQ model to be consistent with this formalism.

c) In case it is not possible to directly calculate the alpha ratio, it is possible to use the data of the previous w_i factors (provided the dose or the survival fraction from which they were obtained is known) to estimate the new ones. This will be described in Section 2.4.2. Again, a correct extraction of the gamma effect from the total neutron beam effect using the LQ model is desired.

It is still not correct to use one w_i^* for other tissues or other facilities, but it can be done (as it is done with the current w_i) if there is no other option. However, the optimal application will be always option a) (or b) with a correct gamma extraction). Therefore, if new radiobiology data is found, the best option is to tabulate these new w_i^* factors, defined in Eq. (2.9), for different tissues, end-points and facilities.

• Knowledge of $\alpha_\gamma/\beta_\gamma$ and α_0/β_0 is also required. For the $\alpha_\gamma/\beta_\gamma$ ratio it is best to use data of irradiations with gamma rays at the same dose rate as in BNCT (around 0.1 Gy/min). If this is not possible, the data for the same tissue (and end-point) with conventional photon irradiation, ratio α_0/β_0, can be used instead. This approximation of $\alpha_\gamma/\beta_\gamma$ to α_0/β_0 can be done as it corresponds to the same type of radiation, although usually with different dose rate. It is not exactly the same, but α_0/β_0 is easier to be found

since is known from a lot of experimental data for many tissues and different biological effects [VanL18, Tham90].

• The biological effect of the BNCT will be given by the photon iso-effective dose, D_0, both for the tumor and for the organs at risk. Therefore, D_0 will be the photon dose with conventional radiotherapy at which the patient would have the same effect as with the BNCT treatment applied. Once the photon iso-effective dose is obtained, the work is to find in bibliography which secondary effects are expected in a patient who receive a dose D_0 in conventional radiotherapy and that such a dose does not exceed the prescribed limit.

2.4 Connection to other formalisms

2.4.1 Gonzalez and Santa-Cruz iso-effective dose formalism

Another formalism, which is based in the same concept of iso-effective dose and the application of the LQ model to BNCT, was presented in 2012 by Gonzalez and Santa Cruz [Gonz12]. This method takes into account the possible synergies between the different types of radiation and the repair mechanisms as a function of time (Lea-Catcheside time factor, $G(\theta)$). By the introduction of all these ideas they reached the following expression:

$$\alpha_R D_R + G(\theta')\beta_R D_R^2 = \sum_{i=1}^{4} \alpha_i D_i + \sum_{i=1}^{4}\sum_{j=1}^{4} G_{ij}(\theta)\sqrt{\beta_i \beta_j}\, D_i D_j \,, \tag{2.19}$$

where sub-index R refers to reference radiation and $i, j = 1,..,4$ refers to each component in BNCT, *i.e.* thermal, fast, γ and boron (See Section 1.2).

This formalism was applied in examples of brain tumor data [Code93] finding that the photon iso-effective dose estimated is different than the one estimated with the fixed-factors dosimetry formalism, especially at high doses. Recently, a retrospective application of the method in the dosimetry calculations of head and neck patients in Finland was presented [Gonz17]. This study has shown that the recalculation with the Gonzalez and Santa-Cruz method agreed better with the real biological effect found in the patients than the prediction with the old dosimetry weighted dose method.

The equation that defines the Gonzalez and Santa-Cruz method can be compared with the presented formalism described in Section 2.3 by Eq.(2.7). Then, it is found that the presented formalism is a particular case of the Gonzalez and Santa-Cruz formalism, when synergies are neglected and the Lea-Catchside factors are assumed to be one. Therefore, the Gonzalez and Santa-Cruz method is physically more reliable. However, most of the parameters are normally impossible to extract from old data and there is no new data available. Also, besides the good definition, this formalism is not established yet by the BNCT community due to the difficult adaptability from the current method (with fixed w_i).

2.4.2 Relation with current formalism

The new weighting factors w_i^* can be related to the dose-dependent conventional RBE factors, w_i. That means that, with the existing data of the w_i, the new factors w_i^* can be calculated. If D_{0i} is the photon dose producing the same effect as the absorbed dose component D_i with $i = t, f, B$, then, by making equal the common effect that corresponds to both doses leads to:

$$\alpha_i D_i + \beta_i D_i^2 = \alpha_0 D_{0i} + \beta_0 D_{0i}^2 \,, \tag{2.20}$$

which can be written as:

$$\frac{\alpha_i}{\alpha_0}\left(D_i + \frac{D_i^2}{\alpha_i/\beta_i}\right) = D_{0i} + \frac{D_{0i}^2}{\alpha_0/\beta_0} \,. \tag{2.21}$$

In this formula we can identify $w_i = D_{0i}/D_i$ and $w_i^* = \alpha_i/\alpha_0$. Then the following relation is found:

$$w_i^* = w_i \frac{1 + \dfrac{D_{0i}}{\alpha_0/\beta_0}}{1 + \dfrac{D_{0i}}{w_i \alpha_i/\beta_i}} \,, \tag{2.22}$$

or equivalently, in terms of D_i we find:

$$w_i^* = w_i \frac{1 + \dfrac{w_i D_i}{\alpha_0/\beta_0}}{1 + \dfrac{D_i}{\alpha_i/\beta_i}} \,. \tag{2.23}$$

In the case that β_i can be neglected, they reduce to:

$$w_i^* = w_i\left(1 + \frac{D_{0i}}{\alpha_0/\beta_0}\right), \tag{2.24}$$

and:

$$w_i^* = w_i\left(1 + \frac{w_i D_i}{\alpha_0/\beta_0}\right). \tag{2.25}$$

In this case it can be clearly seen (taking into account that w_i^* do not depend on D_{0i}), that w_i is a monotonically decreasing function of D_{0i}, and that the w_i^* represent the maximum value of w_i, which happens in the limit $D_{0i} \to 0$. A schematic representation of the behaviour of the weighting factors, both with respect to the dose and to the survival fraction, is displayed in Figure 2.2.

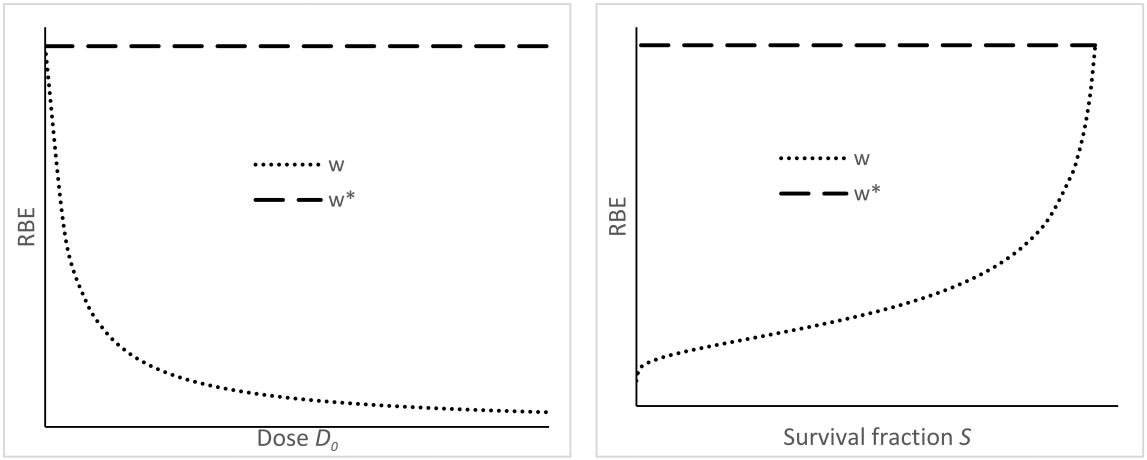

Figure 2.2: Schematic representation of the dose and survival dependence of the current w_i in comparison with the constants w_i^*.

2.5 Examples of application of the new formalism

We will now analyze the data for the new weighting factors that can be estimated from the current radiobiology data and the result in a real treatment planning. The final example will be an actual application of BNCT for brain tumors and it will show the differences between formalisms. Before, we require data of the new weighting factors for similar tissues, *i.e.* glioblastoma for tumor tissue and spinal cord for healthy tissue. We are going to base these on two previous experiments, those of Coderre *et al.* (presented already in Chapter 1) for 9L rat gliosarcoma *in vivo* and *in vitro* [Cod93] and those of Morris *et al.* [Morr94] for myelopathy effects on the spinal cord.

From the Coderre *et al*. experiments [Cod93], data for w_i^* factors will be extracted in two ways: following the equation that defines them, Eq. (2.9), when they will be denoted as w_i^{*b} (because it corresponds to the way b) to apply the formalism shown in Section 2.3.3), or using Eq. (2.23), denoted by w_i^{*c} since it comes from the way c) explained in Section 2.3.3. As we mentioned before, we cannot apply the presented formalism to results of previous measurements where a subtraction of the gamma dose fraction of the neutron irradiation is performed without taking into account the LQ model. However, the Coderre *et al*. experiments are an exception of this, considering that the gamma effect was subtracted from the survival function using the LQ model. This work happens to be the reference work for the values of $w_f = w_t$ and for the tumor values of w_B and is going to be the one used for the forthcoming analysis.

For the values of the factors that correspond to a healthy tissue, the work of Morris *et al*. for rat spinal cord [Morr94] is going to be used. In this irradiation, the gamma subtraction by the use of LQ model is not included, but there is enough information to do it. In this case, w_i^* will be extracted directly applying the formula that defines the formalism, Eq.(2.10) (or the simplified version Eq.(2.13)), because D_0 is known.

As w_i^* will be estimated from previous data, it will be necessary to make some assumptions that those authors made but that are theoretically incorrect following what was described in previous sections. The first assumption, due to the impossibility in previous experiments to separate the effect of epithermal and thermal neutrons, will be that $w_t = w_f = w_n$ (n =neutrons of all energies), therefore $w_t^* = w_f^* = w_n^*$. The effect of the photon reference radiation is presumed to be similar to those from the gamma coming from the beam, therefore $w_\gamma^* = 1$. This last assumption will imply also that $\alpha_\gamma/\beta_\gamma = \alpha_0/\beta_0$.

2.5.1 The neutron weighting factors, w_f^* and w_t^*, for tumor tissue (glioblastoma) from previous data.

The commonly adopted value of 3.2 for w_n, as stated in Ref. [Chad98] comes from the work of Coderre *et al.* [Code93] of 1% survival for rat 9L gliosarcoma model at Brookhaven Medical Research Reactor (See Section 1.3.2 in Chapter 1). In this work they determined the RBE values in terms of the neutron and photon dose for the same survival. They also give the α and

β component for the fitting of the survival curve for the gammas and the neutron irradiation. With all this data we can apply our formalism and estimate the corresponding values for w_n^*, shown in Table 2.2.

	Survival	α_0 **(Gy^{-1})**	β_0 **(Gy^{-2})**	α_n **(Gy^{-1})**	β_n **(Gy^{-2})**	D_{0n} **(Gy)**	D_n **(Gy)**	w_n	w_n^{*b} **Eq.**(2.9)	w_n^{*c} **Eq.**(2.23)
in vitro	0.1	0.13(2)	0.010(1)	0.41(5)	0.17(1)	10(2)	2.7(3)	3.8(7)	3.2(6)	3.1(9)
	0.01	0.13(2)	0.010(1)	0.41(5)	0.17(1)	16(3)	4.1(4)	3.8(7)	3.2(6)	3.0(9)
	0.001	0.13(2)	0.010(1)	0.41(5)	0.17(1)	21(3)	5.3(5)	3.9(7)	3.2(6)	3.0(9)
in vivo	0.1	0.26(3)	0.003(1)	0.50(4)	0.090(8)	8(7)	3.0(5)	3(2)	1.9(3)	2(2)
	0.01	0.26(3)	0.003(1)	0.50(4)	0.090(8)	15(11)	4.9(8)	3(2)	1.9(3)	2(2)
	0.001	0.26(3)	0.003(1)	0.50(4)	0.090(8)	21(14)	6.4(9)	3(2)	1.9(3)	2(2)

Table 2.2: Values of the gamma / neutron doses and the corresponding neutron weighting factors, w_n / w_n^*, extracted from α_0, β_0, α_n and β_n data of Coderre *et al*. [Code93]. The values of the new weighting factors are calculated using the definition given by Eq. (2.9) and from the previous w_n factors, using Eq.(2.23).

D_n is the neutron dose of the BMRR beam with the extraction of the effect due to photons by LQ model. As the extraction was done accordingly to the LQ model in the paper, the calculated w_n are correct and D_n is D_0/w_n.

In the last two columns two different estimations of w_n^* are shown. The first one, w_n^{*b}, is the application of the definition of these factors given by Eq. (2.9). This is the recommended procedure, which can be applied once the α coefficient for both neutrons and photons are known, for the given tissue. When this is not possible, w_n^* can be estimated from the values of w_n using Eq.(2.23) (or Eq.(2.22)), and for illustration we have also included these values, w_n^{*c}, in the last column of Table 2.1. It is evident that w_n^* are close to a constant value for *in vitro* and *in vivo* experiments, in contrast to the varying *in vivo* values of w_n. In addition, it is shown

that Eq.(2.23) approximates well the value provided by Eq. (2.9), accentuating the consistency of the proposed formalism.

It is also remarkable that the error of w_n^{*b} for the *in vivo* samples is considerably lower than for the Coderre *et al.* w_n. When the quadratic coefficient β has a large error, this error will be reflected in the value of the weigthing factor. From this point of view, the presented formalism, which in neutron irradiation supposes normally $\beta_n = 0$ and which weighting factors w_n^* only depends on α_0 and α_n, entails an advantage because will normally lead to lower errors.

2.5.2 The boron weighting factors, w_B^* , for BPA in tumor tissue (glioblastoma)

The commonly adopted value for tumor of w_B and for the compound BPA is 3.8, which was found also in Coderre *et al.*'s experiments [Code93]. In Table 2.3 we show the values of the new weighting factors w_B^* either from Eq. (2.9) (w_B^{*b}, recommended value) or w_B^{*c}, from Eq.(2.23) (which in this case becomes (2.25) because the β_B is zero). It can be noticed how the variability of the w_B values, which is of the order of 10%, is much greater than that of w_B^*, which is of the order of 1%.

	Survival	α_0 (Gy^{-1})	β_0 (Gy^{-2})	α_B (Gy^{-1})	β_B (Gy^{-2})	D_{0n} (Gy)	D_B (Gy)	w_B	w_B^{*b} Eq.(2.9)	w_B^{*c} Eq.(2.23)
in vitro	0.1	0.13(2)	0.010(1)	2.32(9)	0.01(3)	10(2)	1(7)	10(5)	17(3)	18(18)
	0.01	0.13(2)	0.010(1)	2.32(9)	0.01(3)	16(3)	2(13)	8(9)	17(3)	18(18)
	0.001	0.13(2)	0.010(1)	2.32(9)	0.01(3)	21(3)	3(18)	7(7)	17(3)	17(18)
in vivo	0.1	0.26(3)	0.003(1)	1.13(15)	-	8(7)	2.0(3)	4(4)	4.3(8)	4(4)
	0.01	0.26(3)	0.003(1)	1.13(15)	-	15(11)	4.1(5)	3(3)	4.3(8)	4(4)
	0.001	0.26(3)	0.003(1)	1.13(15)	-	21(14)	6.1(8)	3(2)	4.3(8)	4(3)

Table 2.3: Values of the boron weighting factors w_B and w_B^* for tumor and BPA, obtained from the data from the radiobiology experiments of [Code93]. w_B^* calculated using the definition given by Eq. (2.9) and from the previous w_B factors, using Eq.(2.23).

Again, the error in Coderre *et al*. factors, w_B, is larger than in the new weighting factors, w_B^*, due to the error of β_0 and β_B values, that do not affect the new weighting factors (except in the case of w_B^{*c} where Eq (2.23) is used, and because it is based on w_B data, the error of this factor one will be propagated).

2.5.3 The neutron weighting factors, w_f^* and w_t^*, for healthy tissue (spinal cord)

In the work of Morris *et al*. [Morr94] myelopathy effects on the spinal cord of rats were studied as the biological end-point (50% incidence), both for beam-only irradiation and for irradiation with the addition of BSH or BPA. For the beam-only irradiation, a w_{beam} of 1.4 was found, but this value was obtained without taking into account that the beam is a mixed gamma and neutron field. We can reanalyze and reinterpret their results in the light of the present formalism for estimating the new neutron weighting factor. In this case, there is no option to use Eq.(2.9), for the extraction of the values of w_i^*, as there is no data for the fitting factors. The same applies to using Eq. (2.23), since the w_n estimated is incorrect and extracted not using the LQ model. On the other hand, a dose with the same effect is given, *i.e*. the iso-effective dose, so, with the assumptions given in Section 2.5, w_n^* will be extracted by the direct application of Eq. (2.13).

In these experiments, they obtained that the same biological effect was achieved by $13.58 \pm 0.38\ Gy$ of their beam as with a dose of $19 \pm 0.2\ Gy$ of X-rays, taken from Wong *et al.*[Wong93]. The neutron beam is a thermal beam in which the dose delivered by photons to the blood in the vasculature of the spinal cord is 50% of the total beam dose (from the dose rates displayed in the article). Therefore we can estimate that the absorbed dose components are $D_n = D_t + D_f = D_\gamma = 6.79 \pm 0.19\ Gy$. By the use of Eq.(2.23), where D_0 is the 19.0 ± 0.2 Gy of X-ray that have the same effect and the D_n and D_γ the ones just calculated, the new weighting factor for neutrons is $w_n^* = 17.3 \pm 0.6$. For this calculation, the same value used by Wong *et al*. of $\alpha_0/\beta_0 = \alpha_\gamma/\beta_\gamma = 3$ was used [Wong93]. Results are shown on the first line of Table 2.4.

With this analysis, a different value of w_n can be obtained from Eq.(2.25), which gives, for the 50% survival: $w_n = 2.8 \pm 0.1$. However, this value, as it is dose-dependent should not be

applied for neutron doses very different from $D_n = 6.79\ Gy$, whilst $w_n^* = 17.3 \pm 0.6$ can be applied for any dose.

The new weighting factors for neutrons and normal tissue are in this case larger than for the tumor. However, the photon iso-effective dose in normal tissue will remain significantly lower than in the tumor, as it will be seen in Section 2.5.5.

	D_0 (Gy) [Wong93]	D_{beam}(Gy) [Morr94]	D_γ(Gy)	D_n (Gy)	D_B (Gy)	w_n^* (Eq.(2.13))	w_B^* (Eq.(2.13))
BMRR neutron beam	19.0(2)	13.58(38)	6.79(19)	6.79(19)	0	17.3(6)	-
BMRR neutron beam+BPA	19.0(2)	8.88(44)	4.44(22)	4.44(22)	4.93(65)	17.3(6)	11(2)

Table 2.4: Values of the new weighting factors w_n^* and w_B^* for the spinal cord with the BMRR beam alone (first row) and with the use of BPA (second row), both obtained from the radiobiology experiments of Wong *et al*. [Wong93] for D_0, and Morris *et al*. [Morr94] for D_{beam}, D_γ and D_n.

2.5.4 The boron weighting factors, w_B^* , for BPA in healthy tissue

The commonly adopted value for normal tissue of w_B and for the compound BPA is 1.3 (See Section 1.3.2), which was measured in the experiment of Morris *et al*. [Morr94]. In this work, the same biological end-point mentioned in the previous section was found for a total dose of $13.81 \pm 0.49\ Gy$, of which the beam component is $8.88 \pm 0.44\ Gy$ and the boron component $4.93 \pm 0.65\ Gy$. The partial components for the pure neutron and gamma dose are $D_n = D_\gamma = 4.44 \pm 0.22\ Gy$. With the present formalism, using Eq.(2.13), assuming $w_t^* = w_f^* = 17.3 \pm 0.6$, and the same value of $\alpha_0/\beta_0 = 3$, it is found that $w_B^* = 11 \pm 2$ (See Table 2.4). The value of w_B obtained from the present method Eq.(2.25) is 2.26, appreciably greater than the one assumed (1.3).

2.5.5 Example of application of the new formalism to a real BNCT application

In order to illustrate the applications of the presented formalism and the differences with the current one in a real treatment, we will consider the doses applied in a BNCT clinical trial of brain tumors [Joen03]. In this clinical trial, 18 patients with brain tumors were irradiated at the Fir-1 reactor (Finland) using BNCT with BPA. The different absorbed dose components are reported: the average values from all cases of the normal brain maximum (peak) physical doses (in Gy) are: $D_B = 4.46$, $D_\gamma = 3.86$, $D_t = 0.61$, and $D_f = 0.17$.

The biological effect will be compared with a conventional photon radiotherapy treatment. A typical fractionated conventional treatment with photons delivers a total dose of 60 Gy in 30 sessions of 2 Gy [Join16]. For the normal brain, assuming the value of α/β of 3 Gy (same as in Sections 2.5.3 and 2.5.4), this corresponds to a single-session of $15.89\ Gy$, using the BED concept. This will be the prescribed dose, so the dose that prevents adverse effects in normal brain tissue.

The effect of the BNCT treatment, in healthy and tumor tissue, will be:

- **Healthy tissue:** With the current procedure (the one use in this clinical trial), the use of Eq. (1.2) and the current weighting factors, $w_n = w_f = w_t = 3.2$ and $w_B = 1.3$, an equivalent photon dose of $D_w = 12.2\ Gy - Eq$ is obtained.

  Now, we apply the method here presented. We will use the new weighting factors, w^*, calculated in the previous sections, because they were based on two experiments with similar tissue than this BNCT treatment (from Table 2.4). With the data of the spinal cord, $w_n^* = 17.26$ and $w_B^* = 10.5$, we estimate by Eq.(2.14):

$$D_W^* = 17.26 \cdot 0.61 + 17.26 \cdot 0.17 + 3.86 + \frac{3.86^2}{3} + 10.3 \cdot 4.46 = 69.1, \tag{2.26}$$

  which corresponds, following equation (2.12) to a single-fraction photon iso-effective dose of $D_0 = 13.0\ Gy$. Therefore, we found that, even with the larger values of the new weighting factors for normal tissue, the BNCT treatment has delivered a dose to normal brain that does not exceed the prescription of $15.89\ G$y.

The value of $D_0 = 13.0\ Gy$ is close to the weighted dose obtained with the previous formalism, $D_w = 12.2\ Gy - Eq$, but this value was found using $w_B = 1.3$, which in this work has been recalculated using the LQ model resulting in $w_B = 2.26$. With this new more accurate value, the dose with the previous formalism would give $D_w = 16.4\ Gy - Eq$, which overestimates our value of $D_0 = 13.0\ Gy$. This suggests a possible compensation of errors in the current way of determining the dose.

To illustrate another goal of this work, we can also evaluate the iso-effective dose of a fractionated conventional radiation treatment by the use of Eq.(2.18). This gives a value which corresponds to a photon treatment of about 21 sessions of 2Gy, $D_0 = \mathrm{n}\mathrm{d}_0 = 42$ Gy, also a lower value than the conventional radiotherapy protocols.

The results suggest that the dose delivered in the treatment could be slightly increased without exceeding the tolerable dose. However, this cannot be assumed as a definitive conclusion as it is based on very limited data of the weighting factors, but it stimulates further research in order to optimize the treatment planning.

- **Tumor:** We can also estimate the photon iso-effective dose delivered to the tumor. In the tumor, the absorbed dose corresponding to the boron component will be higher, since there is more boron in the tissue and, hence, more captures. According to the values in the same treatment [Joen03], the average value of the tumor total absorbed dose is $15.2\ Gy$. Assuming that the difference with respect to the dose in normal tissue is due to the boron component, D_B has a value of $10.56\ Gy$. The prediction of the current formalism (in this case, as being tumoral tissue, using $w_B = 3.8$) gives a weighted dose of $D_w = 46.6\ Gy - Eq$.

With the presented formalism, and using the values from *in vivo* irradiations from Tables 2.2 and 2.3 ($w_t^* = w_f^* = 1.9$, $w_B^* = 4.3$ and $\alpha_0/\beta_0 = 86.67 Gy$) , a photon iso-effective dose, using Eq.(2.12), of $D_0 = 36.1\ Gy$ is estimated for a single irradiation and of $D_0 = 50\ Gy$ for a 2 Gy/session fractionated treatment, by the use of Eq. (2.17) which corresponds to 25 sessions.

These results are summarized in Table 2.5. In comparison, healthy tissue received approximately the same dose according to both formalisms. In the case of tumor tissue, the presented formalism predicts lower values for final doses. If this prediction is confirmed with

new data, it means that tumors received less dose than the prescribed one, so the tumor control is reduced.

In order to help showing how to estimate the iso-effective dose, in the following link a downloadable excel file can be found:

https://docs.google.com/spreadsheets/d/14hAjAMyS2VIgmF11DmtQ4ttp75AXCxFvUx9HnL4b9Ac/edit?usp=sharing

In this excel file, called "BNCT iso-effective dose calculation", the data and equations used in this example are included. For other examples, data for tissues and absorbed doses can be changed to see the final results in the iso-effective dose and the difference with the current fixed w_i factors formalism. Instructions to use are included in the file denoted as "key".

2.5.6 Example of general behavior of the presented formalism

A further analysis can be done by the use of the obtained data for brain tumors and spinal cord: namely the tendency of effects when the BNCT treatment planning is changed, *i.e.* when the absorbed dose components are different. So the idea is to answer the question of how the formalism compare if different doses (higher or lower) are applied to the patients.

By multiplying by the same number each of the dose components used in Section 2.5.5 (means less dose is applied when the number is less than unity and more dose when number is above unity), we obtain different absorbed doses, while the factors and the tissue-dependent parameters remain the same. With this idea, graphs shown in Figure 2.3 are obtained.

		Dose prescribed with conventional treatment with photons	Weighted Dose for the example of BNCT treatment (current formalism)	Iso-effective Dose for the example of BNCT treatment (presented formalism)
Healthy tissue ($\alpha/\beta = 3$)	Fractionated:	60 Gy (30 sessions of 2 Gy)	-	42 Gy (21 sessions of 2 Gy)
	Single-fraction:	15.9 Gy	12.2 Gy-Eq	13 Gy
Brain tumor ($\alpha/\beta = 86.6$)	Fractionated:	60 Gy (30 sessions of 2 Gy)	-	50 Gy (20 sessions of 2 Gy)
	Single-fraction:	41.5 Gy	48.2 Gy-Eq	36 Gy

Table 2.5: Results of the described example of a BNCT treatment using data of brain tumor patients in FIR-1 from Joensuu *et al.*[Joen03], with both the current (second column) and the presented formalism (last column). Details in Section 2.5.5.

From the graphs, it can be observed that:

• For healthy tissue (low α_0/β_0): at low doses, the presented formalism gives a little higher effect (iso-effective dose) than the current formalism (weighted dose). While, for high doses, the difference is much more pronounced and the effect estimated by the presented formalism seem to be much lower than the current one.

• For tumor tissue (high α_0/β_0): both formalisms are comparable at low doses, nevertheless, as the absorbed dose increases, the difference between the formalisms accentuates, again estimating a much lower effect with the presented formalism.

These results seem to lead to the conclusion that, in past clinical trials, where the treatment planning was done with the current formalism, the effect in tumors, where the absorbed doses are high, was highly overestimated.

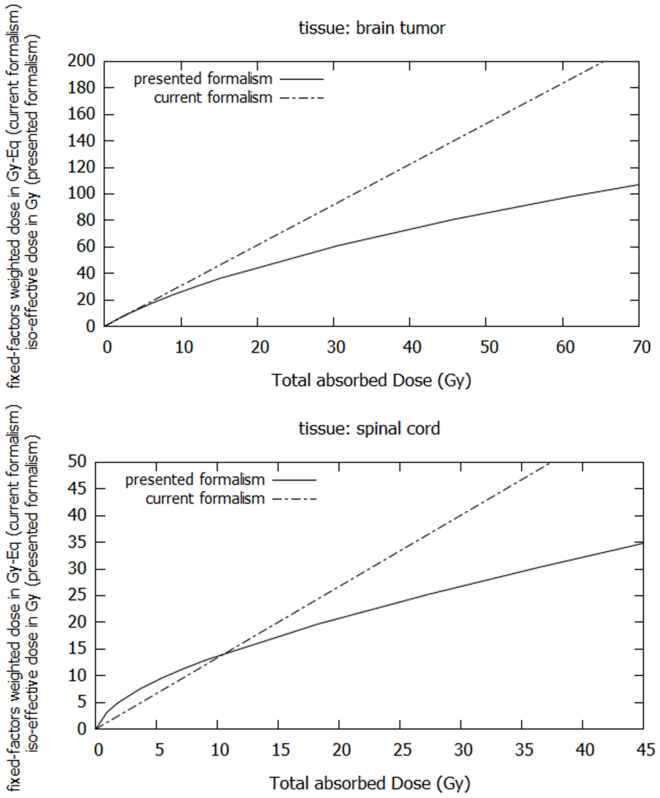

Figure 2.3: Fixed-factor weighted dose (current formalism) and photon iso-effective dose (presented formalism) as a function of the total absorbed dose for brain tumor application. Data used from Sections 2.5.3 and 2.5.4 for the healthy tissue (spinal cord) and Sections 2.5.1 and 2.5.2 for brain tumor.

The first solution to fix this problem could be a simple increase of the dose, to improve the tumor control. However, it is important to take into account that the dose in the healthy tissue will also increase. Given that at low doses, the effect expected in healthy tissue is higher than the old estimation, this solution must be taken with care.

More data for clinical trials would be useful to confirm which formalism is the correct one to be applied in BNCT treatment planning, but unfortunately, there is a big absence of detailed descriptions of absorbed doses and follow-up results in BNCT patients. The new accelerators-based neutron sources should help on having more clinical trials, but it should be accompanied by a worldwide cooperative effort in sharing the results.

Chapter 3

Estimation of the BNCT biological dose and the RBE factors by means of the RBE of the secondary charged particles

In this chapter, a method, that allows the estimation of the iso-effective dose in BNCT based on the biological effect of each secondary charged particles created during neutron irradiation and on Monte Carlo simulations of the neutron fluence, will be presented. First, the standard evaluation of the absorbed dose from the energy deposition of the secondary charged particles via the kerma factors will be described (Sections 3.1 to 3.4). Then, in Section 3.5 weighted kerma factors are defined that will incorporate the RBE of each individual energy deposition from a RBE-LET relationship for the secondary charged particles. Finally, an estimation is obtained for the energy dependence of the neutron weighting factor defined in the previous chapter; this was found to be greater for thermal neutron than for epithermal ones.

3.1 Dose calculation for a given neutron flux

Up to now, the absorbed dose components in BNCT have been discussed as quantities that are known. One of the focus of this chapter is the way in which these values are determined.

During neutron irradiation, different secondary particles that ionize the material are produced; therefore, the calculation of the individual doses deposited by these secondary particles is complex.

The dose, D, is defined as the energy deposited by charged particles per unit mass [ICRP103], in Gy ($J\ kg^{-1}$):

$$D = \frac{dE}{dm}, \tag{3.1}$$

where dE is the energy imparted to a matter of mass dm. As this energy will depend on the ionizing particle, each of the four components in the BNCT dose, (thermal D_t, epithermal D_f, gamma D_γ and boron D_B) needs to be estimated separately and must take into account the energy of all the secondary particles created. Therefore, to calculate the aforesaid deposited energy, it will be necessary to analyse what happens when neutrons penetrate a mass unit of a particular material (or tissue). Neutrons do not deposit energy directly, but by means of charged particles produced by their interactions. Additionally, neutrons also produce secondary photons which in turn deposit their energy by means of the electrons (or positrons) produced by their interactions. Therefore, strictly, the calculation of the dose at a certain mass element dm depends not only on the neutron flux in this element but also on the surroundings.

A good approximation to the dose in certain conditions (discussed later) is the kerma (kinetic energy of charged particles released per unit mass) [ICRP103], which allows the evaluation of the dose from the flux. In this approximation, the energy dE is the energy released by interactions produced at the mass dm.

The energy dE released by the process k with the element j will be described by the number of interactions in the mass element, dN, and the locally absorbed energy from this interaction, ϵ:

$$dE_k = dN_{jk}\, \epsilon_{jk}\,. \tag{3.2}$$

The number of interactions is given by the product of the probability of interaction per unit length, $\frac{dp_{kj}}{dx}$, the displacement dx and the number of incident particles, which can be written in terms of the particle fluence Φ (neutrons/cm^2) as $\Phi\ S\ dx$, if the material volume is considered as $dV = S\ dx$. Thus,

$$dN_{jk} = \Phi \, dV \, \frac{dp_{kj}}{dx} . \tag{3.3}$$

The probability of interaction per unit length depends on the cross section of the process k, σ_{kj}, and the number of targets in the material, n, of the element j:

$$\frac{dp_{kj}}{dx} = \sigma_{kj} n(j) = \sigma_{kj} \rho \frac{x_j}{A_j} N_A . \tag{3.4}$$

Here, the number of targets has been expressed in terms of the material density, ρ, the atomic mass of the particular element, A_j, and its fraction of mass, x_j (N_A is Avogadro's number).

Therefore, the deposited energy from the process k will be:

$$dE_k = \Phi \, dV \, \sigma_{kj} \rho \frac{x_j}{A_j} N_A \epsilon_{jk} . \tag{3.5}$$

For a spectrum of fluence per unit energy $\Phi(E_n)$, the total deposited energy of all the processes k that take place with the different elements j will be:

$$dE = \sum_{j,k} \int dE_n \, \Phi(E_n) \; dV \; \sigma_{kj}(E_n) \, \rho \frac{x_j}{A_j} N_A \, \epsilon_{jk}(E_n) . \tag{3.6}$$

Then, the absorbed dose in a mass element $dm = \rho \, dV$ can be expressed as:

$$D = \frac{dE}{dm} = \sum_{j,k} \int dE_n \, \Phi(E_n) \; \sigma_{kj}(E_n) \; \frac{x_j}{A_j} N_A \, \epsilon_{jk}(E_n) . \tag{3.7}$$

Normally, the quantity sought is the dose rate, since the fluence depends on the irradiation time:

$$\dot{D} = \frac{dE}{dt \, dm} = \sum_{j,k} \int dE_n \, \dot{\Phi}(E_n) \; \sigma_{kj}(E_n) \; \frac{x_j}{A_j} N_A \, \epsilon_{jk}(E_n) , \tag{3.8}$$

where $\dot{\Phi}$ denotes the neutron flux (fluence rate).

3.1.1 Dose-kerma approximation in BNCT and the kerma factor

The approximation of the dose in terms of the kerma definition is valid when the mass element in which the dose is evaluated is under the conditions of charged particle equilibrium: the energy deposited outside dm from interactions produced inside this element compensate

with the energy deposited inside dm from interactions that take place outside it. This usually happens inside any homogeneous material except at points close to the interfaces.

In BNCT, the dominant secondary particles created by neutron interactions (excluding photon production, which is treated separately) are heavy charged particles. Therefore, the previous assumption, which means that they deposit the energy locally, is quite valid for any point in the material with the exception of those located in a range of microns from the interface with other media. This assumption was also used in the calculations performed by Goorley *et al*. [Goor02], which are considered as a reference for BNCT absorbed dose estimation.

As mentioned earlier, neutron capture processes producing photons are not taken into account in Eq. (3.8). Their contribution to the dose must be calculated separately by using the photon flux, which contains both the gammas produced by the neutrons as well as contaminating gammas from the beam (this will be discussed later).

Since we are calculating the kerma, in Eq. (3.7), the expression that will depend on the characteristics of the tissue is called kerma factor. Kerma factors are described by Caswell [Casw82] and a list of data for various tissues, based on cross section data from ENDF/B-VI [ENDFweb], can be found in ICRU 63 [ICRU63]. For neutrons with energy E_n, they can be denoted like:

$$F(E_n) = \sum_{k,j} \sigma_{kj}(E_n)\ \frac{x_j}{A_j} N_A\ \epsilon_{jk}(E_n)\ . \tag{3.9}$$

Then, the dose rate can be expressed as:

$$\dot{D} = \sum \int dE_n F(E_n) \dot{\Phi}(E_n)\ , \tag{3.10}$$

where $\dot{\Phi}(E_n)$ is the particle flux and $F(E_n)$ the defined kerma factor. Usually the spectral flux is discretized in neutron energy bins E_i, and the integral is replaced by a sum:

$$\dot{D} = \sum_{E_i} F(E_i)\, \dot{\Phi}(E_i)\ , \tag{3.11}$$

where $\dot{\Phi}(E_i) = \int_{E_i}^{E_i+\Delta E_i} dE_n\ \dot{\Phi}(E_n)$ means the neutron flux of energies in the interval $E_i + \Delta E_i$.

For each dose component in BNCT, the kerma factor will involve different processes with the different elements in the tissue; hence each component (thermal, fast, boron and gamma) will be defined by its own kerma factor:

$$D_t = \sum_{E_i \leq 0.5eV} F_t(E_i)\ \Phi_n(E_i)\,, \tag{3.12}$$

$$D_f = \sum_{E_i > 0.5eV} F_f(E_i)\ \Phi_n(E_i)\,, \tag{3.13}$$

$$D_B = \sum_{E_i} F_B(E_i)\,\Phi_n(E_i)\,, \tag{3.14}$$

and

$$D_\gamma = \sum_{E_i} F_\gamma(E_i)\,\Phi_\gamma(E_i)\,, \tag{3.15}$$

where $\Phi_n(E_i)$ refers to the neutron fluence and $\Phi_\gamma(E_i)$ to the photon one. An integration over time has been performed implicitly.

3.2 Kerma factors for BNCT dose components

Each kerma factor for each BNCT component shown in Eqs. (3.12), (3.13), (3.14) and (3.15) is going to be analysed individually, taking into account the different processes and secondary particles that are involved in the energy deposit and by calculating what are called partial kerma factors. This analysis is based on the work of Porras *et al.* [Porr14] and will be explained in detail in the section below.

3.2.1 Neutron kerma factors

Following the definition given in Eq. (3.9), each neutron partial kerma factor will be determined by the neutron energy, E_i, the nuclide with which the reaction takes place, j, the type of interaction, k, and the secondary particle produced, q:

$$F_{kjq}(E_i) = \sigma_{kj}(E_i)\,\rho\frac{x_j}{A_j}N_A\,\epsilon_{jk}(E_i), \tag{3.16}$$

where x_j is the mass fraction of the nuclide with atomic mass A_j, N_A is Avogadro's number and ϵ_{kj}^{q} is the energy delivered in the interaction process.

There are two main processes that are involved when neutrons used for BNCT interact with the tissue: collisions and capture reactions. Each of these two processes will have their own partial kerma factor.

Neutron elastic kerma factor

In this case, the k process in Eq.(3.16) is elastic scattering. The average energy imparted to the recoil nucleus in an elastic process is given by:

$$\epsilon_{el} = \frac{2A_j}{\left(1+A_j\right)^2}E_i\,, \tag{3.17}$$

where A_j is the standard atomic weight of the element that interacts with a neutron, that has an energy E_i.

The energy-dependent cross section data can be taken from nuclear data files, but for simplified computation they may be approximated over a limited energy range (0.001eV-10^5eV) with an empirical expression

$$\sigma_{el}(E_i) = a\,\frac{1+bE_i^{\nu}}{1+cE_i^{d}}\,G(E_i), \tag{3.18}$$

where a, b, c, d, ν, $G(E_i)$ are fit parameters and the latter temperature-dependent factor introduces at low energies a strong dependence of the process on the temperature of the scatterer. For a scatterer of mass number A_j it can be expressed as:

$$G(E_i) = \left(1+\frac{kT}{2A_jE_i}\right)\mathrm{erf}\left(\sqrt{\frac{A_jE_i}{kT}}\right) + \frac{\exp(-A_jE_i/kT)}{\sqrt{\pi A_jE_i/kT}}\,. \tag{3.19}$$

Finally, the neutron elastic kerma factor will be given by:

$$F_{el,j}(E_i) = a\,\frac{1+bE_i^{\nu}}{1+cE_i^{d}}\,G(E_i)\,\frac{x_j}{A_j}\,N_A\,\frac{2A_j}{\left(1+A_j\right)^2}\,E_i\,. \tag{3.20}$$

Neutron capture kerma factor

In capture processes, such as occur for nitrogen and boron, there will be one kerma factor for each secondary particle, *i.e.* one for the ejected particle, denoted by P, and one for the recoil nucleus, R.

$$F_{cap,jP}(E_i) = \sigma_{cap,j}(E_i)\,\frac{x_j}{A_j}\,N_A\epsilon_{cap}^{P}\,, \tag{3.21}$$

and

$$F_{cap,jR}(E_i) = \sigma_{cap,j}(E_i)\,\frac{x_j}{A_j}\,N_A\epsilon_{cap}^{R}\,, \tag{3.22}$$

where the energies of each particle that results from a capture interaction are calculated as:

$$\epsilon_{cap}^{P} = \frac{A_R}{A_P + A_R}\left[Q + \left(1 - \frac{1}{A_R}\right)E_i\right], \tag{3.23}$$

and

$$\epsilon_{cap}^{R} = Q + E_i - \epsilon_{cap}^{P}\,. \tag{3.24}$$

Q is the energy liberated in the process diminished by energy lost in form of gamma ray emission, E_i the energy of the initial neutron, and A_R and A_P the atomic weight of each produced particle, P (ejected particle) and R (recoil nucleus).

The cross section for a capture process is normally fitted like:

$$\sigma_{cap}(E_i) = \frac{a}{\sqrt{E_i}}. \tag{3.25}$$

The neutron capture kerma factors expression is then:

$$F_{cap,jP}(E_i) = \frac{a}{\sqrt{E_i}}\,\frac{x_j}{A_j}\,N_A\,\frac{A_R}{A_P + A_R}\left[Q + \left(1 - \frac{1}{A_R}\right)E_i\right], \tag{3.26}$$

for the ejected particle and:

$$F_{cap,jR}(E_i) = \frac{a}{\sqrt{E_i}} \frac{x_j}{A_j} N_A \left(Q + E_i - \epsilon_{cap}^{P}\right), \tag{3.27}$$

for the recoil nucleus.

Neutron total kerma factor

The total kerma factor associated with neutron interactions will be the sum of the partial kerma factors in all the processes with all the elements:

$$F_n(E_i) = \sum_j F_{el,j}(E_i) + \sum_j F_{cap,jP}(E_i) + \sum_j F_{cap,jR}(E_i). \tag{3.28}$$

By definition for $E_i \leq 0.5\ eV$, the neutron kerma factor corresponds to the thermal component and for $E_i > 0.5\ eV$ to the epithermal one:

$$F_n(E_i) \underset{E_i \leq 0.5eV}{-} F_t(E_i), \tag{3.29}$$

$$F_n(E_i) \underset{E_i > 0.5eV}{-} F_f(E_i). \tag{3.30}$$

Previous calculations show how much each of the main elements of a human tissue, brain in the case of the Figure 3.1, influences in the neutron kerma [Goor02]. Generally, in the thermal energy range, the main component of the kerma is due to the nitrogen capture (10^{-12} Gy cm^2/neutrons), followed (two order of magnitude lower) by the hydrogen and the chlorine. In the epithermal range, the hydrogen becomes the most important with the oxygen and carbon two order of magnitude lower and an exception at about $4 \cdot 10^2$ eV of the chlorine resonance, which is a minority element in most of the tissues.

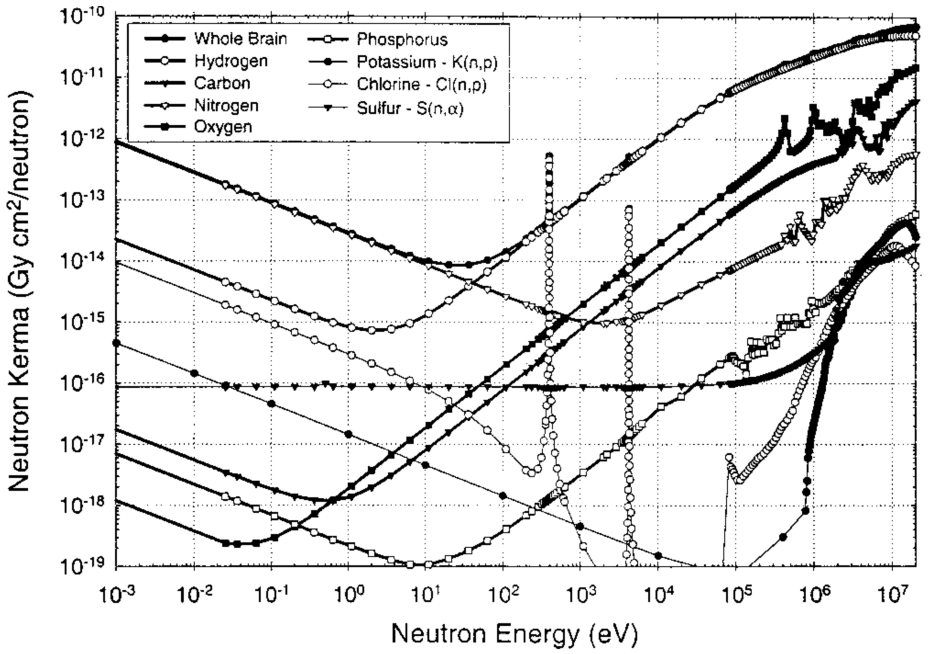

Figure 3.1: Contribution of the different elements to the neutron kerma factor of an adult brain tissue [Goor02].

3.2.2 Boron kerma factor

When there is boron present in the tissue, the interactions of neutrons with boron must be included in order to calculate the boron dose component, D_B. The neutron capture by boron will have high impact on the deposited dose at low energies, but the elastic process should also be included for better accuracy. The kerma factor expressed for neutrons in Eq. (3.28), for interactions with the element boron, will then be:

$$F_n(E_i)_{Boron} F_B(E_i) = F_{el,B}(E_i) + F_{cap,^{10}B,\alpha}(E_i) + F_{cap,^{10}B,Li}(E_i)\,. \tag{3.31}$$

3.2.3 Photon kerma factor

For the gamma component, the kerma factor is calculated by means of X-rays mass attenuation coefficients, specifically, the mass energy-absorption coefficients, $\frac{\mu_{en}}{\rho}$ [Selt93]. These coefficients contain information about the transferred energy of the charged particles after the different types of interaction of photons with matter: photoelectric absorption,

coherent scattering, incoherent (Compton) scattering, pair production in the nuclear- or atomic-field. The quantities, tabulated for different elements and homogeneous material mixtures, can be found in the NIST database [MASSweb].

When the mass energy-absorption coefficients (given in cm^2/g) are multiplied by the photon energy, E_i, the result is the photon kerma factor (Eq.(3.32)). The product of this with the photon fluence, will give the dose (=kerma).

$$F_\gamma(E_i) = E_i \frac{\mu_{en}}{\rho}(E_i) \,. \tag{3.32}$$

3.3 Kerma factors for a standard tissue

Here an **example** for a calculation of partial kerma factors is given. The material chosen is an average adult soft tissue of 4 components called ICRU-33 [ICRU46], with an elemental composition shown in Table 3.1. This tissue includes nitrogen and hydrogen, the main elements for kerma calculation, carbon and oxygen. The composition is simplified as only the dominant isotopes for each element are considered.

Tissue	^{1}H mass fraction	^{12}C mass fraction	^{14}N mass fraction	^{16}O mass fraction
ICRU-33	0.101	0.111	0.026	0.762

Table 3.1: Element composition of the ICRU-33 tissue type [ICRU46], the example selected to display a practical calculation of the kerma factor of the different absorbed dose components in BNCT.

3.3.1 Neutron kerma factor for ICRU-33 standard tissue

For this tissue, each kerma factor corresponding to neutron processes will be:

- For the elastic processes with the 4 elements in the tissue:

$$\sum_j F_{el,j}(E_i) = F_{el,H}(E_i) + F_{el,C}(E_i) + F_{el,N}(E_i) + F_{el,O}(E_i) \,. \tag{3.33}$$

- For the capture in nitrogen 14 (secondary particles are proton p and ^{14}C, denoted with p and C):

$$\sum_{14N} F_{cap,14N,q}(E_i) = F_{cap,14N,p}(E_i) + F_{cap,14N,C}(E_i)\,. \tag{3.34}$$

The first step will be to fit the cross sections for equations (3.18) and (3.25). Taking the last cross section available of ENDF [ENDFweb], the fitting parameters found for the different elements and interaction are specified in Table 3.2[Porr14]. The parameter b is zero for all the processes in this case.

Neutron interaction	a	c	d
elastic scat., ^{1}H	20.467(15)	$9.50(7)\cdot10^{-6}$	0.962(6)
elastic scat., ^{12}C	4.7421(6)	$1.37(14)\cdot10^{-6}$	0.949(9)
elastic scat., ^{14}N	10.00(6)	$2.0(5)\cdot10^{-4}$	0.765(22)
elastic scat., ^{16}O	3.8534(3)	$3.7(18)\cdot10^{-5}$	0.64(4)
capture, ^{14}N	0.290 (5)	-	-

Table 3.2: Parameters of the cross section fitting equations (3.18) and (3.26) used in the estimation of the kerma factors [Porr14]

Having a Q value for nitrogen capture of $0.626\ MeV$, the kerma factor for this type of tissue for all the neutron energies can be calculated (Figure 3.2).

We can see in the figure how the process of capture in the nitrogen 14 contributes more to the kerma at low neutron energies while the elastic processes start gaining importance when the neutron energy increases.

3.3.2 Kerma factor for ICRU-33 standard tissue with boron

In BNCT treatments, ideally boron is taken up mostly in the tumor but also some concentration can be found in normal tissues. In that case, boron capture and elastic scattering with boron can be added and the boron kerma factor will be included for the absorbed dose calculations, following Eq.(3.31).

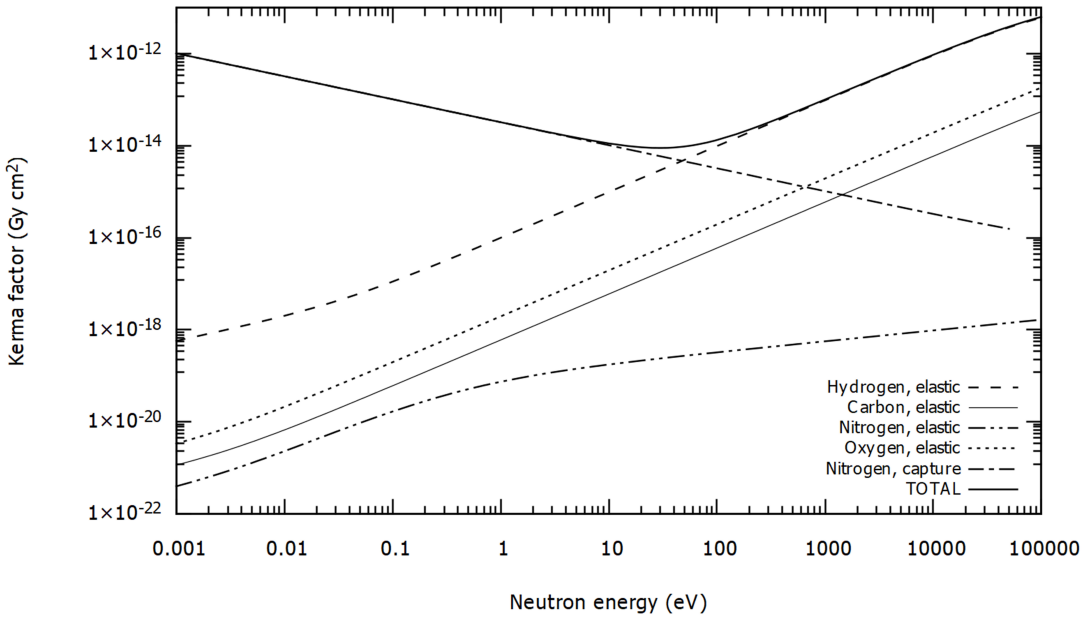

Figure 3.2: Neutron kerma factors for each process involved in neutron interaction with ICRU-33 tissue: Elastic scattering with H, C, N and O and the capture in ^{14}N.

The fitting parameters for boron elastic cross section are going to be [Porr14]: $a = 2.170(29)$, $b = 1.4(1) \cdot 10^{-5}$, $c = 3.0(5) \cdot 10^{-3}$, $d = 0.36(19)$ and $\nu = 0.925(4)$. For the capture cross section [Porr14]: $a = 611.1(14)$.

For a case where a mass fraction of 10^{-5} (10 μg/g) is supposed, the results are shown in Section 3.5 in Figure 3.9, where we can see how the boron kerma increases at low energies and acquires values ten times higher than the kerma of the nitrogen capture.

3.3.3 Photon kerma factor for ICRU-33 standard tissue

For photons, the calculations are quite simple (Eq.(3.32)) since they derive from the product of the mass energy-absorption coefficients for ICRU-33 found in NIST by the photon energy. The resulting units are J/Kg and give the kerma factors in Gy·cm^2. Results are shown in the following figure.

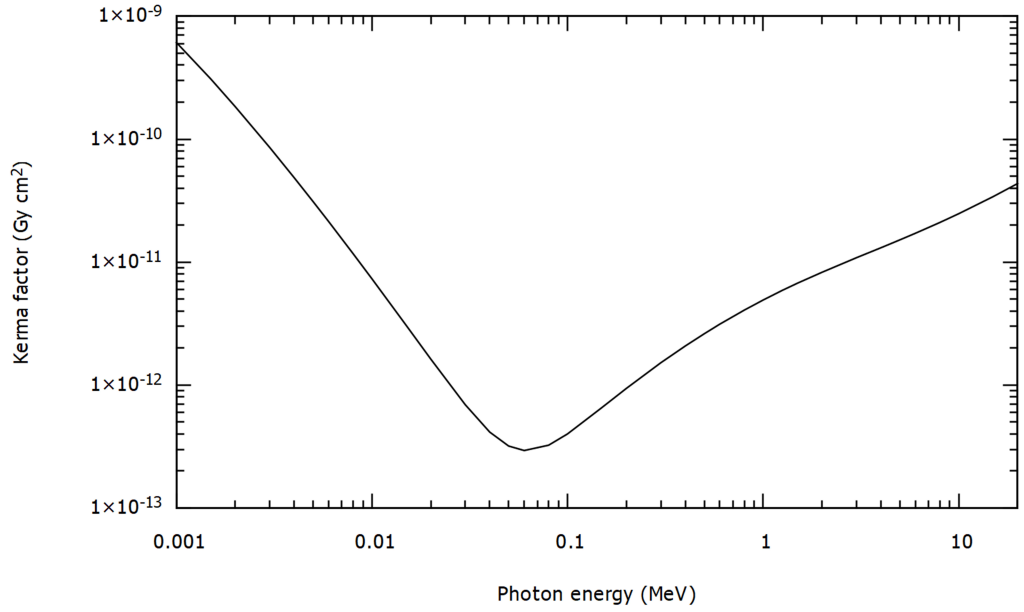

Figure 3.3: Kerma factors for photons in ICRU-33 tissue, obtained based on mass energy-absorption coefficients as a function of the photon energy from NIST.

3.4 Kerma factors and the use in Monte Carlo simulations

Once the kerma factors are calculated, it is still necessary to know the neutron and photon fluence to finally estimate the dose. To know the amount of particles in a certain position it is necessary to follow their behavior across the materials. By deterministic methods, solving the transport equations, what can be obtained is an average of the particle behaviour, but more specific information is needed. Monte Carlo method is the best approach in addressing these transport problems. With this method, particles are treated one by one and can be followed for each step in their lives.

The Monte Carlo method takes into account all the possibilities and events that can occur during a particle "life". This method was born in Los Alamos during World War II by Fermi, von Neumann, Ulam, Metropolis and Richtmyer [MCNP03], who named it in a way that compared it to the games of chance in a casino. As elemental particles do not have a deterministic behavior but follow physical rules for the event probabilities, the behavior can be predicted statistically. If, for example, there is a neutron beam through a fissionable material,

the different possibilities of being scattered, captured, or producing fission for each individual neutron are raffled according to the cross section of each process. Then, secondary particles after each event are followed and raffled again for the next event (See Figure 3.4). By simulating a sufficient amount of particle histories with a physically accurate Monte Carlo method, a result of the particles' behavior can be obtained. In conclusion: a real physical effect is predicted departing from probability distributions that are randomly sampled.

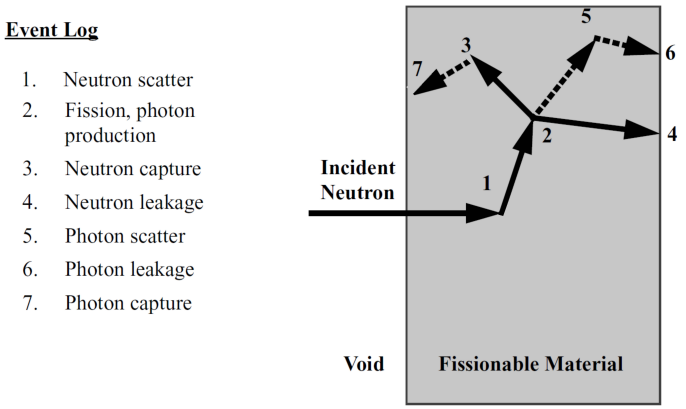

Figure 3.4: Figure extracted from the MCNP5 manual [MCNP11]. Example of the process that a Monte Carlo simulation will follow for one individual neutron entering inside a fissionable material. In the moment where the neutron is in position 1 an event occurs. The program raffles the different processes possible for a neutron with that specific energy. The raffle shows that the neutron is scattered. However, the scattered neutron continues its life and another process occur in position 2. In this case, a fission is produced, resulting in two neutrons and a photon. These particles will be followed as well, finishing their lives in points 4, 6 and 7.

In order to have sufficient histories and the real randomness needed for these types of calculations, a sufficiently powerful computer is required. The simulation program must be physically accurate and include all the probability distributions based on recent data. The MNCPx (named after Monte Carlo Neutron Photon) program [MCNP11] is the one used to simulate particles transport for our dose calculations of the experiments performed (shown in Chapters 4 and 5). MNCPx is a continuation of the previously mentioned work born in Los Alamos. Developed and improved over years, it has become a formidable tool in simulating particles behavior, especially for neutrons. It is written in Fortran 90 language and is the 2005 version of the MCNP program, created in 1977, when the code was merged for neutron simulations, MCN, with MCP, the Monte Carlo code for photons below 1 keV [MCNP03].

It is important to remember that dose calculations following the approach explained in Sections 3.1 and 3.2 must be carried out for very small fractions of tissue. Only volumes where the free path of the neutrons is bigger than the dx chosen are valid. However, in reality, there are large volumes of tissue involved, where the neutrons will change their characteristics in their path along the materials. That means that neutrons will be thermalized inside the tissue, so, for incident epithermal neutrons, processes with higher cross sections for lower energies are going to be more probable with the depth, while dose contributions from elastic scattering will diminish as the neutrons are thermalized. Thus, simulations are required for neutron transport through the materials, and that can follow the change in energy and can give the particle fluence in each position. For this reason, the volume where the dose should be estimated will be divided in little volumes (called voxels), where the dose can be calculated following the dose=kerma explained approach [Goor02].

For our purpose, MCNPx simulations will give the amount of particles and their energy over the different voxels that divide the volume, based on recent cross section data from ENDF. The kerma factor is then included to estimate the dose that those particles will deposit in each voxel. In particular, the MCNPx code, will provide in each voxel what is called "tally 4", which is the average flux within the voxel, per starting particle. This value multiplied by the kerma factor of the corresponding material will be the dose (per source neutron) in the voxel. So, finally, by multiplying this dose by the initial number of neutrons, *i.e*, the flux over the source surface, the dose rate in Gy/s will be obtained for each voxel.

3.5 Weighted kerma factors and their use for neutron RBE factor calculation

Ideally, if the biological effect of each secondary particle from each process could be taking into account, the result should be more accurate compared to the use of an average w factor multiplying each dose component. Once individual biological effects have been quantified, these can be included in the kerma factor to estimate the biological dose, thus weighting each kerma factor instead of the average final dose.

Following this idea, we will introduce a way to take into account the individual biological effect of the secondary particles created by the different processes during neutron irradiation. This approximation will allow us to predict the values of the weighting factors that multiply the dose component in BNCT. With a simple example for ICRU-33 tissue we will see that the assumption of $w_t = w_f = constant$, explained in Chapter 1, is not very appropriate.

3.5.1 Weighted kerma factor

The biological effect will be introduced via RBE factors. In this section, we will use this term to better distinguish from the general w_i factors used to weight the absorbed doses, while taking into account that the physical concept is the same: relative biological effectiveness.

The kerma factor multiplied by the RBE factor of each secondary particle q in a process k with a material j is going to be what we call weighted kerma factor, and it will be denoted with a W-superscript:

$$F_{kjq}^{W}(E_i) = \sum_{j,k,q} \sigma_{kj}(E_i) \frac{x_j}{M_j} N_A \epsilon_{kj}^{q} \, RBE_q \, . \tag{3.35}$$

3.5.2 Relative Biological Effectiveness as a function of the Linear Energy Transfer

In order to calculate this weighted kerma factor, data for the RBE for the specific particle emitted in the process is needed. This particle is going to be a charged particle with an energy that can be deposited in a specific range. The biological effect or RBE must be described as a function of these specific characteristics to be included in the weighted kerma. That information can be found from experimental RBE data of this particular secondary particle or from a general description of RBE as a function of the Linear Energy transfer, LET.

Empirical data about this relation can be found in studies from Barendsen on mammalian cells [Bare94, Bare01]. In particular, these authors worked on the RBE of heavy charged particles by the study of different biological effects and the comparison with photon irradiation. Specifically, they considered cell survival, clonogenic population reduction and breaks in DNA chains. Depending on the biological effect, different RBE are determined. In the work of

Franken *et al*. [Fran11] a compilation of the different experiments for charged particles RBE is given (Figure 3.5). They studied different types of damages or end-points, but also results for different survival percentages can be found. Hence, before choosing which data to use from this RBE-LET relation data, it is necessary to consider which biological effect or end-point is used as experimental observation.

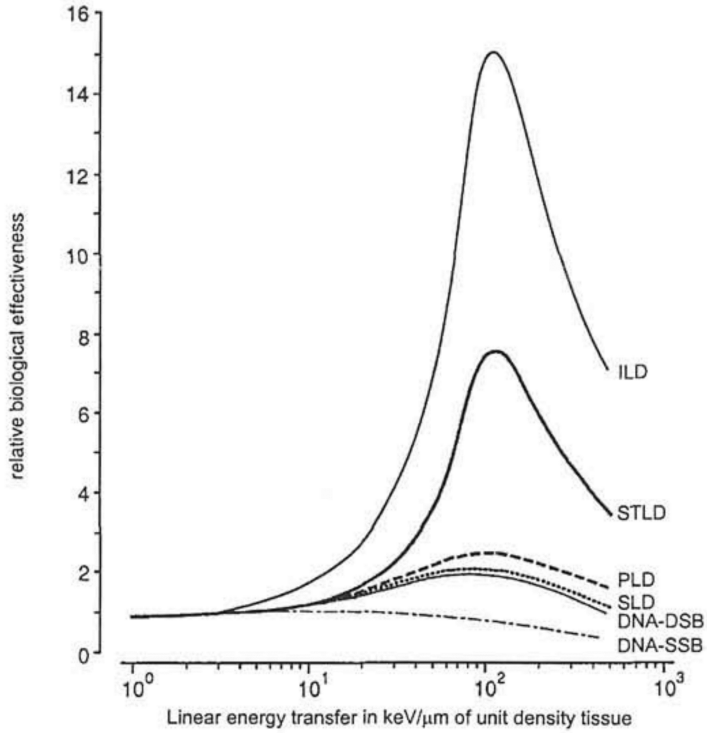

Figure 3.5: Barendsen *et al*. data compilation [Bare01, Fran11], RBE as a function of LET for different types of lethal damage. ILD, PLD and STLD derived as a contribution to the linear coefficient alpha in the LQ model (See chapter 1) in different conditions: irreparable lethal damage (ILD) even when conditions are optimal for repair, potential lethal damage (PLD) when damage is repaired, and single-track lethal damage (STLD), when the reparable damage is not repaired. SLD is the sublethal damage, expressed by beta in the LQ model. DSB and SSB refers to double strand breaks and single strand breaks in DNA, respectively.

3.5.3 Average neutron RBE factors

Once the effect of each secondary particle in each process is weighted with the RBE as a function of LET, the average RBE for neutrons as a function of the neutron energy, E_i, can be estimated by:

$$\overline{RBE_n}(E_i) = \frac{F_n^W(E_i)}{F_n(E_i)}. \tag{3.36}$$

Again, depending on the neutron energy and on the presence of boron in the tissue, the different RBE values corresponding to each dose components (thermal, epithermal and boron) will be:

$$\overline{RBE_n}(E_i) \underset{E_i \leq 0.5eV}{-} \overline{RBE_t}(E_i) = \frac{F_t^W(E_i)}{F_t(E_i)}, \tag{3.37}$$

$$\overline{RBE_n}(E_i) \underset{E_i > 0.5eV}{-} \overline{RBE_f}(E_i) = \frac{F_f^W(E_i)}{F_f(E_i)}, \tag{3.38}$$

and

$$\overline{RBE_n}(E_i) \underset{Boron}{-} \overline{RBE_B}(E_i) = \frac{F_B^W(E_i)}{F_B(E_i)}. \tag{3.39}$$

It must be remembered that photons have also a biological effect, but since they are the reference, their RBE value will be considered as unity.

These average $\overline{RBE_j}(E_i)$ factors can be compared with the w_i factors, if the end-point selected is the same, given that they weight each dose/kerma component. Nevertheless, they still have one main difference, since $\overline{RBE_j}(E_i)$ depend on the neutron energy, and one advantage, since they contain the information of the individual effect of each secondary particle.

3.5.4 Neutron RBE factors estimation for ICRU-33 standard tissue

As an **example** of neutron RBE factors estimation, we are going to see the prediction for ICRU-33 tissue. Data from Section 3.3 will be used. For each process, the weighted kerma factors will then be:

$$F_{el,j}^{W}(E_i) = F_{el,H}(E_i)RBE_H(E_H) + F_{el,C}(E_i)RBE_C(E_C) + F_{el,N}(E_i)RBE_N(E_N) + F_{el,O}(E_i)RBE_O(E_O)\,, \tag{3.40}$$

$$F_{cap,14N,q}^{W}(E_i) = F_{cap,14N,p}(E_i)RBE_p(E_p) + F_{cap,14N,C}(E_i)RBE_C(E_c)\,. \tag{3.41}$$

The RBE-LET dependence used was the one corresponding to single track lethal damage, STLD, from Barendsen *et al.* data [Bare01, Fran11]. The reason for this choice derives from the fact that these values correspond to the ratio of the alpha coefficients for charged particles and photons of the LQ model for this effect, therefore it will provide an estimation to the coefficients w_i^* defined in Chapter 2. These data are fitted to a function of the LET giving the next expression

$$RBE_q = \frac{1 + 0.005(2)\,LET + 0.00027(2)\,LET^2}{1 + 0.0148(4)LET + 0.000102\,(5)LET^2}\,. \tag{3.42}$$

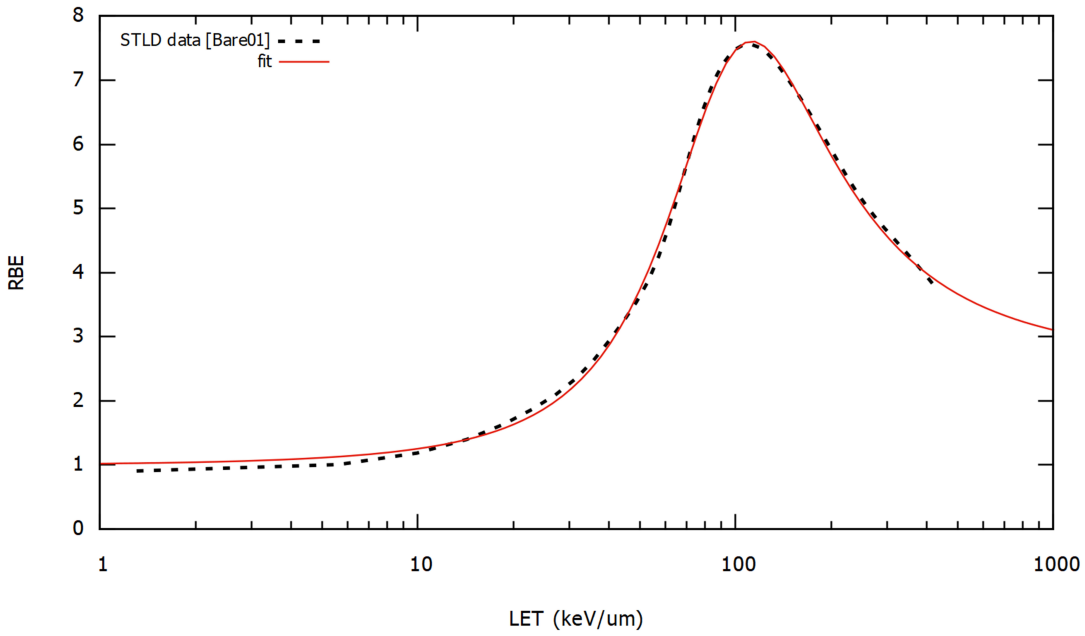

Figure 3.6: Barendsen *et al.* data [Bare01] for mammalian cells and single track lethal damage fitted with Eq. (3.42)

It is necessary then to calculate the LET of each secondary particle. The average LET is the deposited energy per unit distance:

$$LET = \frac{\varepsilon}{R}, \tag{3.43}$$

where ε is the tranfered energy and R the range in the media. To calculate the range of each particle the continuous slowing down approximation (CSDA) was used.

$$R_{A,z}(\varepsilon) = \frac{A}{z^2} R_{1,1}(\varepsilon/A). \tag{3.44}$$

Data from PSTAR at NIST [PSTARweb, ICRU49] data base was applied for energies above 0.001MeV while empirical data from Andersen and Ziegler [Ande77] was used to fit low energies.

With the calculated range, it is possible to calculate the average LET and then the RBE, which will allow to weight each kerma factor of the ICRU-33 tissue obtained in Section 3.3.1, finding final values of weighted kerma factor as a function of the neutron energy shown in red in Figure 3.7.

Once weighted kerma factors are calculated, it is by simply performing the ratio between this value and the non-weighted kerma factors for each neutron energy, to obtain the $\overline{RBE_n}(E_i)$ for this tissue, plotted in black in Figure 3.8. This $\overline{RBE_n}(E_i)$ derived from the STLD from the Barendsen *et al*. data, can be approximated to the w_n^* (Chapter 2), since they refer to the effect of the linear parameter in the LQ model.

If one takes the values of the RBE-LET at a survival of 10% for weighting the kerma and extract the $\overline{RBE_n}(E_i)$ for that end-point, the direct comparison with the current w_n from Coderre experiments [Code93] (Chapter 1) can be done. A similar approach was followed by Blue *et al*. [Blue93, Blue95], where the energy dependence of the RBE of neutrons was calculated and then normalized to the neutron beam of the Brookhaven Medical Research Reactor. Following the results of Barendsen *et al*. at 10% of survival, Blue *et al*. got a RBE-energy dependence that follows the same shape as our results, with a notable minimum around 0.1 keV.

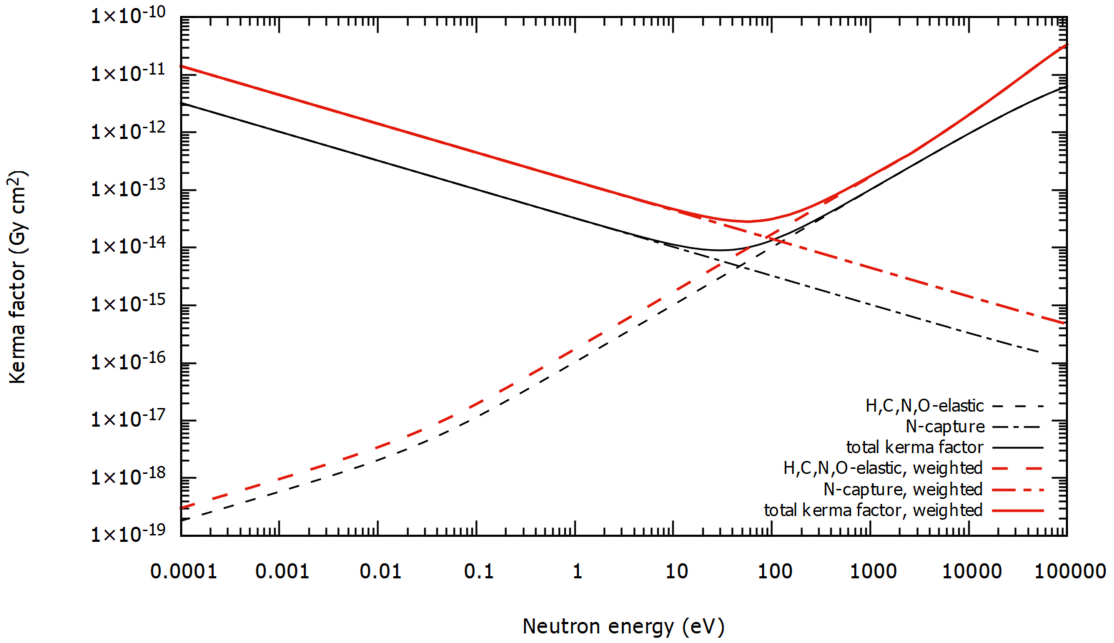

Figure 3.7: Elastic, capture and total kerma factors (black) and weighted kerma factors (red) for ICRU-33 four components tissue calculated following the approach explained in Sections 3.3.1 and 3.5.4, respectively. The ratio between both kerma factors is constant for energies below 10 eV, where the capture on nitrogen is the main process that contributes to the kerma factors. Once the elastic processes start gaining importance, the ratio stops being a constant because of the LET dependence of the weighted kerma factors.

Both, the results of Blue *et al.*'s and the presented one found by our estimation suggest the same conclusions: it is not very accurate to take a constant value for the neutron biological effect, since the RBE-energy dependence is not constant for all the energies. Hence, it is not correct to use the same value for thermal neutrons and for epithermal ones. Even if the $\overline{RBE_n}(E_i)$ have been calculated following some approximations, it is a good way to estimate the theoretical dependence of the biological effect with the energy, since it includes the information about the individual effect of the main secondary particles in a BNCT irradiation.

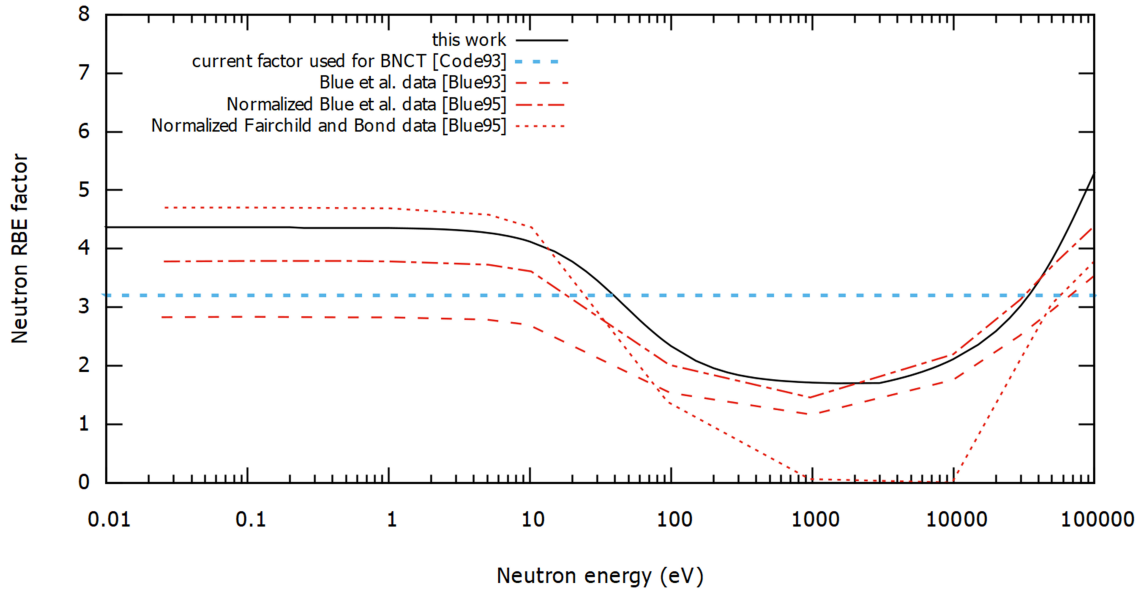

Figure 3.8: $\overline{RBE_n}(E_i)$ (ratio between weighted kerma factor and kerma factor) for ICRU-33 tissue as a function of the neutron energy. Data calculated based on RBE-LET data from Barendsen *et al.* [Bare01]. Black line corresponds to the data described in this section, where STLD data was used and it corresponds with the new weighting factors, w_n^*. Red lines correspond to the data showed in Blue *et al.* [Blue93, Blue95] with and without a normalization to the 3.2 of Coderre and using other authors' method [Fair85], all of them using Barendsen *et al.* data at 10% of survival. Blue line represents the current used 3.2 value of the weighing factor for all neutron energies.

3.5.5 Boron RBE factor estimation for ICRU-33 standard tissue

Following the same reasoning, the weighted kerma corresponding to the interactions of neutrons with boron can be estimated

$$F_B^W(E_i) = F_{el,B}(E_i)RBE_B(E_B) + F_{cap,^{10}B,\alpha}(E_i)RBE_\alpha(E_\alpha) + F_{cap,^{10}B,Li}(E_i)RBE_{Li}(E_{Li})\,. \tag{3.45}$$

The results are shown in Figure 3.9.

The RBE corresponding to the boron dose component can then be calculated from

$$\overline{RBE_B}(E_i) = \frac{F_B^W(E_i)}{F_B(E_i)}, \tag{3.46}$$

obtaining a constant value of 4.4. This value is not boron concentration dependent (same concentration assumed for the numerator and the denominator). The value is higher than the

currently used w_B of 3.8/1.3 [Code93], but it must be remembered that the $\overline{RBE_B}(E_i)$ was calculated following the RBE-LET dependence for an effect of STLD, so the data correspond to the w_B^* (Chapter 2).

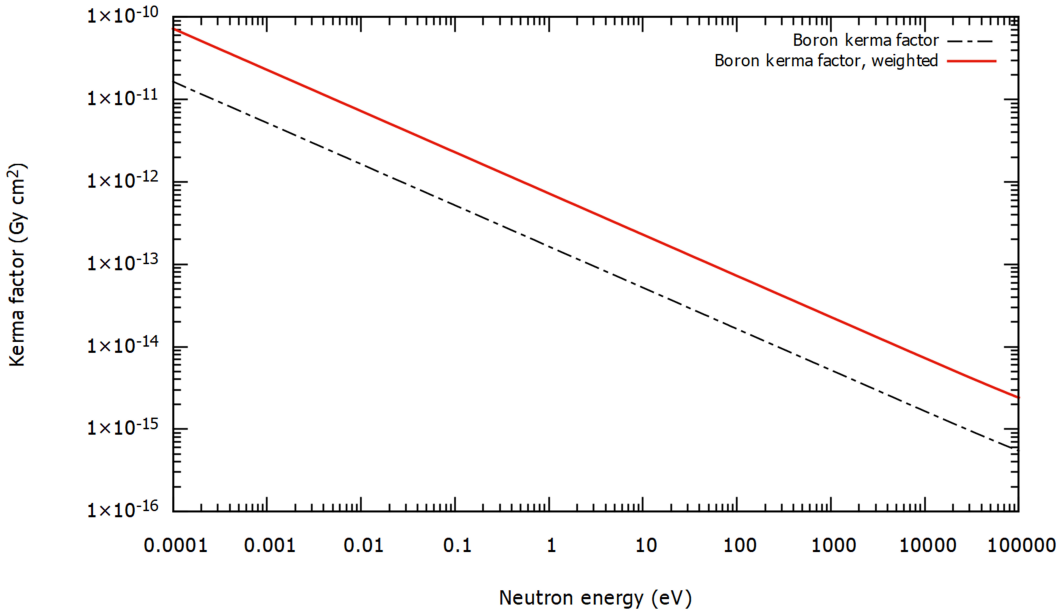

Figure 3.9: Boron kerma factors (black) and boron weighted kerma factors (red) for ICRU-33 with a mass fraction of boron of 10^{-5}.

3.5.6 Predicted values of w_i^* factors

Here we summarize the results for the weighting factors w_i^* as the average RBE from the secondary particles. Some values are displayed in Table 3.3. Some conclusions can be drawn from this table and Figure 3.8:

- The thermal neutron weighting factor w_t^* is a constant and universal factor that can be applied to thermalized neutrons from any beam. This also applies to the boron weighting factor w_B^*.
- The fast neutron weighting factor has a strong energy dependence. From its low energy limit (by definition 0.5 eV) of 4.35 it decreases at epithermal energies, reaching values of $w_f^* \approx 2$ in the range of 100 eV to 1 keV. At higher energies, it increases sharply. Therefore,

the value for a real beam depends on the spectrum. Most of the neutrons from a BNCT beam are in the epithermal range, but the effect of the high energy tail can be quite different depending on the beam (*e. g.* most of the beams from accelerator-based neutron sources are expected to have a less energetic maximum energy due to kinematics than those from reactors). Therefore, the w_f^* should be measured at each facility. An integration of the function displayed in Figure 3.8 with the actual spectrum can give an estimation of this quantity.

Energy:	From thermal to 1 eV		10 eV	100 eV	1 keV	10 keV	100 keV
$\boldsymbol{w_n^*}$**:**	$\boldsymbol{w_t^*}$: 4.35	$\boldsymbol{w_f^*}$:	4.12	2.34	1.72	2.12	5.30
$\boldsymbol{w_B^*}$**:**	4.50 (all energies)						

Table 3.3: Estimated values of the weighting factors for average mammalian cells from the RBE of the secondary charged particles based on RBE-LET STDL Barendsen *et al.* data [Bare01]

We have to keep in mind that these estimations, since they make use of a compilation of RBE values for different mammalian cells, can only be taken as an average estimate. The values are expected to depend on the tissue and they should be measured by radiobiology measurements for each cell/tissue type. This is the aim of the next chapters of this thesis.

Chapter 4

Radiobiology experiments

In this chapter, the irradiation experiments performed will be described. The purpose of all these experiments is to obtain radiobiology data and more precisely neutron RBE factors for the use in BNCT and radioprotection. A list of experiments with their objective and the beams used is presented in Section 4.1. The different experiments are designed to obtain data on the effect of: low-energy neutrons, with and without boron compounds, epithermal neutrons, and the reference irradiation of photons. These data will be acquired for different cells lines: tumor and healthy ones.

Most of the experiments follow the same structure: irradiation of *in vitro* samples followed by survival analysis in order to obtain a survival curve. Therefore, the results will be shown following the structure presented in Figure 4.1. In common with past experiments such as those introduced in Chapter 1, our experiments give a survival curve that will depend on the end-point analyzed after irradiation and on the cell line studied. To obtain this curve, it is necessary to know the dose delivered, which will depend on the beam, as well as a reliable analysis of the survival, which will require correct cell manipulation. The way to obtain these two parameters for each experiment is the central concern of this chapter.

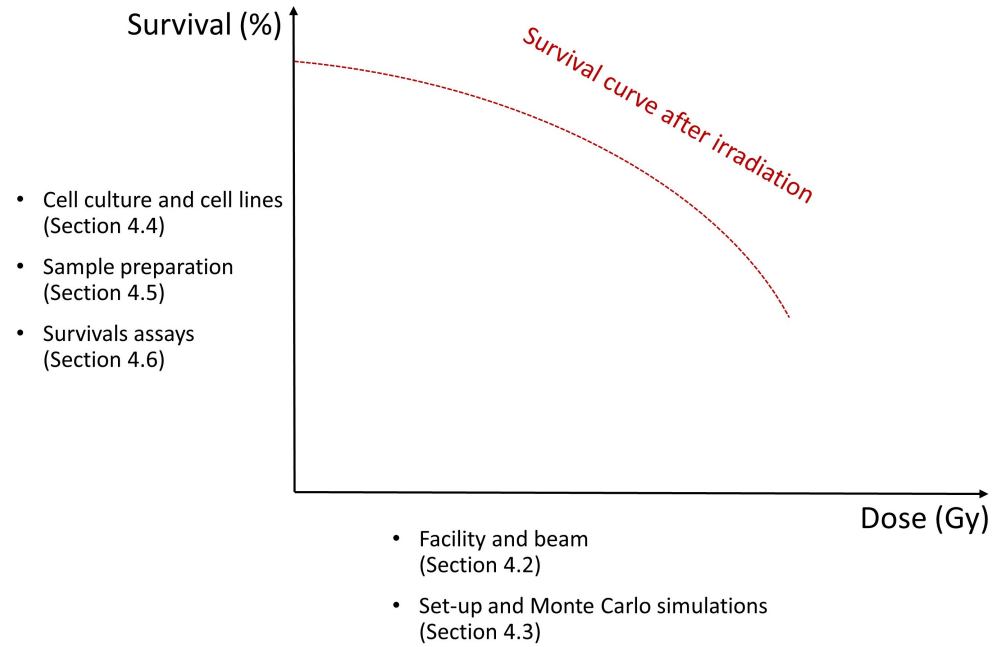

Figure 4.1: Simplification of a typical survival curve obtained from irradiation experiments. Survival as a function of the dose. To calculate the survival it is necessary to select the cell line to irradiate, a sample container where the cells can live during the irradiation, and a proper method to estimate the survival after irradiation. To calculate the dose it is necessary to study the irradiating beam used, to design a good set-up for irradiation, and to make realistic simulations to determine the particle transport. The corresponding section numbers in this chapter are indicated below each task.

4.1 Experiment list and description

Five main experiments are listed in the following table. As noted previously, all focused on the irradiation of mammalian cells with different beams and the subsequent analysis of their survival. Some of them have needed additional sample analysis (*e.g.* Experiments **IIa/b/c**, **IIIa/b**).

Experiment	Facility	Technique	Objective
I	ILL, Grenoble	Cold neutron irradiation	Data for low-energy neutron effects
II	ILL, Grenoble	Cold neutron irradiation, isotope replacement (^{14}N by ^{15}N)	Data for the isolated effect of the neutron capture on ^{14}N and the photons of the beam
IIa	ILL, Grenoble	Thermal neutrons, NRA (Nuclear Reaction Analysis)	^{14}N/^{15}N ratio in samples
IIb	CIC, Granada	Combustion measurements	^{14}N/^{15}N ratio in samples
IIc	CEA, Grenoble	Photon irradiation	Data for photon effects in ^{14}N and ^{15}N samples
III	ILL, Grenoble	Cold neutron irradiation of boron-containing samples	Data for low-energy neutron irradiation in samples with boron
IIIa	LENA, Pavia	Thermal neutrons, NRA (Nuclear Reaction Analysis)	Boron concentration in samples
IIIb	CIC, Granada	ICP-AES analyzer	Boron concentration in samples
IV	CNA, Sevilla	Epithermal neutron irradiation	Data for epithermal neutron effects
V	Virgen de las Nieves Hospital, Granada	Photon irradiation	Data for the reference photon effects

Table 4.1: List of the experiments performed and their objectives. Experiments from I to V are irradiation experiments, where survival is analyzed after the irradiation to extract a biological effect of the irradiation. Experiments IIa, IIb, IIc, IIIa and IIIb are experiments for sample analysis.

Experiment I: The aim of Experiment I was to obtain radiobiology data of mammalian cells after low-energy neutrons irradiation. The ILL PF1b line (described in the next section) provides a beam of slow neutrons, with negligible fast neutron content and a low gamma component.

Experiment II: Performed at the same beam line as Experiment I, it allows, for the first time, the isolation of the effect of the capture reaction of neutrons in nitrogen 14 (^{14}N). ^{15}N has a

neutron capture cross section 10^{-5} times lower than nitrogen ^{14}N, hence cells with ^{15}N instead of ^{14}N would produce much less captures and, therefore, less thermal neutron dose. To this end, we used the human Hek293 cell line (embryonic kidney) labeled with ^{15}N. The residual ^{14}N content in the ^{15}N-isotope replaced cells is not exactly zero and had to be quantified in Experiments IIa and IIb. Experiment IIa makes use of nuclear reaction analysis (NRA) counting the proton recoils of the 14N(n,p) reaction, and Experiment IIb uses combustion in an elemental analyzer to extract the percentage of C, H, N and S in the culture media. Experiment IIc consists of radiation with photons to prove that in this case there is no difference in effects on the labeled and non-labeled samples, since the type of interaction with photons is the same.

Experiment III: This was performed using the same beam as Experiments I and II, and provides the radiobiology for boron capture, by using cell samples previously incubated with the boron compound BPA. To relate the observed effect to the boron concentration, the latter has to be quantified in experiments IIIa and IIIb, using two complementary techniques to quantify the ^{10}B in the cells. The first is again NRA, now counting the alpha recoils of the $^{10}B(n,\alpha)$ reaction. The second one is a direct analysis of the boron content by ICP-AES (Inductively Coupled Plasma Atomic Emission Spectroscopy), where the cell content is dissociated in a high temperature plasma to single atoms and optical emission lines are used for boron quantification. Both techniques will be explained in detail in Section 4.5.1.

Experiment IV: This was carried out in order to test the effect of higher energy neutrons. The approach used an epithermal neutron beam to irradiate cells in order to record radiobiology data for neutrons of energies up to 200 keV. This experiment was performed with just one cell line, giving some preliminary results.

Experiment V: In order to obtain the RBE values in Experiments I and IV, it is necessary to compare with a reference irradiation, *i.e.* photons. In order to obtain RBE factors that allow comparison with clinical conventional radiotherapy, the best choice is using the same type of photon beam as in hospital treatments. This is the reason why we have performed irradiations at a hospital LINAC of the same cell lines irradiated with neutrons.

4.2 Facilities and beams

Figure 4.2: Summary of the facilities used for the different experiments. Top-right, ILL (Grenoble), the research reactor where Experiments I, II and III were carried out. Top-left is CNA (Sevilla), the tandem accelerator where we performed Experiment IV. In bottom-left, the hospital LINAC (Granada) used for Experiment V. Mid-left and bottom-right are ICP in CIC (Granada) and LENA (Pavia), facilities used for sample analysis that will be explained in Section 4.5.1 and 4.5.2.

Cell irradiation and survival studies were carried out at ILL, CNA and Virgen de las Nieves Hospital. These facilities and beams will be explained first. Experiments for sample analysis prior to irradiation were performed in the CIC, at LENA and CEA, and they will be explained in Section 4.5.1-4.5.2.

4.2.1 Institut Laue-Langevin (ILL)

The ILL was used for the main Experiments I, II and III. The biological effect of thermal neutrons, for which this facility provides optimal beams, is one of the most important issues in BNCT, and its determination has been the major goal of this thesis. Therefore, this beam is described more in detail.

The Institut Laue-Langevin (ILL) is an international institute in Grenoble (France) focused on the use of neutrons for studying different fields including biology, chemistry, fundamental

physics, materials science, etc. ILL operates one of the most powerful research reactors in the world, and can produce $1.5 \cdot 10^{15}$ neutrons per second per cm^2, at a thermal power of 58.3 MW. The neutrons are guided to reach more than 45 different instruments with different characteristics, studying elastic or inelastic neutron scattering, neutron-induced reactions or properties of the neutron respectively. Experiments are performed during 3 or 4 reactor cycles per year – each of around 50 days. ILL operates as a service institute for outside users and beam time is distributed based on a peer-reviewed proposal system.

One of the ILL instruments, called *PF1b* [Pf1bweb], was used for our experiments [Pedr20a]. PF1b is situated 80 m from the reactor and is normally dedicated to fundamental particle and nuclear physics. Neutrons from the reactor pass through a cold source, containing liquid deuterium at 25K, where they are moderated down to energies of few meV, *i.e.* cold neutrons. These cold neutrons are guided easily thanks to their small critical angle (total reflection at the surface of material coating of the guide) until they reach the point where PF1b is situated. The characteristics that made us select this instrument for our purposes are:

- It provides an intense neutron beam.

- The H113 ballistic supermirror bent guide transports an intense beam of cold neutrons but avoids fast neutrons and photons reaching the experimental zone, thus resulting in a very "clean" beam of low energy neutrons [Abel06]. In fact, only the low energy neutrons can follow the curvature of the guide by total reflection, while the fast neutrons and γ-rays are not reflected and cannot reach the experimental area (Figure 4.3).

After the H113 guide, a collimation system of 3m was installed in order to obtain a final circular beam of 2 cm diameter. The collimation tube consists of a series of apertures made of boron carbide (with 19.9% natural abundance of ^{10}B), lead (to stop the γ-ray background) and a final enriched ^{6}LiF collimator, which absorbs neutrons outside the 2cm diameter via $^{6}Li(n,\alpha)$ reactions (940 b thermal cross section) without secondary γ-ray emission (Figure 4.4). More details about the collimation can be found in Appendix A.

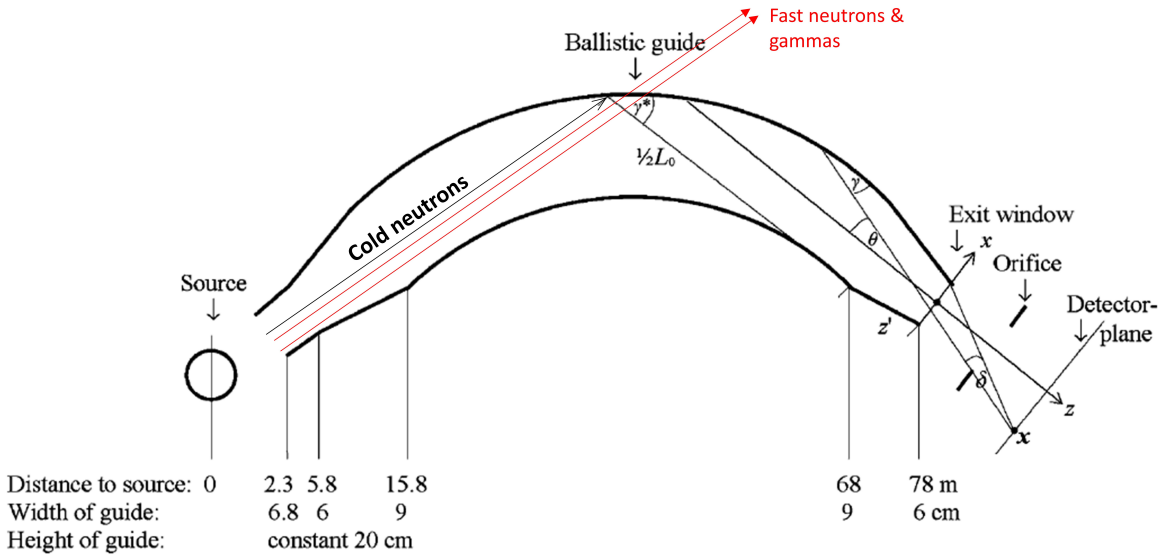

Figure 4.3: Layout of the supermirror bent guide H113 (not to scale) from [Abel06].

The beam spectrum and distribution were simulated using McSTAS, a package for neutron transport and guide simulation [Will04]. The profile of the simulated beam was then compared with the real beam measured with radiochromic films (Gafchromic EBT2) at the sample position. These films allow checking the alignment and homogeneity of the beam.

Before each experiment round, the thermal neutron capture equivalent flux was measured by activation of thin Au foils, finding fluxes between $1.05 \cdot 10^9 n_{th}/cm^2 s$ (September 2018) and $2.85 \cdot 10^9 n_{th}/cm^2 s$ (June 2019). The difference is explained by different entrance collimator sizes of the collimation system and different reactor power in different reactor cycles. For each experiment performed at PF1b, all parameters are checked and then included in the simulated beam to estimate the doses with MCNPx.

In addition to the beam line, there is another installation that helps the *in vitro* experiments at ILL to be carried out: a biological laboratory inside the instrument guide hall. This lab was installed specially for these experiments and it allows the processing of samples faster and more easily. The characteristics of this lab will be presented in Section 4.4.1.

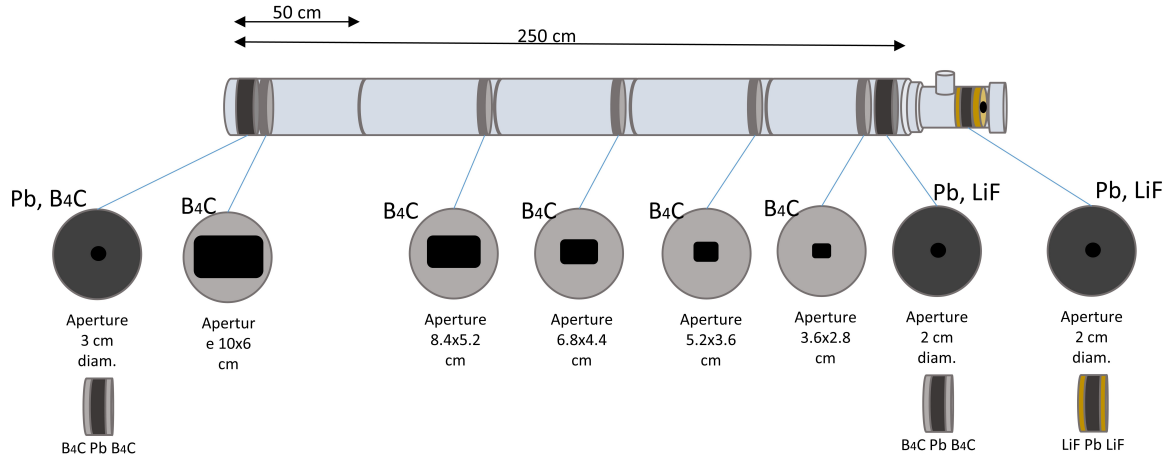

Figure 4.4: Schematic image of the collimation system situated after the H113 bent guide at the PF1b instrument at ILL.

From cold neutron flux to thermal-equivalent capture flux

The objective of the experiments in this beam is to study the effect of low energy neutrons (in samples with and without boron). Here, low energy neutrons means thermal energies and below (<0.5 eV). However, as explained previously, the neutrons at PF1b are cold neutrons, which correspond to energies lower than thermal.

Nevertheless, the effect of thermal neutrons can be studied using this beam thanks to the characteristic of cold neutrons: the capture cross sections follows a $1/v$ behavior, where v is the neutron velocity. Hence, a cold neutron beam will result in more captures than a thermal one with the same particle flux. The effect of one capture in the same element is always the same, meaning that the secondary particles after the capture have always the same characteristics, irrespective of the energy of the initial neutron. This implies that a flux of cold neutrons will have the same effect (same captures) than a higher particle flux of thermal neutrons.

For easier comparison of the number of captures, one defines the so-called thermal-equivalent capture flux or capture flux (expressed in n_{th}/cm^2s) according to the equation [Konr11]:

$$\phi_c = \int_v \phi(v)\frac{v_0}{v}dv\,, \tag{4.1}$$

where the neutron velocities v, are proportional to the square-root of the neutron energy and v_0 corresponds to the thermal velocity.

This description allows direct comparison of the expected number of neutron captures in a beam irrespective if the exact spectrum is thermal, cold or hot (with neutrons faster than thermal neutrons). *De facto*, it also shows that we can measure thermal neutron effects with a cold

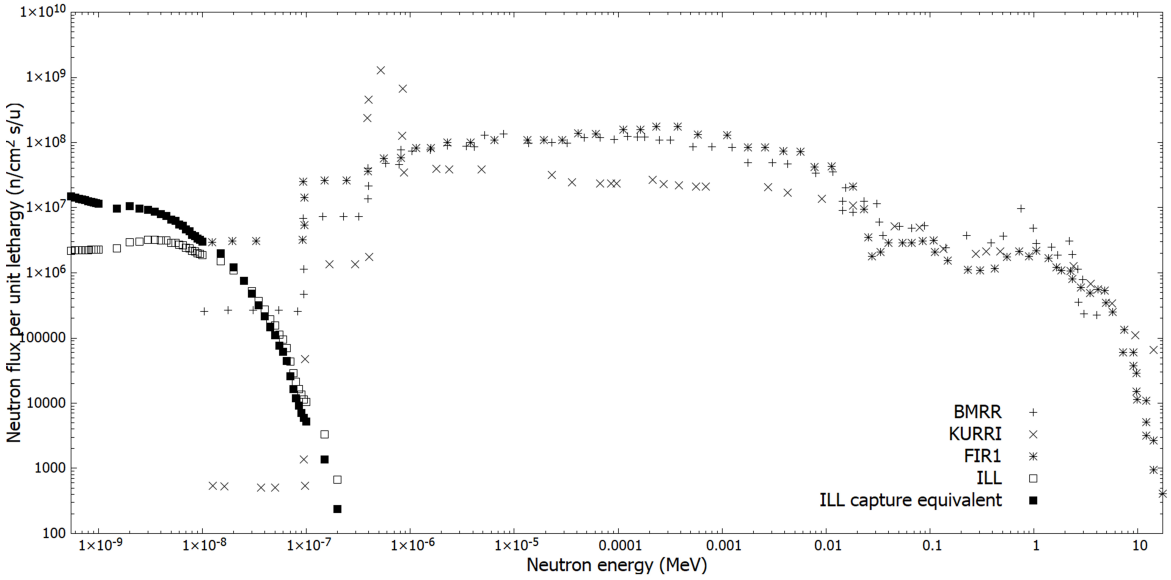

Figure 4.5: Neutron spectrum at the end of the collimation system of the PF1b line at ILL (squares) when compared with epithermal neutron BNCT sources [Aute04]. Data is expressed in neutron flux per unit of lethargy to facilitate the display of the data in the large energy range, where u is the lethargy defined as $u = lnE_0/E$ and $E_0 = 10MeV$. From this image, it can be established that the ILL beam is not suited for (pre-) clinical BNCT of deep-seated tumors, but that it is well suited to low-energy neutron studies and boron compounds analysis, without the disturbing influence of epithermal neutrons. Open symbols show the particle flux (actual neutrons passing) and filled symbols the capture equivalent flux, *i.e.* the corresponding thermal neutron flux that would be required to induce the same number of captures.

4.2.2 Centro Nacional de Aceleradores (CNA)

CNA is a Spanish center situated in Sevilla that has 6 different facilities/systems: a Tandem Van de Graaff accelerator of 3 MV, a cyclotron that provides 18 MeV protons and 9MeV deuterons, a Tandem Cockcroft-Walton accelerator of 1MV, a PET/CT scanner for diagnosis, a radiocarbon dating system and a ^{60}Co irradiator.

The 3 MV Tandem was modified to provide an epithermal neutron beam with almost no thermal neutron component. To obtain a Maxwellian spectrum at kT=30 keV with neutrons of energies from 0 to around 200 keV, protons of 1912 MeV impact in a thick lithium target [Jime18a, Rome18b]. Neutrons are produced through the reaction $p + {}^{7}Li \rightarrow n + {}^{7}Be$, with a fluence of $2.75 \cdot 10^{4}$ cm^{-2} mC^{-1} at 0°[Lede12]. In CNA, a lithium target of 100µm thickness and 0.5cm radius is mounted on a surrounded by a cooling system based in water-cooled copper block [Iraz16]. The cooling system will avoid the melting of the lithium, which can reach high temperature due to the proton stopping power. This beam is normally used for Nuclear Astrophysics experiments, such as the measurement of the ^{197}Au(n,γ) cross section [Jime18b]. In the case of Experiment IV, it was used for the first time for radiobiological purposes.

There is an important aspect to take into account for the cell irradiation with this beam: the flux is much lower compared to the beam at ILL, so irradiation times will be longer. Also, while gamma-ray production by (n,γ) reactions in the sample and environment is low due to the high energy of the neutrons (thus low capture cross sections), 478keV gamma rays are produced by inelastic proton scattering in the lithium target [Lee 99] and their dose needs to be taken into account.

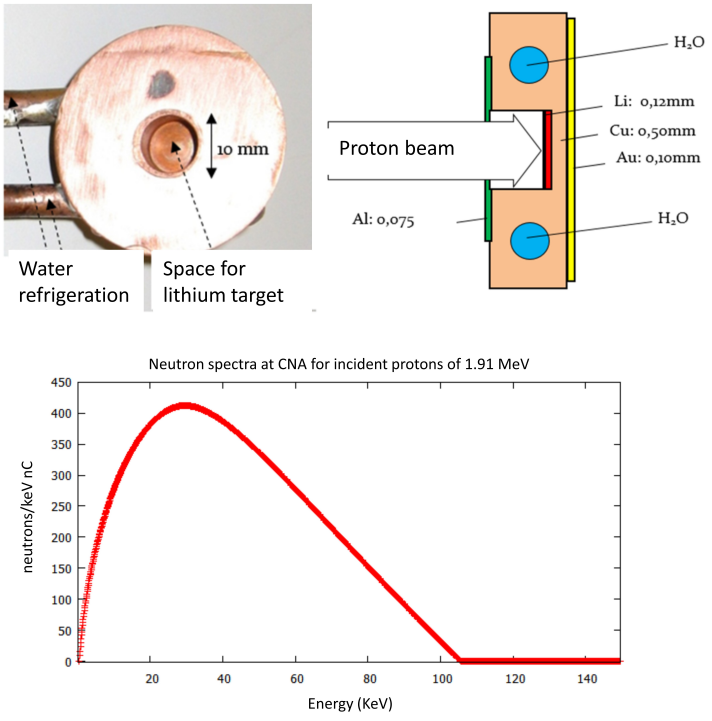

Figure 4.6: Cooling system for the ^{7}Li target installed at the Tandem accelerator in CNA (Sevilla) [Jime18c] and the neutron spectra obtained after the nuclear reaction $p + {}^{7}Li \rightarrow n + {}^{7}Be$.

4.2.3 Hospital LINAC

Many hospitals use photon radiotherapy as a cancer treatment. That it is why it is common to find linear accelerators (LINACs) in big health care facilities. One of these accelerators is situated in the University Hospital "Virgen de las Nieves" in Granada, Spain. This Elekta Versa HD™ accelerator can deliver flattened photon beams of 6MV, 6MV flattening filter-free (FFF), 10 MV, 10 MV FFF, and 18 MV as well as electron beams of 4-15 MeV [Nara16].

In LINACs, electrons are accelerated through a linear path thanks to time-varying electric fields inside a radio-frequency cavity. The electron beam is then stopped in a heavy metal target, resulting in a photon beam. The photon beam is subsequently collimated in a way that is suited to the patient and tumor shape.

As photons damage all the tissue along their track, the key in this kind of treatment is the geometry. The desired high dose is given to the tumor by irradiating from different angles, since the head of the accelerator (also called "gantry") can turn around the patient. Systems to improve the collimation, like multileaf collimators or moving stretchers, are some of the options that these accelerators can include.

For this kind of accelerator, a different unit to measure the dose is used, called monitor units (MU), which is a machine-dependent unit. This dose can change with time, so ionization chambers are used to measure this quantity every day and to make the transformation from this unit to the commonly used Grays.

As they are not designed for *in vitro* experiments but for patient irradiation, the set-up needed adaptation. A big advantage of using a LINAC for our experiments is that, thanks to the treatment planning system, the dose can be calculated accurately with the help of a CT (Computed Tomography) image. The key point is to have a set-up that guarantees the electronic equilibrium. To assure electronic equilibrium, variations of sample density along the track of the photons should be avoided; hence samples are surrounded by a material of the same density.

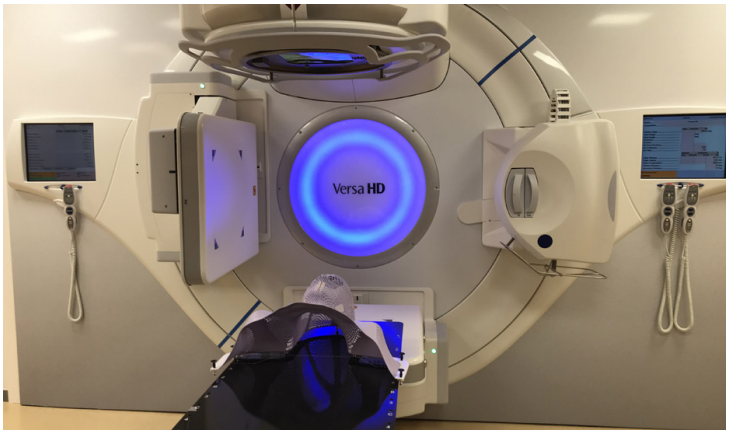

Figure 4.7: Elekta Versa HD™ accelerator at the University Hospital "Virgen de las Nieves" used daily to treat patients with radiotherapy, but also used for *in vitro* irradiations in Experiment V.

4.3 Set-up selection and dose calculations

Each of the three beams (PF1b at ILL, CNA and the LINAC) will require the use of different materials around the samples. Low energy neutrons can be captured easily in some materials such as boron or lithium, so the material selection will be key. Epithermal neutrons penetrate more than thermal ones. Ultimately, photons can penetrate most materials, but for an accurate dose estimation, there has to be electronic equilibrium conditions.

All three different beams are used to irradiate cells, which have to remain alive during the irradiation. Therefore, maintaining the cells in good conditions during the whole process is also an essential part of the experiment design.

The dose has to be estimated as precisely as possible, that is the reason why adherent cells were used in all experiments. Cells will be attached in one thin layer, perpendicular to the beam, where the dose will be constant in all the cells. If the cells are in suspension, it may induce a dose dependence in depth as function of their position inside the container, especially for the cold neutron irradiation, where the beam features change a lot along the path.

Once each set-up is designed, neutron doses will be calculated using the MCNPx simulation code for neutron transport, as explained in Chapter 3. The photon dose in the LINAC will be calculated thanks to the treatment planning program used for patient dose design.

4.3.1 ILL Set-up

As it was explained in Section 4.2.1, the beam at ILL contains mainly cold neutrons. The beam is already very "clean", so the objective of the set-up is to avoid the creation of fast neutrons and gammas as much as possible. Another aspect is crucial: keeping the cells alive during and after the irradiation, and without any bacterial contamination. In this perspective, the set-up must keep an equilibrium between having a good cold neutron beam without a lot of gammas and maintaining the cells "comfortable".

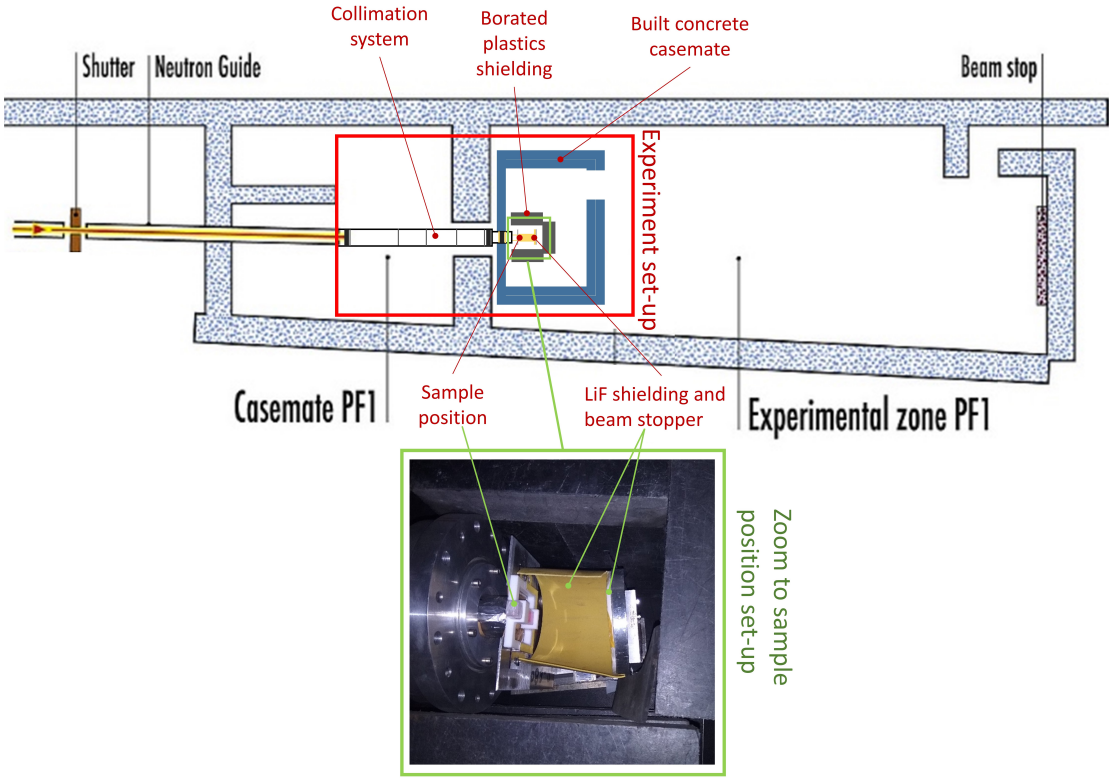

Figure 4.8: Layout of the PF1b zone with the mounted set-up for cell irradiations at ILL (Experiments I, II and III). Indicated in red is the built experiment set-up, including the sample position, the shielding around, the concrete casemate and the collimation system. The photo shows a top view with the samples in quartz cuvettes in place and yellow LiF rubber shielding around.

As PF1b is a "build your own set-up" type of beam line, there is an empty zone with a hole where the H113 guide finishes. That means that sample holder, collimation and shielding should be installed (what we called "experimental set-up" in Figure 4.8). The collimation used has been described in Section 4.2.1. Once the irradiation position is settled, shielding is installed. The shielding consists of (i) a layer of LiF to act like a beam stopper, to stop also

scattered neutrons and to avoid gamma emission and (ii) boron doped polyethylene bricks to capture the few neutrons that could escape the LiF. Surrounding all of this is a concrete casemate with a lead roof to stop particles (mostly gammas), and maintain a secure area around the experimental set-up.

The cell container and set-up at the irradiation position is the next key factor. The material for the container needs to be as transparent as possible for the neutrons, to avoid excessive activation during neutron irradiation, to allow the natural attachment of the cells to its surface, and to be capable of containing media to keep the cells alive. After some trials in 2016 with handmade aluminum and mylar boxes (See Figure 4.9 left), we found that the cells attach naturally to the Hellma quartz cuvettes that are often used for UV/Vis spectroscopy and flow cytometry (Hellma, Müllheim, Germany). Quartz is a good choice of cell material due the low capture (0.11% traversing cold neutrons capture per mm of quartz), the low levels of scattering (2.8% of traversing cold neutrons scatter per mm of quartz) and its transparency, which helps to visually check the cells behavior inside. These were the containers selected for the experiments; they are referred as “cuvettes” from here on.

Figure 4.9: Containers for cell irradiation at ILL. Left - a handmade container made in aluminum and Mylar used in the first trials of ILL irradiations. Right - the Hellma quartz cuvettes of 2mm depth, *i.e.* water layer thickness, that were selected as the final containers for the experiments at ILL.

These cuvettes are filled with 200 µl of cell suspension in culture medium (more information about sample preparation in Section 4.5). Once the cells are attached, the cuvettes will be placed in the beam. A Teflon holder that slides inside a rack maintains the cuvettes in the same position, aligned with the beam, thus allowing all the cells to be irradiated equally (see Figure 4.10) .

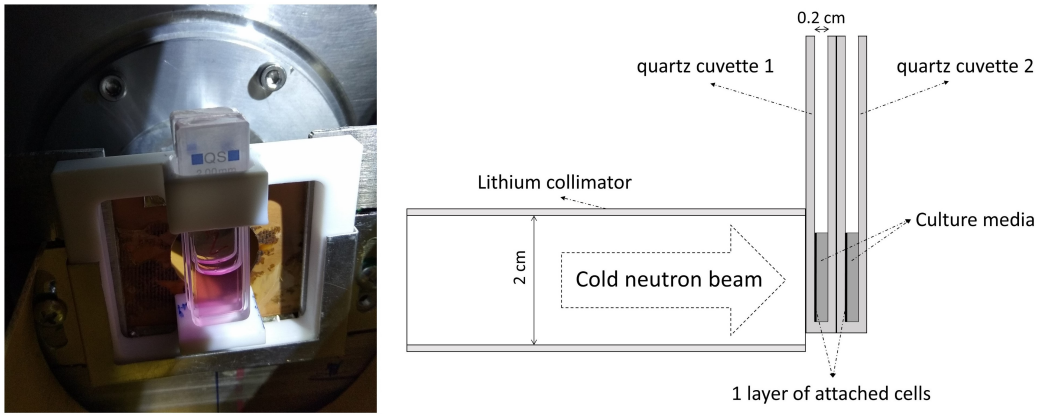

Figure 4.10: Left, picture of the cuvettes, filled with 200 µl of cell suspension, placed at the beam exit inside a teflon holder. On the right, outline of the two cuvettes placed at the end of the beam, with the cells attached in the layer facing the beam and filled with culture media.

The thickness of the cuvettes was also an important issue. A large width allows easy handling of the media. However, larger amounts of media result in more neutron scattering and the creation of more secondary gammas. After various simulations (as summarized in Table 4.2), it was decided to use 2mm wide cuvettes, which allows cells to be extracted using thin pipettes while keeping the gamma ray dose component below half of the total dose. Additionally, since access to ILL beams is highly competitive and beam time may be limited, it was decided to irradiate a stack of two cuvettes at the same time. This allowed the collection of more data per irradiation while still minimizing the gamma level.

Cuvette characteristics	Thermal Dose (Gy/h)	Gamma dose (Gy/h)
 1mm	1.90	0.56
 2mm	2.02	0.79
 3mm	2.05	0.94
 1 cuvette	2.02	0.79
 2 cuvettes	2.03, 0.95	0.80, 0.60
 3 cuvettes	2.04, 0.98, 0.43	0.83, 0.67, 0.42

Table 4.2: MNCPx Simulated thermal and gamma doses in the layer of cells (ICRU-33 tissue) in each cuvette, depending on the set-up. With the idea of having the less gamma dose as possible, as well as maintaining the cells with enough media to survive, the 2mm cuvettes were selected. In order to have more data per irradiation, but still keeping the thermal dose much higher than the gamma in all the samples, two cuvettes were irradiated at the same time. Data is normalized to flux measured in June 2018.

The undesired doses of gammas and epithermal neutron need to be controlled and limited as much as possible. An analysis of these undesired doses is shown in Table 4.3. The capture of neutrons in most materials will result in the creation of gamma rays, especially with the hydrogen of the culture media, so a study about the influence of the different set-up materials to the gamma production was performed (Table 4.3). The first shielding must be LiF, because boron-based shielding would create secondary gammas due to the boron capture. Therefore, the beam stopp and the first shielding layer surrounding the sample was LiF (yellow material in the pictures). This material can create secondary fast neutrons when neutrons are captured by the lithium [Lone80]. In order to estimate this effect, we simulated the beam-stopper in different positions to finally see that, even when it is situated just after the samples, the fast neutron dose is still 10^4 times lower than the thermal one (shown in Table 4.3).

Set-up	Gamma Dose (Gy/h) in cuvette 1
Beam + cells	0.03
Beam + cells + 2 mm culture media	0.45
Beam + cells + 2 mm culture media + quartz cuvette	0.79
Beam + 2 complete quartz cuvettes (real Set-up)	0.80

Set-up	Fast Dose (Gy/h) in cuvette 2
Beam-stopper at 8.1 cm (real Set-up)	10^{-6}
Beam stopper at 0.01 cm	10^{-4}

Table 4.3: Simulation of sources of undesired doses for ICRU-33 tissue at ILL set-up. First, the gamma dose due to the different components of the set-up, simulated in MCNPx. Second, fast dose due to the neutron capture in the LiF. This simulation is based on a beam stop emitting isotropically 10^{-4} fast neutrons per thermal capture [Lone80]. All data is normalized to the flux measured in June 2018.

The final set-up is shown in Figure 4.10 and Figure 4.11. Before each experiment, the beam was aligned with the holder to make sure that all the cells are irradiated.

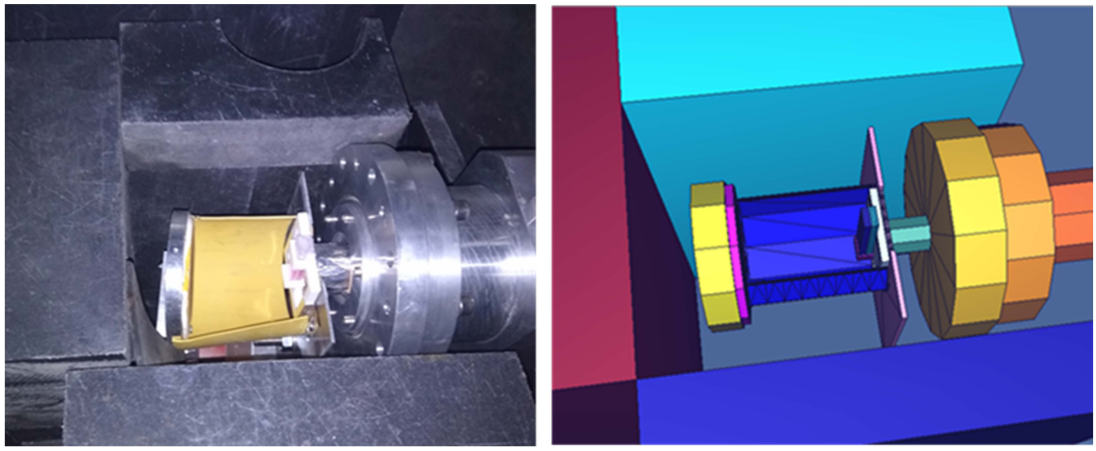

Figure 4.11: Picture of the set-up at Pf1b beam exit for the experiments at ILL, with two cuvettes placed in the sample position. Next to the picture, the geometry of the experiment simulated with MCNPx neutron transport code visualized with the program 3D VisedX-22S.

Doses were calculated using MCNPx simulations, as explained in Chapter 3 and adding some details in Appendix A. The entire set-up after the beam collimation system was included in the simulations, with all the materials and geometries included as accurately as possible (Figure 4.11). The simulated neutron spectra of the beam following collimation for each sample is shown in Figure 4.12. The final dose components for the samples on different irradiation dates

(as the neutron flux can vary) are indicated in Table 4.4. The statistical uncertainties of the fluence from MCNPx simulations are less than 1% and the error of the kerma factor used to calculate the dose is less than 5% (ICRU recommendations). The good temporal stability of the beam and the stable positioning of the samples add a systematic error of no more than 3%. The neutron shutter was operated manually which introduces a scatter in effective irradiation time of 2% on average (up to 5% for the shortest irradiations).

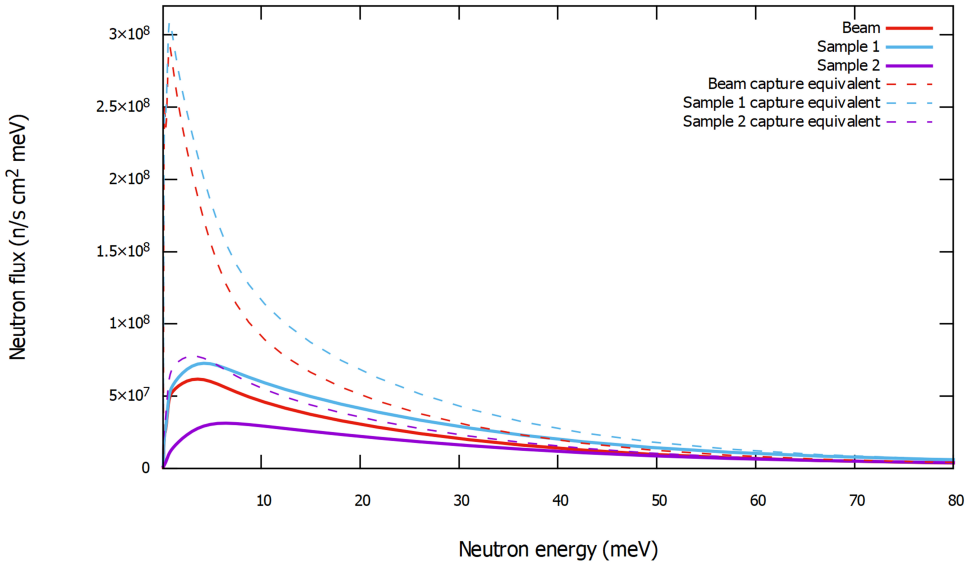

Figure 4.12: PF1b beam spectrum following collimation (red) and the beam spectrum in the two samples (cells inside the cuvettes) irradiated simultaneously (sample 1 in blue and sample 2 in purple), per meV. The neutron flux at sample 1 is higher than in the beam one due to neutrons back-scattered from cuvette 2. Dashed lines correspond to the capture equivalent spectrum (per meV) of the beam and at each sample.

The main objective of the ILL set-up, (which made these experiments different from similar ones in other facilities), was achieved: most of the dose that the cells receive is due to low-energy neutrons. The gamma dose component remains lower than the thermal one in all the irradiations and the fast neutron component is negligible. For cuvette 1, more than 70% of the total dose corresponds to thermal neutrons, while in previous measurements in other facilities the gamma dose was always higher than the thermal one.

This set-up and beam were used in Experiments I, II and III, but the irradiation times depend on the experiment and the measured flux. For Experiment I, times of 15, 30, 60 and 75 minutes were used in order to have a maximum of around 3-4 Gy of total dose, enough to see a strong

effect in the cells due to neutron irradiation. For Experiment II, cells labeled in nitrogen 15 will be less affected, because of the absence of nitrogen capture. Hence, longer irradiation times were set to study the survival effect. For Experiment III, the opposite happens: since the samples contain boron, there are more captures and a strong effect can be seen after short time irradiations.

Sample and date	Thermal dose rate (Gy/h)	Gamma dose rate (Gy/h)	Fast neutron dose rate (Gy/h)	Total dose rate (Gy/h)
Cells in quartz 1 (June 2018)	2.03 (72%)	0.80 (28%)	10^{-6}	2.83
Cells in quartz 1 (September 2018)	1.22 (72%)	0.48 (28%)	10^{-6}	1.70
Cells in quartz 1 (June 2019)	3.25 (72%)	1.28 (28%)	10^{-6}	4.53
Cells in quartz 2 (June 2018)	0.95 (61%)	0.60 (39%)	10^{-6}	1.55
Cells in quartz 2 (September 2018)	0.57 (61%)	0.36 (39%)	10^{-6}	0.93
Cells in quartz 2 (June 2019)	1.52 (61%)	0.96 (39%)	10^{-6}	2.48

Table 4.4: MCNPx simulated dose components for the cells in each of the two cuvettes for a ICRU-33 four components tissue. The different dates correspond to the different beam times where the neutron flux at the set-up varied. For cuvette 1, more than 70% of the dose is due to thermal neutrons. For cuvette 2, around 60% of the total dose is due to thermal neutrons.

More details about characterization of the set-up of the irradiations at ILL are included in Appendix A.

4.3.2 CNA Set-up

The neutron beam at CNA has energies from 10 to 100keV. By comparison with the experiment of the previous section, using the ILL cold neutron beam, the capture probability of these epithermal neutrons was lower, while the scattering probability is higher.

The same quartz cuvettes used at ILL were used in this experiment because of their low probability of neutron interaction and the well stablished protocol for growing cells inside those cuvettes. As the neutron flux is lower than at ILL, the irradiation times were longer. The

epithermal neutrons have higher transmission through the cuvettes, which allowed 4 cuvettes to be irradiated at the same time.

One of the most significant non-desired doses that contaminates the beam and "blur" the effect of the epithermal neutrons is the 478 keV gammas coming from the lithium target [Lee99]. In order to minimize the quantity of these photons interacting with the samples, a 0.4cm layer of lead is situated between the beam and the first cuvette. With this configuration, the photon dose component reaches 30% of the total dose in the 4th cuvette (lower in the other cuvettes).

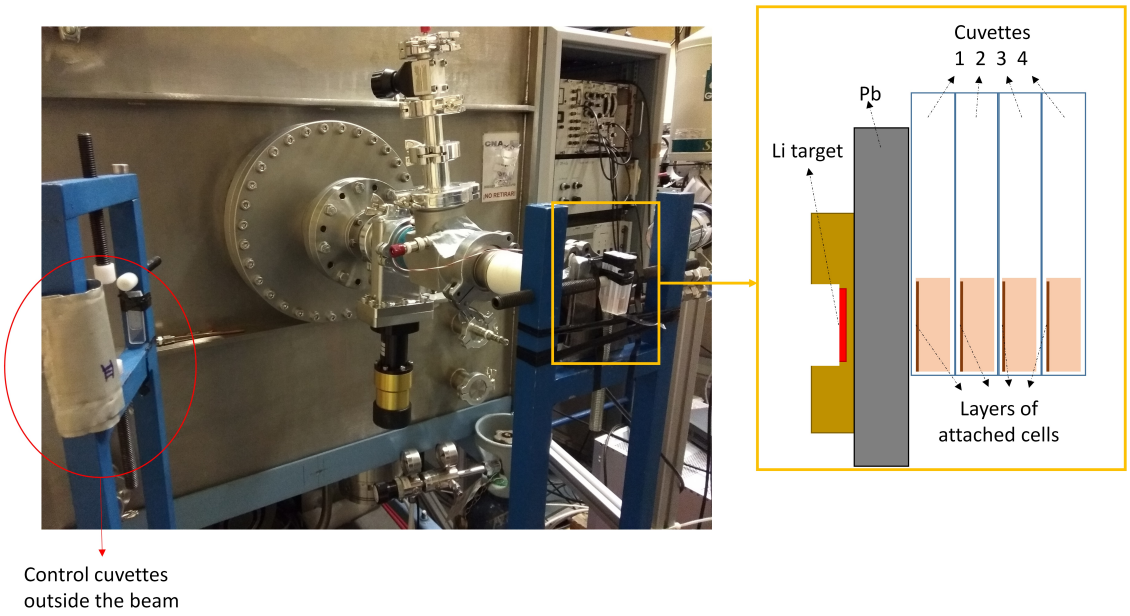

Figure 4.13: Set-up at the CNA epithermal neutron irradiation. The tube of the tandem proton accelerator ends in the lithium target that generates the neutrons. Lead foil stops some of the gammas coming from the target. On the right, the 4 cuvettes following the lead layer are visible. On the left side of the picture, outside the beam, two controls samples are placed, one surrounded by cadmium (gray metal shield).

The set-up consists of 4 quartz cuvettes positioned in a row along the beam axis, filled with 200 µl of culture media and with the cells attached on one of the internal faces of the cuvette (same set-up as at ILL, but with four cuvettes instead of two). Apart from these four irradiated cuvettes, there are four control samples: two outside the irradiation room as a control without any irradiation, and two inside the irradiation room, but situated outside the neutron beam. The objective of the two control cuvettes placed inside the irradiation room is to check the effect of

the thermalized neutron component. One of the inside control cuvettes is surrounded by a cadmium foil, which will capture neutrons. Hence one control receives a larger gamma dose and less neutrons than the other.

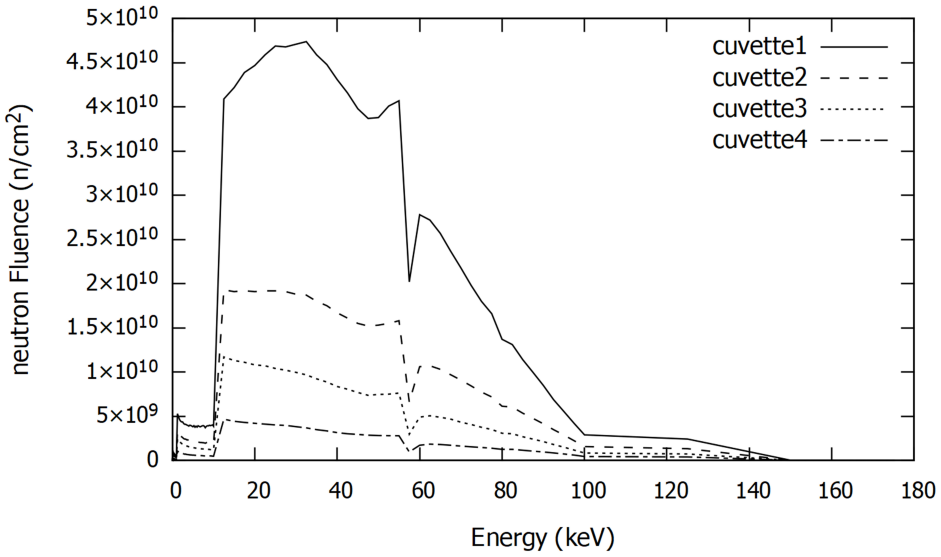

Figure 4.14: neutron spectrum for 5 hours of irradiation in the layer of cells of each cuvette. The dip at 56keV correspond to the silicon elastic scattering resonance.

For a beam of 1.91 MeV protons, $2.41 \cdot 10^{10}$ neutrons/mC are generated [Lee99]. For 5 hours of irradiation at 4μA current, a total of $1.74 \cdot 10^{12}$ initial neutrons are obtained. At the aforesaid proton energy, the number of photons is 6.84 times bigger than the number of neutrons generated in the target, which gives a total of $1.19 \cdot 10^{13}$ photons.

By MCNPx simulations, the dose rate for each component in each cell layer of the cuvettes is obtained and shown in Table 4.5.

Sample	Thermal dose rate (Gy/h)	Gamma dose rate (Gy/h)	Fast neutron dose rate (Gy/h)	Total dose rate (Gy/h)
Cells in cuvette 1	$9.5 \cdot 10^{-6}$ (0.001%)	$2.55 \cdot 10^{-1}$ (28%)	$6.63 \cdot 10^{-1}$ (72%)	$9.19 \cdot 10^{-1}$
Cells in cuvette 2	$8.6 \cdot 10^{-6}$ (0.002%)	$1.00 \cdot 10^{-1}$ (27%)	$2.75 \cdot 10^{-1}$ (73%)	$3.75 \cdot 10^{-1}$
Cells in cuvette 3	$8.5 \cdot 10^{-6}$ (0.004%)	$4.97 \cdot 10^{-2}$ (26%)	$1.39 \cdot 10^{-1}$ (74%)	$1.89 \cdot 10^{-1}$
Cells in cuvette 4	$4.3 \cdot 10^{-6}$ (0.006%)	$2.27 \cdot 10^{-2}$ (30%)	$5.41 \cdot 10^{-2}$ (70%)	$7.69 \cdot 10^{-2}$
Cells in cuvette CT1 (inside the room)	$2.1 \cdot 10^{-7}$ (0.100%)	$1.80 \cdot 10^{-4}$ (89%)	$2.13 \cdot 10^{-4}$ (11%)	$2.02 \cdot 10^{-4}$
Cells in cuvette CT2 (inside the room) + Cd	$1.6 \cdot 10^{-7}$ (0.064%)	$2.33 \cdot 10^{-4}$ (95%)	$1.32 \cdot 10^{-4}$ (5%)	$2.46 \cdot 10^{-4}$

Table 4.5: MCNPx simulated dose components at CNA for A375 cells in each of the four cuvettes placed in the beam and the two controls (CT) inside the room. Current of 4μA.

Given the low availability of the beam and the novel character of the experiment, only 3 irradiations took place at CNA, with the idea of developing more experiments of this kind in the future. For three consecutive days, A375 cells were irradiated for 5 hours under the same conditions in order to obtain the triplicate.

4.3.3 Hospital LINAC Set-up

For the photon irradiations in the hospital LINAC, we worked in collaboration with the radiophysic group of the Hopital Universitario Virgen de las Nieves (Granada). These colleagues took care of the set-up design and dose calculations as well as being part of the team involved in each irradiation.

Cells are placed inside T25 flasks instead of the quartz cuvettes used in neutron irradiations. Since the quartz is not necessary and since plastics have a similar density to water, we chose to use the normal cell culture flasks.

Two flasks were irradiated at the same time to have duplicate data for each irradiation. The flasks need to be completely filled with culture medium and bubbles must be avoided in order not to distort the dose. For the irradiations, as noted in Section 4.2.3, enough dispersed media must be placed around the flask to guarantee the electronic equilibrium. In our case, this media was distilled water and solid water.

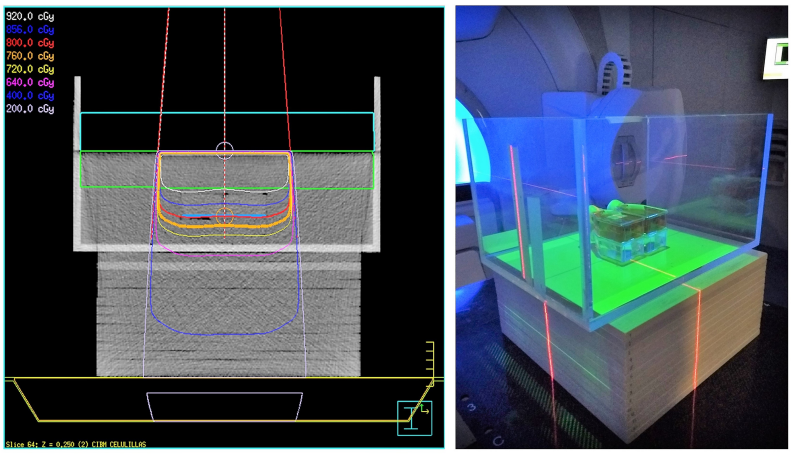

Figure 4.15: Systems used to obtain an accurate dose delivery. Left; CT scan image of the treatment planning program (Pinnacle, Philips). The dose in depth along the beam is calculated and illustrated with different colors. Different densities are taken into account. The dose estimated in the is 800cGy in this case (red marks). Right; laser alignment system to check the position of the flasks before each irradiation.

For the dose estimation, a computed tomography scan (CT scan) image and a treatment planning program (Pinnacle, Philips) were utilized. First, a CT scan image of the set-up is taken (see Figure 4.15) and analyzed to fix the position where the cells will be placed. A field size for which the cells are homogeneously irradiated, is then chosen. In our case, the field used was 15x15 cm. Following this, the dose in the monolayer of cells was calculated with an accuracy of 1%.

To keep a precise dose it is necessary to carry out a daily check before the irradiation. This involves testing the dose in the sample position with an ionization chamber to calculate the factor cGy/MU, a value which depends on the machine and the day.

The final set-up was based on previous works involving similar irradiations [Mack07, Butt10]. It consists of a base of 14cm of solid water plus a poly(methyl methacrylate) cask where the flaks are situated and attached. The container is subsequently filled with distilled water (see Figure 4.16). Thanks to the use of alignment lasers, the holder maintains the flasks in a fixed place and the system is extremely well positioned. Hence the dose estimated for the cells is very accurate.

For Experiment V, photon irradiations of 2, 4 and 6 Gy with a dose rate of 1 Gy/min were performed during the first half of 2019 in four different cell lines.

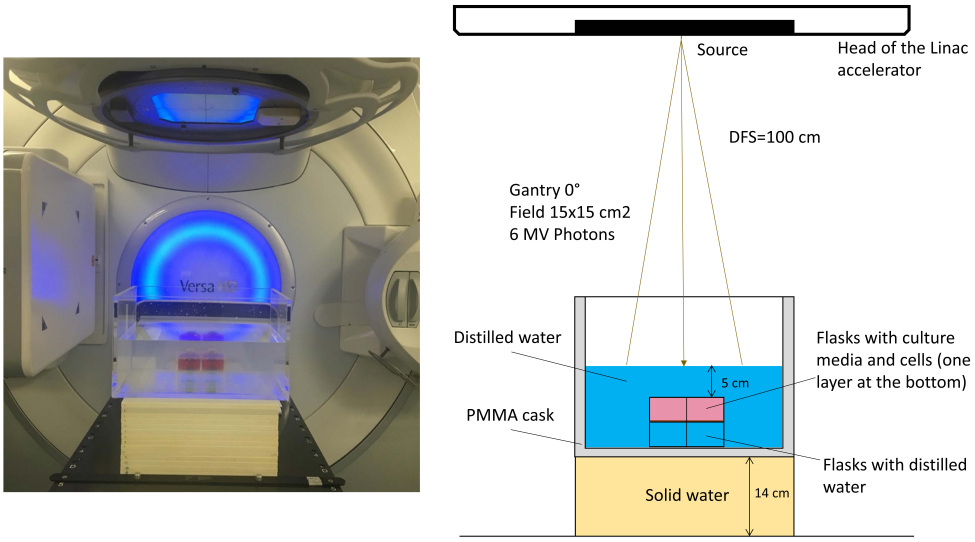

Figure 4.16: Set-up for the irradiations in Experiment V. A picture (left side) and a drawing (right side) are shown of the set-up used in the LINAC, where the two flasks are centered. These are fixed using the holder system and covered with distilled water. DFS for source-sample distance and PMMA for the material Poly-methyl methacrylate.

4.4 Cell culture and cell lines

Human cell lines were chosen because of their availability, easy handling and maintenance in culture. Moreover, the selected tumor cell lines correspond to the type of tumors that have been treated with BNCT (list in Table 4.6). All of them are adherent cells, since it is a requirement in all set-ups. For comparison with normal (non-tumor) cells, the last two cell lines of Table 4.6 were selected.

Most of the cell lines were provided by Dr. Lucie Sancey from Institute of Advance Biosciences, Grenoble. The exception is line Hek293, which was acquired commercially (Thermo Fisher, Massachusetts, UE).

Cells were cultured in DMEM medium (HyClone, Logan, USA) containing 10% fetal bovine serum (FBS; Gibco, California, USA), 1µM L-glutamine (Gibco, California, USA), 100 IU/ml penicillin and 100 IU/ml streptomycin (Sigma-Aldrich, St. Louis, USA) at 37°C in a humidified CO_2, 95% air incubator. Cells were detached with 1% trypsin-EDTA (Sigma-Aldrich, St Louis, MO, USA) when they reached 90% confluence, and then diluted and reseeded with fresh medium.

Cell line	Type	Tissue
A375	Tumor	Human Malignant Melanoma
Cal33	Tumor	Human tongue squamous cell carcinoma
U87	Tumor	Likely glioblastoma, human brain tissue
SQ20	Tumor	Human squamous cell carcinoma
Hek293	Healthy tissue	Human embryonic kidney
MRC5	Healthy tissue	Human lung fibroblast

Table 4.6: Cell lines used in the experiments. In Experiment I, the six cells lines were irradiated. For Experiment II, only Hek293 was used. Experiment III included four of these cell lines. In Experiment IV, as it is a trial, only one cell line was used. Finally, for reference irradiation (Experiment V), four cell lines were used.

Tumor cell lines (A375, Cal33, U87 and SQ20) grow easily and fast, while the MRC5 healthy fibroblasts grow slowly and lose the proliferation capacity after several passes. Hek293 is an especially healthy cell line, as it is transformed with adenovirus type 5 DNA, showing a proliferation ability similar to that of a tumor cell line.

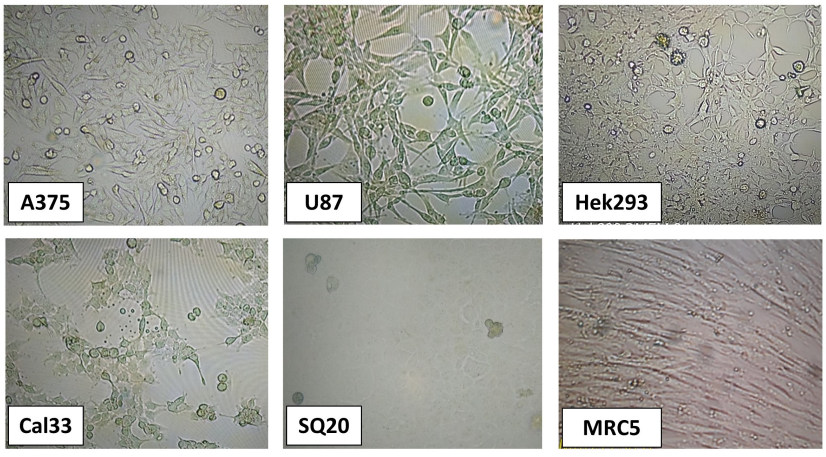

Figure 4.17: The different cell lines viewed under the microscope (Leica DMi1) using 10x magnification.

In order to have good statistics in the results, all the cell lines were irradiated more than once and ideally on different dates so that valid duplicates / triplicates data were acquired. Because of the limited irradiation time and the necessity of irradiating each cell line several times, not

all the cell lines were used in all the experiments. In any case, those that could not be included in these experiment rounds were retained for future work, as well as new cell lines that will contribute to the data available for different tissues.

All the cell lines were irradiated in Experiment I, the low energy neutron data experiment. For Experiment II, only Hek293 cells were used, since the media for nitrogen labeling is limited and it yielded good results. In Experiment III, the boron compound study, the four cell lines giving better results in experiment 1 were used (A375, Cal33, Hek293 and MRC5). In Experiment IV, only melanoma cells were used. Moreover, for Experiment V, four of the cell lines (the same as in Experiment III), that were available in Granada, were irradiated in the hospital LINAC.

All the cell cultures and sample preparations were carried out in the level 2 laboratories situated nearby the facilities. For Experiment V, the laboratory is situated inside the Centro de Investigación Biomédica (CIBM, University of Granada). For Experiment IV, samples were prepared in the Medical and Biophysical Physiology department at the University of Sevilla. For the experiments carried out at ILL (Grenoble), a level 2 lab inside the campus in the Life Science Group was used for cell preparation. In addition, as the irradiated samples are considered radioactive and it is difficult to transport them outside the experimental area, a new cell culture laboratory was installed inside the instrument hall of ILL (details in next sub-section).

4.4.1 Level 2 Laboratory within ILL's instrument hall

The large number of irradiations planned at ILL (Experiments I, II and III) during the limited beam time available resulted in the need for a level 2 lab near the neutron data collection instrument. The installation and management of this new lab was an important part of this thesis work. It was used to prepare the samples before and after the irradiation. As noted above, preparation of the cell lines and posterior analysis were carried out in the laboratories of the Life Sciences Group within the PSB (Partnership for Structural Biology) in the CIBB (Carl-Ivar Brändén) building.

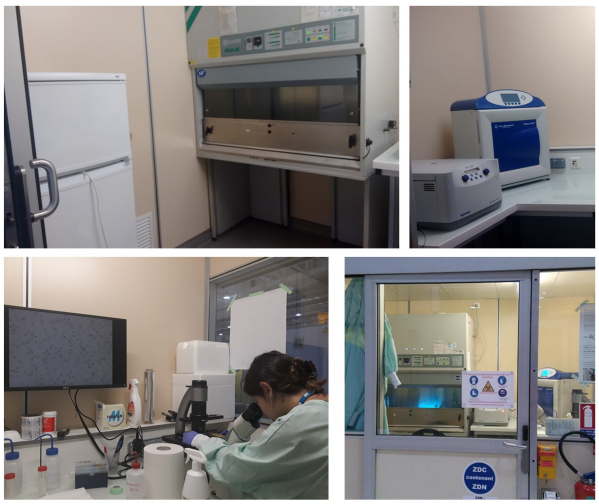

Figure 4.18: The new level 2 laboratory situated inside the controlled area of the experimental guide hall at ILL.

The laboratory is situated within easy walking distance from the PF1b zone, where the irradiations took place. It includes all the equipment necessary for cell culture: a hood, a fridge, a centrifuge, an incubator and a microscope. It does not contain a sink since running water is not permitted inside the radiation-controlled area. For the same reason, the waste, considered as biological and radioactive, is managed in a different way. These arrangements allowed a high quantity of irradiations to be performed in an efficient and practical way.

The installation of this new lab opens the possibility for other groups to perform easily other biological experiments at ILL that involve *in vitro* irradiation.

4.5 Sample preparation

Samples used for neutron irradiation, *i.e.,* Experiments I, II, III and IV, were placed inside the quartz cuvettes (Section 4.3.1) 12-24 hours before the irradiation. Between 150000 and 200000 cells in 200µl culture medium were seeded into the cuvettes. The cuvettes were then left inside the incubator - positioned horizontally to help the cells to attach to the back wall of the quartz after few hours (see Figure 4.19).

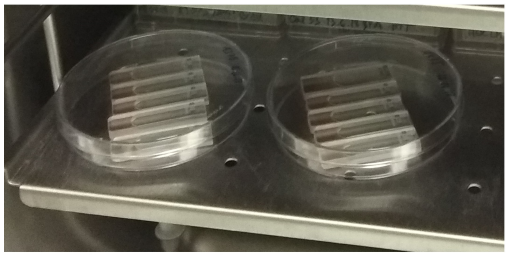

Figure 4.19: Quartz cuvettes with 200µl cell suspension are incubated horizontally inside Petri dishes to avoid contamination. After 12-24 hours incubation, the cells will be attached in one layer in the area covered by culture media.

Samples used for gamma irradiation (Experiment V) were irradiated inside T25 flasks, completely filled with media, with the cells also attached in one layer of the flask.

Before all the irradiations, media was exchanged by fresh media, so that cells not attached or dead could be eliminated.

After the irradiation, the cells were recovered by detaching with 1:100 dilution of trypsin-EDTA (Sigma-Aldrich, St Louis, MO, USA) in PBS (phosphate buffered saline). In the case of the quartz cuvettes, the detachment was performed with the help of long glass Pasteur pipettes so that the bottom of the container could be reached. Finally, each sample was counted and prepared for the different survival assays.

4.5.1 Samples with boron

For samples that contained boron, the compound added to the cells was the most used compound in BNCT, *i.e.* BPA (See Chapter 1).

The ^{10}B enriched BPA (Katchem Ltd, Czech Republic) was prepared at a concentration of 10000ppm of ^{10}B in a 0.1 molar solution of fructose. The pH was adjusted to 9.5-10 to make it soluble, and re-adjusted to 7.4 afterwards [Gara14]. The BPA dilution was then added to culture medium inside the cell container to get the desired concentration of 80 ppm of ^{10}B. Maximum uptake is reached 2-4 hours after the compound addition [Krei01]. Hence samples were incubated with the BPA solution at least 4 hours before irradiation.

Before the irradiation, the medium with the BPA was entirely removed and replaced by normal medium without boron, to ensure that the observations recorded arise from boron inside the cells and not from boron in the medium.

The data for survival following irradiation is in itself insufficient to identify the effect of the boron compound. It is also necessary to know how much boron was inside the irradiated cells. Since boron concentrations inside the cells are no more than few tens ppm of ^{10}B, very sensitive methods are required to measure it.

We have used two ways of analyzing the boron uptake:neutron autoradiography and Inductively Coupled Plasma-Atomic Emission Spectroscopy (ICP-AES).

Boron compound measurements, autoradiography (Experiment IIIa)

Neutron autoradiography is a technique where the samples are situated on a solid state nuclear track detector that will show the tracks of the secondary charged particles created in the sample after the neutron irradiation [Post16]. Following neutron capture, the samples containing boron will release ^{7}Li ions and α particles. In this technique, these secondary particles will be stopped in a solid detector and leave traces that are revealed after chemical etching (example in Figure 4.20, right image). In this way, information both about concentration and position of the boron is yielded as well as information on its homogeneity in the sample. Hence, the method allows simultaneous acquisition of both quantitative and qualitative data.

Neutron autoradiography is complemented by a similar technique called alpha spectrometry [Bort13, Bort14], which uses silicon detectors instead of nuclear track detectors to detect the alpha and lithium recoils.

Specialists have been working for many years on neutron autoradiography at the thermal column of the TRIGA MARK II nuclear reactor at the LENA laboratories of the University of Pavia in Italy [Bort14, Post16], confirming results on boron concentration measurements by comparison with other techniques such as ICP-AES. They have developed a protocol using CR39 as the solid detector and PEW40 ($KOH+C_2H_5OH+H_2O$) as the chemical solution to reveal the tracks. This solution allows the tracks of ^{7}Li and α alone to be revealed in just 10 minutes (improving a previous method with NaOH etching which took 2 hours and sometimes revealed also the tracks of protons). The CR39 films are then transported to the high definition Leica MZ16A microscope, where an image acquisition system sweeps the sample, acquiring images every 0.3 mm. The tracks are then selected by a self-developed program, depending on their roundness and ratio, to separate target data from the background and compared with a calibration standard.

For our samples analyzed in Pavia, cells were cultivated in media containing the boron compound for 4 hours (the same as the one used for irradiations at ILL for Experiment III). The cells were then counted. Four million cells were separated and centrifuged. The liquid supernatant was removed and the pellet diluted in 20 μl of medium, yielding a paste of cells. This drop of paste was deposited on a mylar foil and left to dry for at least 12 hours. Finally, the samples were placed on the CR39 films with adhesive tape and prepared for irradiation. Hence the neutron beam traverses first the tape, then the mylar, then the layer of cells, where neutrons are captured in the presence of boron, and then the CR39, where the secondary particles are stopped.

Samples of the different cell lines with different boron concentrations were prepared in Grenoble and also in Pavia. They were analyzed by using this technique thanks to a collaboration with Dr. Ian Postuma (Istituto Nazionale di Fisica Nucleare, Pavia). Some samples were also irradiated at PF1b in Grenoble so that a comparison of this technique could be made using the two different neutron beams.

Boron compound measurements, ICP (Experiment IIIb)

ICP-AES (also called ICP-OES) is a type of spectrometry that analyzes the optical emission of the elements of a sample after they are excited in a plasma. The aim of the technique is to identify the elements and quantify their concentration. The materials need to be reduced to atoms and without bounding between each other in order to avoid interferences, which is the reason why the sample preparation is a key factor of the process. This powerful technique can detect over 70 elements with a sensitivity of parts per billion (the sensitivity will depend on the element). However, it cannot analyze inert gases or some important non-metals, like C, N, O, H, and it cannot distinguish isotopes. A schematic representation of this technique is given in Figure 4.20.

This approach has proved to be one of the most widely used techniques for boron concentration measurements in BNCT samples [Krei01, Gara11, Gara13], and in patients, where the boron uptake in blood was quickly analyzed after compound injection so as to optimize irradiation doses [Joen03]. We have counted on the collaboration and expertise of Marcela Garabalino (Comisión Nacional de Energía Atómica in Argentina) to adjust the protocol used for our samples.

In the case of our *in vitro* samples, cells were cultivated in similar conditions as the ones that were irradiated. Then, they were digested in a 1:1 mixture of sulphuric and nitric acids for 60 min at more than 100°C. Next, Triton x-100 (at 5%) was added as well as the internal standard solution of Y and Sr. The final volume of the sample was 1 ml. Prior to the measurements, a calibration curve was made with the standard solution and known quantities of boron.

The measurements were carried out at the Centro de Instrumentación Científica (Center of scientific instrumentation) of the University of Granada, where the ICP machine is situated. The spectrometer used was a type ICP-AES Perkim-Elmer Optima 8300. The machine is equipped with two SCD (Segmented-array Charge-coupled Device) detectors covering a spectral range from 163 to 782 nm. Argon gas and a mercury lamp are used for the plasma generation and spray chambers are used for aerosol sample injection. The lamp and tubes are changed before measurements in order to avoid any boron contamination from previous experiments.

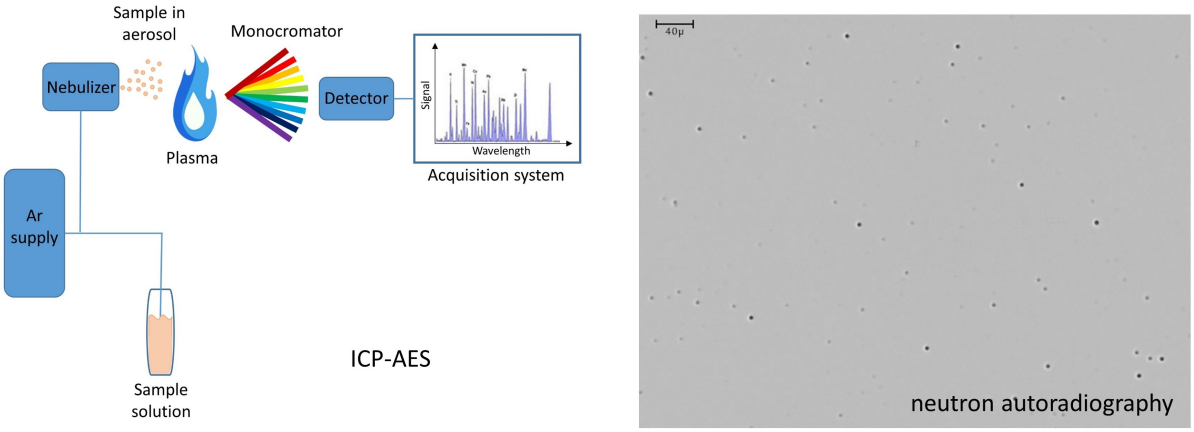

Figure 4.20: The two techniques used for boron concentration analysis. Left, a schematic representation demonstrating how ICP-AES works. Right, alpha and lithium tracks seen in the CR39 films under a microscope (40µm marked with the line in the image) [Post16].

4.5.2 Labeled samples

For the Experiment II, it is necessary to replace the ^{14}N with ^{15}N inside the cells. For this purpose, Bioexpress-6000 mammalian medium (Eurisotop, Cambridge, UK) was used in two forms, the unlabeled version for control and the labeled version (98 % enriched ^{15}N).

The media were supplied in powdered form, and then prepared following the instructions in 200ml of milli-Q water, adjusting the pH to 7.1-7.2, and filtered. The medium is then complemented with 10 % fetal bovine serum (FBS from Gibco, California, USA), previously dialyzed with a 10000K membrane against 0.15 M buffer of NaCl, and 1% of 100 IU/ml streptomycin (Sigma-Aldrich, St. Louis, USA). Hek293 cells were normally incubated in special culture media for more than 8 days, assuring 8 cell divisions and a complete uptake of the cell culture components. Then, the labeled cells would have the same proportion of nitrogen-15 as in the media. Unfortunately, the ^{15}N abundance in the labeled media is not 98%, because of the added FBS and the antibiotics, which will contain natural nitrogen. To avoid as much as possible natural nitrogen, the FBS was dialyzed previously against NaCl.

Cells were grown in unlabeled media in the same conditions than the labeled ones. These were used for comparison, to ensure that the observed effect after the irradiation was due to the nitrogen labeling and not due to the growth in a different medium.

In all other respects, the preparation inside the quartz cuvettes was the same as described for the other experiments.

^{15}N measurements, neutron autoradiography (Experiment IIa)

A similar technique to boron uptake measurements was used for the estimation of the nitrogen ^{14}N replaced by ^{15}N in the samples: neutron autoradiography. The basis of the technique is the same as that used to detect intracellular boron, but in this case, instead of the alpha track, the traces in the solid detectors are from protons emitted in nitrogen capture (see Figure 4.21). Samples having more ^{14}N show more protons tracks.

In order to reveal the proton tracks, the protocol was different than that one for alpha tracks in Experiment IIIa. In the case of Experiment IIa CR39 films were immersed in a solution of NaOH 6.5 Molar at 70°C for 6 hours in order to have proton tracks marked as the ones shown in Figure 4.21.

In this case, the samples were irradiated at ILL beam, but analyzed at LENA (Pavia).

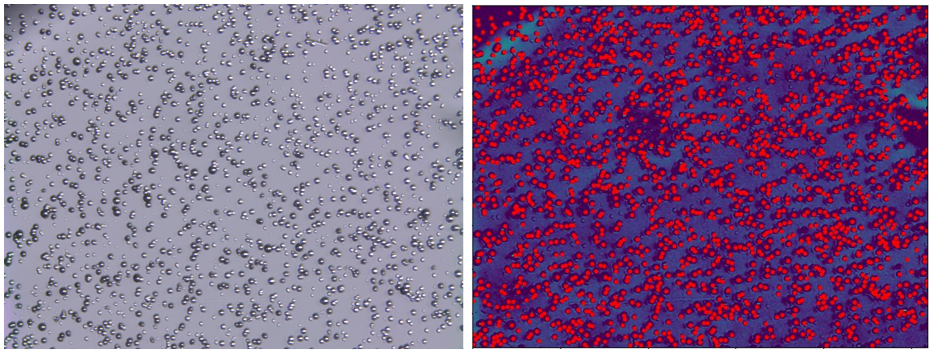

Figure 4.21: Left, microscope image (141x) of proton tracks marked in the CR39 film. Right, counting program selection of tracks (in red).

^{15}N measurements, combustion (Experiment IIb)

Cells for Experiment II were cultured in BIOEXPRESS-6000 + 10% of dialyzed Fetal Bovine Serum (FBS) medium for 8 days. Considering the doubling time of the cells (1 day), it was assumed that the percentage of nitrogen labeled in the cells was the same as that of the medium in which they were grown. If d is the number of days since cells incubation in the BIOEXPRESS-6000 medium, and considering that at day 0 the cells have a natural ^{14}N content ($[^{14}N]_0 = 0.996$), the total ^{15}N content in the cells as a function of time (in days) is given by:

$$[^{15}N\ (in\ cells)] = 1 - (\frac{[^{14}N]_{d-1} + [^{14}N\ (in\ medium)]}{2}). \quad (4.2)$$

From this it can be seen that 8 days is enough to have almost the same percentage of ^{15}N in the cells as in the medium.

The measurement of total nitrogen in the medium is possible thanks to the technique called chemical characterization by combustion in a CHNS Elemental analyzer (THERMO SCIENTIFIC Flash 2000). It is based on the dynamic combustion of a sample. Resultant gases resultant are separated and detected by a thermal conductivity detector (TCD). It can determine the quantity of carbon, nitrogen, hydrogen and sulphur in a single run.

Photon irradiations of labeled samples (Experiment IIc)

In order to prove that the difference in the survivals observed after neutron irradiations for the ^{14}N and ^{15}N samples are only due to variations on numbers of captures on nitrogen, the samples were also irradiated with photons. The exchange of ^{14}N by ^{15}N of the labeled samples in principle has no influence on the effects of photon irradiation, and it was therefore anticipated that no differences in the effect of the unlabeled and labeled samples would be observed. To confirm this, the irradiator at the CEA centre in Grenoble was used, where photons come from a ^{60}Co source immersed in a water pool. The dose rate was 1 Gy/min and dosimetry was controlled using radiochromic films [Chel10].

4.6 Survival assays

Two different types of assay were carried out after the irradiations in all the experiments. One, the clonogenic assay, provides the results for the named survival curves. The other type are colorimetric assays that give information about how many cells are still alive and how many of them can still proliferate. Two of these colorimetric assays were used: BrdU, which shows the DNA synthesis capacity, and Resazurin, which measures the metabolic activity of the cells [Yada14].

4.6.1 Clonogenic assay

The clonogenic method consists of seeding cells following the irradiation and letting them grow for days (depending on the cell line) to see the number of colonies formed (larger than 50 cells each colony). In an ideal case, without any effect on the cells, if n cells are seeded, n colonies should be counted. However, when the cells are affected by irradiation, it is necessary to seed more cells to have a countable minimum number of colonies. For most of the irradiated samples, where there is a very low survival expectancy, it is recommended to seed 10 times more cells than for the control ones (CT). The ratio between the cells seeded and the colonies counted is what is called *plating efficiency*. The survival, S, is then calculated by the comparison of the plating efficiency of the sample and the control, so that the survival of the control sample is equal to 1. The equation used is:

$$S = \frac{PlatingEfficiency_{sample}}{PlatingEfficiency_{CT}}. \quad (4.3)$$

For each cell line, the conditions for the clonogenic assay may change: the plating efficiency is different; the division time, and therefore the time to form the colonies, also varies a lot. The form of the final colonies also changes with the cell line. As we have diverse cell lines that behave differently, it is necessary to analyze them individually before using them for the experiments. This analysis for each cell line consists of trying different numbers of cells seeded and different times of incubation to check the colonies sizes and forms. The optimized values found for each cell line are shown in Table 4.7. These values are the ones used for the control samples in the experiments. The cells seeded following irradiation are estimated depending on the doses and on the growing characteristics of the cell lines.

Cell line	Cells seeded for CT	Time to reach colonies of more than 50 cells (days)	Plating efficiency of CT
A375	200	7-8	(0.4-0.8)
Cal33	400	11-12	(0.4-0.7)
U87	600	14-15	(0.009-0.06)
SQ20	400	11-12	(0.3-0.5)
Hek293	600	8-9	(0.2-0.5)
MRC5	600	14-15	(0.04-0.08)

Table 4.7: Optimal conditions for clonogenic assays found for each cell line. The values of cells seeded (in each well) and plating efficiency correspond to the control sample (CT). For irradiated samples, since they are affected by irradiation, the plating efficiency is lower and the number of cells seeded in each well needs to be higher.

The protocol for clonogenicity was as follows: after irradiation, once the cells were detached and counted, they were suspended in fresh culture medium. For each sample, the corresponding number of cells were seeded in triplicate in a 6-well plate with 2 ml of culture medium. Every four days, the medium was carefully exchanged with new medium. After the time necessary for obtaining of colonies of the desired size (see Table 4.7), the medium was removed and 1-2 ml of 90% ethanol added to each well for 30 min in order to fix the colonies. Then, they were stained by the addition of 1:20 solution of crystal violet for at least 30 min. Once the colonies were easily visible, the crystal violet was removed and the plates cleaned with water.

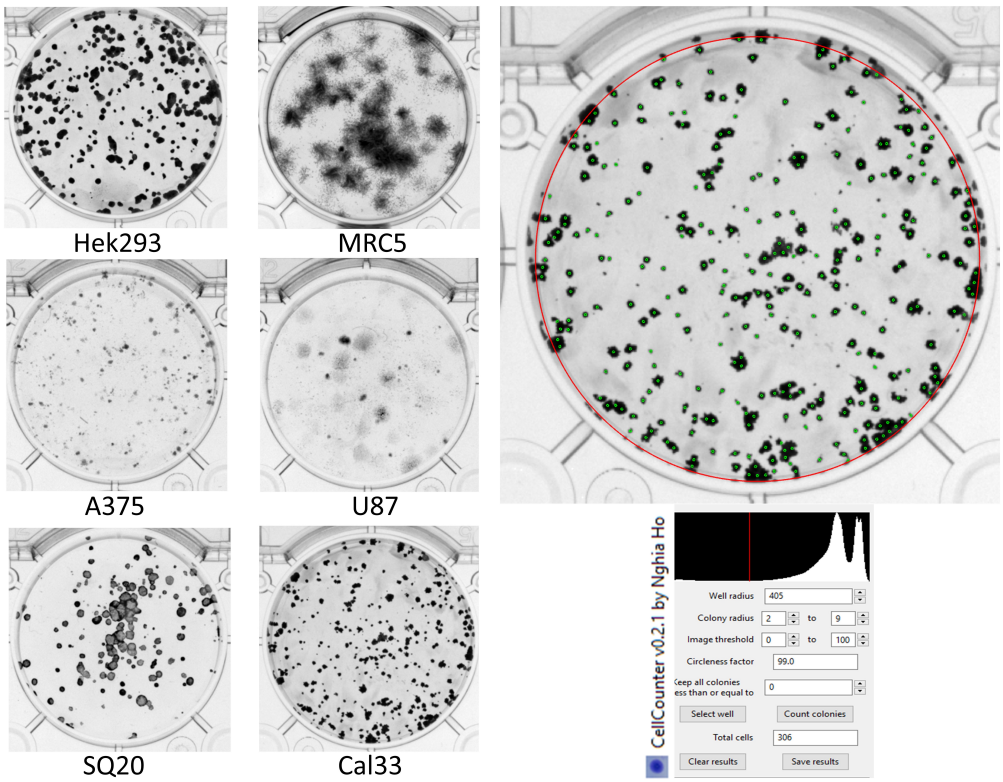

Figure 4.22: Left, cell colonies of the different cell lines. Right-top, Cal33 colonies counted with the Cell Counter program. Counted colonies are marked with green points, following the parameters shown in the bottom right image.

For colony counting, a high quality picture was taken using the BIORAD Molecular Imager CHemiDOc XRS+. Later, each individual well was counted using the open access automatic counter program by Nghia Ho [Nghiweb], which allows parameters to be set as needed. Appropriate parameters are fixed for each cell line depending on the characteristics of the colonies. In addition, each well is checked by eye after the automatic count to discard any false colonies that the program may have identified.

4.6.2 BrdU colorimetric assay

The first colorimetric assay is a 5-bromo-2-deoxyuridine (BrdU) ELISA kit (Roche, Mannheim, Germany). This is a proliferation and viability assay that is an alternative to the classic [3H]-thymide test. The results are comparable to those obtained using the [3H]-thymide assay [Yada14], but a radioactive isotope is not required and it can be easily readable with a microplate reader. The BrdU, an analog of the nucleoside thymidine, is incorporated into

replicating DNA. Viable cells after irradiation (and 24h after BrdU incorporation) are detected by adding a monoclonal antibody (anti-BrdU) conjugated with peroxidase followed by a substrate solution. The peroxide then produces a colored reaction product that can be checked in the BioRad iMark™ microplate absorbance reader.

Samples were prepared after irradiation in 96-well plates, and, unlike the clonogenic assay, the same number of cells were seeded for all doses. Three-four days after irradiation (depending on when it was desired to check the state of the cells), BrdU labeling solution was added to the samples. Twenty-four hours later, the protocol for adding the antibody starts. This process takes a total of 4 hours, after which the plates will be taken to the plate reader to read the absorbance at 405nm (reference wavelength at approx. 490nm).

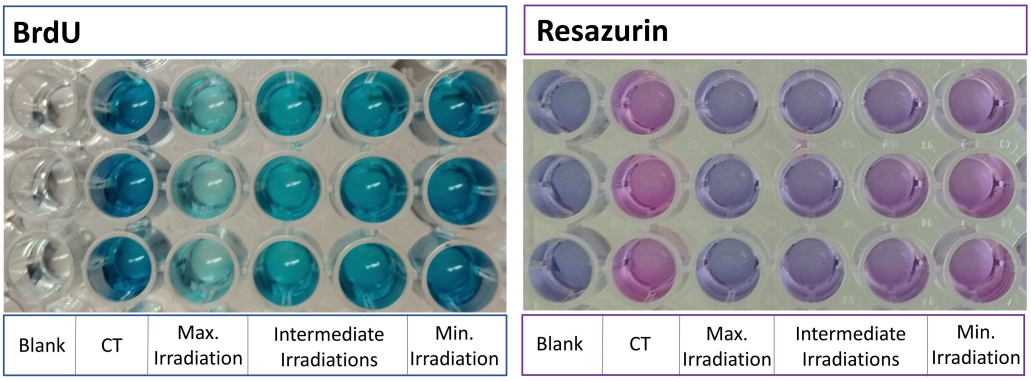

Figure 4.23: Plates with irradiated cells after two different colorimetric assays. The same number of cells were seeded in each well. The BioRad iMark™ microplate absorbance reader will read the wavelength corresponding to each color emission. In BrdU, the blank sample (only culture medium) is mostly transparent, while the control sample (CT), where most of the cells seeded have grown, is dark blue. Hence, in BrdU, the lower the number of cells in the well, the lighter the blue color of the sample. In Resazurin assay, the blank sample is dark purple while the control one is pink. Hence in Resazurin assay, the fewer the number of cells in the well, the darker the color observed.

4.6.3 Resazurin

The second colorimetric assay was done by using the PrestoBlue cell viability reagent (Invitrogen, California, UE). It contains resazurin (7-hydroxy-3H-phenoxazin-3-one-10-oxide), a blue dye that turns to a highly fluorescent pink dye, called resorufin, in metabolically active cells. The redox reactions that accompany the metabolic process of the cells makes the resazurin turn into the pink resorufin. Damaged cells have less metabolic activity; this results in a lower resorufin signal and a less pink color.

As with the BrdU assay, for each cell line, the same number of cells for each sample were seeded in a 96-well plate after irradiation (three wells per sample), changing the number of cells seeded, from 500 to 2000, depending on the cell line. Then, 4 or 5 days after irradiation, the medium in each well was changed and 10 μl of the reagent was added. After 4 hours incubation, the color changes and the absorbance could be measured in the plate reader at 562nm (reference wavelength at approx. 630nm). The fluorescence emission could also be read and it gave a higher signal, but since a comparison of the two proliferation assays was required, only absorbance was measured.

The differences observable by eye between the two different colorimetric assays can be seen in Figure 4.23.

Chapter 5

Results

In this chapter, the results of the experiments explained in Chapter 4 will be described. In order to maintain consistency in the development of the chapter, the order of the experiment results will be given as follows: firstly, Experiment V (LINAC irradiations), whose data will be used as a reference in the subsequent ones. Secondly, the results of Experiments I and III (irradiations at ILL, without and with BPA) will be given; the analyses used for both type of experiments are similar. The innovative Experiment II (irradiation of labeled samples) will then be described and the results shown. Finally, the preliminary results of Experiment IV (CNA irradiations) will be presented.

From each irradiation experiment survival curves as a function of the radiation dose were obtained after counting the colonies grown in the prepared plates. Simulations of each set of experimental conditions were necessary to estimate the irradiation dose.

The most interesting results arise from the comparison of those obtained from the different types of irradiation.

5.1 Experiment V: results of photons irradiation

Four cell lines were irradiated at a hospital LINAC for Experiment V. Colonies were counted for each cell line (Chapter 4, Table 4.6) and compared with data from the control sample to evaluate the survival. The dose was simulated in the treatment planning program, as explained in Chapter 4, Section 4.3.3. Results for the survival, S_0, due to the photon irradiation with dose D_0 in Figure 1.1 are fitted following the linear quadratic model:

$$S_0 = e^{-\alpha_0 D_0 - \beta_0 D_0^2}. \tag{5.1}$$

After fitting the survival data, the α_0 and β_0 coefficients corresponding to each cell line were obtained (Table 5.1). Errors in the survival data are estimated by standard deviation (SD) and by error propagation, selecting the largest one as the final value. This will possibly overestimate the errors, which in some cases are huge. In Table 5.1 the values of the ratio α_0/β_0, a relevant radiobiological parameter, has also been included.

There is a clear difference between the results for the different cell lines, since the response to irradiation and the possibility of repair depend on the tissue (results plotted together in Figure 5.2). The most radioresistant cell line turns out to be Cal33, while A375 proves the most radiosensitive one. With respect to the parameter α_0/β_0, it turns out to be high (typical of tumors) for the normal cell line MRC5, a result that can be addressed to the particular features (in terms of proliferation) of these cells. Also, the Cal33 cell line shows a very low ratio (typical of normal tissues). However, for this last cell line the uncertainties in the parameters are high and no quantitative prediction for this ratio can be extracted.

The results of this experiment will now be designated as those corresponding to reference photon dose. They will be used for a comparison when the effect of other types of irradiation needs to be known.

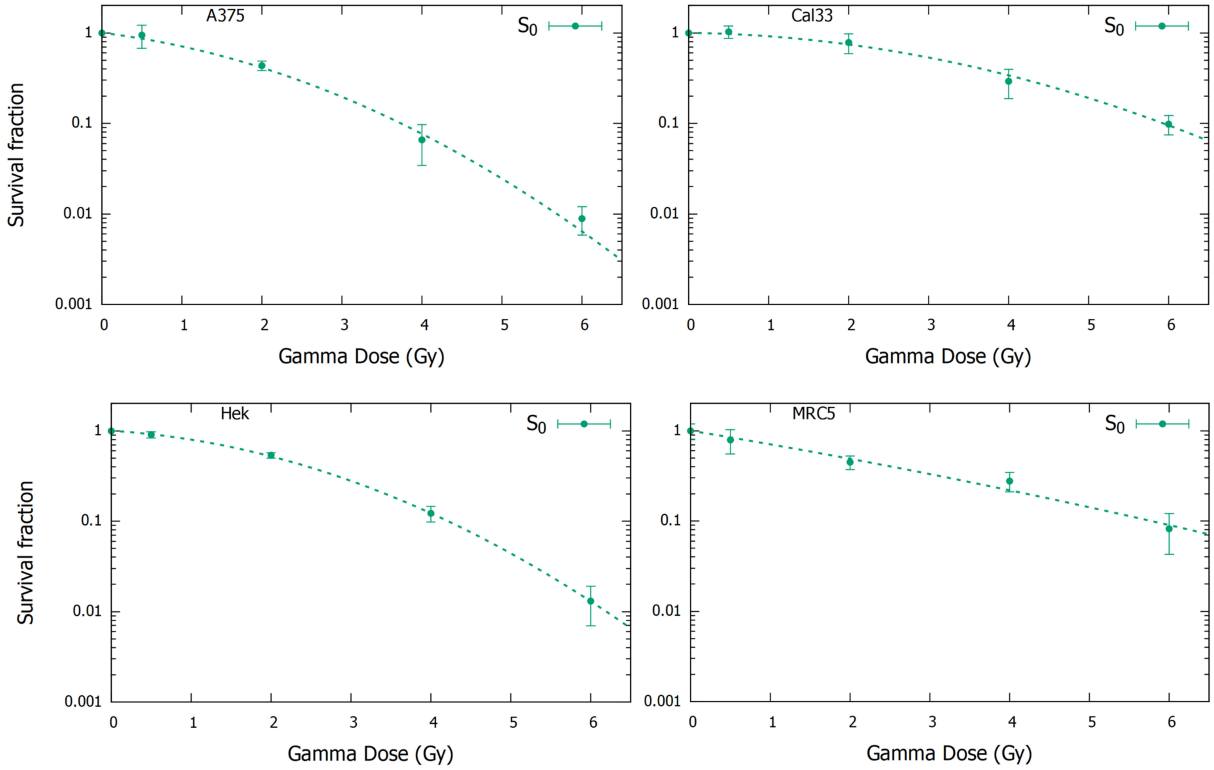

Figure 5.1: Survival data and fitting curves of each cell line after photon irradiations at the LINAC in Granada Hospital with a dose rate of 1Gy/min.

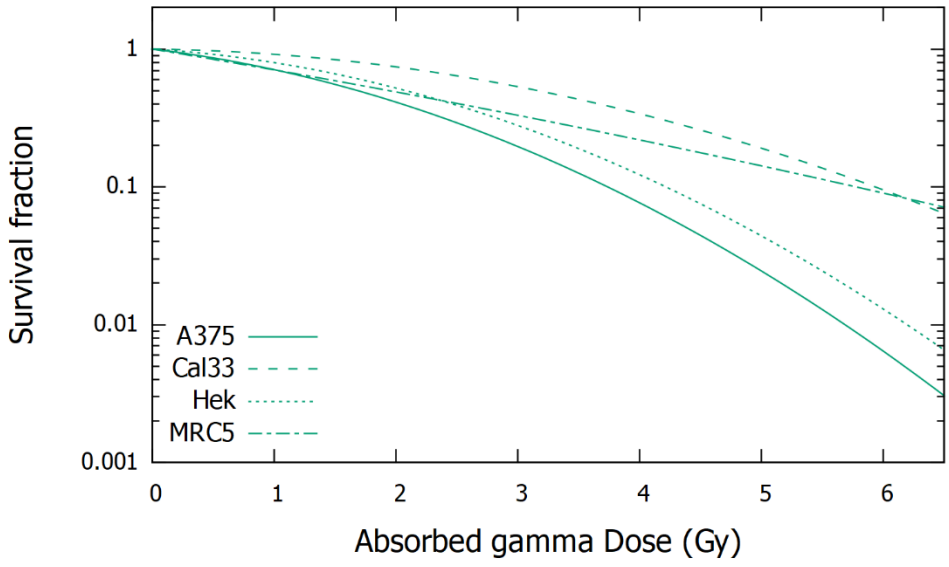

Figure 5.2: Survival curves of the irradiated samples in Experiment V plotted together, where the variation between the different cell lines can be observed.

	$\alpha_0(Gy^{-1})$	$\beta_0(Gy^{-2})$	$\alpha_0/\beta_0(Gy)$
A375	0.244±0.084	0.01±0.02	24
Cal33	0.026±0.052	0.06±0.10	0.4
Hek	0.127±0.009	0.099±0.002	1.3
MRC5	0.337±0.07	0.01±0.02	31

Table 5.1: α_0 and β_0 coefficients of the reference photon dose, D_0, estimated with the fitting of the results of the four cell lines irradiated at the LINAC. The ratio between the two coefficients, as it is the usual quantity expressed in radiobiology, is indicated in the last column.

The low availability of the beam restricted our measurements to only four cell lines. Data shortage in some cases has led to large errors in the fitting, as has occurred for example with the parameters for the Cal33 cell line or β_0 for the A375 and MRC5 cell lines. Nevertheless, the well-designed experimental arrangement and the convenience of using irradiation at a LINAC as the reference dose encourage us to continue performing photon irradiations under these conditions and to improve the results obtained.

5.2 Experiment I: results from cold neutron irradiation

Six cell lines were irradiated at the PF1b beam line at ILL during the experiments in June 2018 and September 2018. Colonies formed after the irradiation were counted and compared to the corresponding control data, yielding the survival data. The survival of each irradiated sample (cuvette 1 and cuvette 2) as a function of the neutron fluence (flux over time) is illustrated in Figure 5.3.

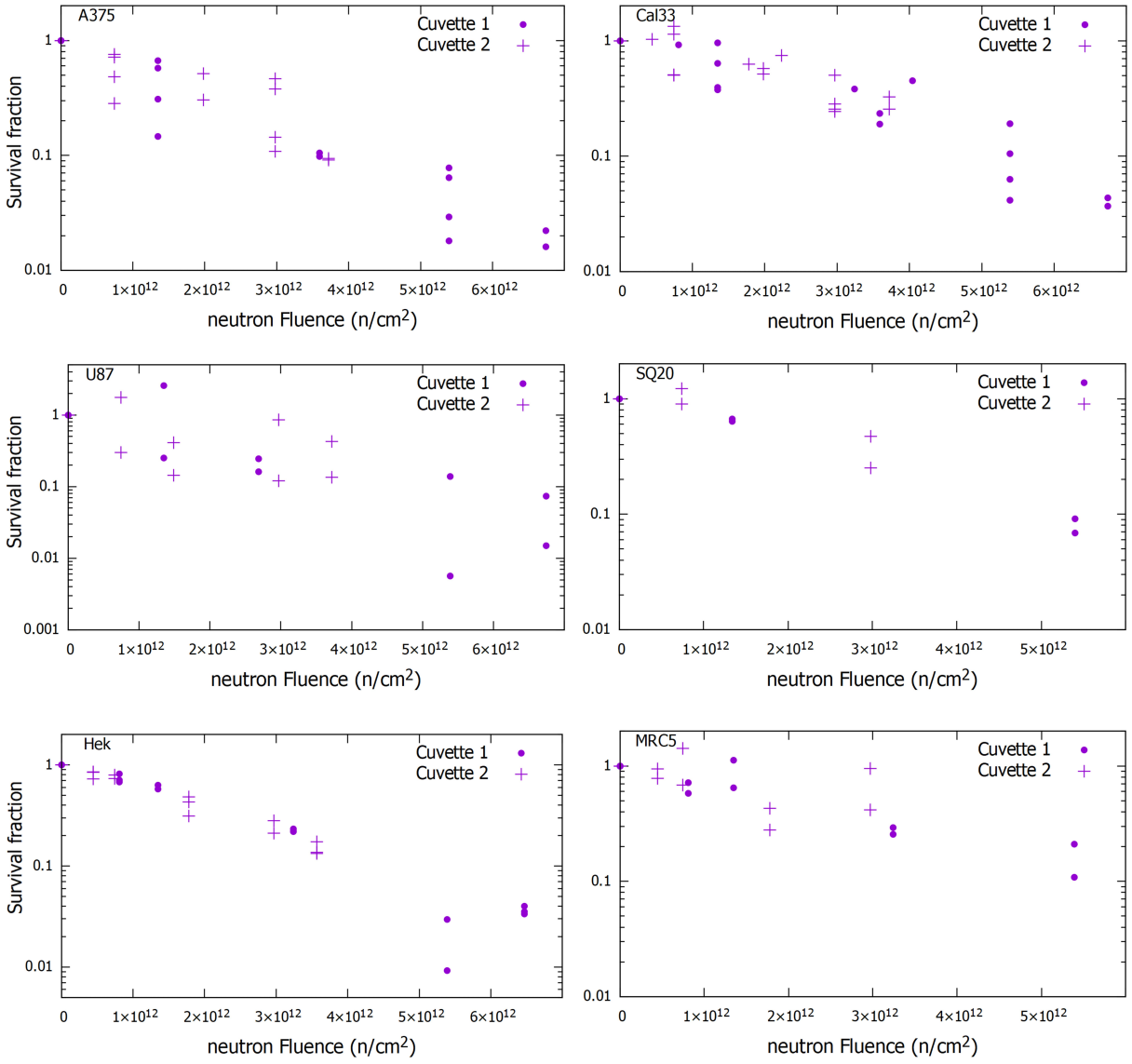

Figure 5.3: Survival data of each cuvette and each irradiation for the six cell lines irradiated at ILL, shown as a function of the neutron fluence.

The survival data after irradiation at the ILL cold neutron beam is due to the total absorbed dose, D_{ILL}, which is the sum of the neutron dose, mostly from captures in nitrogen, and photon dose, mostly from photons emitted after capture by hydrogen:

$$D_{ILL}(Q_i) = \dot{D}_n(Q_i) \cdot t + \dot{D}_\gamma(Q_i) \cdot t. \tag{5.2}$$

For each cuvette, Q_1 and Q_2, the fraction of each dose component will be different. t refers to the irradiation time and $\dot{D}_n$ and $\dot{D}_\gamma$ are the dose rate of each component (extracted from the MCNPx simulations). Cuvette 1 has a higher percentage of neutron dose than cuvette 2, since it is closer to the beam incidence. In both cuvettes, the biggest dose component is the one corresponding to neutrons, the subject of study in this experiment. Each dose rate will also

depend on the composition of the cells, where those with more nitrogen will have a higher neutron component (see Chapter 1 Section 1.2 for dose components definition).

By the use of kerma factors and knowing the nitrogen composition of each cell line, the dose corresponding to each fluence is calculated. For more details about these calculations, see Appendix A which is focused on the ILL beam simulations. The uncertainty in the dose comes mostly from the uncertainty of the neutron shutter that is operated manually. The simulation error is less than 1% and that for the kerma factor used in the dose calculation is less than 5% (ICRU recommendations). Since the reactor is operated at constant power during each cycle, the beam is stable. The positioning of the samples is also quite stable given the holder design, introducing an error of no more than 3%. An assumed thickness variation of ± 10% of the cell layer (13.5 to 16.5 μm) results in ± 2% uncertainty of the incomplete CPE correction of the thermal dose (see Appendix A).

Survival data at the same dose are grouped together (plotted in Figure 5.4), estimating the error as the standard deviation (SD) and applying error propagation.

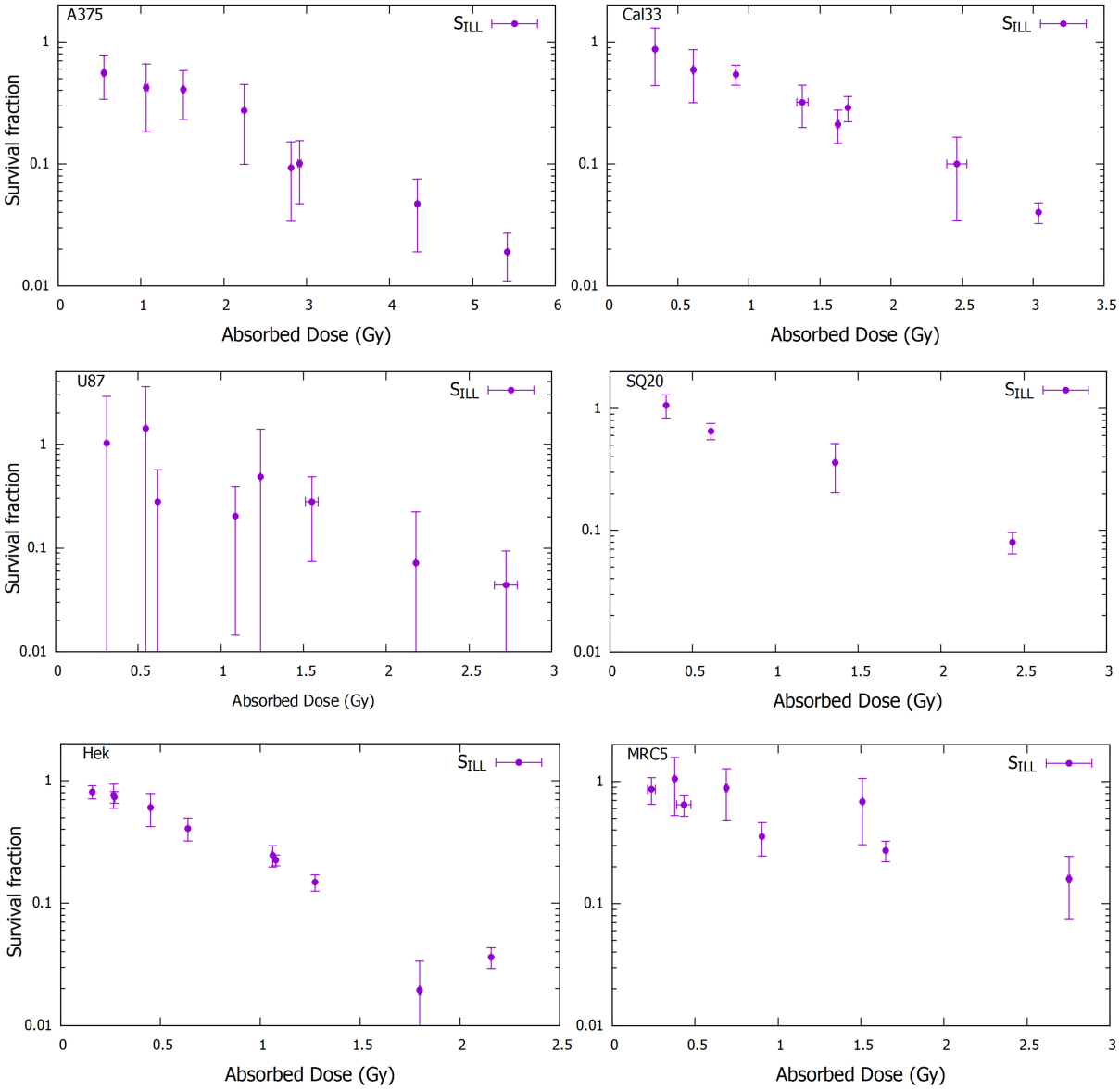

Figure 5.4: Survival as a function of the dose of the six cell lines irradiated at ILL. The effect is due to the irradiation at the ILL beam, S_{ILL}, *i.e.* low-energy neutrons plus gamma rays.

As it was found in Experiment V, the difference in the profile of the survival results amongst the diverse cell lines is appreciable. For similar cell lines (*e.g.* Cal33 and SQ20), it can be seen that the shape is similar (more clearly shown in Figure 5.5). This demonstrates the dependence of the survival effect on the tissue (or cell line) for the same neutron irradiation.

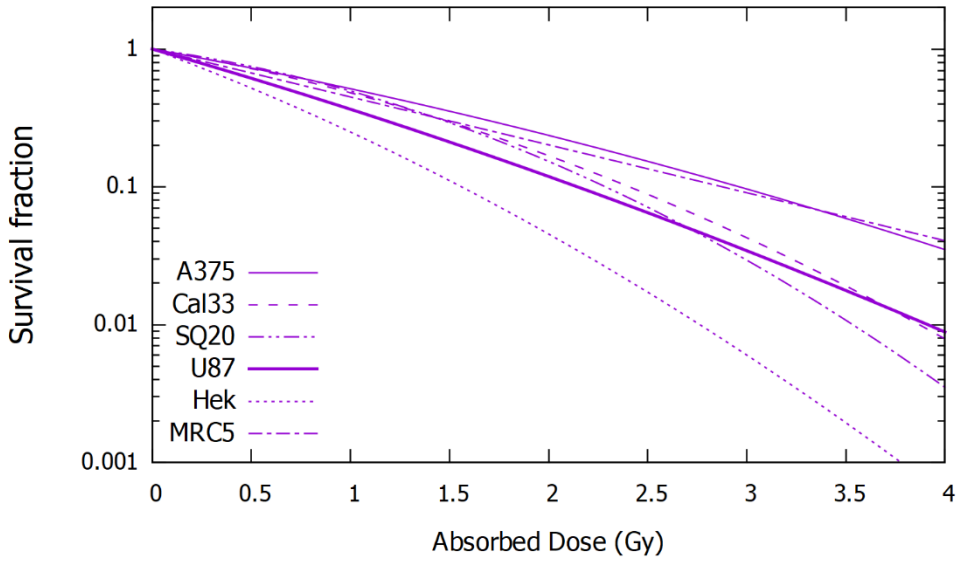

Figure 5.5: Survival curves for the irradiated samples in Experiment I plotted together. The variation between the response of the different cell lines irradiated at ILL can be seen.

Each point of the observed survival due to the total absorbed dose is:

$$S_{ILL}(Q_i) = S_n(Q_i) \cdot S_\gamma(Q_i) = e^{-\alpha_n D_n(Q_i) - \beta_n D_n^2(Q_i)} \cdot e^{-\alpha_\gamma D_\gamma(Q_i) - \beta_\gamma D_\gamma^2(Q_i)}, \tag{5.3}$$

where the coefficients α_n, β_n, α_γ, β_γ are constants that describe the survival curves and depends on the cell line and irradiation type.

From now on, a series of assumptions are going to be made in the treatment of the results, for this experiment and for the following ones:

a) The effect of low energy neutrons is considered as of high LET radiation, consequently, the quadratic term for neutrons in Eq.(5.3) will be zero:

$$\beta_n = 0. \tag{5.4}$$

This assumption will be checked for each result when extracted and fitting the S_n, confirming that data fits to a linear function instead of a quadratic one.

b) When no data about the isolated effect due to the gammas coming from the beam exist, as is the case for Experiments I, III and IV, the effect of those gamma rays will be considered the same as the effect of the gamma rays taken as a reference (from experiment V or from bibliography data):

$$a_\gamma, \beta_\gamma = a_0, \beta_0. \tag{5.5}$$

This hypothesis assumes that the reference photons from experiments at the LINAC or from bibliography data have similar characteristics and tissue response as those coming from the beam. At ILL this may not be the case, since the gamma dose rate in the ILL beam is much lower than it is in the LINAC. The fact that the ILL beam has such a low gamma dose makes this error smaller than for other beams.

In this case, the data for the reference photon dose not only is a reference for RBE calculation, but it is also used to represent the gamma component of the dose in the neutron beam.

Following the two assumptions a) and b), the only unknown terms in (5.3) are the damage that corresponds to just the low energy neutrons in the ILL beam, S_n, and the coefficient which describes it, α_n.The D_n and D_g corresponding to each cuvette $Q_{i=1,2}$ can be calculated with the percentage of the total dose they entail, X_n and X_γ (known from the simulations), multiplied by each irradiation dose:

$$D_n(Q_i) = X_n(Q_i) D_{ILL}, \tag{5.6}$$

$$D_\gamma(Q_i) = X_\gamma(Q_i) D_{ILL}. \tag{5.7}$$

S_n can be obtained from S_{ILL} and S_γ for each dose by:

$$S_n(Q_i) = \frac{S_{ILL}(Q_i)}{S_\gamma(Q_i)} = \frac{S_{ILL}(Q_i)}{e^{-\alpha_\gamma D_\gamma(Q1) - \beta_\gamma D_\gamma^2(Q_i)}}. \tag{5.8}$$

For this purpose, reference radiation data from Section 5.1 are used, with the assumption b) and Eq. (5.5) used to calculate S_γ. Subsequently, equation (5.8) is applied to extract S_n. Hence, several points that correspond to data of S_n against D_n are obtained (black points in Figure 5.6).

These points are then fitted, yielding the α_n coefficient (values in Table 5.2) which describes the damage that the cells would have if 100% of the dose would arise only from neutrons (purple line in Figure 5.6).

	$\alpha_n(Gy^{-1})$
A375	0.84±0.05
Cal33	1.38±0.05
U87	1.60±0.18
SQ20	1.37±0.12
Hek	2.57±0.10
MRC5	0.98±0.13

Table 5.2: α_n coefficients corresponding to the survival S_n, shown in Figure 5.6, with a neutron dose D_n, estimated from the results of the six cell lines irradiated at the ILL and Eq. (5.8). For A375 and Hek cell lines, the photon dose coefficients are the ones extracted from Experiment V. For Cal 33 and SQ20, photon dose coefficients from [Baue10], for U87 from [Baya19] and for MRC5 from [Ding13] are used.

For those cell lines for which no data have been extracted in Experiment V and for those in which the data extracted had a considerable error, data from other authors have been used as photon data to subtract the S_n from the S_{ILL}. For the U87 cell line, data from Bayart *et al*, obtained with a Varian NDI 226 X-ray tube of 200 kVp (kilovolt peak) at a dose rate of 1.2 Gy/min, were used [Baya19]. For MRC5, for which errors in Experiment V are high, data from Ding *et al*. [Ding13] were used. In this reference, the authors irradiated MRC5 cells using a Faxitron RX-650 operated with 100 kVp and 5 mA at a dose rate of 1.33 Gy/min. A strange behavior in Cal33 cells was noted in some of the irradiations so data from Bauer *et al*. [Baue10] were used in their place. Bauer *et al*. used ^{137}Cs γ-irradiations for studies of Cal33 at 0.54 Gy/min. It was not possible to irradiate the SQ20 cell line at the LINAC and (because of the unique origin of these cells) no previous reference was found; however the cell type is similar to Cal33 (they both are squamous cell carcinomas), and the same data for this last cell line was also used for SQ20.

The observation of Figure 5.6 shows that the values of S_n are well fitted by a single exponential. This confirms the validity of hypothesis a) above and the adequate removal of the photon effect, allowing to quantify the pure neutron effect.

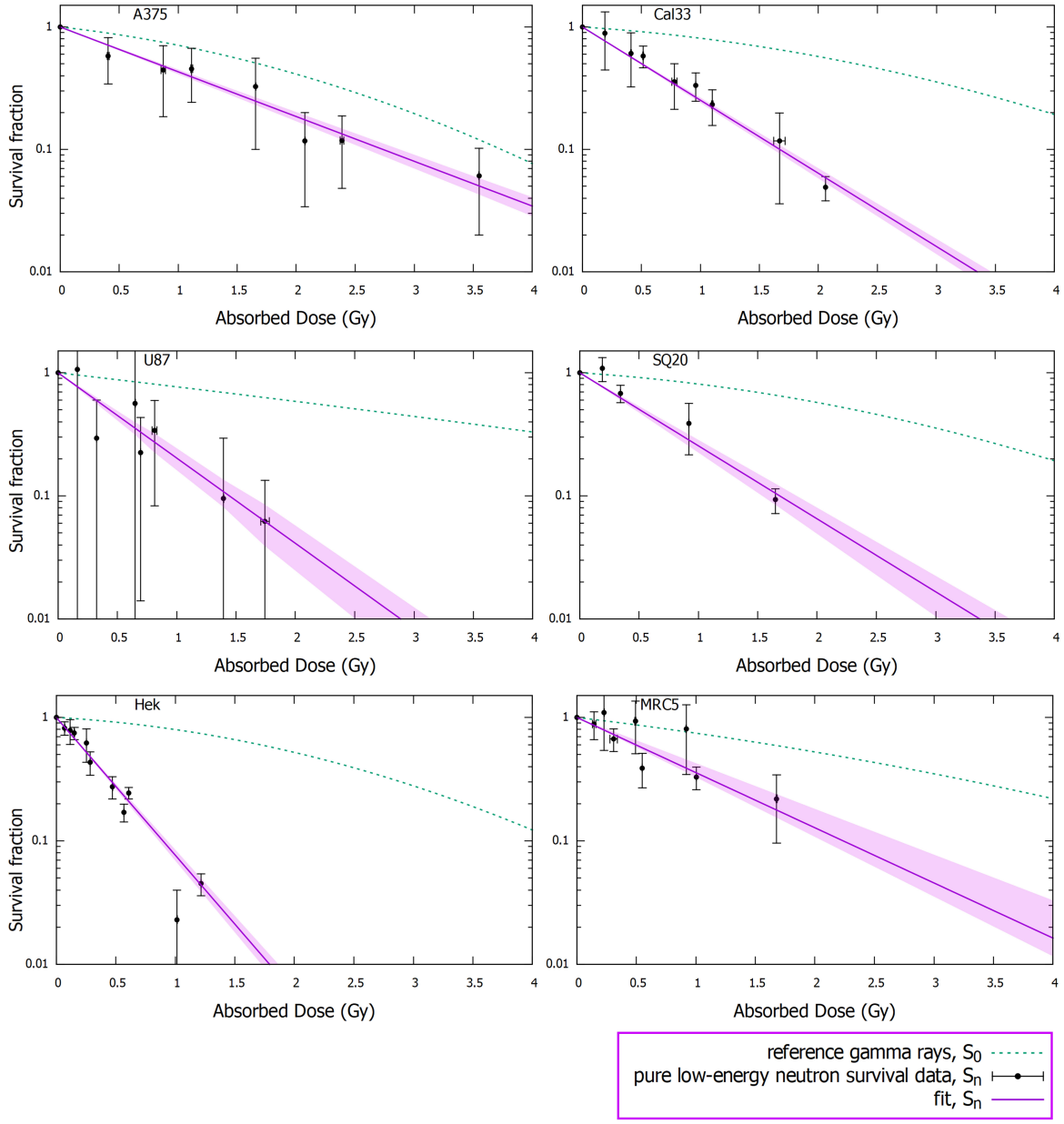

Figure 5.6: Survival curves of the reference photon dose, D_0, and the low-energy neutron dose, D_n, for each cell line. Green lines correspond to the survival when the dose is only gammas, S_0, obtained in Section 5.1 or from references ([Baue10] for Cal33 and SQ20, [Baya19] for U87 and [Ding13] for MRC5). The purple line is the survival, S_n, when the dose arises from the low-energy neutrons alone, D_n, extracted in this section from the data after irradiation at ILL and by fitting the obtained black points. The error of the fitting is shown by the purple shadow

5.2.1 Low-energy neutrons weighting factor, w_t

All the necessary data for the calculation of the RBE corresponding to low-energy neutrons are then found. The reference photon dose and neutron dose, D_0 and D_n, can be estimated using

the calculated coefficients, α_n, α_0 and β_0. In this way, the value of RBE for several percentages of survival is determined (by applying Eq.(1.3) in Chapter 1) and expressed in Table 5.3, as well as the value of the new defined weighting factors, w_t^*, which correspond to the α_n/α_0 ratio, in Table 5.4.

Again, for those cell lines with no acceptable data from Experiment V, data from the same references as described previously in Section 5.2 were used as the reference photon dose.

A strong variability between the different survivals and the various cell lines is noted. Melanoma A375 cells, despite their high nitrogen content, appear to be resistant to low-energy neutrons irradiation. In BNCT treatment of melanoma, the RBE used is actually lower than the general values used (the 3.2 from Coderre *et al.*): 2.5 is used in Kyoto [Fuku03] and 3 in Argentina [Blau04]. According to our data, for a normal melanoma treatment, where the neutron doses are between 1.3 and 3.5 Gy [Fuku03], the RBE corresponds to values that are lower than 2.

Hek cells demonstrate the opposite tendency; they have a low nitrogen content, but the effect following low-energy neutron irradiations is strong. Their embryonic origin may explain their strong radiosensitivity to neutrons. For Glioblastoma U87 cells, while they are shown to be one of the most radio-resistant to photon irradiations (the α_0 is high), they have a higher effect than other lines after neutron irradiation.

The observed variability with the survival fraction is one of the arguments for the application of the constant weighting factors, w_t^*, explained in Chapter 2. w_t^* remain constant in survival and dose for each cell line.

In previous work, the RBE data are illustrated without errors; this may have been done because the errors are typically high. Here the errors are displayed to show how they are low when the data they are based on have good certainty, whereas cells that grow in “cloudy” colonies (*eg* U87 and MRC5) will require much more data to improve the statistics.

A375	α_n=0.84±0.05	α_0=0.244±0.084 β_0=0.010±0.021		**Cal33**	α_n=1.38±0.05	α_0=0.144±0.028 [Baue10] β_0=0.067±0.007	
S	D_n(Gy)	D_0(Gy)	RBE_t or w_t	**S**	D_n(Gy)	D_0(Gy)	RBE_t or w_t
50%	0.82±0.04	1.68±0.26	**2.05±0.43**	**50%**	0.50±0.02	2.32±0.20	**4.60±0.56**
37%	1.18±0.06	2.16±0.37	**1.83±0.42**	**37%**	0.72±0.03	2.93±0.28	**4.05±0.52**
10%	2.73±0.15	3.74±0.72	**1.37±0.34**	**10%**	1.67±0.06	4.89±0.51	**2.92±0.41**
1%	5.47±0.29	5.68±1.14	**1.04±0.26**	**1%**	3.35±0.12	7.29±0.79	**2.18±0.31**
U87	α_n=1.60±0.18	α_0=0.258±0.017 [Baya19] β_0=0.005±0.003		**SQ20**	α_n=1.37±0.12	α_0=0.144±0.028 [Baue10] β_0=0.067±0.007	
S	D_n(Gy)	D_0(Gy)	RBE_t or w_t	**S**	D_n(Gy)	D_0(Gy)	RBE_t or w_t
50%	0.43±0.05	2.56±0.90	**5.90±2.74**	**50%**	0.51±0.04	2.32±0.20	**4.57±0.79**
37%	0.62±0.07	3.61±1.48	**5.79±3.03**	**37%**	0.73±0.06	2.93±0.28	**4.02±0.73**
10%	1.44±0.16	7.80±3.79	**5.40±3.23**	**10%**	1.69±0.15	4.89±0.51	**2.90±0.56**
1%	2.89±0.32	14.15±7.26	**4.90±3.07**	**1%**	3.37±0.29	7.29±0.79	**2.16±0.42**
Hek	α_n=2.57±0.10	α_0=0.127±0.009 β_0=0.099±0.002		**MRC5**	α_n=0.98±0.13	α_0=0.265±0.023 [Ding13] β_0=0.028±0.005	
S	D_n(Gy)	D_0(Gy)	RBE_t or w_t	**S**	D_n(Gy)	D_0(Gy)	RBE_t or w_t
50%	0.27±0.01	2.08±0.03	**7.70±0.42**	**50%**	0.67±0.08	2.13±0.24	**3.16±0.73**
37%	0.39±0.02	2.59±0.04	**6.69±0.38**	**37%**	0.97±0.11	2.87±0.37	**2.97±0.74**
10%	0.90±0.04	4.21±0.08	**4.70±0.27**	**10%**	2.24±0.26	5.47±0.82	**2.45±0.66**
1%	1.79±0.07	6.19±0.12	**3.46±0.20**	**1%**	4.48±0.53	8.89±1.40	**1.99±0.55**

Table 5.3: Thermal RBE factor (or w_t factor), in purple, for different survival percentage of the six cell lines irradiated at ILL. The reference photon dose for each survival, D_0, is calculated from the α_0 and β_0 obtained in Section 5.1 and from references cited therein. The low-energy neutron dose, D_n, is calculated from the α_n obtained in Section 5.2.

Cell line	w_t^*
A375	**3.5±1.4**
Cal33	**9.5±2.2**
U87	**6.2±1.1**
SQ20	**9.5±2.6**
Hek	**20.3±2.3**
MRC5	**3.9±0.8**

Table 5.4: Values of new constant thermal factors: w_t^* , presented in Chapter 2, Section 2.3.2, for the six cell lines irradiated at ILL, calculated as the ratio of α_n and α_0.

5.2.2 Comparison with previous experiments

The objective of this section is to explain why it is advantageous to extract the effect of thermal neutrons using irradiations data from ILL.

The effect due to neutron irradiation, $\ln(S_n)$, is calculated from the survival observed after irradiation, S_{beam}, and by subtracting the survival observed following photon irradiation, S_γ, following equation (5.8). The error associated with this is assumed to be:

$$\Delta S_n = \left|\frac{\partial S_n}{\partial S_{beam}}\right| \Delta S_{beam} + \left|\frac{\partial S_n}{\partial S_\gamma}\right| \Delta S_\gamma = \frac{\Delta S_{beam}}{S_\gamma} + \frac{S_{beam}}{S_\gamma^2} \Delta S_\gamma. \tag{5.9}$$

From this expression it can be deduced that the lower the photon survival (as would be expected for higher irradiation doses), the greater the error will be in the subtraction of neutron survival. The following expression shows that, as the percentage of the total dose (D_{beam}) due to photons, X_γ, increases, the survival S_γ is lower.

$$S_\gamma = e^{-\alpha_\gamma X_\gamma D_{beam} - \beta_\gamma X_\gamma^2 D_{beam}^2}. \tag{5.10}$$

Hence studies aimed at probing the effect of neutron irradiation S_n with high certainty should seek a X_γ as small as possible. Therefore, the first beam example given in Table 5.5, with 69% of the dose due to photons, will lead to values with high error for neutron effect.

Another advantage of the ILL beam used in these studies will be now explained through a comparison with a neutron beam at the Brookhaven Medical Research Reactor (BMRR). This beam has characteristics that are typical of BNCT irradiations and irradiation of biological

tissues. A comparison of the dose components of each beam in shown in Table 5.5. For BMRR it can be seen that, even in the case of a low gamma component, there will be a problem in the neutron survival subtraction: the S_n estimated will be due to a mix between epithermal neutrons (called fast neutrons in the BNCT field) and thermal neutrons.

	Themal neutron dose	Fast neutron dose	Gamma dose
BMRR thermal [Arch71]	23%	9%	69%
BMRR epithermal [Code93]	24%	43%	33%
ILL beam (cuvette 1)	64%	0%	36%

Table 5.5: Dose components of two beams used for biological studies in BNCT: the reactor of Brookhaven (BMRR), in two modes, and the cold neutron beam at ILL. For the ILL beam, the dose components correspond to U87 cells (with 2.2% of nitrogen) and the first cuvette (see Appendix A, table A.5 for dose components of each cuvette and cell line).

The results obtained for the glioblastoma U87 cells in Experiment I can be compared with those obtained from the studies of Coderre, a major reference for neutron RBE studies [Cod93]. At BMRR, rat gliosarcoma cells were irradiated in the epithermal mode with and without the addition of boron compounds. It is interesting to compare the results obtained by these workers and those obtained for the U87 glioblastoma cell lines irradiated at ILL given that they both relate to the same type of tumor.

The differences in the response to irradiation in the two beams are shown by the survival results displayed in Figure 5.7. In Figure 5.7a) it is appreciable that at the BMRR beam, the cell survival (S_{BMRR}), is higher. In contrast, the survival of cells irradiated at ILL (S_{ILL}), where most of the dose is thermal, was found to be lower and less quadratic, bringing its behavior closer to that of a beam composed only of low-energy neutrons.

The isolated effect of neutrons for both beams is extracted using their corresponding reference photon dose, both with similar dose rates (1.23 Gy/min for the U87 cells [Baya19] and 0.9 Gy/min for the rat gliosarcoma cells [Code93]) and shown in Figure 5.7b). It is notable how the effect of a mixture of epithermal and thermal neutrons (shown in BMRR results, $S_{n(BMRR)}$), is lower than that shown for the ILL results, $S_{n,(ILL)}$, where the effect corresponds to only thermal neutrons. This observation could be considered as demonstrative that the effects of thermal and epithermal neutrons are different and, in addition, that the epithermal effect is lower, since the survival observed when irradiating with the more epithermal beam (BMRR) is higher (purple dashed line in Figure 5.7b)).

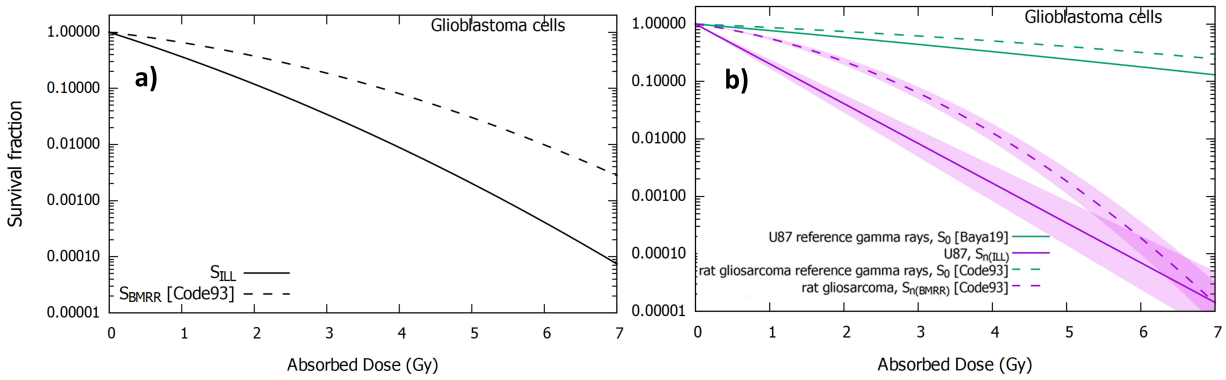

Figure 5.7: Results of irradiation of glioblastoma/gliosarcoma cells in two different beams: the epithermal beam at Brookhaven reactor (BMRR) and the cold neutron beam at ILL, as a function of the absorbed dose. a) Results of the total survival after the irradiation. b) Results of the survival due to neutrons of each beam (in purple) extracted from the total survival and the reference photon data (in green). The error of the fitting is shown with the purple shadow.

5.2.3 Sensitivity of the data to the reference dose

The survival after photon irradiation plays a key role in the neutron RBE calculations. It is used to estimate the photon effect in the survival data for a mixed beam, where the parameters a_γ and β_γ are required. Photon irradiations are subsequently used for the direct estimation of the RBE values when using a reference photon dose described with a_0 and β_0. The fact that the direct determination of a_γ and β_γ is not possible generally requires the use of the assumption described by Eq. (5.5) in neutron irradiation experiments with different beams. In this section it will be demonstrated that the error of using a_0 and β_0 as a_γ and β_γ for neutron survival extraction is not that significant if the beam has low gamma dose component (as is the case for the ILL beam). Additionally, in Section (5.4) (related to Experiment II), an innovative method by which the a_γ and β_γ parameters can be obtained will be described.

An analysis was done for the cell line A375, in order to extract the low-energy neutron effect in the same way as described in Section 5.2, but using nine different reference photon dose results. Seven studies were found in the literature for photon irradiation of A375: four of them were from a ^{137}Cs irradiator [Muns05, Muns06, Gome12], with dose rates of 2-4.5 Gy/min; three used an X-ray tube of around 200kVp [Schi15, Buon18, Min05], with dose rates of 0.2-6.4 Gy/min; and one used a 6MV Linac [Li15] at 3 Gy/min (all illustrated in the top graph of Figure 5.8).

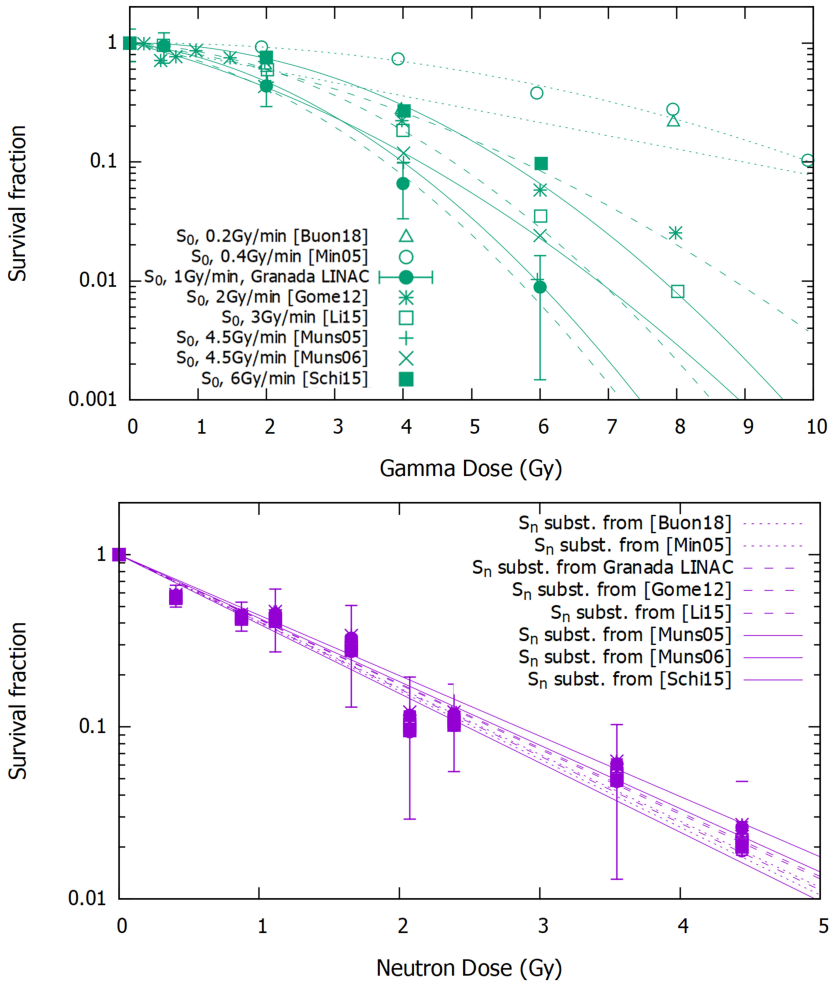

Figure 5.8: Top: survival curves for different photon irradiations of A375 cells. Bottom: survival curve results for low-energy neutron irradiation obtained at ILL and using the various photon data to extract the survival due to neutron irradiation alone. Dotted lines show low dose rate data fitting (0.2-0.4 Gy/min), dashed lines are used for medium dose rate data fitting (1-3 Gy/min), and solid lines for high dose rate data fitting (4-6 Gy/min).

The nine photon survival curves were used for the S_n extraction from ILL survival, yielding the data shown in Figure 5.8 (bottom graph). It can be seen that the big difference in the photon data does not result in major differences in the S_n and α_n values (0.80-0.92). This is because the main dose component at ILL are the neutrons, and the different data used for the extraction of the low gamma fraction of the dose do not have a strong effect. For cell lines with low nitrogen content, the neutron dose rate will be lower, and the error of choosing wrong α_γ and β_γ will thus be higher.

The problem arrives when a diversity of photon data are used as reference in calculating the corresponding w_t. Here, values from 1.06 to 3.47 are found at 1% survival and from 1.50 to 6.02 at 37% survival.

The last results indicate that neutron RBE calculated for data collected at various facilities cannot be reliably compared if they did not use the same reference photon data.

By always obtaining the reference photon dose parameters a_0 and β_0 from the same specific experimental arrangement and dose rate, the values of the RBE can be established with greater confidence.

This section is based on two crucial facts: firstly that the ILL experiments have the big advantage of having a high fraction of neutron dose, and secondly that the selection of a reference photon irradiation at a specific dose rate for all RBE calculations will help the comparison of data obtained by different researchers.

5.2.4 Sensitivity of the data with the nitrogen concentration

Given that the captures in nitrogen are the most important reactions for the dose delivered in the irradiations at ILL, it is essential for the dose calculation to have a good estimate of the nitrogen content for the cells under study. The nitrogen abundance of each cell line is presented in Table 5.6. For Cal33 and SQ20, without any reference found, the standard four-components tissue ICRU-33 (used also in Chapter 3 in Section 3.3) was selected.

	% of nitrogen	Reference
A375	5.6 (Melanoma)	[Maug97]
Cal33	2.6 (ICRU-33)	-
U87	2.2 (Brain)	[ICRU46]
SQ20	2.6 (ICRU-33)	-
Hek	1.6 (Kidney, Fetus)	[Bouc03, ICRU46]
MRC5	3.1 (Lung)	[ICRU46]

Table 5.6: Nitrogen content of the six cell lines irradiated at ILL.

In the dose estimation, as shown in Chapter 3, the kerma factor of the captures in nitrogen is proportional to the nitrogen mass fraction. This kerma entails more than 99% of the total kerma for the thermal dose, *i.e.* the thermal dose will be proportional to the nitrogen content. For the

ILL irradiations, the thermal neutron dose component is the most important, so the total dose will change considerably with the nitrogen content.

An analysis of this influence was carried out for the survival results of A375 cell line. In Figure 5.9, the survival obtained for A375 considering different doses corresponding to different nitrogen composition is shown. The solid line corresponds to the nitrogen content of 5.6% used in this work and extracted from [Maug97]. The upper and lower bounds, determined assuming an uncertainty of 10% for the nitrogen content estimation, are displayed by the dashed lines. Finally, the dotted line corresponds to a nitrogen content according to the ICRU-33 standard tissue.

In Figure 5.9 it can be seen that, for given survival results, a difference in the nitrogen content translates to a difference in the survival curves that define the effect of the ILL beam; the same survival for lower dose implies a larger effect resulting from the neutrons. This figure shows how important is to evaluate the nitrogen content of each tissue for the dose calculation and the subsequent study of the effect of low-energy neutrons. It also demonstrates that the choice of an incorrect tissue nitrogen content (*e. g.* for Cal33 cells) could lead to large errors in the data for that cell line; however, the absence of any previous data left us without alternatives in the case of Cal33 and SQ20 cell lines.

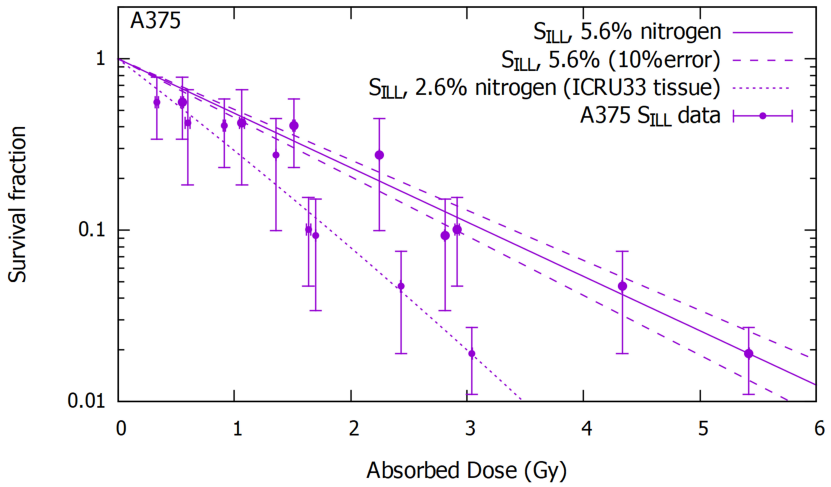

Figure 5.9: A375 survival results of the irradiations at ILL (points) represented for different doses calculated for different nitrogen content. 5.6% of nitrogen corresponds to the content that is assumed in this study [Maug97] giving the survival curve shown with a solid line. If this nitrogen content is determined with 10% of error, the survival curves could vary between the two dashed lines. If a standard tissue (ICRU-33) nitrogen content of 1.6% is supposed, the same survival data fit to the survival curve shown as dotted line.

For reducing uncertainties in future measurements, the accurate measurement of the nitrogen content of the cell lines under study is required.

5.3 Experiment III: results of cold neutron irradiation of samples with boron

Four different cell lines were irradiated at the PF1b line at ILL for Experiment III. In each case, the compound BPA (^{10}B-enriched) was added to the cell medium prior to the irradiation. The cells are cultured in the medium with boron for 4-6 hours in the cuvettes, when they reach saturated uptake [Krei01]. Before irradiation, the medium is exchanged for medium without boron, with a good washing to eliminate any trace of the previous medium with BPA and avoid undesired captures in the medium. Finally, cuvettes are irradiated in the neutron beam and processed for analysis in the same way as described for Experiment I.

In contrast to the irradiation data recorded for samples not containing boron (where irradiation times of more than 1 hour were required to observe a low survival in the cells), irradiation times of just 1-3 min were seen to be enough to observe an effect on the survival of the boron-containing cells. This gives a simple picture of the strong effect of the secondary particles on cell survival following neutron capture in ^{10}B - the main idea underlying BNCT. This can be seen in Figure 5.10 where, comparing with the data shown in Figure 5.3, illustrates the lower irradiation time necessary. For example, in A375 cells, a 10% of survival is observed for a fluence of around $4 \cdot 10^{12}$ n/cm^2 for cells without boron, while in Figure 5.10 the same survival is noted with a fluence of only $2.5 \cdot 10^{11}$ n/cm^2.

For MRC5 the irradiation times are higher because it is expected that they have lower ^{10}B uptake due to their slower metabolism.

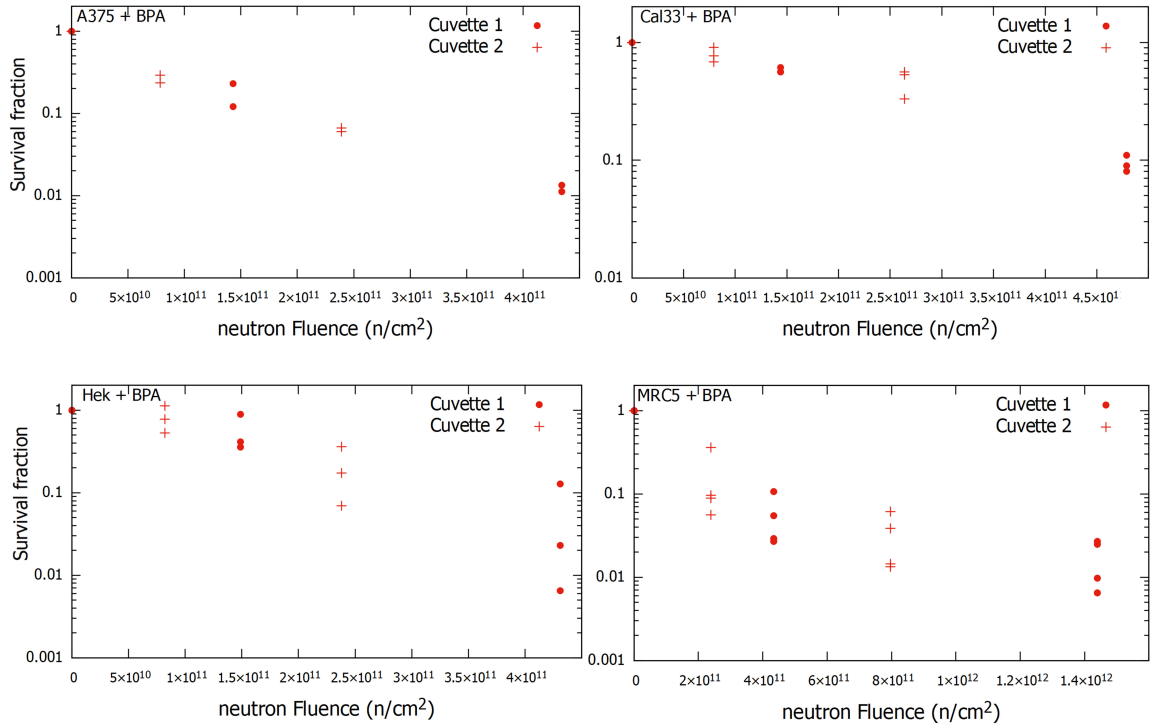

Figure 5.10: Survival data for each cuvette and each irradiation of the four BPA-containing cell lines studied at ILL shown as a function of the neutron fluence.

The total dose is composed of three dose components: the neutron one, the gamma dose, and that arising from captures in boron (called boron dose). The boron dose rate will depend on the sample position, since cuvette 1 (Q_1) will receive a higher neutron flux than the cuvette 2 (Q_2). There is also a dependence on the boron concentration$[^{10}B]$, which in turn will depend on the cell line under study. The total dose for boron-containing cells will be:

$$D_{ILL+BPA}(Q_i) = \dot{D}_n(Q_i) \cdot t + \dot{D}_\gamma(Q_i) \cdot t + \dot{D}_B\left(Q_i, [^{10}B]\right) \cdot t. \quad (5.11)$$

In order to estimate the dose, the boron uptake needs to be measured (Experiments IIIa and IIIb). Following the methods previously explained in Chapter 4, the values displayed in Table 5.7 were estimated for the boron uptake. Some discrepancies were found in some cell lines between the ICP measurements and the boron autoradiography, since some of the conditions used in sample preparation were not exactly the same. Finally, only the data of boron autoradiography of the samples prepared at the same time and in the same conditions of the samples for irradiations were taken.

	A375	Cal33	Hek	MRC5
^{10}B **ppm**	33±4	44±2	13±5	26±2

Table 5.7: Boron uptake in ppm (atoms of ^{10}B) measured in each cell line by boron autoradiography (Experiment IIIa).

Hence the dose can be estimated with the help of the simulations and the kerma factors corresponding to each boron uptake, getting the data for the survival curves that correspond to the irradiations at ILL of boron-containing cells (Figure 5.11). Errors in the dose are bigger due to the uncertainty in the boron uptake.

In this case, the total survival $S_{ILL+BPA}$ in each cuvette Q_i is expressed as:

$$S_{ILL+BPA}(Q_i) = S_n(Q_i) \cdot S_\gamma(Q_i) \cdot S_B(Q_i) = e^{-\alpha_n D_n(Q_i)} \cdot e^{-\alpha_\gamma D_\gamma(Q1) - \beta_\gamma D_\gamma^2(Q_i)} \cdot e^{-\alpha_B D_B(Q_i,[^{10}B])}. \quad (5.12)$$

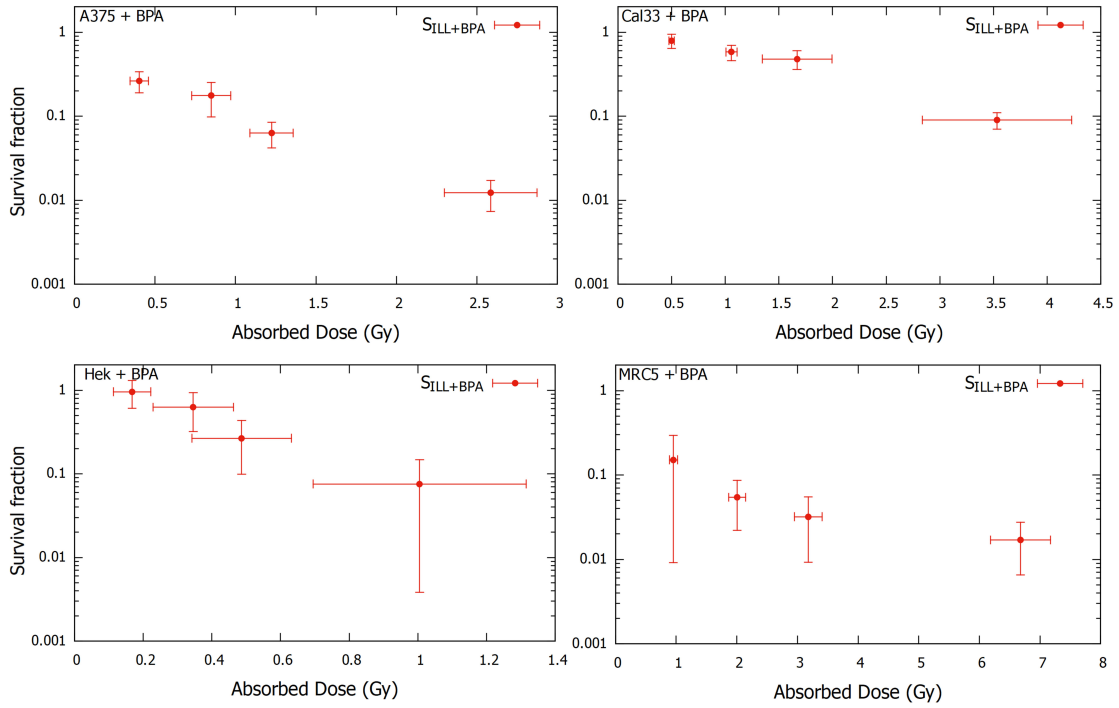

Figure 5.11: Survival ($S_{ILL+BPA}$) as a function of the irradiation dose at ILL for the six cell lines previously cultivated in BPA-containing media.

Boron and neutron survivals, S_B and S_n, are both considered as result of high LET radiation, assuming a quadratic component equal to zero. The neutron effect is known thanks to the

previous experiment on cells without boron. Subsequently, and by following a process similar to the one followed in Section 5.2, the effect which arises only from captures in boron can be calculated from $S_{ILL,BPA}$, S_γ (described with the known α_γ and D_γ) and S_n (described with the known α_n and D_n). The dose components are calculated with the fraction of the total dose they suppose, X_j:

$$D_n(Q_i) = X_n(Q_i)D_{ILL+BPA}, \tag{5.13}$$

$$D_\gamma(Q_i) = X_\gamma(Q_i)D_{ILL+BPA}, \tag{5.14}$$

$$D_B\left(Q_i, [^{10}B]\right) = X_B\left(Q_i, [^{10}B]\right)D_{ILL+BPA}. \tag{5.15}$$

The results for the calculated S_B for each boron dose D_B are the black points shown in Figure 5.12. The effect of the boron capture was estimated using α_B determined by fitting these points. By using the data from the two previous experiments (the gamma irradiations and the irradiations with low-energy neutrons), the effect due to boron capture alone was extracted. In this case, the error of the fitting will be larger due to the uncertainty on the boron uptake which affects the estimated error in the dose.

It is remarkable that for the Cal33 data, the nitrogen content of the cells was not possible to find, so a standard tissue (ICRU-33) nitrogen content was used. As shown in Section 5.2.4, the nitrogen content is a decisive factor for the neutron dose calculation. If the content in nitrogen of Cal33 is different than the 2.6% supposed, the effect of nitrogen captures could be different than that calculated in the previous section and therefore the effect of boron captures extracted from it would be different too. Consequently, data of Cal33 should be viewed taking this into account.

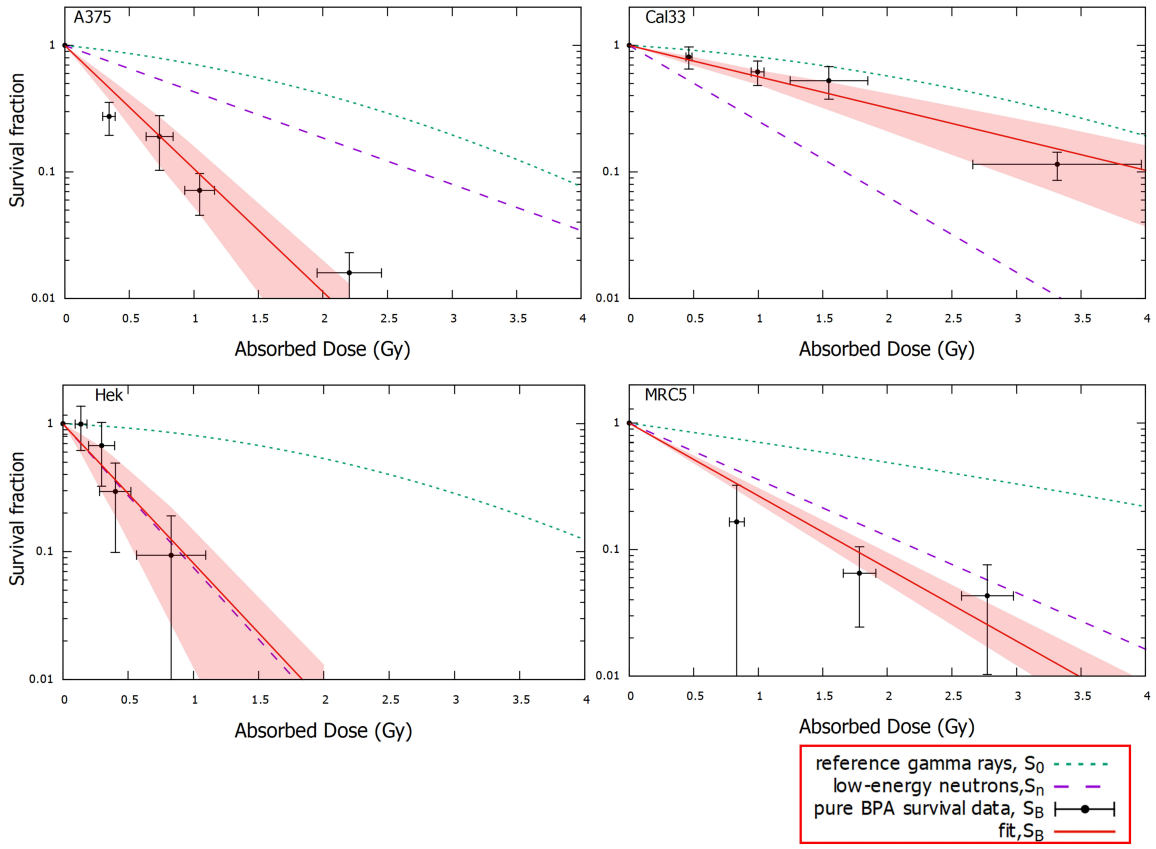

Figure 5.12: Survival curves for the reference photon dose, D_0, the low-energy neutron dose, D_n, and the boron dose, D_B, of each cell line. The green line corresponds to the survival when the dose is only due to gammas, S_0, and the purple line is the survival when the dose is from low-energy neutrons alone, S_n, both obtained as described in Section 5.2. The red line represents the survival due to the boron dose alone, extracted as described in this section by fitting the obtained black points, with the error represented as the red shadow.

The survival results corresponding to captures in boron shown in red in Figure 5.12 and extracted using Eq.(5.12) - (5.15), are non-dependent on the boron uptake, since dependence has been already taken into account in the dose calculations in Eq. (5.15). Thus what this red line represents is the survival effect due to dose D_B for each cell line when BPA is added. In general, this survival is expected to be lower than that from photons alone or from neutrons alone, because captures in boron have the strongest effect between the different doses in BNCT. This is noted for A375 and MRC5 cells. However, this is not the case for Cal33 cells; this cell line appears to be relatively radio-resistant to boron dose, but taking into account that the dose calculations are not reliable due to the unknown nitrogen content, we cannot jump into any conclusion. Hek cells show a strong response to boron dose, comparable to that of neutrons alone.

Healthy cells are expected to uptake less BPA due to their slower metabolism, but even when considering the same uptake as in a tumor tissue, sometimes a lower effect is observed. This fact could be explained with a different microdistribution inside the cells [Sato18] or the different metabolism and DNA response. It might be the case for Hek cells, where the survival arising from captures in boron, S_B, is similar to the one corresponding to low energy neutron irradiation, S_n.

The same interpretation could explain the result on Cal33 cells. However, as these cells are from tumors that have a high uptake and a strong response for BNCT treatment [Kato04, Kank11b], there should be another reason for the high survival, S_B. An incorrect selection of nitrogen content for dose calculation (we chose the one for ICRU-33 tissue) could be an explanation. Another explanation could be a release of boron to the media during the irradiation: for the BPA-containing samples, the medium surrounding the cells is exchanged before the irradiation by a medium that is boron free. The idea in doing this is to avoid the results being compromised by boron capture in the residual solvent in which the cells are immersed. However, this step may in itself be problematic and may result in 'back exchange' of boron from the cells into the surrounding medium [Meni09]. If this were to happen, the data in Table 5.7 may not agree with the real boron inside the cells during the irradiation, because the samples for boron uptake measuring did not follow this step of medium exchanged and therefore they cannot have the 'back exchange' of boron as the irradiated samples. If the cells have released boron, the dose will be lower, which, for the obtained survival data, makes the effect arising from captures in boron higher (the same survival corresponding to less dose means a higher effect).

In Figure 5.13 (left), the Cal33 results are shown; these assume a release similar to that found for endothelial cells in the work of Menichetti [Meni09] (32% after 45min). Nonetheless, S_n is still lower than S_B. It is found that only presuming a release of more than 64% of boron, the observed effect of the captures in boron for Cal33 is higher than the one from captures in nitrogen (Figure 5.13 right).

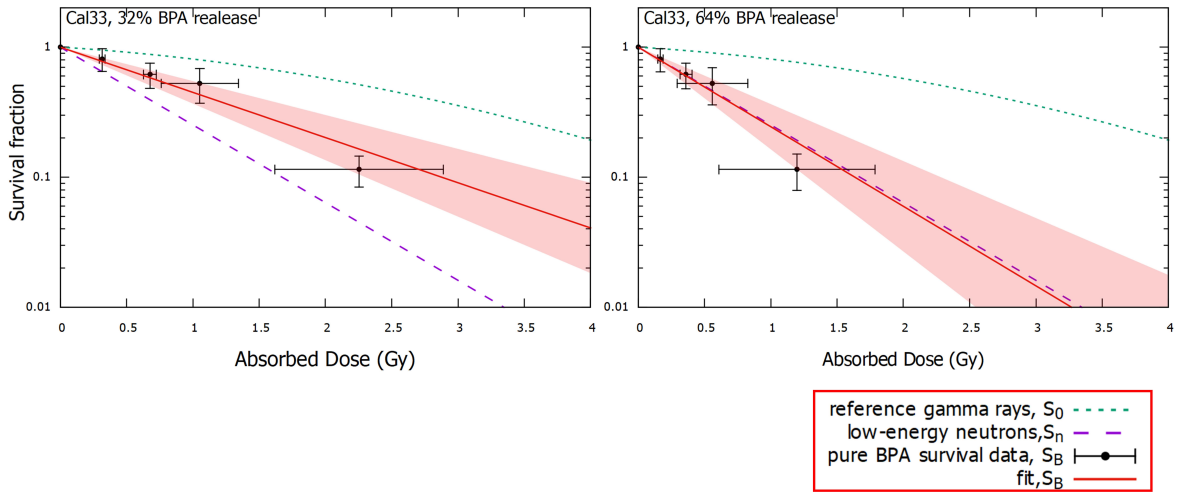

Figure 5.13: Survival curves of the reference photon dose, S_0 [Baue10], the low-energy neutron dose, S_n, and the boron dose, S_B, of Cal33 cells assuming different quantity of boron release.

The possibility of boron released to the medium has to be kept in mind and studied also for the other cell lines, so the dose estimated in Figure 5.12 may change. In order to avoid this, in future experiments, samples for boron uptake measurements should be prepared in the same way as for irradiations: leaving the cells in a non-boron-containing medium for around 45 min (similar to the time that the cells are in medium without boron during the irradiations in Experiment III) and then prepare the samples for ICP or boron autoradiography. Another possibility is to avoid the medium exchange before the irradiations and estimating the effect of this on the total dose.

5.3.1 Boron weighting factor, w_B

Following a strategy parallel to that described in Section 5.2.1, it is only necessary to compare the reference photon dose from Experiment V and references, D_0, with the dose results for captures in boron, D_B, to obtain the weighting factor RBE_B of BPA (called CBE considering its compound dependence). The data obtained is shown in Table 5.8

Values of the CBE are usually higher than the corresponding RBE_t values – apart from those for the Cal33 and Hek cells, which may vary as a result of the issues explained in the previous Section 5.3.

A375	α_B=2.24±0.25	α_0=0.244±0.084 β_0=0.010±0.021		**Cal33**	α_B=0.57±0.05	α_0=0.144±0.028 [Baue10] β_0=0.067±0.007	
S	D_B(Gy)	D_0(Gy)	CBE or w_B	**S**	D_B(Gy)	D_0(Gy)	CBE or w_B
50%	0.31±0.03	1.68±0.59	**5.5±2.5**	**50%**	1.22±0.11	2.32±0.20	**1.9±0.4**
37%	0.44±0.05	2.16±0.76	**4.9±2.3**	**37%**	1.75±0.15	2.93±0.28	**1.7±0.3**
10%	1.03±0.11	3.74±1.31	**3.6±1.7**	**10%**	4.05±0.06	4.89±0.51	**1.2±0.2**
1%	2.05±0.23	5.68±2.00	**2.8±1.3**	**1%**	8.11±0.71	7.29±0.79	**0.9±0.2**
Hek	α_B=2.51±0.44	α_0=0.127±0.009 β_0=0.099.±0.002		**MRC5**	α_B=1.32±0.15	α_0=0.265±0.023 [Ding13] β_0=0.028±0.005	
S	D_B(Gy)	D_0(Gy)	CBE or w_B	**S**	D_B(Gy)	D_0(Gy)	CBE or w_B
50%	0.28±0.05	2.08±0.04	**7.5±1.5**	**50%**	0.52±0.06	2.13±0.33	**4.1±1.1**
37%	0.40±0.07	2.59±0.05	**6.5±1.3**	**37%**	0.75±0.08	2.87±0.45	**3.8±1.0**
10%	0.92±0.16	4.21±0.08	**4.6±0.9**	**10%**	1.74±0.19	5.47±0.87	**3.1±0.9**
1%	1.84±0.32	6.19±0.11	**3.4±0.7**	**1%**	3.48±0.38	8.89±1.42	**2.6±0.7**

Table 5.8: Boron CBE (or w_B factor), in red, for different survival percentage of the four cell lines irradiated at ILL. The reference photon dose of each survival, D_0, is calculated from the α_0 and β_0 obtained in Section 5.1 and from references indicated. The boron dose, D_B, is calculated from the α_B obtained from the fitting in Figure 5.12.

Cell line	$w_B^*(CBE)$
A375	**9.2±6.8**
Cal33	**3.9±1.1**
Hek	**20±5**
MRC5	**5.0±1.0**

Table 5.9: Values of the new constant CBE factors, w_B^*, presented in Chapter 2 Section 2.3.2, for the four ^{10}B-containing (BPA compound) cells lines irradiated at ILL, calculated as the ratio of α_B and α_0.

5.4 Experiment II: results of ^{15}N-labeled sample irradiations

The main objective of this experiment was to isolate, by means of a single experiment, two different effects: the effect purely associated with the neutrons and the effect of the produced photons, both following irradiation using the ILL beam. In order to accomplish this objective,

we are going to leverage the much lower capture cross section of the ^{15}N and different reaction compared to that on ^{14}N (see Figure 5.14). ^{15}N has not only nearly five orders of magnitude lower capture cross section, but thermal neutron captures are exclusively (n,γ) reactions leading to tiny local energy deposition from 0.16 keV ^{16}N recoils (16 times less compared to deuteron recoils from neutron capture on hydrogen) and the subsequent beta decay of ^{16}N. In contrast thermal neutron capture on ^{14}N leads dominantly to (n,p) reactions with 626 keV local energy deposition from the proton and ^{14}C recoils. Thus, compared to usual tissue with 99.6% isotopic abundance of ^{14}N, in a tissue highly enriched in ^{15}N the nitrogen dose is basically "switched off".

Hek cell line was selected for this experiment and two types of samples were used: the labeled samples, referred as "N15", and the non-labeled ones, designated "N14". The non-labeled samples were grown in a BIOEXPRESS-6000 unlabeled medium. The N15 cultures were grown in the labeled BIOEXPRESS-6000 medium in which 98% of the nitrogen was replaced by ^{15}N. Both, N14 and N15 cultures of Hek cells were maintained in the corresponding BIOEXPRESS-6000 medium for 8 days prior to irradiation.

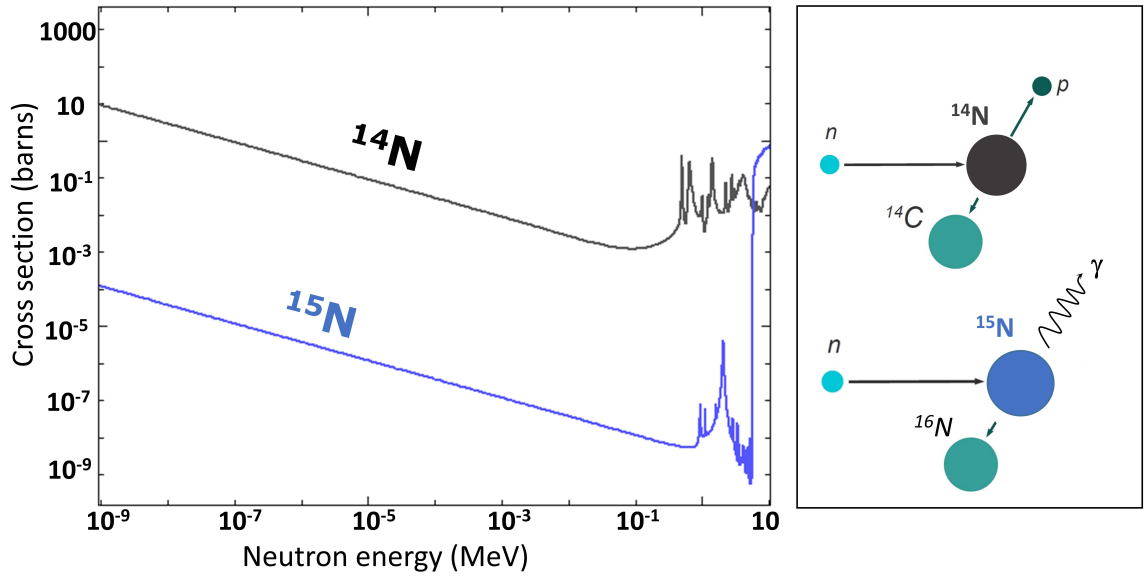

Figure 5.14: The graph shows the capture cross section of ^{14}N compared to that of ^{15}N. The sketch shows the most probable reaction of thermal neutrons captured on ^{14}N namely an (n,p) reaction, and for capture on ^{15}N, namely an (n,γ) reaction.

For each cuvette, depending on whether they are N14 or N15 samples, the dose is:

$$D_{ILL}^{N14}(Q_i) = \dot{D}_n^{N14}(Q_i) \cdot t + \dot{D}_\gamma(Q_i) \cdot t, \tag{5.16}$$

$$D_{ILL}^{N15}(Q_i) = \dot{D}_n^{N15}(Q_i) \cdot t + \dot{D}_\gamma(Q_i) \cdot t, \tag{5.17}$$

where $\dot{D}_n^{N14}$ is the neutron dose rate for the non-labeled samples and $\dot{D}_n^{N15}$ the neutron dose rate for the labeled ones. In the case of the labeled samples, the larger the extent of the ^{15}N replacement, the less captures in nitrogen would occur. The neutron dose for the labeled (N15) samples is therefore much lower than that for the N14 samples:

$$\dot{D}_n^{N15} \ll \dot{D}_n^{N14} \rightarrow S_{ILL}^{15} \gg S_{ILL}^{14}. \tag{5.18}$$

This is illustrated clearly in Figure 5.15, where the difference in the survival data for N14 and N15 samples following irradiations at ILL is shown.

In contrast, in the results of Experiment IIc (Figure 5.16) there is no appreciable difference, because the irradiation was performed with gamma rays. Isotope labeling would not be expected to have any effect on results arising from photon irradiation, since ^{14}N or ^{15}N will have the same photon interaction. The results shown in Figure 5.15 and Figure 5.16 therefore demonstrate the effects of the ^{14}N/^{15}N isotope exchange and show that the difference in the survival between the two samples is caused by the neutron captures and not by isotope-dependent artifacts (efficiency of repair mechanisms, etc.) which could cause a different radiobiological response.

During the irradiations at ILL, the gamma dose rate in each cuvette, $\dot{D}_\gamma(Q_i)$, will be the same for both N14 and N15, while the neutron dose rate is different. This implies that the total dose is different in N14 and N15 ($D_{ILL}^{N14} \neq D_{ILL}^{N15}$) and that the fractions of each dose component, $X_{j=n,\gamma}^{N14}$ and $X_{j=n,\gamma}^{N15}$, are different too.

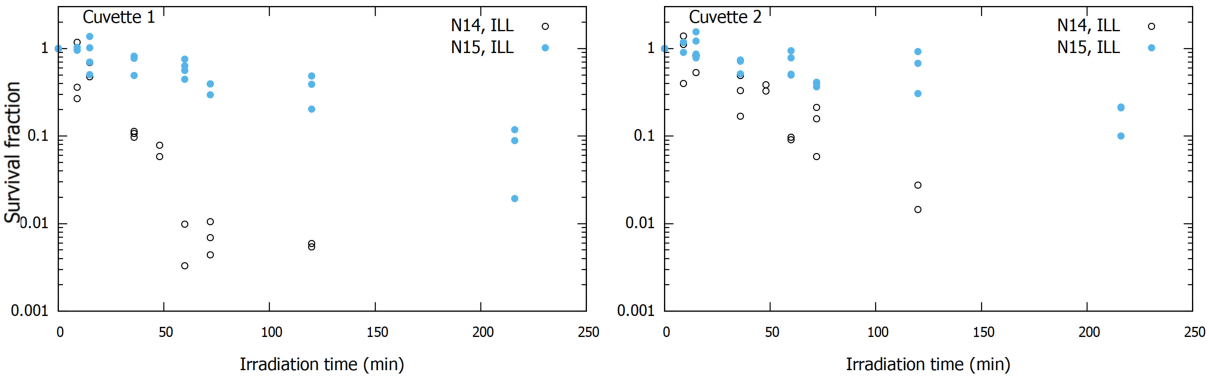

Figure 5.15: Results of Experiment II, irradiations at ILL of the samples grown in special medium non-labeled (N14) and the samples grown in special ^{15}N labeled medium (N15). Survival data shown as a function of the irradiation time (min).

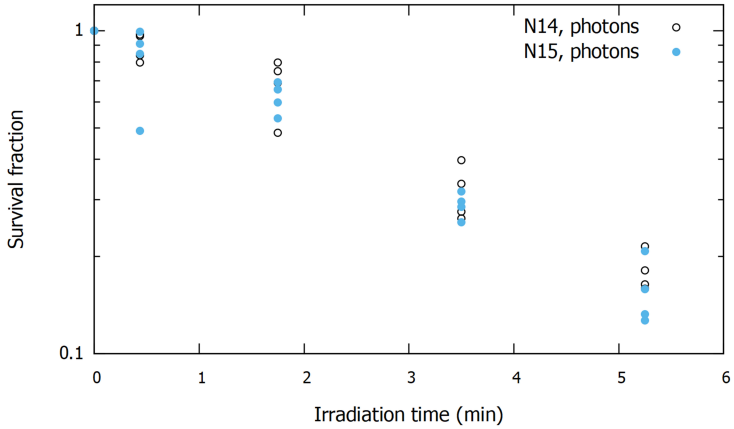

Figure 5.16: Results of Experiment IIc (photon irradiation carried out at CEA) of non-labeled samples (N14) and labeled samples (N15). Survival data shown as a function of the irradiation time (min).

The survival of the two type of samples, N14 and N15, after irradiations at ILL will be:

$$S_{ILL}^{N14}(Q_i) = S_n^{N14}(Q_i) \cdot S_\gamma^{N14}(Q_i) = e^{-\alpha_n D_n^{N14}(Q_i)} \cdot e^{-\alpha_\gamma D_\gamma^{N14}(Q1) - \beta_\gamma \left(D_\gamma^{N14}(Q_i)\right)^2}, \quad (5.19)$$

$$S_{ILL}^{N15}(Q_i) = S_n^{N15}(Q_i) \cdot S_\gamma^{N15}(Q_i) = e^{-\alpha_n D_n^{N15}(Q_i)} \cdot e^{-\alpha_\gamma D_\gamma^{N15}(Q1) - \beta_\gamma \left(D_\gamma^{N15}(Q_i)\right)^2}, \quad (5.20)$$

where the dose components can be defined as a function of the total doses D_{ILL}^{N14} and D_{ILL}^{N15}:

$$D_n^{N14}(Q_i) = X_n^{N14}(Q_i) D_{ILL}^{N14}, \quad (5.21)$$

$$D_\gamma^{N14}(Q_i) = X_\gamma^{N14}(Q_i) D_{ILL}^{N14}, \quad (5.22)$$

and

$$D_n^{N15}(Q_i) = X_n^{N15}(Q_i) D_{ILL}^{N15}, \tag{5.23}$$

$$D_\gamma^{N15}(Q_i) = X_\gamma^{N15}(Q_i) D_{ILL}^{N15}. \tag{5.24}$$

The final effect after ILL irradiation can be expressed with the survival as a function of the total doses:

$$S_{ILL}^{N14}(Q_i) = e^{-\alpha_{N14} D_{ILL}^{N14} - \beta_{N14} \left(D_{ILL}^{N14}\right)^2}, \tag{5.25}$$

$$S_{ILL}^{N15}(Q_i) = e^{-\alpha_{N15} D_{ILL}^{N15} - \beta_{N15} \left(D_{ILL}^{N15}\right)^2}, \tag{5.26}$$

where each alpha and beta are defined as:

$$\alpha_{N14} = \alpha_n X_n^{N14} + \alpha_\gamma X_\gamma^{N14}, \tag{5.27}$$

$$\alpha_{N15} = \alpha_n X_n^{N15} + \alpha_\gamma X_\gamma^{N15}, \tag{5.28}$$

$$\beta_{N14} = \beta_\gamma \left(X_\gamma^{N14}\right)^2, \tag{5.29}$$

$$\beta_{N15} = \beta_\gamma \left(X_\gamma^{N15}\right)^2. \tag{5.30}$$

The results from the ILL irradiations gave $S_{ILL}^{N14}(Q_i)$ and $S_{ILL}^{N15}(Q_i)$. The total doses were calculated using MCNPx simulations.

The total dose corresponding to the N14 samples, D_{ILL}^{N14}, can be estimated in the same way as for the Hek cells in Experiment I (see Section 5.2) and the survival curve should be similar, since the only change is the growing medium, but not the quantity of ^{14}N (they are both unlabeled samples). In Figure 5.17 it is appreciable that the same behavior is shown after ILL irradiation of Hek from Experiment I (called “Hek”) and the N14 samples grown in BIOEXPRESS-6000 unlabeled medium. With these results, it is demonstrated that the culture in BIOEXPRESS-6000 medium does not interfere with the radiation response of the cells.

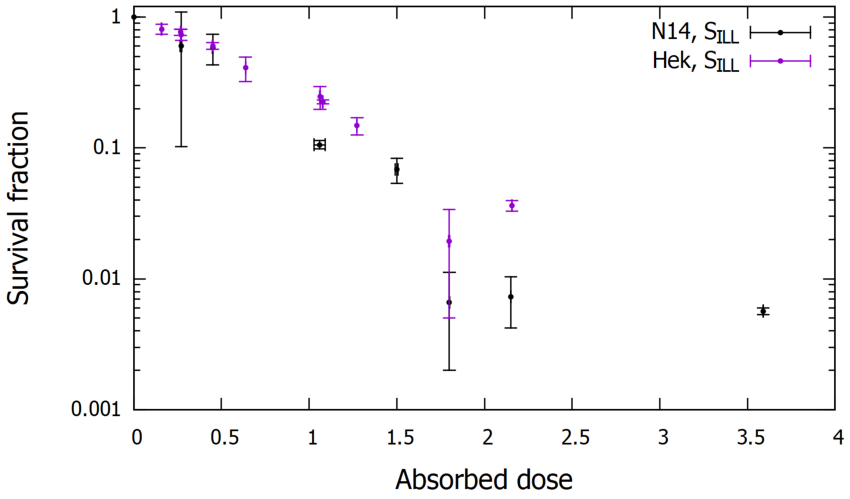

Figure 5.17: Survival data for the Hek unlabeled cells after ILL irradiation. "N14" for cells grown in the non-labeled BIOEXPRESS-6000 medium and "Hek" for cells in Experiment I, grown in the regular DMEM medium.

For dose calculations of N15 samples, D_{ILL}^{N15}, it was necessary to know the concentration of residual ^{14}N in the ^{15}N labeled cells. Experiment II is carried out to isolate the pure effect of the nitrogen dose, therefore the residual ^{14}N content has to be quantified.

According to the measurements from experiments IIa and IIb, explained in detail in the following subsection, the isotopic enrichment of ^{15}N in the cells was 75±3%.

Once doses are simulated, N14 and N15 survival curves of each cuvette are plotted (Figure 5.18), then, equations (5.25) and (5.26) can be fitted and the system of equations (5.27) and (5.28) can be solved to extract the values of α_n and α_γ. The coefficient β_γ can be estimated from (5.29) or (5.30). The same process to obtain α_n, α_γ and β_γ can be followed for cuvette 1 and for cuvette 2, and the same results should be obtained in both cases.

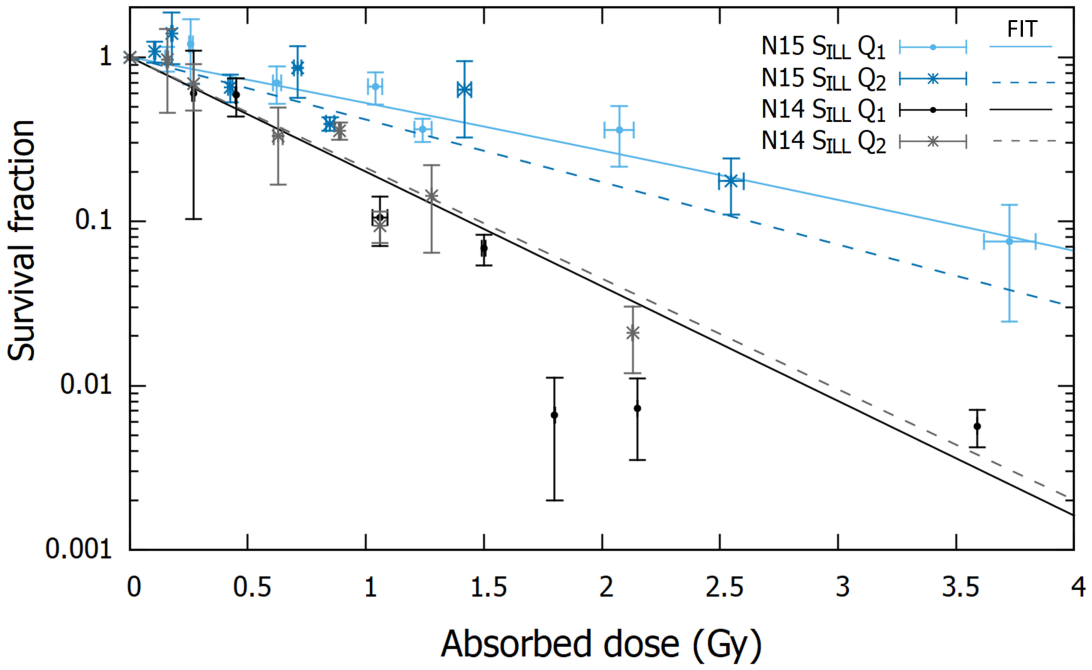

Figure 5.18: Survival curves fitted for S_{ILL}^{N14} and S_{ILL}^{N15} data of each cuvette Q_1 and Q_2. N15 samples with dose estimated supposing 75%±3% of ^{15}N labeling.

For the first cuvette Q_1, the dose simulated for N14 samples gives dose fractions of $X_n^{N14} = 0.56$ and $X_\gamma^{N14} = 0.44$. Thereafter, the fitting parameters of the survival curve (the black solid line in Figure 5.18) are $\alpha_{N14} = 1.61 \pm 0.42$ and $\beta_{N14} = 1 \cdot 10^{-6} \pm 0.13$. For the N15 samples, in blue in Figure 5.18, the neutron dose fraction is $X_n^{N15} = 0.24$ and the photon one $X_\gamma^{N15} = 0.76$, while the fitting parameters are $\alpha_{N15} = 0.63 \pm 0.15$ and $\beta_{N15} = 0.01 \pm 0.07$. The same process is followed for cuvette 2, where the data used for N14 samples are $X_n^{N14} = 0.45$, $X_\gamma^{N14} = 0.55$, $\alpha_{N14} = 1.55 \pm 0.47$ and $\beta_{N14} = 0.0 \pm 0.4$. The data for cuvette 2, N15 samples are $X_n^{N15} = 0.17$, $X_\gamma^{N15} = 0.83$, $\alpha_{N15} = 0.88 \pm 0.25$ and $\beta_{N15} = 0.00 \pm 0.16$.

By the use of this data, average values of $\alpha_n = 2.9 \pm 1.3$ for describing the effect of the neutrons from ILL and $\alpha_\gamma = 0.2 \pm 0.6$ and $\beta_\gamma = 0.0 \pm 0.2$ for the photons are obtained. The errors in parameters α_n, α_γ and β_γ come from the error of the fitting parameters from survival curves in Figure 5.18. These errors can be decreased by increasing the data, thus improving the fitting. For a better estimation of the quadratic coefficient β_γ, irradiations of N15 samples at higher doses may help to represent the curve tendency characteristic of photon irradiation. Additionally, using another cell line with more nitrogen content will increment the difference

between X_n^{N14} and X_γ^{N14}, which will make easier to differentiate the effect caused by neutrons from the one arising from gammas and will lead to lower errors.

The parameters obtained in this experiment for the photons of the beam, α_γ and β_γ, should be compared with the ones obtained for the same cell line at the LINAC α_0=0.127±0.009 and β_0=0.099±0.002 (Figure 5.19). These LINAC data were used in Experiment I to subtract the neutron effect in Hek cells, obtaining $\alpha_n(Exp.I)$=2.57±0.10, that should be compared with the α_n here obtained (α_n = 2.9±1.3). Results are compatible, but the large errors of the results from this experiment prevent us from reaching clear conclusions.

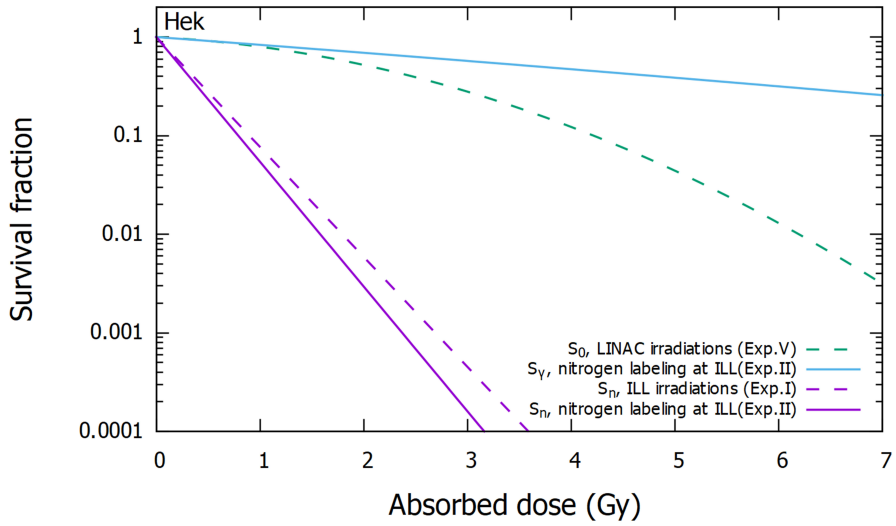

Figure 5.19: In green, survival curves of photons from LINAC irradiation (Experiment V) and, in blue, from the photons in the ILL beam (Experiment II) for Hek cells. In purple, survival curves corresponding to the effect of ILL neutrons alone, from data of Experiment I (dashed line) and from Experiment II (solid line).

This is the only experiment where we did not have to use the assumption of taking data extracted with a photon beam to describe the effect of the photons in the neutron beam (Eq. (5.5) Section 5.2), because the effect of the photons of the beam could be isolated. With only one experiment it is possible to calculate α_n, α_γ, β_n and β_γ of the ILL beam without any presupposition (like Eq.(5.4) and (5.5)) or any previous data. The clear conclusion is then the potential of this nitrogen labeling experiment. The good idea and design favor that with an increase of data we could reach very interesting results.

5.4.1 ^{15}N content, results of experiments IIa and IIb

Experiment IIa

This experiment had the objective of determining the residual ^{14}N concentration in nitrogen labeled N15 samples. For this purpose, the N14 and N15 samples were deposited on CR39 films (see Chapter 4 Section 4.5.1 and 4.5.2) and irradiated for 33 s at the PF1b cold neutron beam at ILL. Both types of samples were irradiated for the same time, and one expects to find a number of proton tracks marked in the CR39 (easily appreciable in the Figure 5.20) proportional to the ^{14}N amount. The ratio of the number of tracks between the N15 samples and the N14 (with a suitable subtraction of the background), gives the ratio of ^{14}N content between the samples. The counting is performed with the same self-developed program (by Ian Postuma), used for alpha tracks in Experiment IIIa, but adjusting the size to the tracks of protons.

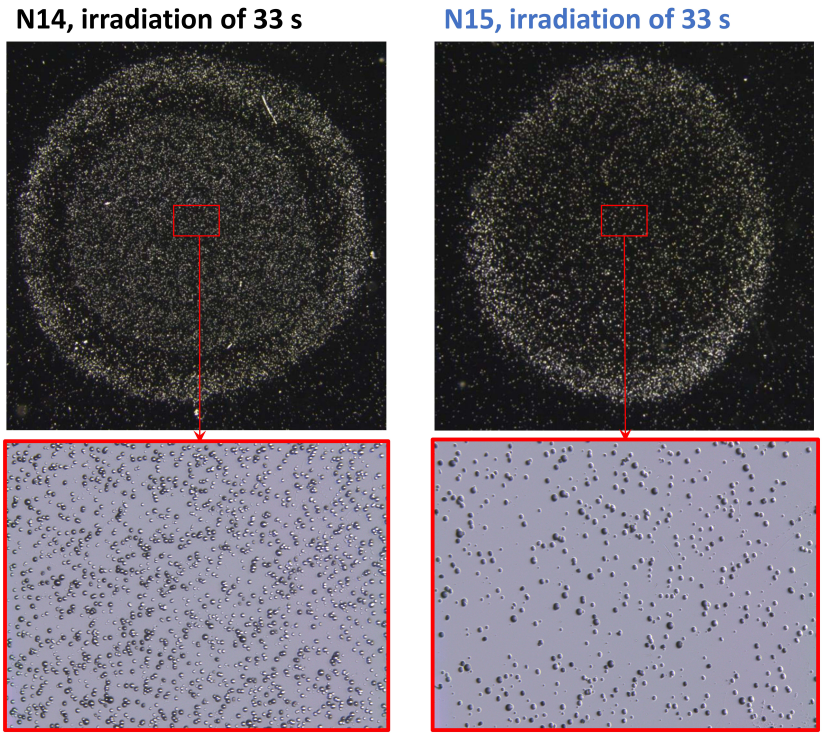

Figure 5.20: Proton tracks marked in the CR39 film of the samples irradiated for 33s at PF1b and their images under the microscope (141x).

The track ratio estimation gives a result of 4 times more ^{14}N in N14 samples than in N15 samples. A final value of 25%±3% of labeling is then used in Experiment II.

Experiment IIb

This sample analysis, explained in Chapter 4 Section 4.5.2, has the objective of analyzing the $^{14}N/^{15}N$ content of the culture medium and supposes that the cells have then the same one. The BIOEXPRESS-6000 labeled medium is known to have 98% of nitrogen labeled to ^{15}N, but, with the addition of the dialyzed FBS, more ^{14}N is included in the dilution. The elemental analysis technique gives the total amount of nitrogen in the samples, so by a comparison between the nitrogen content of the medium with and without FBS, the ^{14}N provided by the FBS in the dilution can be deduced. Four samples have been analyzed with the elemental analysis technique: BIOEXPRESS-6000 labeled medium, BIOEXPRESS-6000 labeled medium completed with dialyzed FBS, FBS and dialyzed FBS; finding the results shown in Table 5.10.

sample	% N (±0.3 %)	% C (±0.3 %)	% H (±0.3 %)
BIOEXPRESS-6000 labeled medium	0.02	0.32	1.44
BIOEXPRESS-6000 labeled medium complete (+ 10% dialyzed FBS)	0.09	0.51	8.97
FBS	0.76	2.48	8.84
Dialyzed FBS	0.51	1.84	9.40

Table 5.10: Nitrogen, carbon and hydrogen percentage content of labeled medium and FBS samples obtained by elemental analysis (combustion).

The results suggest a ^{15}N labeling of the medium less than 50%, but due the low values of nitrogen content of the media joined with the big errors of the technique, made us discard these results for Experiment II calculations.

However, some conclusions can be drawn from these results, such as that dialyzing the FBS decreases the nitrogen content in it and that adding the FBS increases the nitrogen content (^{14}N) in the medium. Also, this technique, which although not valid for the measurement of the low nitrogen content of BIOEXPRESS-6000 medium, it may be the optimum way of measurement the total nitrogen content in the different cell lines (a key point in dose calculation of Experiments I-III) and thus not have to depend on the references found. An attempt of measuring the nitrogen content of a cell line have been made for Hek, with results shown in Appendix A, and it is planned to continue for the other cell lines.

5.5 Experiment IV: preliminary results of epithermal neutron irradiation

A375 cells were irradiated at the CNA epithermal neutron beam. A similar procedure to that described for Experiments I and III was followed: colonies were counted some days after the irradiation, yielding survival data that were compared with the data of the control colonies. The fluence and dose were calculated using a MCNPx simulation of the specific set-up used (See Chapter 4 Section 4.3.2). The results can be seen in Figure 5.21 a) and b).

In this experiment, the biggest dose component was due to the epithermal neutrons (called also the fast dose), $D_{n(fast)}$; the second largest (around 30%), corresponds to the gamma dose, D_γ. By irradiating four cuvettes at the same time, for each cuvette, $Q_{i=1,2,3,4}$, the doses are:

$$D_{CNA}(Q_i) = \dot{D}_{n(fast)}(Q_i) \cdot t + \dot{D}_\gamma(Q_i) \cdot t\,. \tag{5.31}$$

The dose is simulated by a reproduction of the irradiation conditions in MCNPx Monte Carlo simulator, as performed for the ILL irradiations, but including the epithermal beam. 4 μA was assumed for the beam intensity, however this intensity may fluctuate during irradiation time, implying a systematic uncertainty in the dose. The study of this dose variation is planned to be performed afterwards a better knowledge of the beam.

Once the survival curve corresponding to the CNA beam was checked, the effect specifically derived from the epithermal neutrons for each dose was extracted from:

$$S_{n(fast)}(D_n) = \frac{S_{CNA}}{S_\gamma} = \frac{S_{CNA}}{e^{-\alpha_\gamma D_\gamma(Q_i) - \beta_\gamma D_\gamma^2(Q_i)}}, \tag{5.32}$$

where S_{CNA} is the survival after the CNA irradiation, S_γ the survival corresponding to only photons from the beam and $S_{n(fast)}$ the survival arising from the epithermal neutrons alone.

$D_{n(fast)}$ and D_γ of each cuvette are defined as the fraction of dose arising from neutrons (mostly epithermal), $X_n(Q_i)$, and the fraction corresponding to photons, $X_\gamma(Q_i)$, following:

$$D_{n(fast)} = X_n(Q_i) D_{CNA}\,, \tag{5.33}$$

$$D_\gamma = X_\gamma(Q_i) D_{CNA} \,. \tag{5.34}$$

The values of the dose fractions of each cuvette can be found in Chapter 4, in the description of the CNA experimental set-up (Chapter 4 Section 4.3.2).

Once this analysis was completed, the black points in Figure 5.21c) were obtained and plotted. These points were fitted in order to obtain the $\alpha_{n(fast)}$, that describes the effect of CNA neutrons alone (mostly epithermal):

$$S_{n(fast)} = e^{\alpha_{n(fast)} D_{n(fast)}} \,. \tag{5.35}$$

A $\alpha_{n(fast)} = 0.31 \pm 0.08$ was found for the A375 melanoma cells irradiated. The value is lower than the corresponding to low-energy neutrons (Experiment I), with a value of 0.84 ± 0.05, which translates into a minor effect of epithermal neutrons. The $w_f^* = 1.3 \pm 0.8$ calculated value is therefore smaller than the one for low-energy neutron in Section 5.2.1, $w_t^* = 3.5 \pm 1.4$.

	$\alpha_{n(fast)}(Gy^{-1})$
A375	**0.31±0.08**

Table 5.11: α_n coefficients corresponding to the survival S_n shown in Figure 5.21c) with the epithermal neutron dose D_n, estimated from the results of the A375 cell line irradiated at the CNA.

The fitted line is shown in yellow on the right graph in Figure 5.21. It can be seen that the effect of the epithermal neutrons is lower (*i.e.* the survival is higher) than that of the reference photon dose (green). This implies that a higher dose of CNA epithermal neutrons (with energies of 10-100 keV) is necessary to observe the same effect as with photon irradiation. This apparent result is another manifestation of the unreliability of reference photon data (Experiment V and literature) and its impact on radiobiological experiments in mixed beams with large photon component.

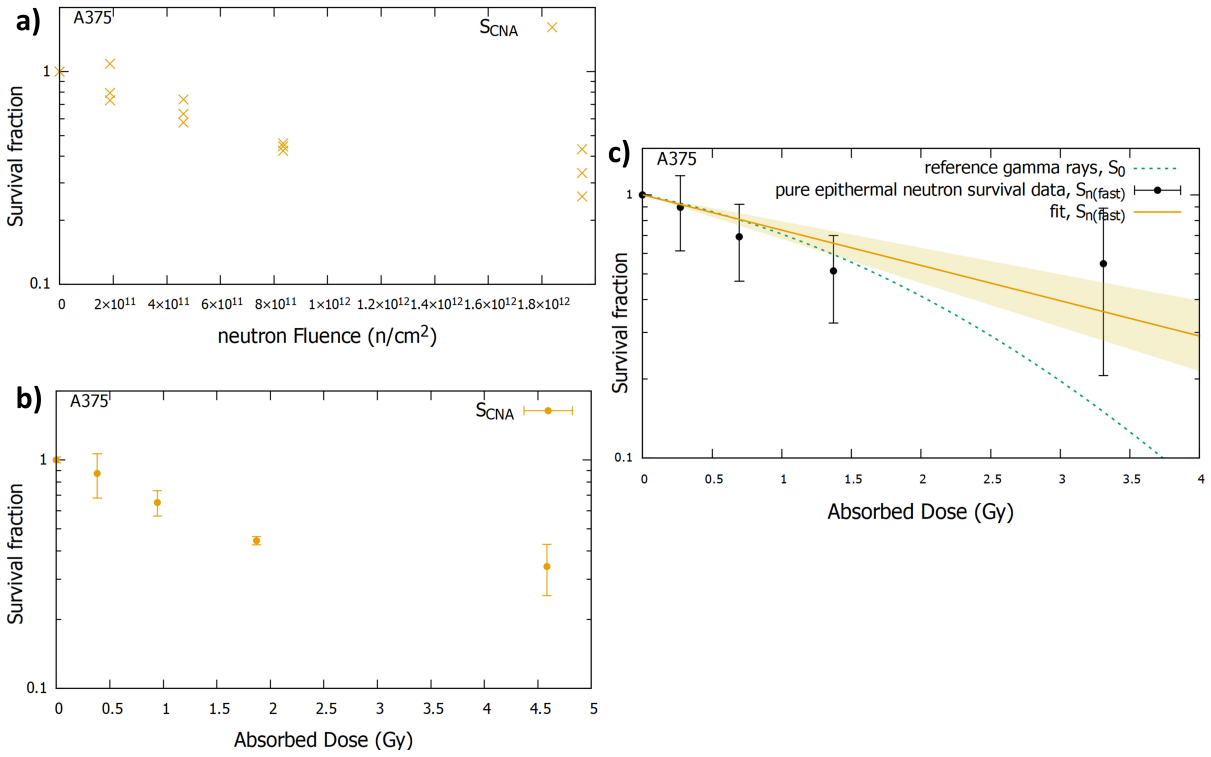

Figure 5.21: Results of irradiation of A375 cells with epithermal neutrons at CNA, Seville. a) Results as a function of the neutron fluence and b) as a function of the neutron dose. c) Survival corresponding to only neutrons of CNA beam (mostly epithermal), subtracted by using photon data from Experiment V.

Taking a look at the data, a different tendency is seen at low dose than at high dose, where the point at high dose present a survival higher than expected. The assumption for high-LET radiation in Eq.(5.4) of $\beta = 0$ is more accurate as the dose is lower, since the quadratic behavior only plays a role for large doses. Following this argument we have fitted again the values of S_n, but taking into account only the first three points (Figure 5.22). In this case, the $\alpha_{n(fast)} = 0.49 \pm 0.1$ which lead to a $w_f^* = 2.0 \pm 0.7$. This is a RBE factor still lower than the one found for low-energy neutrons ($w_t^* = 3.45$), so the decrease of the neutron effect at 10-100 keV predicted in Chapter 3 Section 3.5.4 is confirmed again. Discarding the apparently anomalous data at the highest dose, it can be seen in Figure 5.22 how the fit of the pure neutron survival effect keeps below the photon one at low doses, showing the expected stronger effect of the neutron than the photon irradiation.

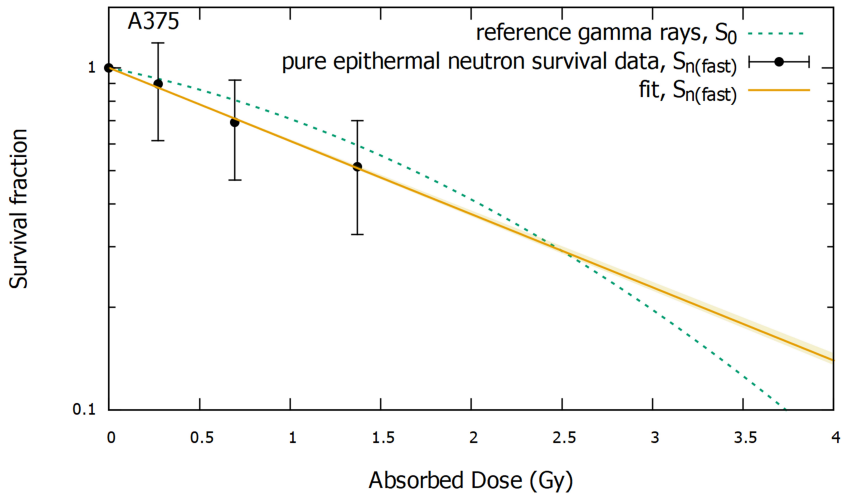

Figure 5.22: Survival at low dose corresponding to only neutrons of CNA beam (mostly epithermal), subtracted by using photon data from Experiment V.

Despite the fact that this experiment was a first trial to establish if the CNA beam could be used for radiobiological data collection, the results encourage from the point of view of future irradiations. Data for additional cell lines would be useful as well as more data for A375 to improve certainty in the values obtained.

5.6 Discussion of the results

Only one end-point (effect after irradiation), the one corresponding to clonogenic assays, was shown and used to analyze the effect in Experiments I-V. The results of the other study, the colorimetric assays, that express the proliferation end-point, are displayed in Appendix B.

Generally, the evaluation of the biological effect of relevance in healthy tissue should be carried out with a different end-point: the normal tissue tolerance, since the essential in healthy tissue is that the tissue survives with minimum adverse effects. This end-point could be correlated with the *in vitro* survival [Burn92], but ideally should be study *in vivo*, therefore it would be interesting to carry out similar experiments on animals in the future.

In all the experiments a variability of response between the different cell lines was observed. Therefore, extrapolating weighting factors (RBE or CBE) to different tissues is not a recommended practice; the individual study of biological response for each tissue/cell line is necessary.

The composition of each cell line proved to be key in the calculation of the dose, especially the percentage of nitrogen and hydrogen. In this way, the CHNS elemental analysis used for Experiment IIa should be used to analyze the composition of all irradiated cell lines and thus not depend on the accuracy of the data found in the literature.

Boron uptake measurements are fundamental for a good calculation of the dose delivered to the cells. ICP and neutron autoradiography have proven to be excellent techniques for boron uptake analysis, as the large amount of boron compounds studies in BNCT have also demonstrated.

Irradiations in a pure neutron beam such as that at ILL have allowed to show that the error made in the extraction of the neutron survival does not have a great effect on the final result, whatever photon data are used in the extraction. However, a decrease in the photon dose component at the ILL beam would yield still better results. As the photon dose arises mainly from captures in hydrogen in the culture medium, finding an experimental arrangement that allows the use of less medium would help to reduce the error in the S_n data. The first step would be irradiation of individual cuvettes, *i.e.* pushing the trade-off between optimum neutron-to-gamma ratio and efficient use of beam time towards the former. The next step would be the use of cuvettes with only 1 mm or even 0.5 mm thickness of water layer instead of 2 mm now. This would render the cell transfers more delicate but does not appear impossible.

The accuracy of the photon irradiation data is important when used as a reference radiation in the comparison of neutrons for the RBE estimation. A type of reference photon radiation, at a specific dose rate, generally stipulated, is desirable. Irradiation at LINACs at dose rates of few Gy/min are a good option in acquiring data for the reference photon dose, providing a comparison with a standard irradiation field for which there is a lot of clinical experience.

The inability to obtain data directly from photons of a beam has been overcome with Experiment II. This experiment was shown to be designed appropriately for extracting results for the effect of photons and neutrons, without using data from other experiments. Only one cell line has been studied for now, but since the idea of the experiment seems relevant, more cells and tissues should be studied.

One of the most remarkable results is the comparison of the data obtained for the cell line irradiated in Experiments I, III, IV and V: A375. This was the only one for which all the effects from the different BNCT dose components were studied. The effect of low-energy neutrons

appears to be higher than the epithermal one and $w_t^* > w_f^*$. This result supports one of the main arguments of the thesis: that the use of the same RBE for thermal and fast neutrons is not advisable. This is also in consistence with the graph 3.7 illustrated in Chapter 3, where the w^* factor for an average of mammalian tissue showed a RBE value higher for the thermal than for the epithermal region of 0.01 keV-100 keV, a range that coincides mostly with the energies of the irradiations at CNA.

Conclusions

This work has been based on the proposal of theoretical revisions and the provision of data aimed at achieving a better estimation of the dose administered and the cellular damage resulting from BNCT neutron irradiation.

There has been illustrated how the currently used RBE factors for the different dose components depend on the dose delivered, therefore using fixed factors may provide wrong estimations of the biological effects when extrapolating to different doses. This is corrected in the present proposal of a new formalism, which combines the simplicity of the currently used one with the physically realistic photon iso-effective one. This new formalism allows also using previous radiobiological data and adapting them to this new form of calculation. It is expected that the proposed formalism brings the views of physicians and physicists closer, and that the effect on patients can be efficiently and more accurately estimated.

A study of the effect of the secondary particles emitted in the interaction of neutrons with tissues has shown how the effect of neutrons depends on their energy. Hence, the RBE factors describing this effect should not be taken as a constant.

Since the cellular damage arising from neutron irradiation depends on different factors, its study requires a wide range of experimental data. In order to extend the available data relating to the effect of neutron irradiation, several experiments at different facilities were designed and carried out using various cell lines. This was initiated with irradiation studies of photons as a good reference dose, followed by irradiation studies using low-energy neutrons, and subsequently a dedicated research facility that provides epithermal neutrons. A broad range of experimental approaches was used in this work, involving extensive collaboration and bringing to the results variability and quality.

It has been shown how with an appropriate set up and a clean cold neutron beam, such as the one at ILL, the radiobiological coefficients α_n for thermal neutrons can be obtained with more precision than in previous work. Here they have been obtained with an uncertainty of less than 15% for some tumor and normal cell lines. However, the same accuracy for the RBE factors requires similar precision for the photon radiobiological data. A setup for obtaining these from a hospital LINAC has been proposed.

Experiments carried out using the cold neutron beam at ILL has proved very useful for the study of the thermal dose associated with BNCT, as well as for the analysis of the efficacy of the boron compounds in use. Moreover, for the first time they have allowed the effect of the photons in the beam to be isolated from that of the neutrons through the use of nitrogen isotopic labelling of the cells under study.

Preliminary results from the CNA Sevilla epithermal beam illustrated the dependence of the RBE on neutron energy. More irradiations will be carried out at this facility, but as the fast component can be different for different beams, it is advisable for each BNCT epithermal neutron facility to measure specifically their own fast neutron RBE factors (w_f^* or w_f).

The large amount of data obtained from the different irradiation studies of the various cell lines will be of value for a better understanding of BNCT dosing, and thus for a better individual adaptation of the treatment to individual patients. Since a major aspect of the response to BNCT depends on the tissue being irradiated, the experiments described here should be extended to the study of other cell lines and boron compounds and, eventually, to tissues and animals.

Another conclusion that has been reached is the necessity to standardize the photon reference dose. This will be very helpful in future studies of the effect of neutrons in BNCT and will help make the results obtained worldwide easily comparable to each other. We intend to continue the irradiation work at the LINAC and to study how the dose rate affects the biological effect so as to find an optimal photon dose rate.

As a result of this study and of other similar ones carried out by other groups, the collection of data on the effect of neutrons and boron compounds is very extensive. It is suggested here that there would be considerable benefit in assembling a database that could be easily accessible to researchers in this and related fields, and that this would help push the BNCT research through diffusion and sharing. The creation of this database as well as the continuation

and development of the irradiation experiments in the various facilities is a major priority for the future.

Conclusiones

Este trabajo se ha basado en la propuesta de revisiones teóricas y la provisión de datos experimentales destinados a lograr una mejor estimación de la dosis administrada y el daño celular resultante de la irradiación con neutrones para BNCT.

Se ha mostrado cómo los factores RBE utilizados actualmente para los diferentes componentes de la dosis en BNCT dependen de la dosis administrada y, por lo tanto, el uso de factores fijos puede proporcionar estimaciones erróneas de los efectos biológicos cuando se extrapola a diferentes dosis. Esto se corrige en la propuesta actual de un nuevo formalismo, que combina la simplicidad del formalismo que se usa actualmente con el físicamente realista denominado iso-efectivo. Además, este nuevo formalismo permite el uso de datos radiobiológicos anteriores, adaptados para esta nueva estimación del efecto biológico. Se espera que el formalismo propuesto acerque los puntos de vista de médicos y físicos, y que el efecto sobre los pacientes pueda estimarse de manera eficiente y, a la vez, más precisa.

Un estudio del efecto de las partículas secundarias emitidas en la interacción de los neutrones con los tejidos ha demostrado cómo el efecto de los neutrones depende de su energía, por lo que, el uso actual de los factores RBE de neutrones que describen este efecto como constante no es recomendable.

Dado que el daño celular derivado de la irradiación con neutrones depende de diferentes factores, su estudio requiere una amplia gama de datos experimentales. Para ampliar los datos disponibles se diseñaron y llevaron a cabo varios experimentos en distintas instalaciones utilizando diversas líneas celulares. Comenzando con estudios de irradiación con fotones para la obtención de una dosis de referencia adecuada, seguidos de estudios de irradiación con neutrones de baja energía, y finalizando con estudios en un haz que proporciona neutrones epitérmicos, en este trabajo se ha utilizado una amplia gama de enfoques experimentales, que implican una amplia colaboración y aportan a los resultados variabilidad y calidad.

Se ha demostrado que, con una configuración adecuada y un haz de neutrones fríos carente de gran contaminación de neutrones de alta energía y fotones, como el utilizado en las irradiaciones en ILL, los coeficientes radiobiológicos α_n para describir el daño por neutrones térmicos se pueden obtener con más precisión que en trabajos anteriores. En este trabajo se han obtenido con una incertidumbre de menos del 15% para algunas líneas celulares tumorales y sanas. Sin embargo, para una buena precisión en la obtención de los factores RBE requiere que los datos radiobiológicos de fotones sean obtenidos con una precisión similar a la de los neutrones. Con este objetivo, se ha propuesto una configuración para obtener estos datos de fotones en un LINAC hospitalario.

Los experimentos realizados con el haz de neutrones fríos de ILL han demostrado ser muy útiles para el estudio de la dosis térmica asociada con BNCT, así como para el análisis de la eficacia de los compuestos de boro. Además, han permitido que, por primera vez, el efecto de los fotones en el haz se aísle del de los neutrones, gracias a la técnica de reemplazo isotópico de nitrógeno en las células.

Los resultados preliminares con el haz epitérmico del CNA en Sevilla ilustraron la dependencia del RBE con la energía de neutrones al obtener en las células un efecto menor que el obtenido con neutrones de baja energía en ILL. Se realizarán más irradiaciones en esta instalación, pero como el componente correspondiente puede ser diferente para diferentes haces, es aconsejable que cada instalación de neutrones epitérmicos de BNCT mida específicamente sus propios factores de RBE de neutrones epitérmicos (w_f^* o w_f).

La gran cantidad de datos obtenidos en los diferentes estudios de irradiación de las diversas líneas celulares será valiosa para una mejor comprensión de la dosis en BNCT y, por lo tanto, para una mejor adaptación individual del tratamiento a los pacientes. Dado que la respuesta a la BNCT depende del tejido que se irradia, los experimentos descritos aquí deberían extenderse al estudio de otras líneas celulares y compuestos de boro y, finalmente, a tejidos y modelos animales.

Otra conclusión a la que se ha llegado es la necesidad de estandarizar la dosis de referencia de fotones. Esto sería muy útil para futuros estudios sobre el efecto de los neutrones en BNCT y ayudaría a que los resultados obtenidos en todo el mundo fueran fácilmente comparables entre sí. Por nuestra parte, tenemos la intención de continuar las irradiaciones en el LINAC

hospitalario y estudiar cómo afecta la tasa de dosis en el efecto biológico para encontrar una tasa de dosis óptima de fotones.

Como resultado de estos estudios y de otros similares realizados por otros grupos, la colección de datos sobre el efecto biológico de los neutrones y los compuestos de boro es muy extensa. Sería beneficioso llevar a cabo una recopilación de estos resultados en una base de datos que pudiera ser fácilmente accesible para los investigadores en este y otros campos relacionados. Esto ayudaría a impulsar la investigación en BNCT a través de la difusión y el intercambio. La creación de esta base de datos, así como la continuación y el desarrollo de los experimentos de irradiación en las diversas instalaciones es una prioridad importante para el futuro del proyecto.

Appendix A

ILL beam and set-up simulations

Appendix A describes the simulations used for the dose calculation of the ILL irradiations at the PF1b beam line, corresponding to Experiments I-III.

A.1 Collimation

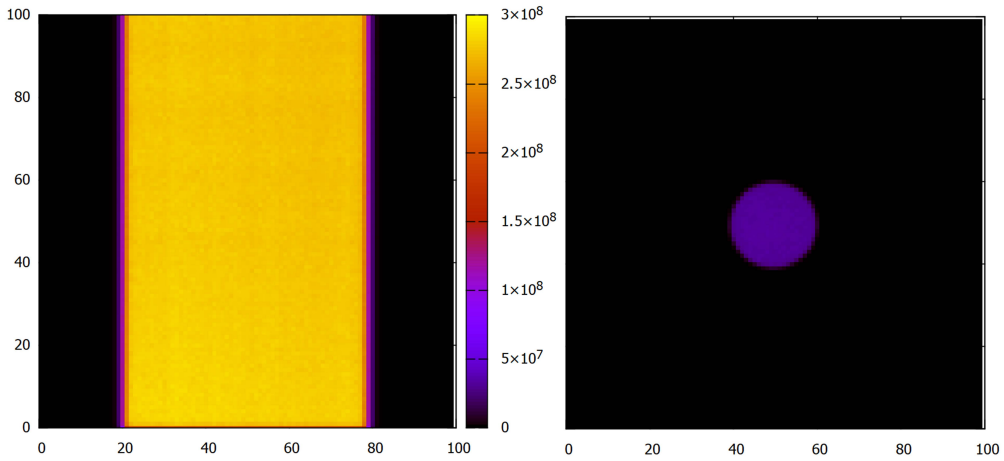

Figure A.1: Left, size (in mm) and intensity of the neutron beam at the end of the H113 guide at the PF1b line used for ILL irradiations during Experiments I-III. Right, size and intensity of the neutron beam after the collimation system, at the sample position.

The collimation used on PF1b at ILL is installed at the end of the H113 guide with the purpose of focusing the 10 cm x 6 cm neutron beam to a circular one of 2cm diameter. The collimation system consists of a succession of tubes with a total length of ~3 meters containing B_4C collimators. This system has been installed with a view to minimizing the photon content of the neutron beam. There are three 5cm thick lead pieces along the tubes, one after the first collimator and two after the last two collimators (see Figure 4.4 in Chapter 4 or points 1,2 and

3 in Figure A.2). The last collimator is made of LiF (+ Pb) in order to avoid the secondary production of photons, such as those created after neutrons are captured by B_4C.

The collimation system was simulated using the McSTAS and MCNPx programs. McSTAS allows the neutron transportation to be defined; it also allows a detailed characterization of the neutron beam at the end of the tubes. MCNPx simulates both photons and neutrons, in order to define the low quantity of photons that are in the beam. In Figure A.2 the MCNPx simulation of the collimation system is shown, with the irradiation area at the end of it (empty and only including the beamstop). In the figure, neutrons are clearly collimated at the sample position and stopped after it. Photons are created mainly in the two B_4C collimators (points 1 and 2), but stopped in the lead just after them. The irradiation area where samples are placed thus has low gamma contamination.

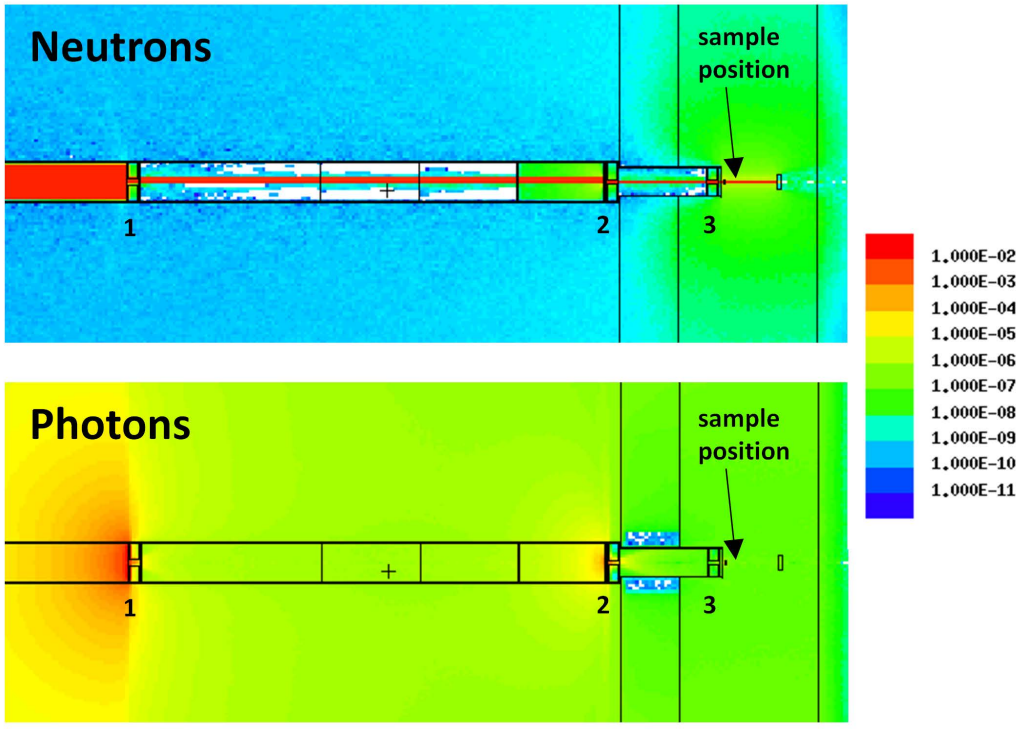

Figure A.2: MCNPx simulation of the collimation system. Neutron and photon intensity is represented per starting particle (neutrons).

The neutron flux is reduced by one order of magnitude by the collimation system. At the sample position, a gamma flux of $3.2 \cdot 10^7$ γ/cm^2s is found compared to the neutron flux of $1.5 \cdot 10^9 n/cm^2s$ which means that only 2% of the irradiating beam are photons.

A.2 Homogeneity

Due to the importance that all the cells in the samples are equally irradiated, it was essential to check the beam homogeneity. McSTAS simulations, that include all the collimation system after the H113 guide, resulted in a beam with less than 5% inhomogeneity over the sample area. The alignment of the beam was done taking the maximum intensity point as a reference for the center.

Radiochromic films (Gafchromic EBT2) were irradiated for a range of exposure times. A gray mark appeared where the neutrons passed through the film (see figure 4.6). An analysis of the grey scale intensity was performed for the different irradiation times, allowing the flux to be calibrated against the measured grayscale value.

From the analysis of all the films of the gray values along the *x* and *y* axis, we found that the measurements corroborate the simulations that the beam is very homogeneous, with less than 5% deviation from the mean flux over the sample area.

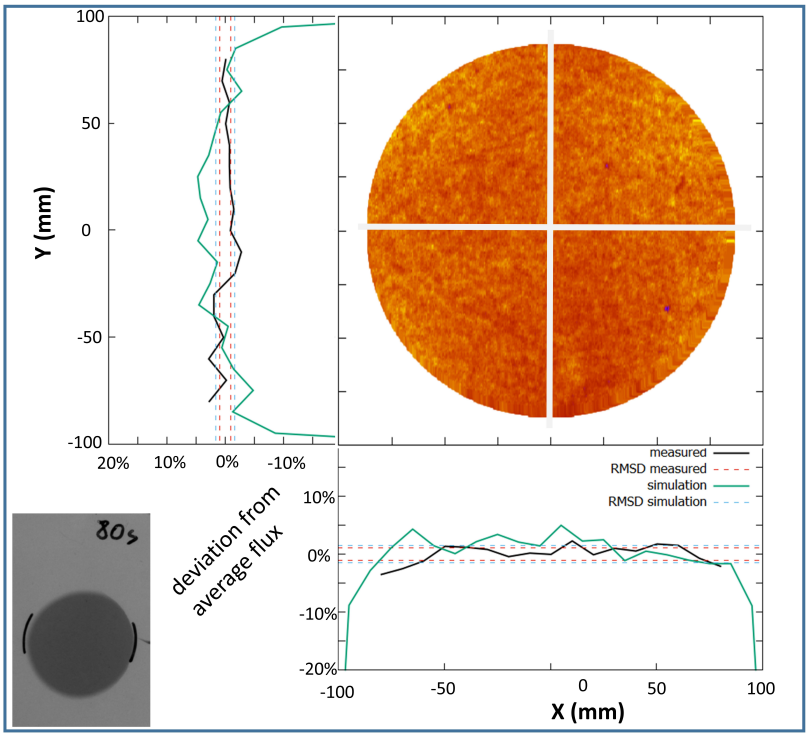

Figure A.3: Results of the analysis of homogeneity of the Pf1b beam. The bottom-left shows a picture of a film irradiated for 80 seconds, with the exposure of the neutron beam clearly visible. The gray scale values are represented in orange gradient. The deviation from the average flux along the axis (where the white lines are marked) are represented in the two graphs. The RMSD (root-mean-square deviation) is less than 2%, for both measured and simulated data.

Additionally, Cu foils were activated in different positions of the beam and the resulting ^{64}Cu activity was analyzed. Again, there was not more than 5% of difference between left side and right side of the beam.

Having confirmed the beam homogeneity, the McSTAS beam simulation results were used as input to the MCNPx simulations of the experimental set-up.

A.3 Materials

A good definition of the material is essential for realistic simulations of particle interactions following irradiation. In some cases the elemental composition is known while for others it can be found from previously published studies – see for example [McCo11]. The composition of the culture media used in this workwas estimated from their biochemical content and data sheets provided by suppliers.. The estimated elemental composition of DMEM medium is given in Table A.1.

DMEM

Components	Molecular Weight (g/mol)	Concentration (mg/L)	mM	Formula	n atoms total	%
Amino Acids						
Glycine	75.0647	30	0.4	NH2-CH2-COOH	10	0.0017
L-Arginine hydrochloride	210.6578	84	0.398104	C6H15ClN4O2	28	0.0049
L-Cystine 2HCl	313.2174	63	0.201278	C6H14Cl2N2O4S2	30	0.0037
L-Glutamine	146.1404	584	4		20	0.034
L-Histidine hydrochloride-H2O	191.6111	42	0.2	C6H10ClN3O2	22	0.0024
L-Isoleucine	131.1687	105	0.801527	C6H13NO2	22	0.0061
L-Leucine	131.1687	105	0.801527	C6H13NO2	22	0.0061
L-Lysine hydrochloride	182.6444	146	0.797814	C6H15ClN2O2	26	0.0085
L-Methionine	149.2077	30	0.201342	C5H11NO2S	20	0.0017
L-Phenylalanine	165.1827	66	0.4	C9H11NO2	23	0.0038
L-Serine	105.0897	42	0.4	C3H7NO3	14	0.0024
L-Threonine	119.1157	95	0.798319	C4H9NO3	17	0.0055
L-Tryptophan	204.2174	16	0.078431	C11H12N2O2	27	0.0009
L-Tyrosine disodium salt dihydrate	261.175238	104	0.398467	C9H13NNa2O5	30	0.0061
L-Valine	117.1427	94	0.803419	C5H11NO2	19	0.0055
Vitamins	0					
Choline chloride	139.6207	4	0.028571	C5H14ClNO	22	0.0002
D-Calcium pantothenate	476.5174	4	0.008386	C18H32CaN2O10	63	0.0002
Folic Acid	441.3829	4	0.00907	C19H19N7O6	51	0.0002
Niacinamide	122.1204	4	0.032787	C6H6N2O	15	0.0002
Pyridoxine hydrochloride	205.6327	4	0.019417	C8H12ClNO3	25	0.0002
Riboflavin	376.3508	0.4	0.001064	C17H20N4O6	47	2E-05
Thiamine hydrochloride	337.2608	4	0.011869	C12H18Cl2N4OS	38	0.0002
i-Inositol	180.15	7.2	0.04	C6H12O6	24	0.0004
Inorganic Salts	0					
Calcium Chloride	110.984	200	1.801802	CaCl2	3	0.0116
Ferric Nitrate	403.9911	0.1	2.48E-04	FeH18N3O18	40	6E-06
Magnesium Sulfate	120.366	97.67	0.813917	MgSO4	6	0.0057
Potassium Chloride	74.5513	400	5.333334	KCl	2	0.0233
Sodium Bicarbonate	84.004769	3700	44.04762	NaHCO3	6	0.2153
Sodium Chloride	58.442769	6400	110.3448	NaCl	2	0.3724
Sodium Phosphate monobasic	137.990531	125	0.905797	NaH2PO4-H2O	11	0.0073
Other Components	0					
D-Glucose (Dextrose)	180.15	4500	25	C6H12O6	24	0.2619
Phenol Red	354.362	15	0.039851	C19H14O5S	39	0.0009
Sodium Pyruvate	110.040769	110	1	C3H3NaO3	10	0.0064
TOTAL	6416.723276	17185.37	200.1188		758	0.0172

DMEM solution

Dilution	Concentration (g/L)	%
DMEM	17.18537	0.0172
Water	982.81463	0.9828

Table A.1: Elemental analysis of the DMEM medium following the molecular information provided by the company (HyClone, Logan, USA); 1st-4th columns.

The information of the element composition of the materials used in the simulations are expressed in Table A.2. Nitrogen labeled culture media element concentration has been obtained from a CHNS Elemental analyzer (THERMO SCIENTIFIC Flash 2000), like in Experiment IIb (see Chapter 4).

Material	Composition, mass fraction
Quartz	^{16}O 0.53, Si 0.46
DMEM medium	^{1}H 0.11, ^{12}C 0.003, ^{14}N 0.00025, ^{16}O 0.87798, ^{23}Na 0.00359, ^{35}Cl 0.0043 (Others 0.00088: Mg, ^{31}P, ^{32}S, ^{39}K, ^{40}Ca, Fe)
BIOEXPRESS-6000 media	^{1}H 0.0897, ^{12}C 0.0051, ^{14}N 0.0009 , ^{16}O 0.90 (CHNS Elemental analyzer)
Cells (A375)	^{1}H 0.094, ^{12}C 0.241, ^{14}N 0.056, ^{16}O 0.615 [Maug97]
Cells (U87)	^{1}H 0.107, ^{12}C 0.145, ^{14}N 0.022, ^{16}O 0.712 [ICRU46]
Cells (Hek)	^{1}H 0.107, ^{12}C 0.064, ^{14}N 0.016, ^{16}O 0.804 [ICRU46]
Cells (MRC5)	^{1}H 0.103, ^{12}C 0.105, ^{14}N 0.031, ^{16}O 0.749 [ICRU46]
Cells (ICRU-33)	^{1}H 0.10, ^{12}C 0.11, ^{14}N 0.03, ^{16}O 0.76 [ICRU46]
Air	C 0.0001, ^{14}N 0.75, ^{16}O 0.24, Ar 0.01
Lithium Fluoride	^{6}Li 0.27, ^{19}F 0.73
Polyethylene Borated (5-10%)	^{1}H 0.13, B 0.10, C 0.77
Boron carbide rubber	^{1}H 0.06, B 0.39, C 0.55
Teflon	C 0.24, ^{19}F 0.76
Concrete	^{1}H 0.01, ^{16}O 0.532, ^{23}Na 0.029, ^{27}Al 0.034, Si 0.337, Ca 0.044, Fe 0.014 [McCo11]

Table A.2: Elemental composition of the materials used in the MCNPx simulations of the ILL experiments. No mass number indicated represents the natural element, with the natural abundance of each isotope included.

The data used in the simulations for the cells and culture media include the effect of hydrogen molecularly bound in the water, so slow neutron cross-section data is enclosed.

A.4 Flux measurements vs simulations

Gold and zirconium foils were used to characterize the beam flux for each experiment. Variations in reactor power during individual experimental sessions may occur as well as changes in the collimation system. Table A.3 summarizes the measured neutron capture fluxes for the different irradiation dates.

	Capture flux (n_{th}/cm^2 s)
June 2018	$1.75 \cdot 10^9$
September 2018	$1.05 \cdot 10^9$
June 2019	$2.80 \cdot 10^9$

Table A.3: Measured neutron capture flux at sample position for each experimental campaign.

Gold foils measurements for the various arrangements were used to measure the flux; these were then compared with simulations. The results are shown in Figure A.4 and Figure A.5. First graphs row in Figure A.4 corresponds to gold foils situated before and after each cuvette, for different dates and using the same diameter of the foils. The standard one cm diameter foils could have border effects if they are not situated exactly in the center of the sample, *i.e.* particles passing through the borders of the foil would have traversed through the lateral quartz walls of the cuvette instead of being attenuated by the medium. Because of this reason foils of 0.6 cm diameter were used too. The second row of graphs includes experiments using this 0.6 cm foils and cuvettes filled with D_2O. Figure A.5 include experiments using only 1 cuvette but with distinct thickness. The last row includes the arrangement of only 1 cuvette of 2 mm thickness (the one used in cell irradiation experiments) and the one corresponding to Zr foils inside the cuvettes.

In spite of the measured/simulated differences observed in Figure A.4 and Figure A.5, it is appreciable that the error is similar for the different cases. Since the simulations, from the beam with McSTAS to the geometry/materials in MCNPx, have assumed perfect conditions (perfect guide, homogeneous materials, samples exactly perpendicular to the beam and centered), some differences between measured and simulated data can be expected. Independently of the normalization factor used, the particle transportation is well simulated, since the average error in the flux ratio between the foils comparing measured and simulated is less than 10%.

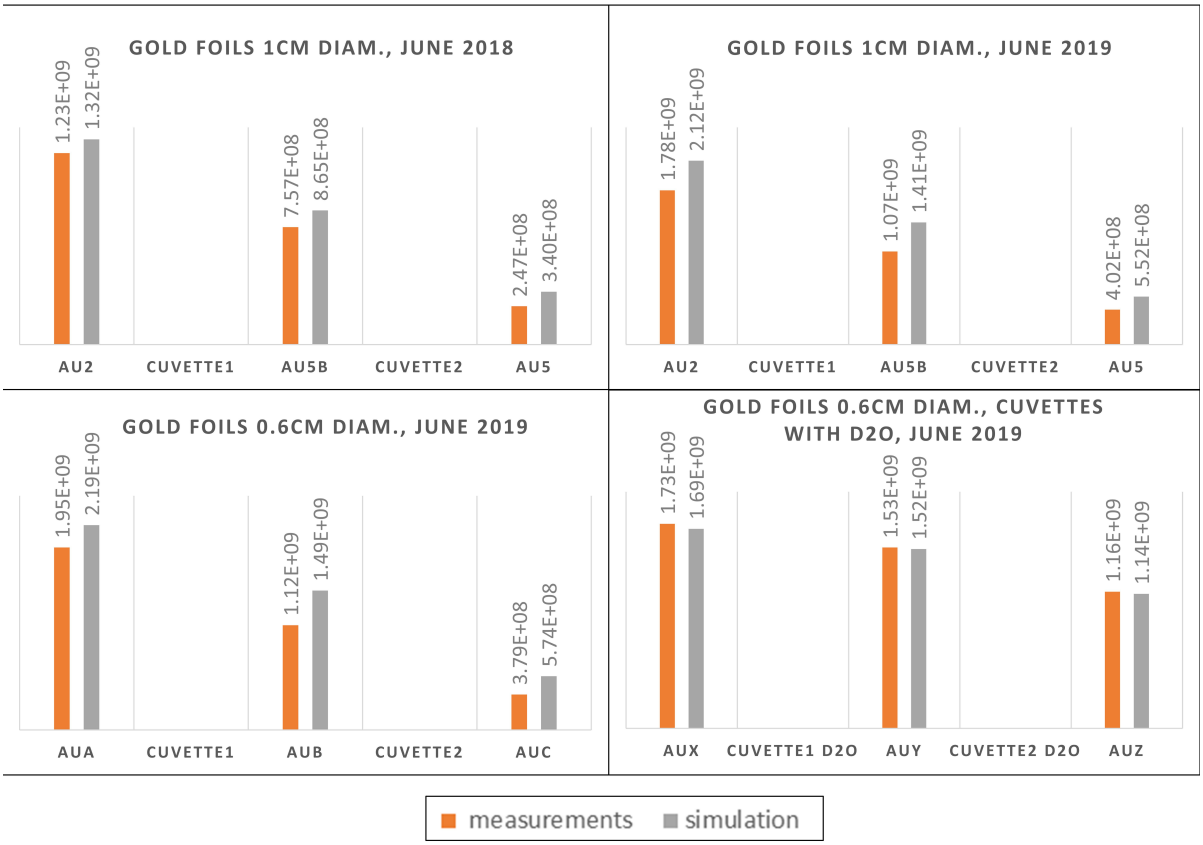

Figure A.4: Measured and simulated flux (n/cm^2 s) comparison for the different foils used in the various experimental arrangements: two cuvettes filled with culture medium (same set-up as for cell irradiation), or D_2O in the last graph, and gold foils situated before and after each cuvette.

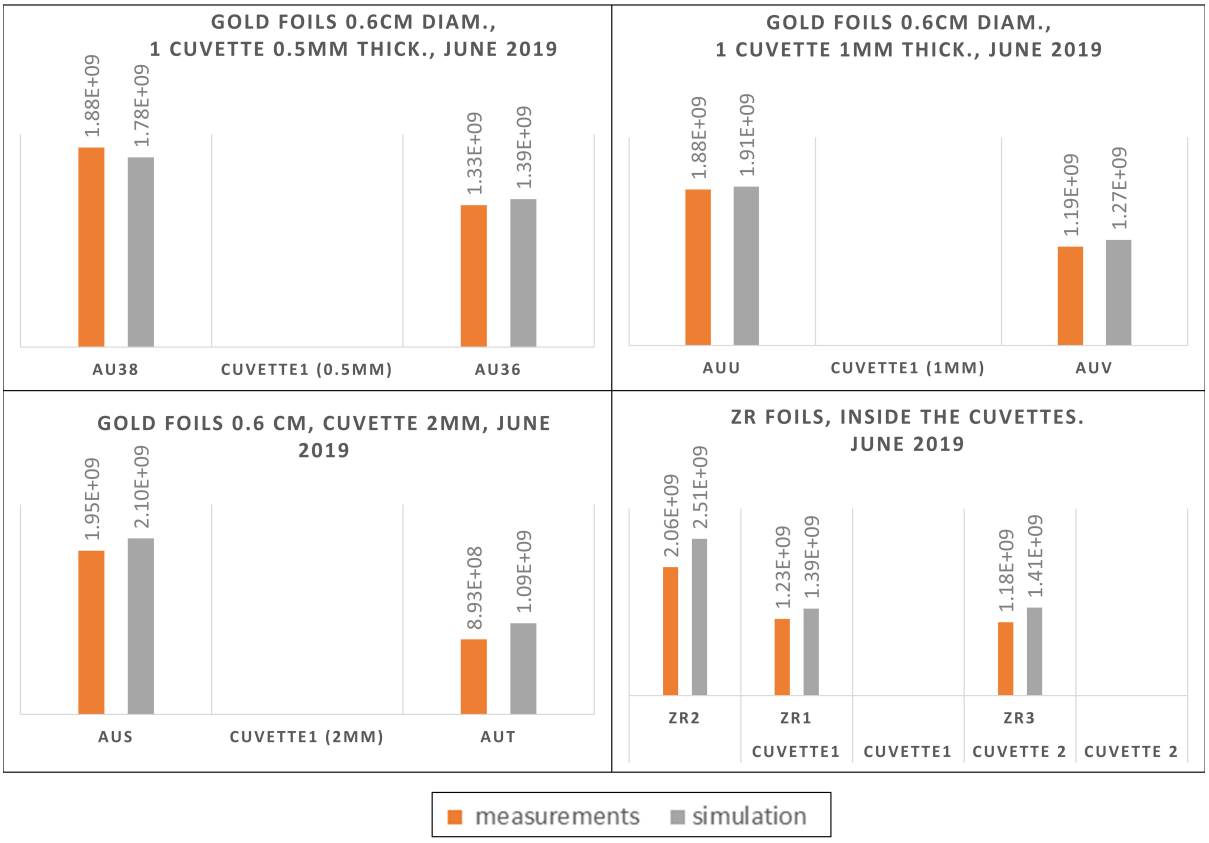

Figure A.5: Measured and simulated flux (n/cm^2 s) comparison for the different foils used in the various experimental arrangements: one cuvette of different thickness for the first three graphs and two cuvettes with Zr foils inside for the last one.

A.5 Dose, kerma and the charge-particle equilibrium effect

An important assumption was explained and justified in Chapter 3: that the dose can be approximated to the kerma when it is assumed that all energy is deposited locally. In the case of the ILL irradiation experiments, this means that to calculate the dose by means of the kerma, it is assumed that all secondary particles emitted in the neutron irradiation leave their energy in the cell layer. In general this is a reasonable assumption, since the secondary particles usually have a low range. However, the protons emitted after the capture of neutrons in nitrogen near the boundaries may deposit some of their energy outside the cell layer. When those particles that escape outside the area of interest are compensated with others of the same characteristics that enter from the adjacent materials, it is said that the charge particle equilibrium (CPE) is

fulfilled and the kerma approximation to the dose is accurate. That is, the energy of the protons that deposit energy outside is compensated by that from the protons from outside that deposit energy inside, coming from outside. This balance is not fulfilled in our case, because the adjacent materials are quartz, that lack in nitrogen, and culture medium, which concentration of nitrogen is 100 times smaller than in cells (Figure A.6 includes a schematic representation of the effect). Hence, the dose can be calculated using the kerma, but it must be taken into account the fact that the CPE is not accomplished and that part of the energy escapes from the area of study.

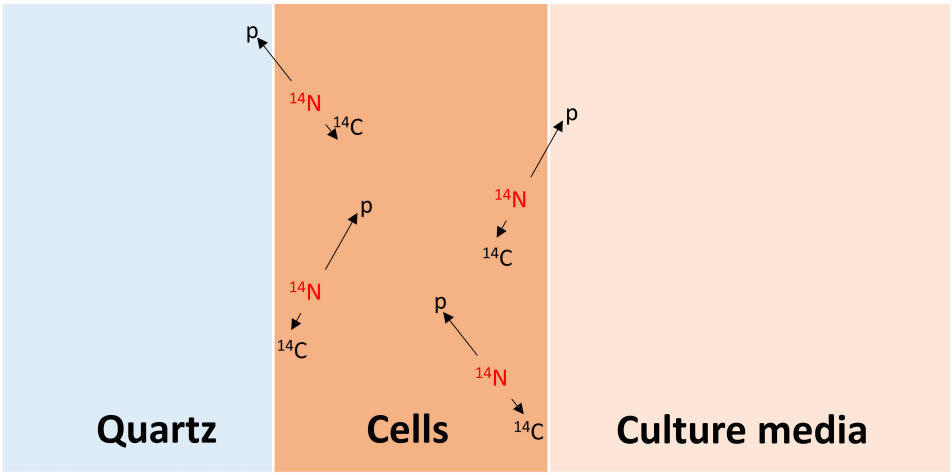

Figure A.6: Drawing of the incomplete Charge Particle Equilibrium effect in the sample arrangement used. Proton emission following neutron capture occurs very differently in the quartz, cell, and culture parts of the sample.

This effect must therefore be taken into account in the calculation of the thermal dose, which depends on the capture in the nitrogenous parts of the sample system. The effect varies according to the width of the cell layer. A lower thickness will allow more protons to escape so the dose inside the cell layer will be lower. A study was carried out by simulating (with MCNPx) the amount of protons emitted in the cell layer and those which deposit their energy out of it, taking into account that the 42 keV from the ^{12}C recoils were dominantly deposited inside. The dose percentage lost was then extracted from this study for different cell layer thickness (Table A.4).

Cell layer thickness (μm)	Percentage proton energy lost (respect to proton energy)	Percentage proton energy lost (respect to the reaction energy)
10	27.7 %	25.8%
15	18.5 %	17.3%
20	14.0 %	13.1%

Table A.4: Percentage of emitted protons, after the neutron captured in nitrogen, that deposit their energy outside of the cell layer

A wide range of references have described the size of the cell lines irradiated as between 11-19 μm [Echa07] [Luo14] [webBio]. These results were corroborated by measurements using a cell counter Countess™ II (Thermo Fisher Scientific, Waltham, USA). In the simulations, a thickness of 15 μm was therefore assumed for the cell layer.

The amount of nitrogen in the cell line together with the assumed width of the layer, with the CPE effect included, makes the dose of neutrons arising from the captures in nitrogen (the thermal dose) dependent on the cell line used. In the following table the dose components for ILL irradiations for each cell line in each cuvette are given, assuming the measured flux value for the June 2019 campaign.

	Thermal dose (Gy/min)		Gamma dose (Gy/min)		Boron dose (Gy/min/[^{10}B]ppm)	
	Cuvette 1	**Cuvette 2**	**Cuvette 1**	**Cuvette 2**	**Cuvette 1**	**Cuvette 2**
A375	0.095	0.044	0.021	0.016	0.022	0.010
U87	0.037	0.017	0.021	0.016	0.022	0.010
Hek	0.027	0.013	0.021	0.016	0.022	0.010
MRC5	0.052	0.024	0.021	0.016	0.022	0.010
Cal33/SQ20 (ICRU-33)	0.044	0.021	0.021	0.016	0.022	0.010

Table A.5: Dose rates of the different cell lines irradiated at the ILL PF1b beam line. Simulations included the effect of material composition and of the CPE effect.

Appendix B

Another end-point: proliferative ability

The proliferative ability of irradiated cells has been another end-point studied in most of the experiments by Resazurin and BrdU based-assays. In this way, most of the survival results shown in Chapter 5 are complemented with the additional information that these studies provide. The difference between the different types of irradiation or the equivalence with the survival results of Chapter 5 can be checked. For Experiments II and IV this additional study was not performed, while the results of Experiments I, III and V will be displayed.

B.1 Proliferation results of experiments I, III and V

As explained in Chapter 4 (Sections 4.6.2 and 4.6.3), Resazurin and BrdU provide colorimetric assays that are commonly used to measure cell proliferation. Thus, this end-point is represented by the absorbance, relative to the control, as a function of the absorbed dose. The results will be presented as in Chapter 5: firstly those corresponding to photons for Experiment V and then those corresponding to irradiations with neutrons of samples without and with BPA respectively. The following three figures are the analog of the survival results shown in Chapter 5 for these experiments. Similarities between the two end-points, survival and proliferation, are found, and parallel conclusions can be reached.

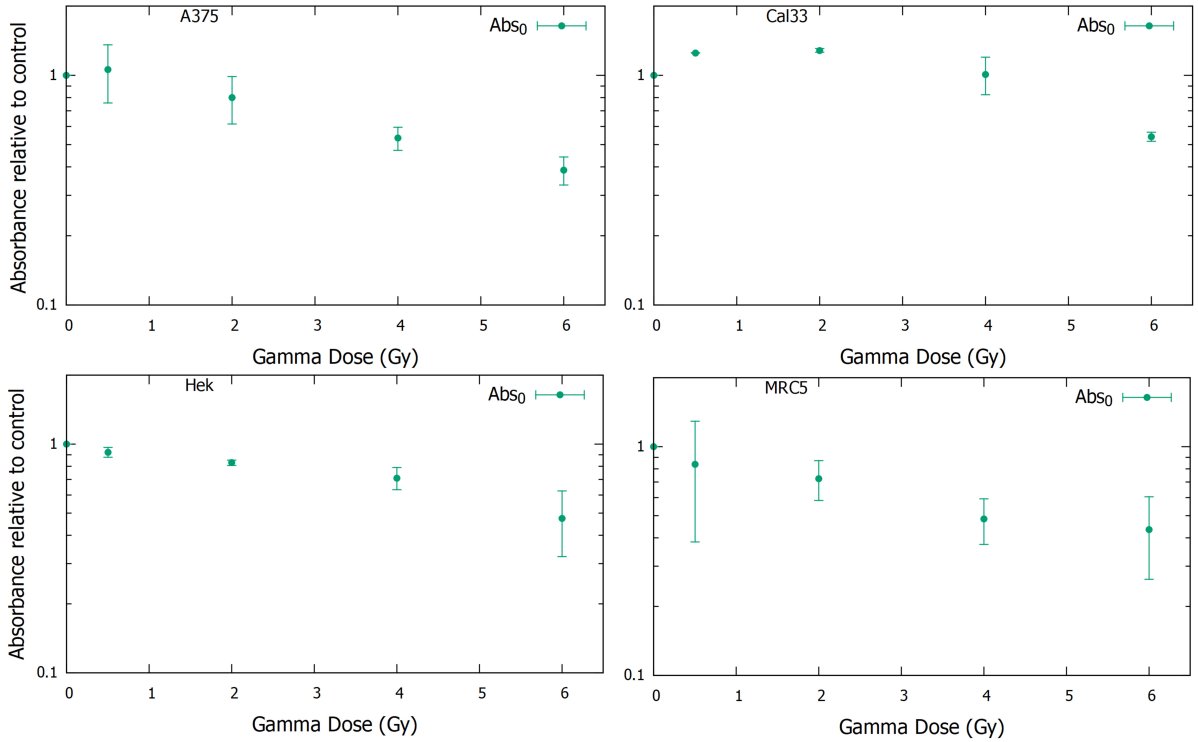

Figure B.1: Proliferation results for Experiment V by Resazurin colorimetric assay. Results are supplementary to the clonogenic assay shown in Figure 5.1 Chapter 5.

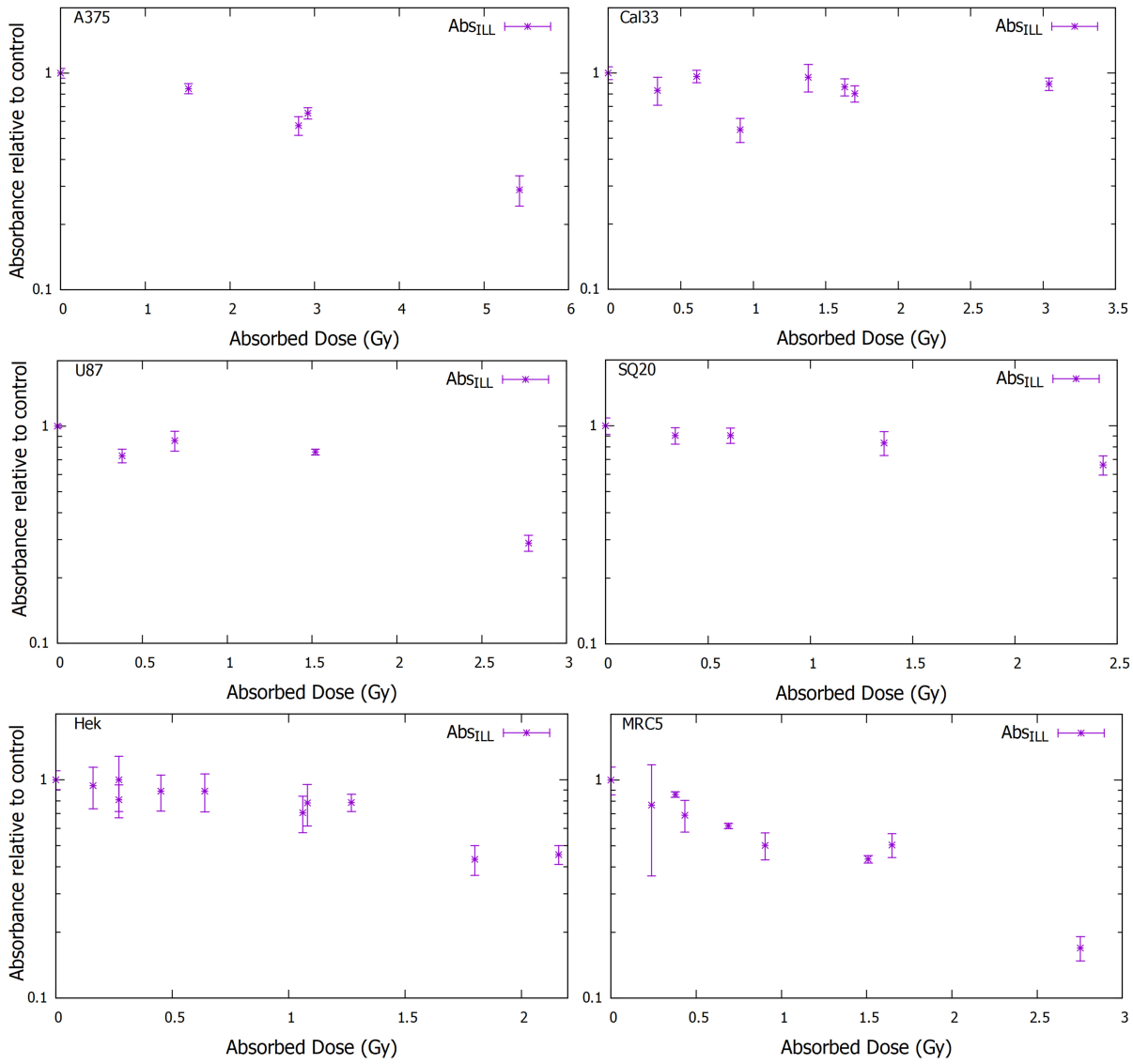

Figure B.2: Colorimetric BrdU assay results for Experiment I, using low-energy neutron irradiation. These data complement those shown in Figure 5.4 in Chapter 5.

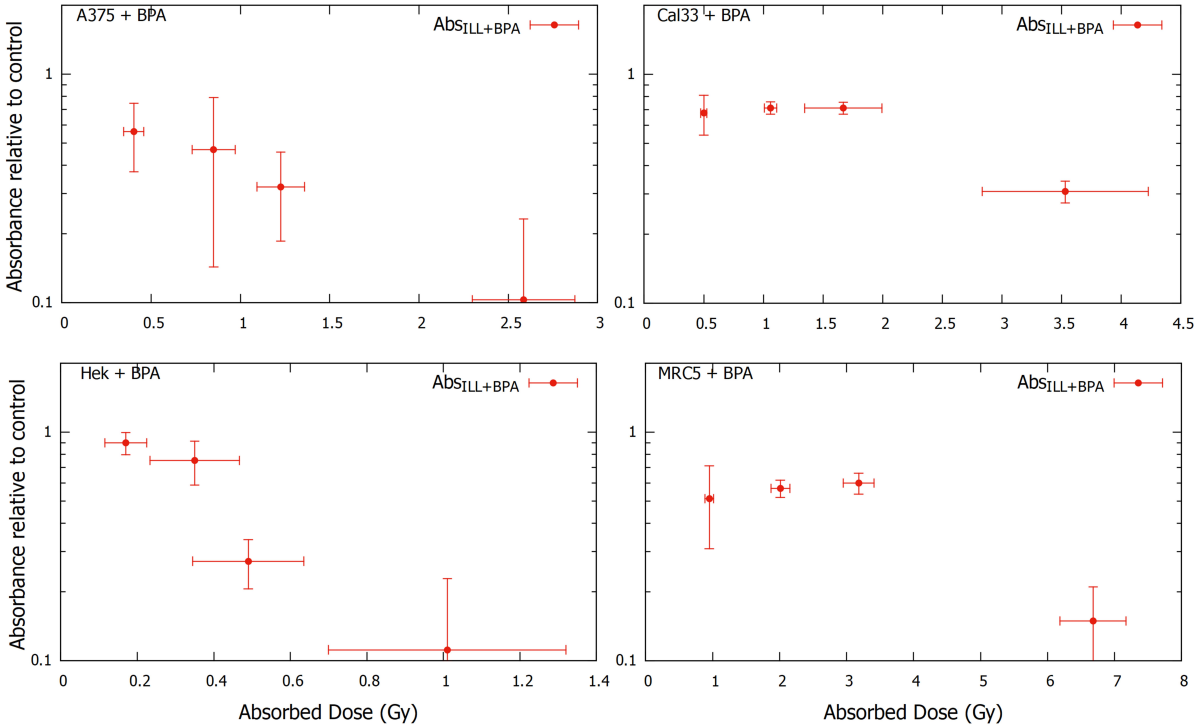

Figure B.3: Proliferation results for the samples of Experiment III, containing boron compound, performed with Resazurin colorimetric assay. The data are additional to those shown in Chapter 5 Figure 5.11.

With this study, a different response in the various tissues is found for the same irradiation type. In addition, low-energy neutron irradiations induce a stronger effect than the photon ones. The neutron irradiations of boron-containing cells yield to the lowest survival, therefore to the strongest effect on the cells. All of these results are similar of what it was observed in the results of the clonogenic assays shown in Sections 5.1, 5.2 and 5.3.

B.2 Resazurin – BrdU comparison

One of the reasons that these assay data are not included in the results analysis in Chapter 5 is because different assays were performed for the different experiments. While the Resazurin assay was used for photon irradiation and for the neutron irradiation of boron-containing samples, the BrdU assay was used for the studies for low-energy neutron irradiation (Experiment I). The equivalence between the two different approaches is not clear given that

the Resazurin assay is based on the metabolic activity of life cells whereas the BrdU assay is based onDNA synthesis during cell division. Hence a comparison of the results from photon irradiation and neutron irradiation is not straightforward and must be carries out with caution. In Figure B.4 a comparison between the two colorimetric assays was performed for the samples corresponding to Experiment III. A correlation is found for A375 and Hek, while for Cal33 and MRC5 high disparities are found.

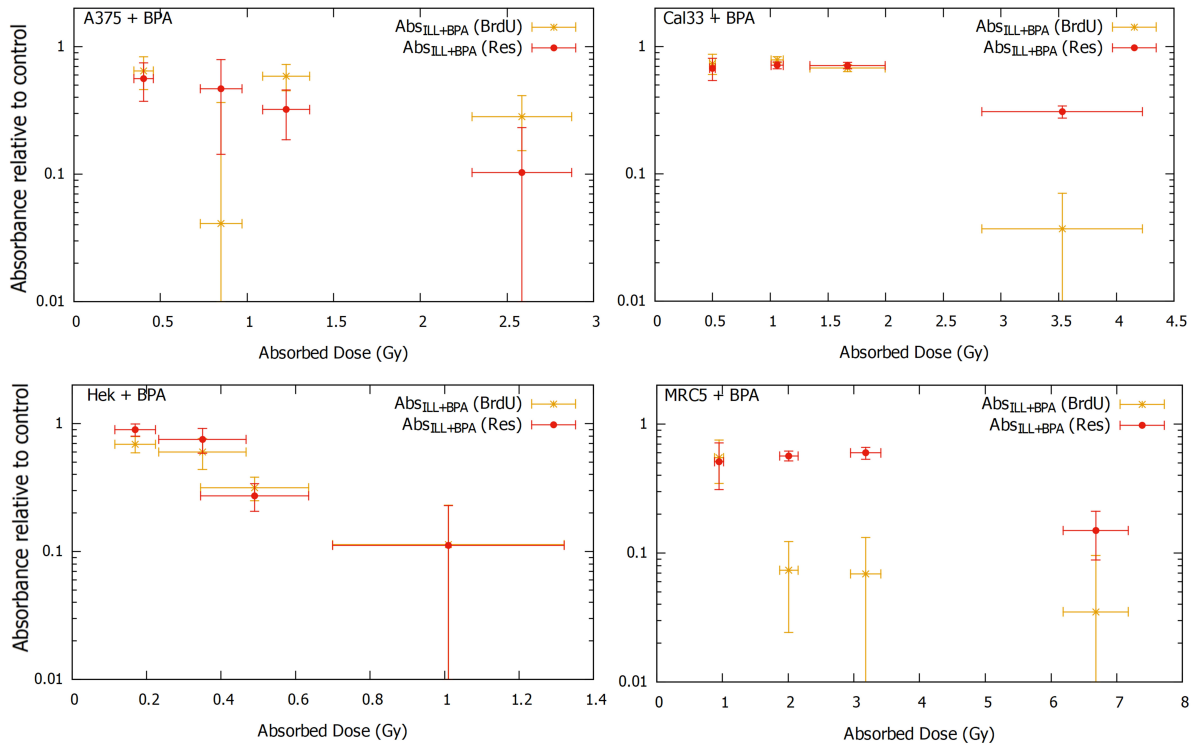

Figure B.4: Absorbance relative to control for the two difference colorimetric assays: BrdU and Resazurin (expressed like "Res" in the graphs). Samples corresponds to BPA containing cells irradiated at ILL, *i.e.* Experiment III.

References

[Abel06] Abele H. et al. (2006). Characterization of a ballistic supermirror neutron guide. Nuclear Instruments and Methods in *Physics Research Section A: Accelerators, Spectrometers, Detectors and Associated Equipment 562*, 407-417.

[Aiya11] Aiyama H. *et al.* (2011). A clinical trial protocol for second line treatment of malignant brain tumors with BNCT at University of Tsukuba. *Applied Radiation and Isotopes 69*, 1819-1822.

[Aley11] Aleynik V. *et al.* (2011). BINP accelerator based epithermal neutron source. *Applied Radiation and Isotopes 69*, 1635-1638

[Ande77] Andersen H. H., Ziegler J. F. (1977). Hydrogen: Stopping Powers and Ranges in All Elements. Vol. 3 of *The Stopping and Ranges of Ions in Matter* (Pergamon Press, Elmsford, New York).

[Arch71] Archambeau J. O., Fairchild R. G., Brenneis H. J. (1971). The Response of the Skin of Swine to Increasing Absorbed Doses of Radiation from a Thermal Neutron Beam, a Degraded Fission Neutron Beam, and the $^{10}B(n,\alpha)^{7}Li$ Reaction. *Radiation Research 45*, 145-165.

[Aute04] Auterinen I., Serén T., Anttila K., Kosunen A., Savolainen S. (2004). Measurement of free beam neutron spectra at eight BNCT facilities worldwide. *Applied Radiation and Isotopes 6*, 1021-1026.

[Bare94] Barendsen G. W. (1994). The relationships between RBE and LET for different types of lethal damage in mammalian cells: biophysical and molecular mechanisms. *Radiation Research 139*, 257-270.

[Bare01] Barendsen G. W., Van Bree C., Franken, N. A. (2001). Importance of cell proliferative state and potentially lethal damage repair on radiation effectiveness: implications for combined tumor treatments. *International Journal of Oncology 19*, 247-256.

[Bart05]Barth R. F., Coderre J. A., Vicente M. G. H., Blue T. E. (2005). Boron neutron capture therapy of cancer: current status and future prospects. *Clinical Cancer Research 11*, 3987-4002.

[Bart12] Barth R. F. *et al.* (2012). Current status of boron neutron capture therapy of high grade gliomas and recurrent head and neck cancer. *Radiation Oncology 7*, 146.

[Baue10] Bauer V. L. *et al.* (2010). Establishment and molecular cytogenetic characterization of a cell culture model of head and neck squamous cell carcinoma (HNSCC). *Genes 1*, 388-412.

[Bava17] Bavarnegin E., Kasesaz Y., Wagner F. M. (2017). Neutron beams implemented at nuclear research reactors for BNCT. *Journal of Instrumentation 12*, P05005.

[Baya19] Bayart E. *et al*. (2019). Fast dose fractionation using ultra-short laser accelerated proton pulses can increase cancer cell mortality, which relies on functional PARP1 protein. *Scientific Report* 9, 10132.

[Bell89] Belli M., Cherubini R., Finotto S., Moschini G., Sapora O., Simone G., Tabocchini M. A. (1989). RBE-LET relationship for the survival of V79 cells irradiated with low energy protons. *International Journal of Radiation Biology 55*, 93-104.

[Blau04] Blaumann H. R., González S. J., Longhino J., Santa Cruz G. A., Calzetta Larrieu O. A., Bonomi M. R., Roth B. M. C. (2004). Boron neutron capture therapy of skin melanomas at the RA-6 reactor: A procedural approach to beam set up and performance evaluation for upcoming clinical trials. *Medical Physics 31*, 70-80.

[Blue93] Blue T. E., Gupta N., Woollard, J. E. (1993). A calculation of the energy dependence of the RBE of neutrons. *Physics in Medicine & Biology 38*, 1693.

[Blue95] Blue T. E., Woollard J. E., Gupta N., Greskovich Jr, J. F. (1995). An expression for the RBE of neutrons as a function of neutron energy. *Physics in Medicine & Biology 40*, 757.

[Bort13] Bortolussi S., Altieri S. (2013). Boron concentration measurement in biological tissues by charged particle spectrometry. *Radiation and Environmental Biophysics 52*, 493-503.

[Bort14] Bortolussi S. *et al*. (2014). Boron concentration measurements by alpha spectrometry and quantitative neutron autoradiography in cells and tissues treated with different boronated formulations and administration protocols. *Applied Radiation and Isotopes 88*, 78-80.

[Bouc03] Bouchet L. G. *et al*. (2003). MIRD Pamphlet No. 19: Absorbed fractions and radionuclide S values for six age-dependent multiregion models of the kidney. *Journal of Nuclear Medicine 44*, 1113-1147.

[Buon18] Buontempo F. *et al*. (2018). Enhancing radiosensitivity of melanoma cells through very high dose rate pulses released by a plasma focus device. *PloS one 13*, e0199312.

[Burn92] Burnet N. G., Wurm R., Yarnold J. R., Peacock J. H., Nyman J., Turesson I. (1992). Prediction of normal-tissue tolerance to radiotherapy from in-vitro cellular radiation sensitivity. *The Lancet 339*, 1570-1571.

[Butt10] Butterworth K. T., McGarry C. K., O'Sullivan J. M., Hounsell A. R., Prise K. M. (2010). A study of the biological effects of modulated 6 MV radiation fields. *Physics in Medicine & Biology 55*, 1607.

[Casw82] Caswell R. S., Coyne J. J., Randolph M. L. (1982). Kerma factors of elements and compounds for neutron energies below 30 MeV. *The International Journal of Applied Radiation and Isotopes 33*, 1227-1262.

[Ceba11] Ceballos C., Esposito J., Agosteo S., Colautti P., Conte V., Moro D., Pola A. (2011). Towards the final BSA modeling for the accelerator-driven BNCT facility at INFN LNL. *Applied Radiation and Isotopes 69*, 1660-1663.

[Chad98] Chadha M. *et al*. (1998). Boron neutron-capture therapy (BNCT) for glioblastoma multiforme (GBM) using the epithermal neutron beam at the Brookhaven National Laboratory. *International Journal of Radiation Oncology* Biology* Physics 40*, 829-834.

[Chel10] Chełmiński K., *et al*. (2010). Energy dependence of radiochromic dosimetry films for use in radiotherapy verification. *Reports of Practical Oncology & Radiotherapy 15*, 40-46.

[CICSweb] Home page of CICS, Inc. http://www.cics.jp/nct/category_1.html

[Ciud03]Ciudad J, Guirado D., Sanchez-Reyes A., Sanjuanbenito, W. Velazquez S. (2003) Radiobiología clínica © Sociedad española de física médica.

[Code93] Coderre J. A. *et al*. (1993). Derivations of relative biological effectiveness for the high-LET radiations produced during boron neutron capture irradiations of the 9L rat gliosarcoma in vitro and in vivo. *International Journal of Radiation Oncology* Biology* Physics 27*, 1121-1129.

[Code95] Coderre J. A., Morris G. M., Micca P. L., Fisher C. D., Ross G. A. (1995). Comparative assessment of single-dose and fractionated boron neutron capture therapy. *Radiation Research 144*, 310-317.

[Code99] Coderre J. A., Morris G. M. (1999). The radiation biology of boron neutron capture therapy. *Radiation research 151*, 1-18.

[Dbal02] Dbaly V. *et al*. (2003). Contemporary state of neutron capture therapy in the Czech Republic.(Part 2). *Ceska a Slovenska Neurologie a Neurochirurgie 66*(1), 60-63.

[Ding13] Ding N. *et al*. (2013). Simulated studies on the biological effects of space radiation on quiescent human fibroblasts. *Advances in Space Research 52*, 1314-1319.

[Echa07] Echave P., Conlon I. J., Lloyd A. C. (2007). Cell size regulation in mammalian cells. *Cell Cycle 6*, 218-224.

[Edwa97] Edwards A. A. (1997). The use of chromosomal aberrations in human lymphocytes for biological dosimetry. *Radiation Research 148*, S39-S44.

[ENDFweb] http://www-nds.iaea.org/endf/.

[Fair85] Fairchild R. G., Bond V. P. (1985). Current status of 10B-neutron capture therapy: enhancement of tumor dose via beam filtration and dose rate, and the effects of these parameters on minimum boron content: a theoretical evaluation. *International Journal of Radiation Oncology* Biology* Physics 11*, 831-840.

[Farr54] Farr L.E. *et al*. (1954) Neutron capture therapy with boron in the treatment of glioblastoma miltiforme. *Am. J. Roentgenol. 71*, 279.

[Fowl89] Fowler J. F. (1989). The linear-quadratic formula and progress in fractionated radiotherapy. *The British Journal of Radiology 62*, 679-694.

[Fowl90] Fowler J. F. (1990). How worthwhile are short schedules in radiotherapy?: A series of exploratory calculations. *Radiotherapy and Oncology 18*, 165-181.

[Fran11] Franken N. A., *et al.* (2011). Comparison of RBE values of high-LET α-particles for the induction of DNA-DSBs, chromosome aberrations and cell reproductive death. *Radiation Oncology 6*, 64.

[Fuku03] Fukuda H. *et al*. (2003). Boron neutron capture therapy (BNCT) for malignant melanoma with special reference to absorbed doses to the normal skin and tumor. *Australasian Physics & Engineering Sciences in Medicine 26*(3), 97.

[Fuku89] Fukuda H., Ichihashi M., Kobayashi T., Matsuzawa D., Kanda K., Mishima Y. (1989). Biological effectiveness of thermal neutrons and 10B (n, α) 7Li reaction on cultured cells. *Pigment Cell Research 2*, 333-336.

[Gabe84] Gabel D., Fairchild R. G., Larsson B., Börner H. G. (1984). The relative biological effectiveness in V79 Chinese hamster cells of the neutron capture reactions in boron and nitrogen. *Radiation Research 98*, 307-316.

[Gara11] Garabalino M. A. *et al*. (2011). Boron neutron capture therapy (BNCT) for the treatment of liver metastases: biodistribution studies of boron compounds in an experimental model. *Radiation and Environmental Biophysics 50*, 199-207

[Gara13] Garabalino M. A. *et al*. (2013). Biodistribution of sodium borocaptate (BSH) for boron neutron capture therapy (BNCT) in an oral cancer model. *Radiation and Environmental Biophysics 52*, 351-361.

[Gara14] Garabalino, M. A *et al*. (2014). Boron biodistribution for BNCT in the hamster cheek pouch oral cancer model: Combined administration of BSH and BPA. *Applied Radiation and Isotopes 88*, 64-68.

[Gavi94] Gavin P. R., Kraft S. L., Dehaan C. E., Swartz C. D., Griebenow M. L. (1994). Large animal normal tissue tolerance with boron neutron capture. *International Journal of Radiation Oncology* Biology* Physics 28*, 1099-1106.

[Gavi97] Gavin P. R., Kraft S. L., Huiskamp R., Coderre J. A. (1997). A review: CNS effects and normal tissue tolerance in dogs. *Journal of Neuro-Oncology 33*, 71-80.

[Gree12] Green S. *et al*. (2012). The Birmingham BNCT Project: Developments towards selective internal particle therapy. *Radiotherapy and Oncology 102*, S164-S165.

[Gome12] Gómez-Millán J. *et al*. (2012). The importance of bystander effects in radiation therapy in melanoma skin-cancer cells and umbilical-cord stromal stem cells. *Radiotherapy and Oncology 102*, 450-458.

[Gonz12] González S. J., Santa-Cruz G. A. (2012). The photon-isoeffective dose in boron neutron capture therapy. *Radiation Research 178*, 609-621.

[Gonz17] Gonzalez S. J., Pozzi E. C. C., Hughes A. M., Provenzano L., Koivunoro, H., Carando, D. G. (2017). Photon iso-effective dose for cancer treatment with mixed field radiation based on dose–

response assessment from human and an animal model: clinical application to boron neutron capture therapy for head and neck cancer. *Physics in Medicine & Biology 62*, 7938.

[Goor02] Goorley J. T., Kiger W. S., Zamenhof R. G. (2002). Reference dosimetry calculations for neutron capture therapy with comparison of analytical and voxel models. *Medical Physics 29*, 145-156.

[Half11] Halfon S. *et al*. (2011). High-power liquid-lithium target prototype for accelerator-based boron neutron capture therapy. *Applied Radiation and Isotopes 69*, 1654-1656.

[Hall75] Hall E. J., Novak J. K., Kellerer A. M., Rossi H. H., Marino S., Goodman L. J. (1975). RBE as a function of neutron energy: I. Experimental observations. *Radiation Research 64*, 245-255.

[Hata75] Hatanaka H. (1975). A revised boron-neutron capture therapy for malignant brain tumors. *Journal of Neurology 209*, 81-94.

[Hope11] Hopewell J. W., Morris G., Schwint A., Coderre J. A. (2011). The radiobiological principles of boron neutron capture therapy: a critical review. *Applied radiation and isotopes 69*, 1756-1759.

[IAEA01] International Atomic Energy Agency, IAEA-TECDOC-1223 (2001).

[ICRP60] ICRP publication 60 (1991). *Ann ICRP 21*,1-3.

[ICRP97] Valentin J. (2003). Relative biological effectiveness (RBE), quality factor (Q), and radiation weighting factor (w_R): ICRP Publication 92. *Annals of the ICRP 33*, 1-121.

[ICRP103] ICRP publication 103 (2007). *Ann ICRP 37*, 2.

[ICRU46] ICRU 46 (1992) Photon, electron, proton, and neutron interaction data for body tissues. International Commission on Radiation Units and Measurements, Bethesda, MD.

[ICRU49] International Commission on Radiation Units and Measurements report 49 (1993). International Commission on Radiation Units and Measurements. *ICRU Report 49*, *Stopping Powers and Ranges for Protons and Alpha Particles*.

[ICRU63] Malmer C. J. (2001). ICRU report 63, Nuclear data for neutron and proton radiotherapy and for radiation protection. *Medical Physics 28*, 861-861.

[Iraz16] Irazola L. *et al*. (2016). Using a Tandem Pelletron accelerator to produce a thermal neutron beam for detector testing purposes. *Applied Radiation and Isotopes 107*, 330-334.

[Jime18a] Jiménez-Bonilla P., Praena J., Quesada J. M. (2018). Maxwellian Neutron Spectrum generation and Stellar Cross-Section measurements: measurement of the 197Au (n, $\boldsymbol{\gamma}$) MACS. *Journal of Physics: Conference Series 940*, 012044.

[Jime18b] Jiménez-Bonilla P., Praena J. (2018) Measurement of the 197 Au (n, $\boldsymbol{\gamma}$) stellar cross section at kT= 30 keV by activation. *XIII Nuclei in the Cosmos proceedings.*

[Jime18c] Jiménez-Bonilla P. (2018). Experimentos de activación en astrofísica nuclear para la medida de secciones eficaces estelares de captura de neutrones: Revisión del método y medida experimental de la sección eficaz estelar de la reacción (*Doctoral dissertation, Universidad de Sevilla*).

[Joen03] Joensuu H. *et al*. (2003). Boron neutron capture therapy of brain tumors: clinical trials at the Finnish facility using boronophenylalanine. *Journal of neuro-oncology 62*, 123-134.

[Join16] Joiner M. C., Van der Kogel A. (Eds.). (2016). Basic clinical radiobiology. Ed. CRC Press.

[Kage97] Kageji T., Nakagawa Y., Kitamura K., Matsumoto K. Hatanaka H. (1997). Pharmacokinetics and boron uptake of BSH (Na2B12H11SH) in patients with intracranial tumors. *Journal of Neuro-Oncology 33*, 117-130.

[Kank11] Kankaanranta L. *et al*. (2011). L-boronophenylalanine-mediated boron neutron capture therapy for malignant glioma progressing after external beam radiation therapy: a Phase I study. *International Journal of Radiation Oncology* Biology* Physics 80*, 369-376.

[Kank11b] Kankaanranta L., Saarilahti K., Mäkitie A., Välimäki P., Tenhunen M., Joensuu H. (2011). Boron neutron capture therapy (BNCT) followed by intensity modulated chemoradiotherapy as primary treatment of large head and neck cancer with intracranial involvement. *Radiotherapy and Oncology 99*, 98-99.

[Kank12] Kankaanranta L., Seppälä T., Koivunoro H., Saarilahti K., Atula T., Collan J., Mäkitie, A. (2012). Boron neutron capture therapy in the treatment of locally recurred head-and-neck cancer: final analysis of a phase I/II trial. *International Journal of Radiation Oncology* Biology* Physics 82*, e67-e75.

[Kato04] Kato I. *et al*. (2004). Effectiveness of BNCT for recurrent head and neck malignancies. *Applied Radiation and Isotopes 61*, 1069-1073.

[Kato09] Kato I. *et al*. (2009). Effectiveness of boron neutron capture therapy for recurrent head and neck malignancies. *Applied Radiation and Isotopes 67*, S37-S42.

[Kawa09] Kawabata S. *et al*. (2009). Boron neutron capture therapy for newly diagnosed glioblastoma. *Journal of Radiation Research 50*, 51-60.

[Kiya12] Kiyanagi Y. *et al*. (2012). A project of boron neutron capture therapy system based on a proton linac neutron source. *Physics Procedia 26*, 223-230.

[Konr11] Konrad G.R. (2011) Measurement of the Proton Recoil Spectrum in Neutron Beta Decay with the Spectrometer aSPECT: Study of Systematic Effects. (*Doctoral dissertation, Johannes Gutenberg-Universität*)

[Kono04] Kononov O. E. *et al*. (2004). Optimization of an accelerator-based epithermal neutron source for neutron capture therapy. *Applied Radiation and Isotopes 61*, 1009-1013.

[Kono06] Kononov V. N., Bokhovko M. V., Kononov O. E., Soloviev N. A., Chu W. T., Nigg D. (2006). Accelerator-based fast neutron sources for neutron therapy. *Nuclear Instruments and Methods in Physics Research Section A: Accelerators, Spectrometers, Detectors and Associated Equipment 564*, 525-531.

[Krei01] Kreimann E. L., Itoiz M. E., Dagrosa A., Garavaglia R., Farías S., Batistoni D., Schwint, A. E. (2001). The hamster cheek pouch as a model of oral cancer for boron neutron capture therapy studies: selective delivery of boron by boronophenylalanine. *Cancer Research 61*, 8775-8781

[Krei14] Kreiner A. J. *et al*. (2014). Development of high power electrostatic accelerators for nuclear and medical purposes in Argentina. *Physics Procedia 60*, 39-44.

[Krei16] Kreiner A. J. *et al*. (2016). Present status of accelerator-based BNCT. *Reports of Practical Oncology & Radiotherapy 21*, 95-101.

[Kuma14] Kumada H. *et al*. (2014). Project for the development of the linac based NCT facility in University of Tsukuba. *Applied Radiation and Isotopes 88*, 211-215.

[Kwan95] Kwan J. W., Anderson O. A., Reginato L. L., Vella M. C., Yu S. S. (1995). A 2.5 MeV electrostatic quadrupole DC accelerator for BNCT application. *Nuclear Instruments and Methods in Physics Research Section B: Beam Interactions with Materials and Atoms 99*, 710-712.

[Lede12] Lederer, C. *et al*. (2012). Definition of a standard neutron field with the ^{7}Li (p, n)^{7}Be reaction. *Physical Review C 85*, 055809.

[Lee99] Lee C. L., Zhou X. L., Kudchadker R. J., Harmon F., Harker Y. D. (2000). A Monte Carlo dosimetry-based evaluation of the reaction near threshold for accelerator boron neutron capture therapy. *Medical Physics 27*, 192-202.

[Li15] Li P., Shi Y. W., Li B. X., Xu W. C., Shi Z. L., Zhou C., Fu S. (2015). Photo-thermal effect enhances the efficiency of radiotherapy using Arg-Gly-Asp peptides-conjugated gold nanorods that target αvβ3 in melanoma cancer cells. *Journal of Nanobiotechnology 13*, 52.

[Loch36] Locher G. L. (1936). Biological effects and therapeutic possibilities of neutrons. *Am J Roentgenol 36*, 1-13.

[Lone80] Lone M. A., Santry D. C., Inglis W. M. (1980). MeV neutron production from thermal neutron capture in Li and B compounds. *Nuclear Instruments and Methods 174*, 521-529.

[Luo14] Luo X. et al. (2014). Isolation and molecular characterization of circulating melanoma cells. *Cell Reports 7*, 645-653.

[Mack07] Mackonis E. C., Suchowerska N., Zhang M., Ebert M., McKenzie D. R., Jackson M. (2007). Cellular response to modulated radiation fields. *Physics in Medicine & Biology 52*, 5469.

[MASSweb] NIST Standard Reference Database 126, https://physics.nist.gov/PhysRefData/XrayMassCoef/tab4.html

[Maso11] Mason A. J., Giusti V., Green S., af Rosenschöld P. M., Beynon T. D., Hopewell J. W. (2011). Interaction between the biological effects of high-and low-LET radiation dose components in a mixed field exposure. *International Journal of Radiation Biology 87*, 1162-1172.

[Maug97] Maughan R. L., Chuba P. J., Porter A. T., Ben-Josef E., Lucas D. R. (1997). The elemental composition of tumors: Kerma data for neutrons. *Medical physics 24*, 1241-1244.

[McCo11] McConn R. J., Gesh C. J., Pagh R. T., Rucker R. A., Williams III R. (2011). Compendium of material composition data for radiation transport modeling. No. PNNL-15870 Rev. 1. *Pacific Northwest National Lab.(PNNL)*, Richland, WA (United States).

[MCNP03] X-5 Monte Carlo Team. (2003). MCNP—A General Monte Carlo N-Particle Transport Code, Version 5. *LA-UR-03-1987 1*.

[MCNP11] Pelowitz D.B. (2011) MCNPX Users Manual Version 2.7.0. *LA-CP-11-00438*.

[Mene09] Menéndez P. R., Roth B. M. C., Pereira M. D., Casal M. R., González S. J., Feld D. B., Rebagliati R. J. (2009). BNCT for skin melanoma in extremities: updated Argentine clinical results. *Applied Radiation and Isotopes 67*, S50-S53.

[Meni09] Menichetti L *et al*. (2009). In vitro neutron irradiation of glioma and endothelial cultured cells. *Applied Radiation and Isotopes 67*, S336-S340.

[Min05] Min F. L., Zhang H., Li W. J., Gao Q. X., Zhou G. M. (2005). Effect of exogenous wild-type p53 on melanoma cell death pathways induced by irradiation at different linear energy transfer. *In Vitro Cellular & Developmental Biology-Animal 41*, 284-288.

[Mish89] Mishima Y. *et al*. (1989). First human clinical trial of melanoma neutron capture. Diagnosis and therapy. *Strahlentherapie und Onkologie*, *165*, 251-254.

[Miya05] Miyatake S. I. *et al*. (2005). Modified boron neutron capture therapy for malignant gliomas performed using epithermal neutron and two boron compounds with different accumulation mechanisms: an efficacy study based on findings on neuroimages. *Journal of Neurosurgery 103*, 1000-1009.

[Miya13] Miyatake S. I., Furuse M., Kawabata S., Maruyama T., Kumabe T., Kuroiwa T., Ono K. (2013). Bevacizumab treatment of symptomatic pseudoprogression after boron neutron capture therapy for recurrent malignant gliomas. Report of 2 cases. *Neuro-Oncology 15*, 650-655.

[Morg88] Morgan G. R., Mill A. J., Roberts C. J., Newman S., Holt P. D. (1988). The radiobiology of 24 keV neutrons. *The British journal of radiology 61*, 1127-1135.

[Morr94] Morris G. M., Coderre J. A., Hopewell J. W., Micca P. L., Rezvani M. (1994). Response of rat skin to boron neutron capture therapy with p-boronophenylalanine or borocaptate sodium. *Radiotherapy and Oncology 32*, 144-153

[Morr94b] Morris G. M., Coderre J. A., Hopewell J. W., Micca P. L., Nawrocky M. M., Liu H. B., Bywaters A. (1994). Response of the central nervous system to boron neutron capture irradiation: Evaluation using rat spinal cord model. *Radiotherapy and Oncology 32*, 249-255.

[Moss14] Moss R. L. (2014). Critical review, with an optimistic outlook, on Boron Neutron Capture Therapy (BNCT). *Applied Radiation and Isotopes 88*, 2-11.

[Muns05] Munshi, A. *et al*. (2005). Histone deacetylase inhibitors radiosensitize human melanoma cells by suppressing DNA repair activity. *Clinical Cancer Research 11*, 4912-4922.

[Muns06] Munshi, A., Tanaka, T., Hobbs, M. L., Tucker, S. L., Richon, V. M., Meyn, R. E. (2006). Vorinostat, a histone deacetylase inhibitor, enhances the response of human tumor cells to ionizing radiation through prolongation of γ-H2AX foci. *Molecular Cancer Therapeutics 5*, 1967-1974.

[Naka09] Nakagawa Y., Kageji T., Mizobuchi Y., Kumada H., Nakagawa Y. (2009). Clinical results of BNCT for malignant brain tumors in children. *Applied Radiation and Isotopes 67*, S27-S30.

[Naka11] Nakai K. *et al*. (2011). Boron neutron capture therapy combined with fractionated photon irradiation for glioblastoma: a recursive partitioning analysis of BNCT patients. *Applied Radiation and Isotopes 69*, 1790-1792.

[Nara16] Narayanasamy G., Saenz D., Cruz W., Ha C. S., Papanikolaou N., Stathakis S. (2016). Commissioning an Elekta Versa HD linear accelerator. *Journal of Applied Clinical Medical Physics 17*, 179-191

[Nghiweb] https://github.com/nghiaho12/CellCounter

[Otto15] Ottolenghi A., Baiocco G., Smyth V., Trott K. (2015). The ANDANTE project: a multidisciplinary approach to neutron RBE. *Radiation Protection Dosimetry 166*, 311-315.

[Pedr20a] Pedrosa-Rivera M. *et al*. (2020). Neutron radiobiology studies with a pure cold neutron beam. *Nuclear Instruments and Methods in Physics Research Section B: Beam Interactions with Materials and Atoms 462*, 24-31.

[Pedr20b] Pedrosa-Rivera M., Praena J., Porras I., Ruiz-Magaña M. J., Ruiz-Ruiz C. (2020). A simple approximation for the evaluation of the photon iso-effective dose in Boron Neutron Capture Therapy based on dose-independent weighting factors. *Applied Radiation and Isotopes 157*, 109018.

[Perr86] Perris A., Pialoglou P., Katsanos A. A., Sideris E. G. (1986). Biological effectiveness of low energy protons. I. Survival of Chinese hamster cells. *International Journal of Radiation Biology and Related Studies in Physics, Chemistry and Medicine 50*, 1093-1101.

[Pf1bweb]http://www.ill.eu/instruments-support/instruments-groups/instruments/PF1b/characteristics/

[Phoe09] Phoenix B., Green S., Hill M. A., Jones B., Mill A., Stevens D. L. (2009). Do the various radiations present in BNCT act synergistically? Cell survival experiments in mixed alpha-particle and gamma-ray fields. *Applied Radiation and Isotopes 67*, S318-S320.

[Porr14] Porras I., Sabaté-Gilarte M., Praena J., Quesada J. M., Esquinas P. L. (2014). ^{33}S for neutron capture therapy: nuclear data for Monte Carlo calculations. *Nuclear Data Sheets 120*, 246-249.

[Post16] Postuma I. *et al*. (2016). An improved neutron autoradiography set-up for ^{10}B concentration measurements in biological samples. *Reports of Practical Oncology & Radiotherapy 21*, 123-128.

[PSTARweb] NIST Standard Reference Database 124, https://physics.nist.gov/PhysRefData/Star/Text/PSTAR-t.html

[Rome18] Romero-Expósito M., Viñals, S., Ortega-Gelabert, O., Fernández, B., Jiménez-Bonilla, P., Praena, J., Domingo, C. (2018). Characterization of the epithermal neutron field produced by p+ ^{7}Li reaction in a Tandem accelerator using a Bonner sphere spectrometer. *Radiation Protection Dosimetry 180*, 80-84.

[Sato18] Sato T., Masunaga S. I., Kumada H., Hamada N. (2018). Microdosimetric modeling of biological effectiveness for boron neutron capture therapy considering intra-and intercellular heterogeneity in 10 B distribution. *Scientific Reports 8*, 1-14.

[Saue02] Sauerwein W., Zurlo A. EORTC Boron Neutron Capture Therapy Group. (2002). The EORTC boron neutron capture therapy (BNCT) group: achievements and future projects. *European Journal of Cancer 38*, 31-34.

[Saue12] Sauerwein W. A., Wittig A., Moss R. & Nakagawa Y. (Eds.). (2012). *Neutron capture therapy: principles and applications*. Springer Science & Business Media.

[Schi15] Schick U. *et al*. (2015). Trametinib radiosensitises RAS-and BRAF-mutated melanoma by perturbing cell cycle and inducing senescence. *Radiotherapy and Oncology 117*, 364-375.

[Selt93] Seltzer S. M. (1993). Calculation of photon mass energy-transfer and mass energy-absorption coefficients. *Radiation Research 136*, 147-170.

[Solo67] Soloway A. H., Hatanaka H., Davis M. A. (1967). Penetration of brain and brain tumor. VII. Tumor-binding sulfhydryl boron compounds. *Journal of Medicinal Chemistry 10*, 714-717.

[Suzu12] Suzuki M. *et al*. (2012, October). Reirradiation for locally recurrent lung cancer in the chest wall with boron neutron capture therapy (BNCT). In *International Cancer Conference Journal 1,* 235-238

[Swee51] Sweet W. H. (1951). The uses of nuclear disintegration in the diagnosis and treatment of brain tumor. *New England Journal of Medicine 245*, 875-878.

[Tana11] Tanaka H. *et al*. (2011). Experimental verification of beam characteristics for cyclotron-based epithermal neutron source (C-BENS). *Applied Radiation and Isotopes 69*, 1642-1645.

[Tham90] Thames H. D., Bentzen S. M., Turesson I., Overgaard M., Van den Bogaert W. (1990). Time-dose factors in radiotherapy: a review of the human data. *Radiotherapy and Oncology 19*, 219-235.

[VanL18] Van Leeuwen C. M. *et al*. (2018). The alfa and beta of tumours: a review of parameters of the linear-quadratic model, derived from clinical radiotherapy studies. *Radiation Oncology 13*, 96.

[Wang11] Wang L. W., Wang S. J., Chu P. Y., Ho C. Y., Jiang S. H., Liu Y. H., Yen, S. H. (2011). BNCT for locally recurrent head and neck cancer: preliminary clinical experience from a phase I/II trial at Tsing Hua open-pool reactor. *Applied Radiation and Isotopes 69*, 1803-1806.

[Wang18] Wang L. W., Liu Y. W. H., Chou F. I., Jiang S. H. (2018). Clinical trials for treating recurrent head and neck cancer with boron neutron capture therapy using the Tsing-Hua Open Pool Reactor. *Cancer Communications 38*, 37.

[webBio] https://bionumbers.hms.harvard.edu

[Will04] Willendrup P., Farhi E., Lefmann K. (2004). McStas 1.7-a new version of the flexible Monte Carlo neutron scattering package. *Physica B: Condensed Matter 350*, E735-E737.

[Wong93] Wong CS, Poon JK, Hill RP. (1993). Re-irradiation tolerance in the rat spinal cord: influence of level of initial damage. *Radiotherapy and Oncology 26*, 132-138.

[Yada14] Yadav K., Singhal N., Rishi V., Yadav H. (2014). Cell Proliferation Assays. *eLS, John Wiley & Sons, Ltd* (Ed.).

[Yama61] Yamamoto Y. L. (1961). The biological effectiveness of thermal neutrons and of the heavy particles from the B10(n,alpha)Li7 reaction for the rabbit's ear and its utilization for neutron capture therapy. *Yokohama medical bulletin 12*, 4-22.

[Yama04] Yamamoto T. *et al*. (2004). Current clinical results of the Tsukuba BNCT trial. *Applied Radiation and Isotopes 61*, 1089-1093.

[Yama11] Yamamoto T. *et al*. (2011). The status of Tsukuba BNCT trial: BPA-based boron neutron capture therapy combined with X-ray irradiation. *Applied Radiation and Isotopes 69*, 1817-1818.

[Zont09] Zonta A. *et al*. (2009). Extra-corporeal liver BNCT for the treatment of diffuse metastases: what was learned and what is still to be learned. *Applied Radiation and Isotopes 67*, S67-S75.

List of publications

• Pedrosa-Rivera M., Praena J., Porras I., Ruiz-Magaña M. J., Ruiz-Ruiz C. (2020). A simple approximation for the evaluation of the photon iso-effective dose in Boron Neutron Capture Therapy based on dose-independent weighting factors. *Applied Radiation and Isotopes 157*, 109018.
DOI: 10.1016/j.apradiso.2019.109018

• Pedrosa-Rivera M. *et al.* (2020). Neutron radiobiology studies with a pure cold neutron beam. *Nuclear Instruments and Methods in Physics Research Section B: Beam Interactions with Materials and Atoms*, *462*, 24-31.
DOI: 10.1016/j.nimb.2019.10.027

• Porras I., Pedrosa M., Praena J., Saavedra F., Sabariego M. P., Ogállar F., Torres-Sánchez P. (2019). Perspectives on Neutron Capture Therapy of Cancer. *CERN Conference: C18-06-11.10 Proceedings*, 295-304.
DOI: 10.23727/CERN-PROCEEDINGS-2019-001

• Pedrosa-Rivera M., Porras I., Praena J., Ruiz-Magaña M. J., Ruiz-Ruiz C. (2017). Radiobiology for improving Boron Neutron Capture Therapy treatment planning. *New trends from young scientists in Molecular and Atomic Physics*. Ed. Secretariado de Recursos Audiovisuales y Nuevas Tecnologías (Universidad de Sevilla).
ISBN: 978-84-16784-65-3

• Porras I., Praena J., Arias de Saavedra F., Pedrosa M., Esquinas P. L., Jiménez-Bonilla P. (2015). Epithermal neutron beams from the 7Li (p, n) reaction near the threshold for neutron capture therapy. *Il Nuovo Cimento 38,* 179.
DOI: 10.1393/ncc/i2015-15179-9

El doctorando / The *doctoral candidate* **[María Pedrosa Rivera]** y los directores de la tesis / and the thesis supervisor/s: **[José Ignacio Porras Sánchez y María Carmen Ruiz Ruiz]**

Garantizamos, al firmar esta tesis doctoral, que el trabajo ha sido realizado por el doctorando bajo la dirección de los directores de la tesis y hasta donde nuestro conocimiento alcanza, en la realización del trabajo, se han respetado los derechos de otros autores a ser citados, cuando se han utilizado sus resultados o publicaciones.

/

Guarantee, by signing this doctoral thesis, that the work has been done by the doctoral candidate under the direction of the thesis supervisor/s and, as far as our knowledge reaches, in the performance of the work, the rights of other authors to be cited (when their results or publications have been used) have been respected.

Lugar y fecha / Place and date: Granada 11/02/2020

Director/es de la Tesis / *Thesis supervisor/s;*

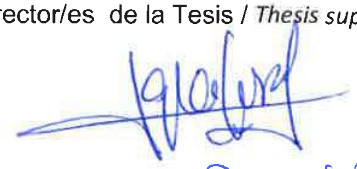

Fdo: J. Ignacio Porras Sánchez

Fdo. Mª CARMEN RUIZ RUIZ

Firma / Signed

Doctorando / *Doctoral candidate*:

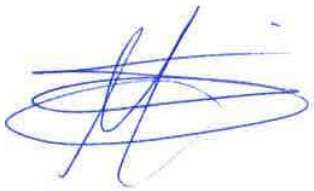

Firma / Signed